Australian Government
Bureau of Meteorology

The Centre for Australian Weather and Climate Research
A partnership between CSIRO and the Bureau of Meteorology

CSIRO

Understanding and Prediction of Monsoon Weather and Climate - abstracts of the sixth CAWCR Workshop 12 November - 15 November 2012, Melbourne, Australia

CAWCR Technical Report No. 056

Keith A. Day (editor)

November 2012

www.cawcr.gov.au

Understanding and Prediction of Monsoon Weather and Climate - abstracts of the sixth CAWCR Workshop 12 November - 15 November 2012, Melbourne, Australia

Keith A. Day (Editor)

Centre for Australian Weather and Climate Research,
GPO Box 1289, Melbourne, VIC 3001, Australia

CAWCR Technical Report No. 056

November 2012

National Library of Australia Cataloguing-in-Publication entry

Author: CAWCR 6th Annual Workshop; Understanding and Prediction of Monsoon Weather and Climate (2012: Melbourne, Victoria)

Title: Understanding and Prediction of Monsoon Weather and Climate - abstracts of the sixth CAWCR Workshop 12 November - 15 November 2012, Melbourne, Australia / Editor Keith. A. Day.

ISBN: 978-0-643-10959-9

Series: CAWCR technical report; No. 56

Notes: Includes index.

Subjects: Meteorology--Research--Congresses.

Enquiries should be addressed to:

Keith Day
Centre for Australian Weather and Climate Research:
A partnership between the Bureau of Meteorology and CSIRO
GPO Box 1289
Melbourne VIC 3001
Australia

k.day@bom.gov.au
Phone: 61 3 9669 8311
Fax: 61 3 9669 4660

Copyright and Disclaimer

All images reproduced in grayscale. A colour version of CAWCR Technical Report No.056 is available online: http://www.cawcr.gov.au

Contents

FOREWORD

The Centre for Australian Weather and Climate Research (CAWCR) is a partnership between Australia's leading atmosphere and ocean research agencies – CSIRO) and the Bureau of Meteorology. CAWCR, established in 2007, jointly manages the science capability within the Bureau and CMAR providing a single centre of research excellence. This year's CAWCR Workshop, *"Understanding and Prediction of Monsoon Weather and Climate"* is the sixth Annual Workshop under the auspices of the Centre, continuing the series originating within the Bureau of Meteorology Research Centre.

The focus of the workshop on monsoons is motivated by the primary role that the Australian-Asian monsoon plays in the climate of Australia and the need to better predict and simulate monsoon weather and climate in order to provide more useful advice on weather and climate variability and change to society. However, monsoons are fundamental to many other regions of the world; hence the focus of the workshop is not limited to the Australian-Asian monsoon.

The aims of the meeting are to:
1) Review and assess the current understanding of the processes involved in monsoon climate (especially for Australia) on time scales from weather to seasonal to climate;
2) Identify major challenges in simulating the monsoon in the Australasian region and globally at these time scales; and
3) Provide a forum for monsoon researchers from different disciplines (weather, seasonal prediction, climate and climate change) to share ideas, enhance collaboration and develop a coordinated approach to address challenges in monsoon prediction and simulation in Australasia.

The key themes covered in this year's workshop are:

(i) Observed monsoon Variability from Weather to Climate;
(ii) Prediction of monsoon weather;
(iii) Representing monsoons in weather and climate models;
(iv) Intra-seasonal/Seasonal Prediction of the Monsoon;
(v) Monsoon Decadal Prediction and Climate Change

A number of prominent scientists and experts from overseas, Australian research agencies and universities have been invited to give presentations. Keynote speakers include Dr Gareth Berry (Monash University, Australia), Dr William Boos (Yale University, USA), Dr Akio Kitoh (Climate Research Department, Meteorological Research Institute, Tsukuba, Japan), Dr Eric Maloney (Department of Atmospheric Science, Colorado State University, USA), Dr Gill Martin (Met Office, Exeter, UK), Dr Peter May (CAWCR, Bureau of Meteorology, Australia), Dr Sean Milton (Global Model Evaluation and Development, Met Office, Exeter, UK), Dr Masayuki Nakagawa (Numerical Prediction Division, Japan Meteorological Agency, Tokyo, Japan), Dr Leon Rotstayn (CAWCR, CSIRO Marine and Atmospheric Research, Australia), Dr Kenneth Sperber (Program for Climate Model Diagnosis and Intercomparison, Lawrence Livermore National Laboratory, USA), Dr Matt Wheeler (CAWCR, Bureau of Meteorology, Australia), and Dr Chidong Zhang (Division of Meteorology and Physical Oceanography, University of Miami, Miami, USA),

The Workshop also includes two panel session aimed to address important questions in the field of seasonal prediction of monsoon and monsoon under climate change. We are grateful for these expert contributions and to all the participants' contributions to the debate and discussions.

This workshop is sponsored by the Bureau of Meteorology, the Australian Climate Change Science Program (ACCSP), the Pacific-Australian Climate Change Science and Adaptation Planning Program (PACCSAP), and CSIRO (Climate Adaptation Flagship, CMAR and the Climate and Atmosphere

Theme). We are also particularly grateful to Fujitsu and Intel for their generous support of this workshop.

Finally, we would like to thank the members of the organising committee for their efforts, comprising: Aurel Moise (Chair), Harry Hendon, Christian Jakob, Shoni Maguire, Leon Rotstayn, and John McBride. Meryl Wiseman, Val Jemmeson, Mark Bervanakis, Anu Arora and Julie Sortino provided excellent administrative support.

Tom Keenan

Director
Centre for Australian Weather and Climate Research:
A partnership between the Australian Bureau of Meteorology and CSIRO

November 2012

GENERAL OVERVIEW ON OBSERVATION OF AUSTRALIAN MONSOON

Peter May

Centre for Australian Weather and Climate Research: A partnership between the Bureau of Meteorology and CSIRO, Melbourne, Australia.

Abstract

I will review the recent work that has been undertaken in the Darwin area in the context of past analysis and field projects including the classic work of Troup and the findings from AMEX/EMEX/STEP that revolutionised our understanding of the Australian monsoon.

The talk will include some discussion on mesoscale circulations leading to major events and their predictability using the TWPICE MCS as an example where there is apparent large scale predictability for an event that was initiated by complex small scale interactions.

COHERENT SYNOPTIC DISTURBANCES IN THE AUSTRALIAN MONSOON

Gareth J. Berry[1], Michael J. Reeder[1] and Christian Jakob[2]

[1] Monash Weather and Climate, School of Mathematical Sciences, Monash University, Clayton, Victoria, Australia

[2] ARC Centre of Excellence for Climate System Science, School of Mathematical Sciences, Monash University, Clayton, Victoria, Australia

Introduction

Synoptic scale weather systems are frequently observed in the tropics and are intimately linked to disturbed local weather conditions. Perhaps the best documented synoptic systems are African Easterly Waves (AEWs; e.g. Reed et al., 1977) and monsoon lows over the Indian subcontinent (e.g. Godbole, 1977), both of which are important organisers of rainfall in their respective regions. AEWs and Indian monsoon lows are most frequently observed during summer and are generated within a monsoon environment. The aim of the research presented here is to explore synoptic analogues in the Australian monsoon in order to generate a climatology and to estimate their effect on regional rainfall.

Over tropical North Africa, AEWs are generated over the central and eastern parts of the continent and propagate westwards through the West African monsoon, intensifying as they move towards the Atlantic Ocean. As these disturbances continue to move westwards over the ocean they may act as precursors for tropical cyclones in the tropical Atlantic or eastern Pacific. It has been shown that AEWs are fuelled by baroclinic and barotropic energy conversions from the monsoon scale environment (particularly the mid-tropospheric African Easterly Jet) as well as from deep moist convection embedded within the disturbance (see e.g. Berry and Thorncroft, 2012). AEWs have a length scale of order 3000 km and can persist for a week or more as they traverse the African continent and the Atlantic Ocean.

By comparison, Indian monsoon lows are generated around the Bay of Bengal and propagate inland toward the continental heat low. These systems tend to be shorter lived than AEWs (2-5 days) and have smaller horizontal scales (approximately 1500 km), which may reflect differences in the environment. Composite studies of Indian monsoon lows show that these disturbances are characterised by strong cyclonic vorticity from the surface to the upper troposphere, with relatively little vertical tilt. At the surface, these disturbances have been associated with wind gusts exceeding 40 kts and heavy rainfall of 120 mm day^{-1} or more on their western (leading) edge.

Monsoon depressions are also found within the Australian monsoon system during Austral summer, although they have received considerably less attention than AEWs or Indian monsoon lows in the literature. The majority of studies concerned with Australian disturbances are focussed on particular high impact cases (e.g. Davidson and Holland, 1987). The broad consensus from these studies is that Australian monsoon disturbances are similar to Indian monsoon depressions, although little is known about their lifecycle or if the few events examined are representative. The similar geography of Australia and North Africa was noted by Dickinson and Molinari (2000) who compared the large-scale summertime basic state from an isentropic potential vorticity (PV) perspective and used band-pass (2-10 days) filtered winds as a metric of synoptic activity. These authors determined that the background mean gradients of PV necessary to support small amplitude, growing disturbances in the absence of convection were similar over both Australia and Africa, but found the synoptic activity over Australia was very weak and no evidence of growing synoptic scale disturbances was found. These authors suggested that this lack of synoptic activity could be linked to the smaller horizontal extent of the Australian monsoon or the lack of high terrain compared to the African region.

Methodology

Long-lived cyclonic disturbances are identified in the isentropic PV field from the ECMWF ERA-Interim (ERAI) reanalysis dataset and tracked using a simple automated technique. The ERAI reanalysis data used here are provided on a 1.5 x 1.5^{o} horizontal grid every six hours for the period 1989 – 2009. The analysis is confined to the three isentropic surfaces, 315 K, 330 K and 350 K, during the Southern Hemisphere warm season (November to March). The PV field is multiplied by negative one so that a PV maximum refers to a cyclonic feature throughout this study.

The tracking algorithm comprises four steps with necessary threshold values determined through direct experimentation and comparison with daily maps. First, the PV field is smoothed with two passes of a 5-point averaging operator. Second, the data at each timestep are scanned for all local PV maxima exceeding 0.01 PVU (where PVU = 10^{-6} K m^{2} kg s^{-1}) that are separated by at least 3^{o} from adjacent maxima. This radius threshold with the smoothing effectively means that only PV maxima of around 500 km and larger (i.e. meso and synoptic scale) are tracked. Third, the horizontal wind components on each surface are interpolated to the location of each local maximum and used to forecast the position of the each maximum at the next time step. Finally, the position of PV maxima at the subsequent time step are detected and their locations compared to the forecast positions of PV maxima detected at the initial time. Those within a radius of 5^{o} are associated with one another and joined to form a track. Only complete tracks lasting more than 24 hours are retained to ensure the PV maxima detected are coherent weather systems.

An example demonstrating the identification and tracking technique on the 315 K isentropic surface in the ERA-Interim reanalysis is shown in Fig. 1. There are several PV maxima over northern Australia that are all sub-synoptic scale and conform to our conceptual expectations based on previous literature. The tracks overlaid show that each PV maximum has propagated more than 1000 km from the east. Long-lived isolated PV maxima are also detected at higher latitudes (e.g. near 36^{o}S, 167^{o}E), although it should be recognised that tracking only commences once the feature becomes an isolated maximum, meaning that elongated maxima such as PV troughs or streamers are not detected or analysed. Composites of synoptic structures are formed from the ERA-Interim datasets and the Global Precipitation Climatology Project (GPCP) daily precipitation dataset. Because rainfall in the Australian monsoon has a clear seasonal progression, GPCP anomalies are computed as a deviation from a time-varying mean. This time-varying mean is constructed by a low pass filter of the daily means that retains only the first four harmonics of the seasonal cycle.

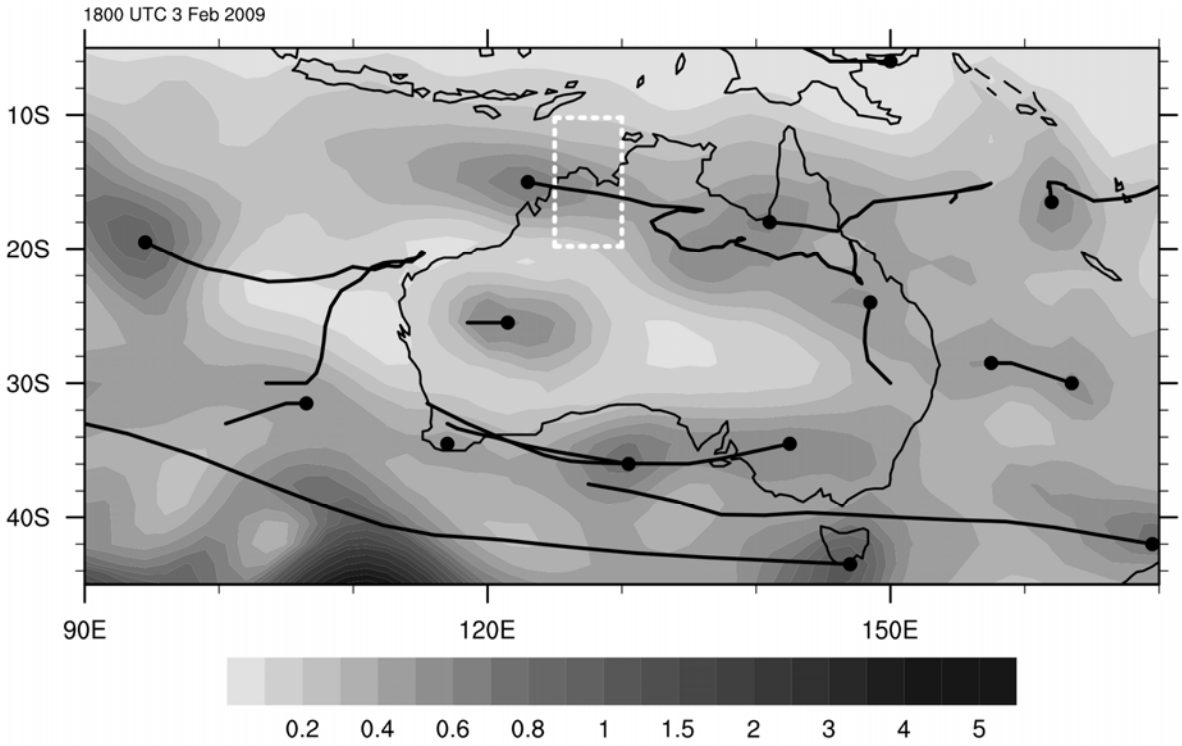

Fig. 1 *- Example of the PV maxima tracking algorithm. Shading shows the 315 K PV field (legend below panel) and the black dots denote the location of PV maxima identified by the tracking algorithm at the example time. Black lines show the tracks of the detected PV maxima from previous time periods. The boxes overlaid show the area used to define a region used to construct the synoptic composite (short white dashes).*

Overall PV centre behaviour.

The total track density of coherent PV maxima on each of the isentropic levels is shown in Fig. 2. There is a track density maximum over northern Australia on all three levels, extending from the Gulf of Carpentaria into the eastern Indian Ocean, suggestive of a tropical 'storm track'. Poleward of 40^{o}S at all three levels the track density is relatively low, presumably as a consequence of the PV maxima being defined by closed contours of PV; at these latitudes the PV maxima are likely to be associated with extended troughs. At the lowest level (315 K, Fig. 2a), the track density is high over north central Queensland (near 20^{o}S), which may be an eastward extension of the tropical storm track. In general, track densities equatorward of 40^{o}S are uniform, with an exception of near the continental heat low (centred near 15^{o}S, 130^{o}E), which is likely connected with the bowing of isentropes towards (and sometimes intersection with) the Earth's surface. The heat low is not evident at 330 K (Fig. 2b), where the track density tends to decrease gradually away from the tropical storm track. At the upper level (350 K, Fig. 2c), there is also a subtropical track density maximum near 35^{o}S, which peaks over southwestern and southeastern Australia. These are preferred regions for the breaking of extratropical Rossby waves (e.g. Postel and Hitchman 1999). The maximum presumably reflects the formation of isolated PV maxima from the breaking waves.

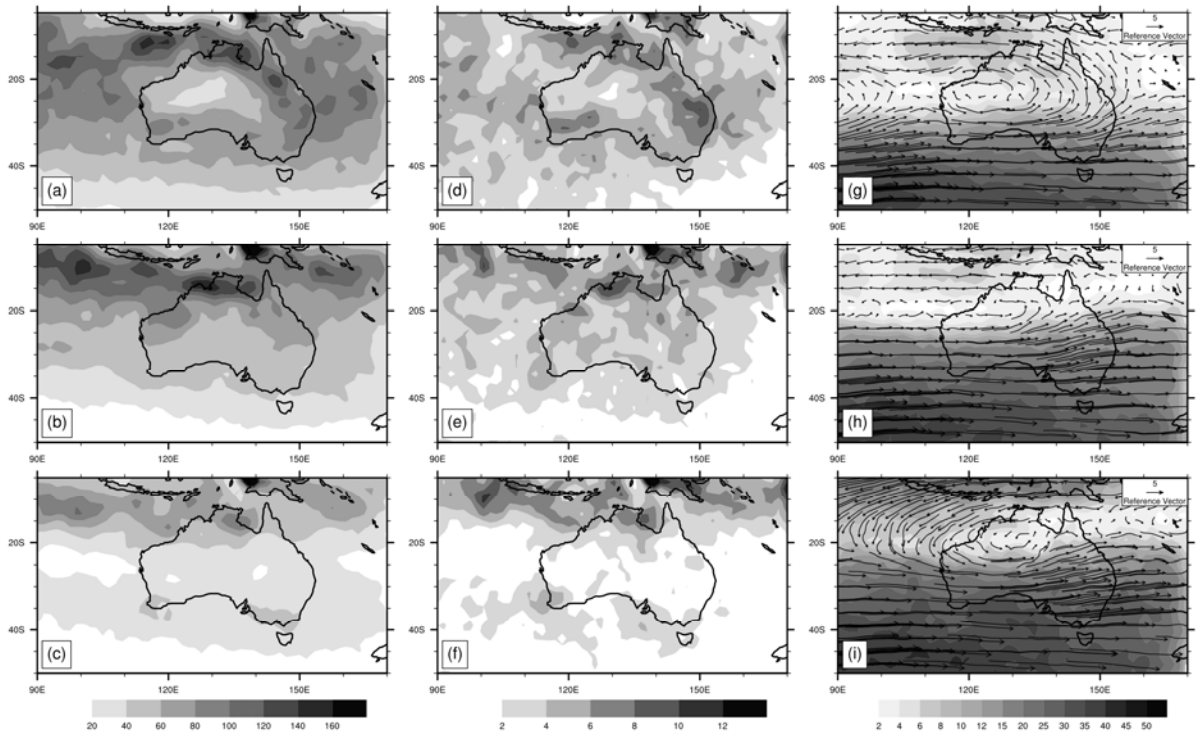

Fig. 2 - *Statistics of tracking at each of the ERA-Interim grid points at 315 K (top row), 330 K (middle row) and 350 K (bottom row). Left column: Track density at the ERA-Interim grid points (total number of tracks for the period 1989-2009). Middle column: Count of initial locations of PV maxima (i.e. first tracked location using all tracks during the period 1989-2009) on the ERA-Interim grid points. Right column: Propagation speed (shaded, ms^{-1}) and direction (vector) averaged across all tracks 1989-2009. Legends for each field are displayed at the bottom of each column.*

The origin of a coherent PV maximum is defined as the first location at which its track was recorded. Generally, the high genesis regions are close to the high track densities shown in Fig. 2a-c, with a tendency for the genesis to peak upstream of the maximum track densities (c.f. Fig. 2g-i). This indicates that most maxima originate in the 'storm tracks'. The main exception to this is found at 315 K (Fig. 2d), where there is a genesis maximum over southern Queensland (near 30^{o}S, 150^{o}E), away from a corresponding track density maximum. Figure 2g-i displays the mean motion vector of all tracked PV maxima at each gridpoint on the three isentropic levels. At all levels, poleward of about 25^{o}S the motion of coherent PV centres is predominantly west to east and equatorward of this latitude the motion is generally slower and in the opposite direction. In the tropics on the 315 K level, the motion vectors show that PV maxima move equatorward over the eastern half of the Australian continent and curve anticyclonically toward the monsoon region. PV maxima within the monsoon accelerate westwards and attain their peak motion (approximately 10 ms^{-1}) over the Timor Sea. This is consistent with the broad anticyclonic flow associated with the heat troughs over Northern Australia and indicates that PV maxima at 315 K frequently move from the subtropics into the tropics. There is little evidence at 330 K (Fig. 2h) of similar behaviour over eastern Australia. Instead, the mean motion of the PV maxima in the tropics is generally slowly westward, with maximum motion again over the Timor Sea. At the uppermost level (Fig. 2i), the mean motion vectors over much of northern Australia are very small with a slight preference for westward motion. However, the mean motion within 5^{o} of the equator is strongly westwards and over the eastern Indian Ocean (west of about 115^{o}E) the PV maxima move poleward, consistent with mean upper level divergence near the equator. This contrasts with PV maxima at 315 K over eastern Australia, where PV maxima tend to move from the subtropics into the tropics.

Composite synoptic structure

The composite structure of all 315 K PV maxima passing through the box 10 - 20^{o}S, 125 - 130^{o}E (box shown on Fig. 1) at 315 K is shown in Fig. 3. In total, this composite comprises 454 individual cases. Composites on other levels give virtually identical results as the PV maxima tend to be vertically aligned (c.f. Fig. 3c, d). The location of the box is selected as there is a relatively dense observation network in this region, including regular soundings from Darwin (12.5^{o}S 130.9^{o}E), thus it is expected that the ERA-Interim data are highly constrained by observations. This region is close to the track density maximum at 315 K and 330 K (Fig. 2a, b) and close to where PV maxima moving through the monsoon cross from land to ocean (see Fig. 3g-i).

As anticipated from the tracking technique, the composite 315 K PV maximum (Fig. 3a) is marked by a closed contour of PV exceeding 0.3 PVU near 130^{o}E. The disturbance is of the order 1000 km across, similar to sub-synoptic scale PV maxima embedded within African Easterly Waves (Berry and Thorncroft, 2005). The PV maximum is located at the end of a region of relatively high PV that extends north-westwards from central Queensland, approximately following the composite 315 K flow vectors. The composite GPCP anomaly shows that the PV maximum is collocated with a significant modulation of the mean rainfall; an area of enhancement of similar size to the PV maximum and peaking near 3 mm day^{-1} is found on the western (upstream) side of the PV maximum. Given that isentropes slope downwards and equatorward (towards the inland desert) in the presence of cyclonic flow around the PV maximum, this rainfall occurs in a region of mean isentropic ascent. There are areas of suppressed rainfall of similar size and amplitude both upstream and downstream of the PV maxima (near 120^{o}E and 140^{o}E), suggesting that the disturbance has a characteristic length scale of around 2000 km, which is less than that of composite African easterly waves.

The composite horizontal wind vectors with specific humidity and temperature fields at 900 hPa are shown in Fig. 3b. The cyclonic circulation of the PV maxima is evident along the northern coast, although it is relatively weak, with wind vectors of the order 1 ms^{-1}. The highest moisture content is located at low latitudes (equatorward of 10^{o}S), but there is a local maximum on the eastern side of the cyclonic circulation, near Darwin. This is essentially in the wake of the highest rainfall rates (Fig.3 a), so this could reflect both increased local evaporation as well as advection of moisture from the adjacent ocean. Although the magnitude of the wind vectors is small, the flow pattern around the disturbance acts across the gradients of specific humidity and advects moisture into the interior of the Australian continent. The advection of moisture, especially from around the Gulf of Carpentaria was found to be a key component in promoting rainfall in the interior of the continent by Berry et al. (2011), who speculated that transient synoptic disturbances modulate the moisture transport in the manner shown by the composite wind pattern in Fig. 3b and increase the likelihood of rainfall in the desert interior.

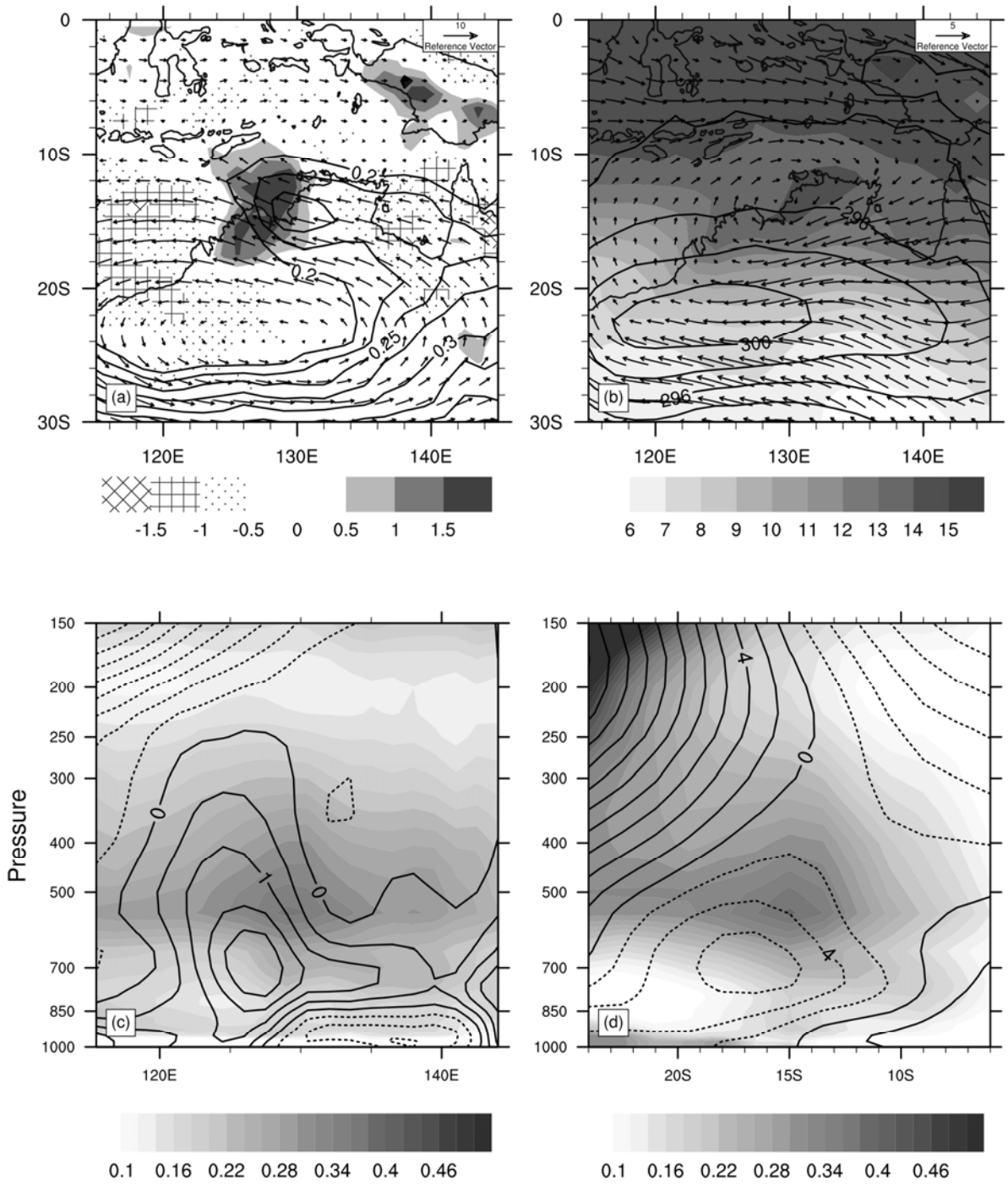

Fig. 3 *– Composite synoptic structure of all tracked 315 K PV maxima passing through the box 10°S -20°S, 125°E -130°E, shown in Fig. 1 (total 454 cases).* ***(a)*** *315 K PV (contoured every 0.1 PVU greater 0.2 PVU) and wind vectors overlaid on rainfall anomaly from time-varying GPCP climatology (mm day^{-1}).* ***(b)*** *900 hPa mixing ratio (shaded, g kg^{-1}) wind vectors and potential temperature (black contours, K).* ***(c)*** *Vertical cross-section taken West-East along 14°S showing PV (shaded, PVU) and meridional wind (black contours, dashed negative, ms^{-1}).* ***(d)*** *Vertical cross-section taken south-north along 130°E showing PV (shaded, PVU) and zonal wind (black contours, dashed negative, ms^{-1}).*

Vertical cross-sections of PV and wind through the centre of the composite PV maximum (14°S, 130°E) in the zonal and meridional plane are displayed in Fig. 3c and d. The PV maximum shows no preferred vertical tilt and is maximised just below 500 hPa (5 km, approximately 330 K), with relatively low values above and below this level. Poleward of the disturbance (Fig. 7d) the boundary layer of the interior desert is marked by near zero PV values up to about 700 hPa as a result of low static stability associated with the well-mixed boundary layer. Strong horizontal PV gradients exist at upper levels in high latitudes in association with the subtropical jet stream. Around the tropical PV maximum, the strongest winds are found near 700 hPa near the strongest horizontal PV gradient on the periphery of the desert boundary layer. There is a weak jet (peak zonal wind values around 7 ms^{-1}) poleward of and below the PV maximum (Fig. 3d), with relatively weak zonal winds elsewhere near the disturbance. Southerlies around 2 ms^{-1} exist on the western (upstream) flank of the PV maximum, again where the horizontal PV gradients are strongest. Ahead of the PV maximum, southerly winds still are evident up to around 300 hPa and there is some hint of the relative maximum tilting against the mean zonal shear (Fig. 3d). Behind the PV maximum the meridional flow is relatively weak at the latitude of the cross section, although there is a shallow layer of northerlies up to the 850 hPa level that could be regionally important for the transport of moisture (c.f. Berry et al., 2011). This composite PV maximum is located in a monsoon environment and is associated with a maximum in rainfall. Consequently, it is expected that the vertical distribution of PV is, in part, determined by the profile of diabatic heating. To first order the effect of latent heating on the PV field is to generate cyclonic PV where the vertical gradient of heating is positive and to destroy it where the vertical gradient is negative, effectively redistributing cyclonic PV along the negative of the local absolute vorticity vector. The PV distribution shown in Fig. 3c is consistent with a peak in diabatic heating near 8 km (300 hPa) and peak diabatic cooling near 2 km (approximately 850 hPa). This is essentially the heating profile associated with deep organised convection in the tropics (e.g. Houze, 1982), suggesting that at this stage of the PV maximum life cycle convective processes play an important role.

Discussion and conclusions

Using an objective tracking scheme applied to reanalysis data, the statistics and main characteristics of synoptic scale disturbances in the Australian monsoon region have been calculated. One of the key findings is that coherent, long-lived PV maxima are present over northern Australia throughout the summer. This result contradicts previous work (e.g. Dickinson and Molinari, 2000), which found relatively little synoptic activity in this region. This difference may be an artifact of analysis techniques that rely on band-pass filtering to describe synoptic activity. The systems associated with the PV maxima are regionally important as they significantly modulate the mean rainfall (see e.g. Fig. 3a). Moreover, it is estimated that of order half of the summertime rainfall in parts of northwestern Australia occurs in the vicinity of the tracked PV maxima.

Although it might be tempting to view these disturbances as being the dynamic response to locally generated organised convection, it is important to consider that the horizontal scale of the PV maxima is larger than that of a typical mesoscale convective vortex and the rainfall rate is modulated over a large area (Fig. 3a). Additionally, rainfall is enhanced most where quasigeostrophic theory predicts ascent (i.e. ahead of the disturbance). In many aspects, these Australian systems resemble African Easterly Waves, albeit with significantly smaller amplitudes (c.f. Reed et al., 1977). Perhaps the most intriguing result presented here is the apparent connection between extratropical disturbances and the coherent PV maxima in the monsoon region. The geographic distribution at 315 K (Fig. 2) shows that there is a PV maxima genesis peak over Queensland at 315 K and these maxima move northwestwards, approximately following the coastline. This region is on the equatorward (anticyclonic shear) side of the exit of the mean subtropical jet, where extratropical Rossby waves are most likely to overturn and break (see e.g. Postel and Hitchman 1999). It is hypothesized that the PV maxima that are first detected over Queensland could form as a result of Rossby wave breaking along the eastern coast of Australia; effectively these maxima are the debris of wave breaking, which are subsequently transported into the tropics by the large-scale flow. Once in the tropics these

extratropical features could act as the focus for convection and further intensify through diabatic processes.

References

Berry, G. J. and Thorncroft, C. 2005: Case study of an intense African easterly wave. *Mon. Wea. Rev.*, 133, 752–766.

Berry, G. J., Reeder, M. J. and Jakob, C. 2011: Physical mechanisms regulating summertime rainfall over northwestern Australia. *J. Climate*, 24, 3705–3717.

Berry, G. J. and Thorncroft, C. 2012: African Easterly Wave dynamics in a mesoscale numerical model: The upscale role of convection. *J. Atmos. Sci. in press.*

Davidson, N. E. and Holland, G. J. 1987: A diagnostic analysis of two intense monsoon depressions over Australia. *Mon. Wea. Rev.*, 115, 380–392.

Dickinson, M. and Molinari, J. 2000: Climatology of sign reversals of the meridional potential vorticity gradient over Africa and Australia. *Mon. Wea. Rev.*, 128, 3890–3900.

Godbole, R.V. 1977: The composite structure of the monsoon depression. Tellus, 29: 25–40. doi:10.1111/j.2153-3490.1977.tb00706.x

Houze, R. A. Jr. 1982: Cloud clusters and large-scale vertical motions in the tropics. *J. Meteor. Soc. Japan,* 60, 396-410

Postel, G.A. and Hitchman, M.H. 1999: A climatology of Rossby wave breaking along the subtropical tropopause. *J. Atmos. Sci.*, 56, 359–373.

Reed, R.J., Norquist, D.C. and Recker, E.E. 1977: The structure and properties of African wave disturbances as observed during phase III of GATE. *Mon. Wea. Rev.*, 105, 317–333.

Tapp, R.G. and Barrell, S.L. 1984. The North-West Australian cloud band: climatology, characteristics and factors associated with development. *J. Climatol*., 4, 411-424.

CONTRIBUTION OF TROPICAL CYCLONES TO NORTH AUSTRALIAN RAINFALL

Sally Lavender and Debbie Abbs

Centre for Australian Weather and Climate Research
CSIRO Marine and Atmospheric Research, PMB1, Aspendale, 3195.

Introduction

The majority of rainfall over northern Australia occurs during the monsoon and tropical cyclone season. It is no coincidence that these seasons occur at the same time since the formation of tropical cyclones is largely influenced by the location of the monsoon trough. All tropical cyclone formation regions, with the exception of the North Atlantic, are also influenced by a monsoon (McBride 1995). In the Australian region, the development of tropical cyclones predominantly occurs due to disturbances in the monsoon trough (McBride and Keenan 1982).
Approximately 12 tropical cyclones occur in the Australian region per year. On average, five of these will make landfall (Dare and Davidson 2004). As well as extensive damage due to severe winds, tropical cyclones can lead to extreme rainfall events. In addition to tropical cyclones, other closed low pressure systems deliver a large amount of rainfall to tropical Australia (Lavender and Abbs 2012). The proportion of north Australian rainfall that can be attributed to these systems is analysed in this study.

Contribution of tropical cyclones and other closed low systems

Tropical cyclone best-track data from the International Best Track Archive for Climate Stewardship dataset (IBTrACS, Knapp et al. 2010) were compared with precipitation data from the Australian water availability project (AWAP, Raupach et al. 2009) over a 40-year period (1970-2009). Tropical cyclones account for around 10% of annual rainfall over the whole of northern Australia and up to 35% in northwestern Australia (Fig. 1a). When extreme rainfall is considered (defined as rainfall above the 99th percentile, Fig. 1b), up to 30% of annual extreme rainfall in coastal areas and over 45% over northwestern Australia occur as a result of tropical cyclones.

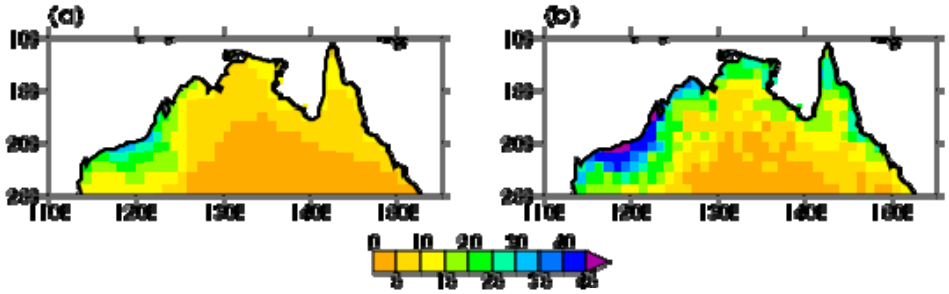

Fig. 1: *Percentage of (a) annual precipitation and (b) extreme precipitation due to tropical cyclones over the period 1970-2009. Colouring is shown by the legend. Tropical cyclones are assumed to influence a 500 km radius.*

Other closed low pressure systems also provide rainfall to the Australian region; these include monsoon lows and tropical storms that do not develop into a tropical cyclone. Australian region closed low pressure systems are detected in ERA-Interim data and compared with AWAP data over a shorter 21-year period (1989-2009). Over 40% of annual rainfall and 50% of extreme rainfall over the

majority of northern Australia can be attributed to the influence of some variety of closed low pressure system (including tropical cyclones) passing within 500 km.

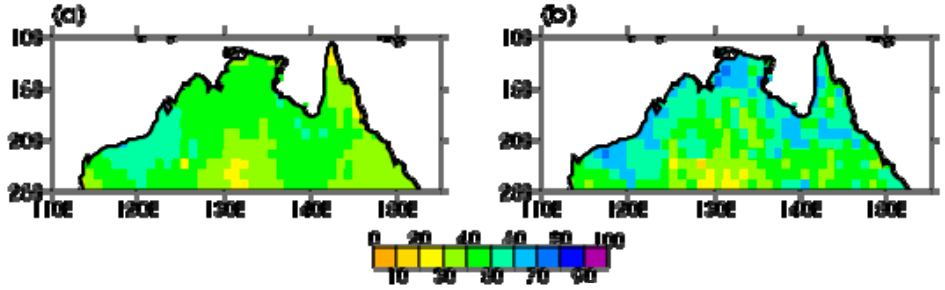

***Fig. 2**: Percentage of (a) annual precipitation and (b) extreme precipitation due to closed low pressure systems, detected over the period 1989-2009. Colouring is shown by the legend. Closed lows are assumed to influence a 500 km radius.*

Trends in north Australian rainfall

A positive trend in rainfall over northern Australia has been evident in the period since the late 1980s (Fig. 3a). This trend is mainly evident during the monsoon season. Since the contribution of closed low pressure systems to rainfall is large, it is intuitive to ask if changes in these systems are contributing to these changes in rainfall. The percentage of annual trend in rainfall that can be attributed to closed low pressure systems is shown in Fig. 3b. Where the trend is greatest, over 60% of the rainfall trend is associated with changes in precipitation within 500 km of a closed low pressure system. Further examination of these trends in closed low-related rainfall found that the precipitation efficiency, defined as the amount of rainfall per closed low day, has been increasing with a very similar spatial pattern as the rainfall trends (Fig. 3c).

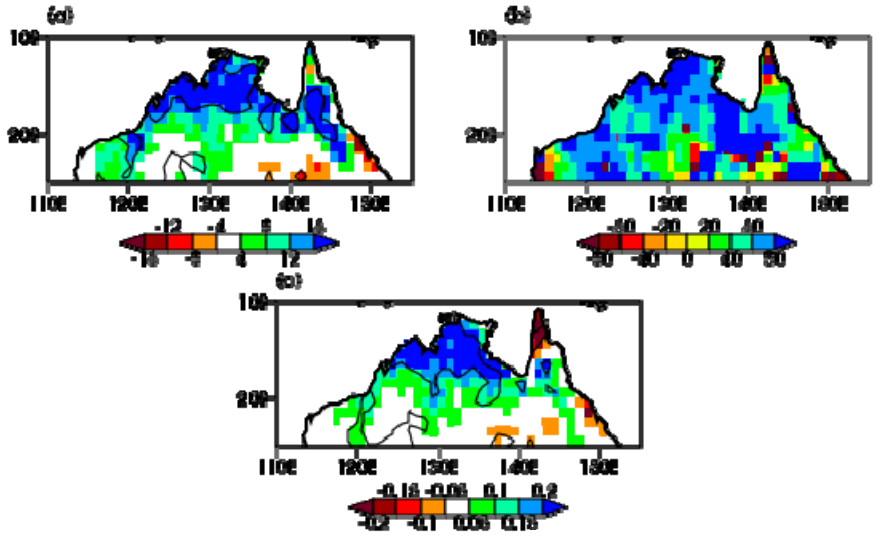

***Fig. 3**: (a) Trend in annual precipitation [mm year^{-1}], (b) Percentage [%] of the trend in rainfall shown in (a) that can be attributed to closed low pressure systems. (c) Trend in the amount of precipitation [mm] per closed low day per year. All trends over the period 1989-2009. Colourings are shown by the legend. Black lines highlight values significant at the 90% level.*

Summary

Tropical cyclones alone account for around 10% of annual rainfall over northern Australia, increasing to 35% on the northwest coastline. The majority of this annual rainfall falls in the monsoon season. When the analysis is extended to include all Australian region closed low pressure systems, over 40% of annual rainfall over the majority of northern Australia can be accounted for.
Recent increases in rainfall over northern Australia can, at least partially, be explained by an increase in the rainfall producing efficiency of Australian closed low pressure systems, including tropical cyclones.

References

Dare, R.A. and Davidson, N. E. 2004. Characteristics of tropical cyclones in the Australian region, *Mon. Weather Rev.*, 132, 3049–3065.

Knapp, K.R., Kruk, M.C., Levinson, D.H., Diamond, H.J., and Neumann, C.J. 2010. The international best track archive for climate stewardship (IBTrACS): Unifying tropical cyclone best track data. *Bull. Am. Met. Soc.,* 91, 363–376

Lavender, S.L. and Abbs, D.J. 2012. Trends in Australian rainfall: contribution of tropical cyclones and closed lows, *Clim. Dyn.*, DOI 10.1007/s00382-012-1566-y

McBride, J.L. 1995: Tropical cyclone formation, *Chapter 3, Global Perspectives on Tropical Cyclones*, R. L. Elsberry, Editor. Tech. Doc. WMO/TD No. 693, World Meteorological Organization, Geneva, Switzerland, 63-105.

McBride, J.L. and Keenan, T.D. 1982. Climatology of tropical cyclone genesis in the Australian region, *J. Climatology*, 2. 13-33

Raupach M.R., Briggs, P.R., Haverd, V., King, E.A., Paget, M. and Trudinger, C.M. 2009. Australian Water Availability Project (AWAP): CSIRO Marine and Atmospheric Research Com ponent: Final report for phase 3. *Tech. Rep. 013, CAWCR*

RADAR OBSERVATIONS OF DARWIN MONSOON CONVECTION

Vickal V. Kumar[1,2], Alain Protat[2], Peter T. May[2], Guillaume Penide[3] Christian Jakob[1]

[1]School of Mathematical Sciences, Monash University, Australia.
[2]Centre for Australian Weather and Climate Research: A partnership between the Bureau of Meteorology and CSIRO, Melbourne, Australia.
[3]Université Sciences et Technologie de Lille, UFR de Physique Bâtiment P5 Laboratoire d'optique atmosphérique.

Abstract

This paper provides a brief summary of some of the recent research completed using radar observations of convective cloud systems associated with the North-Australian monsoon. The key focus is to describe the variability of convective cloud system properties as a function of the large scale regimes characterizing the region. This latter work is linked with the evaluation of the ACCESS model and the development of new convective parameterisation.

Introduction

Darwin hosts what is probably the most comprehensive observing network anywhere in the tropics with a C-band polarimetric weather radar (CPOL), an operational Doppler radar, an U.S. Department of Energy Atmospheric Radiation Measurement (ARM) site with cloud radars, lidars 50 and 920 MHz wind profilers and the Bureau's operational network. The Darwin radar reflectivities, Doppler velocities, and other polarimetric radar retrievals, such as drop size distribution (DSD) and precipitating water contents, have been investigated by several researchers. This paper summarizes some of the recent works done in Protat et al. (2011), May et al. (2012), Kumar et al. (2012) and Penide et al. (2012) using the Darwin radar observations.

Darwin experiences a classic monsoon regime with periods of widespread convection with a largely oceanic character interspersed with "break" periods where convection is suppressed on the large scale but there are plentiful intense storms triggered by local circulations. Recent cluster analysis of thermodynamic sounding data using 49 wet seasons (defined as October to April) showed that the Darwin wet season could be subdivided into five objective large-scale regimes (Pope et al. 2009), instead of the simple monsoon / break separation. Such a separation give an ideal framework for the evaluation and development of convective parameterizations in models as it can help better identify how well the relationship between the large-scale state and small-scale cloud properties is reproduced by the models.

Results

Overview of the five large-scale atmospheric regimes

Figure 1 shows the vertical profile of wind vectors and relative humidity, together with the total daily rainfall during the five large-scale atmospheric regimes using two wet seasons of data (October 2005 – April 2006 and October 2006 – April 2007).

The Dry Easterly (DE) regime typically occurs for about 10 % of the wet season time. The lowest rain accumulation and raining area in this regime (Fig. 1c) is consistent with the lowest relative humidity (Fig. 1b), which is due to a dry continental air mass being advected from the southeast over Darwin

(Pope et al. 2009a). Approximately 70% of the rain contribution in this regime is from convective rain.

The Easterly (E) regime is the least frequent and accounts for only 7 % of time. This regime has a higher average rain accumulation and raining area than the DE regime, but still smaller compared to the other regimes. Like the DE regime, the convective rain contribution is higher than the stratiform contribution in the E regime. The large-scale synoptic environment advects an airmass from the Coral Sea over Darwin (Pope et al. 2009a), which creates a moister environment than that of the DE regime. The Deep Westerly (DW) regime is associated with typical monsoon conditions, and accounts for about 18 % of the wet season time. The large-scale synoptic environment indicates the presence of northwesterly winds at low levels (Fig. 1a) transporting an airmass of equatorial origin into the region (Pope et al. 2009a). This regime had the highest amount of rainfall and raining area, consistent with the highest relative humidity of all regimes (Fig. 1b). The contribution of the stratiform rain is the highest in this regime.

The Shallow Westerly (SW) regime occurs when the active monsoon region moves to the east of Darwin (Pope et al. 2009a). It occurs 16 % of the sample time. This regime has the second highest raining accumulation and raining area, with amounts similar to the Moist Easterly (ME) regime. The contribution of convective rain to the total accumulation is the highest in this regime compared to the other two frequently occurring regimes.

The ME regime corresponds to the typical break monsoon period. This regime is the most frequent, occurring 48 % of the sample time. The large-scale synoptic environment indicates the presence of easterly wind anomalies transporting an airmass of equatorial origin, together with a large region of convergence over Darwin (Pope et al. 2009a).

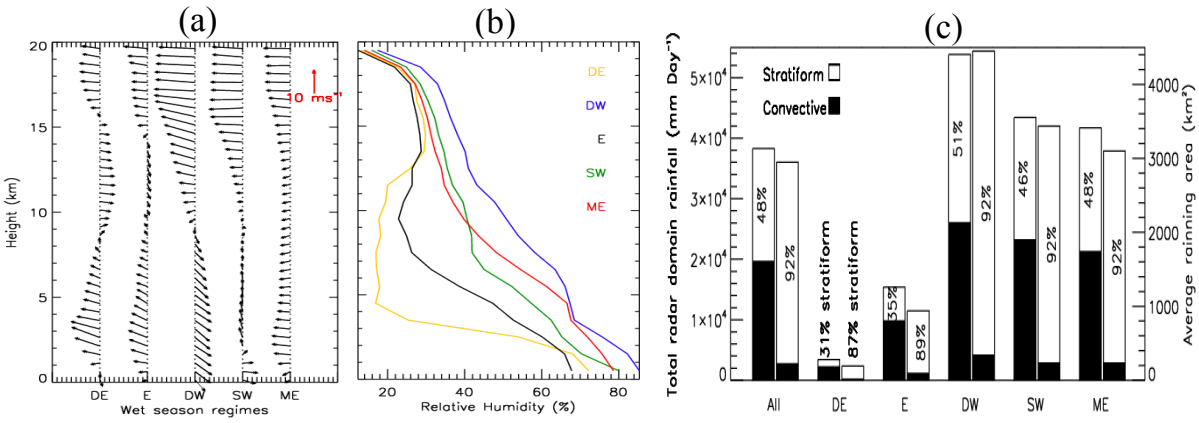

***Fig. 1**: Two-year mean profile of radiosonde measurements of (a) horizontal winds and (b) relative humidity, for the five large-scale atmospheric regimes. (c) Bar graph of daily rainfall accumulation and average raining area within 120 km of the Darwin CPOL radar. Amounts that are convective in nature are shaded in black and the remaining white parts represent the stratiform contributions.*

Diurnal variability in the radar observations

In this section we compare the diurnal pattern from CPOL and radar-lidar observations during the five scales regimes with the spatiotemporal patterns in total rainfall which is separated into the two simple break / monsoon regimes. The DE regime results are not shown due to poor sampling.

In the E regime, convective echo top height (ETH) occurrence is highest in the afternoon and in the early morning period (Fig. 2a). It appears that, especially in the afternoon period, the clouds are generally shallow during the early growth phase and progressively develop into deeper clouds in the mature stage. This diurnal cycle is consistent with that of the non-precipitating ice clouds (Fig. 2b)

which suggests that in the E regime, non-precipitating ice clouds are predominantly convectively generated.

The DW (active monsoon) regime shows a prolonged period of occurrence of convective clouds from midnight through the morning with a peak around midday, and a clear occurrence minimum in the evening. Unlike the E regime, the frequency of occurrence of non-precipitating ice clouds in the DW is very different from the convective ETH statistics obtained here. The maximum in non-precipitating ice cloud occurrence occurs later than the convective ETH occurrence maximum, between 15:00-20:00 LT. This comparison suggests that during the DW regime, thick non-precipitating anvils and cirrus decks produced by deep convection are much longer-lived than during other regimes. Comparison of the spatiotemporal variation in rainfall total (Fig. 2c) with the DW regimes shows that the diurnal pattern in total monsoon rainfall bear greater resemblance with the convective cloud occurrence frequency. Consequently, most of the early morning peak in convective activity in the DW regime generally occurs over the western half of the radar domain. The lack of a strong evening peak in the occurrence of convection and rainfall during this regime is due to the presence of continuous cloud cover reducing daytime heating that prevents the establishment of sea breeze convergence.
During the SW regime, the ETH occurrence frequency shows two peaks, one in the morning and one in the afternoon. The peak in non-precipitating ice cloud occurrence is shifted to a later time, again suggesting the production of extended anvils by deep convection associated with the SW regime, as is the case for the DW regime as well. Neither the monsoon nor the break spatiotemporal patterns in rainfall (Fig. 2c) seem to be consistent with the convective cloud frequency in the SW regime. This suggests that the SW regime is unique, maybe a mixture of monsoon and break conditions.
.

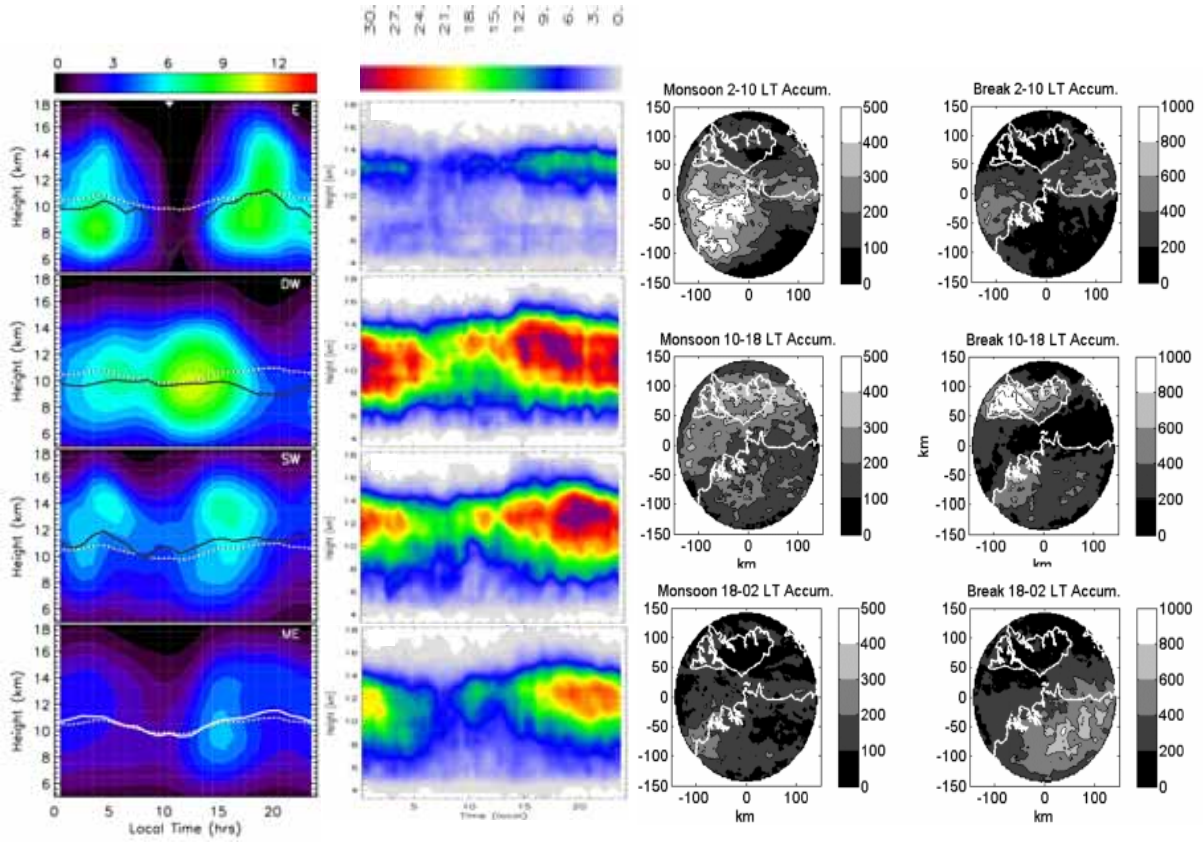

***Fig 2**: Diurnal variation of (a) convective echo top height occurrence frequency measured with CPOL radar, (b) ice cloud occurrence frequency measured with the vertically pointing radar-lidar observation at the Darwin for the four convective activity large-scale regimes. (c) Spatial map of C-POL rainfall accumulation in the monsoon and break conditions during the early morning (02-10 LT), afternoon (10-18 LT) and evening (18-02 UT).*

During the most frequent ME regime, the results reveal that the early phase of storm development occurs at ~15:00 LT with a peak height of 9 km (Fig. 2a). These cells mature within a few hours, becoming towering cumulonimbus clouds with a peak occurrence height of 14 km. This diurnal cycle is consistent with that of the non-precipitating ice clouds in this regime (Fig. 2b). This suggests that thick anvils and cirrus decks produced by deep convection are shorter-lived than during the DW and SW regimes. From the evening through the night the convective systems gradually decay causing a gradual drop in ETH. This drop is also found in the non-precipitating ice cloud statistics (Fig. 2b). Overall, the patterns in convective ETH and non-precipitating ice cloud occurrence frequency in this regime seem to be consistent with the break total rainfall patterns.

Variability in Drop size distribution parameters

Figure 3 indicates that the probability of heavy rain-rates is lowest in the DW regime compared to other regimes. This is consistent with the PDF of the DSD parameters, as this regime is mainly formed of small particles in high concentration compared to the other regimes. Thus the cause for the highest daily rain accumulation in this regime is due increase in the raining area domain (Fig. 1c) and raining time (Fig. 2a). Another important difference is the width of the PDF for all the DSD parameters in the DW regime is much narrow compared to the other regimes and could be due to a lesser impact of the ice microphysics on the rain formation (e.g., warm rain process) compared to the other regimes. In contrast, rainfall properties in the driest regimes (DE/E) are mostly of convective origin, therefore DE and E rain rates are higher than in the moister regimes (DW/ME). These two regimes had large droplets in relatively low concentration due to a larger contribution of the ice microphysical processes.

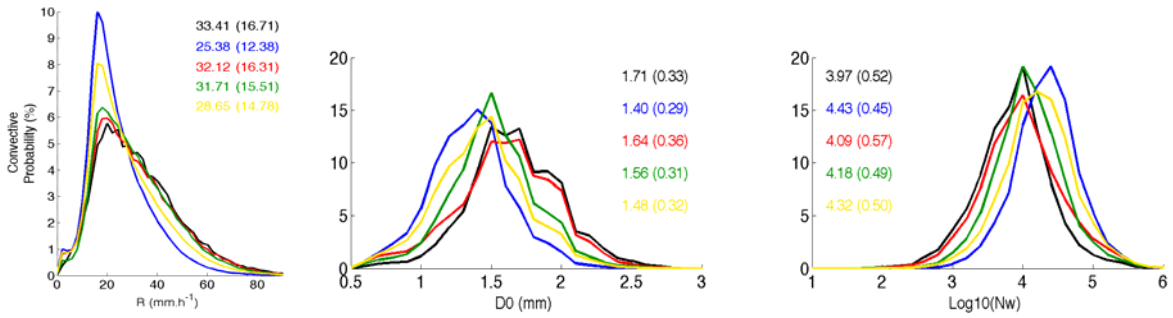

***Fig 3**: Probability Density Function (PDF) of convective a) rain rates, b) D_0 and c) $log_{10}(N_w)$ for the 5 large-scale regimes. Means and standard deviations (in brackets) for each PDF are also represented. The DE regime is represented in black, DW blue, E red, SW green and ME yellow.*

Conclusion

The above radar observations, which has been published in a series of papers, ascertain that the Darwin monsoon convections have significant different properties during the five large-scale atmospheric regimes. We are currently working with the ACCESS modeling community to search for similar regime dependence signatures in their simulations of tropical convection.

References

Kumar V.V., Protat A., May P.T., Jacob C., Penide G., Kumar S. and Davies L. 2012. On the effects of large-scale environment and surface types on convective cloud characteristics over Darwin, Australia. *Mon Wea. Rev.,* in press.

May, P.T., Long, C. and Protat, A. 2012. The diurnal cycle of the boundary layer, convection, clouds, and surface radiation in a coastal monsoon environment (Darwin Australia). J. Climate. doi:10.1175/JCLI-D-11-00538.1, in press.

Penide, G., Kumar, V.V., Protat, A. and May, P.T. 2012. Statistics of drop size distribution and rain rates for stratiform and convective precipitation during the north Australian wet season. *Mon Wea. Rev.,* (submitted).

Pope, M., Jakob, C. and Reeder, M.2009. Regimes of the North Australian Wet Season. *J. Climate*, **22**, 6699-6715.

Protat, A., Delanoë, J. May, P.T., Haynes, J ., Jakob, C., O'Connor, E., Pope, M. and Wheeler, M.C. 2011. The variability of tropical ice cloud properties as a function of the large-scale context from ground-based radar-lidar observations over Darwin, Australia. Atmos. Chem. Phys., **11**, 8363–8384.

THE INITIATION OF EQUATORIAL ROSSBY WAVES IN THE PACIFIC DURING THE NORTH AUSTRALIAN WET SEASON AND THEIR EFFECT ON THE SYNOPTIC FLOW AND THE RAINFALL OVER THE AUSTRALIAN TROPICS AND ADJOINING WATERS

Fernon, J.

Abstract

The passage of Equatorial Rossby Waves (ERW) through Australian longitudes affects the deep layer flow and precipitation over north Australia and adjoining waters during the north Australian Wet Season (November-April). In those instances where there is a pre-existing monsoon trough the trough is reinvigorated and moves southward. Flow north of the trough becomes stronger and more northerly. Circulations within the trough form and sometimes reach tropical cyclone intensity. For those other scenarios, where there is a pre-existing near Equatorial trough and easterly low to mid-level flow over North Australia, the Southern Hemisphere member of the ERW twin losses its structure as it traverses Papua New Guinea then rapidly reforms in the Banda Sea, thus initiating the formation of the monsoon trough to the north of Australia. Subsequent development and movement of the trough affects the flow and precipitation over North Australia. In many instances the circulation reaches tropical cyclone intensity- initially moving to the west and then recurving to the southeast and making landfall on the Northwest Australian coast.

Nine ERW events from 1993-2007 were investigated using ERA-Interim reanalysis, TRMM 3B42 and NOAA Interpolated outgoing long-wave radiation (OLR) data. Also investigate relation TC development and phase/strength ER waves 1978-2011 over slightly larger domain.
The formation of the ERW and the associated twin circulations were also investigated. In all events studied the southern hemisphere twin formed in an area of enhanced convection located on the northwest flank of the South Pacific Convergence Zone (SPCZ). The formation occurred during a phase in the evolution of the SPCZ when its convective focus was in its northwestern sector. In all the scenarios consistent sequence of events occurred starting with potential vorticity intrusions (evident at 350K) in both hemispheres in the eastern Pacific. In the southern hemisphere this precipitated the amplification of low to middle level mid-latitude trough and development of a cloud band. This trough and cloud band and then moved westward and as it did so an easterly low to middle level trough to the north developed and amplified. Convection developed in the low to middle level convergent flow to the east of this trough. It was then a small step to the formation of the SPCZ with discrete circulation / s in the trough north of the subtropical ridge (STR) and northwesterly convergent flow northeast ward of circulation/s. The SPCZ and associated convection moved westward, with the focus of the convection moving to the northwest.

THE METEOROLOGY OF THE AUSTRALIAN MONSOON FLOODS OF 2010-2011

John L McBride

Emeritus Fellow, Centre for Australian Weather and Climate Research, Australia
Associate Professor (Principal Fellow), Dept. Earth Sciences, University of Melbourne, Australia

Major rainfall events in the monsoon tropics are rarely documented in the literature. It is important that such a knowledge base is built up as a step towards advancing our knowledge and understanding of the global and regional monsoon systems. During the North Australian summer monsoon of 2010-2011, the State of Queensland experienced prolonged flooding associated with extreme rainfall over several months. Thirty-three people died. More than 78 per cent of the state (an area bigger than France and Germany combined) was declared a disaster zone; over 2.5 million people were affected. A dramatic impact of the event was the flooding and evacuation of the City of Brisbane.

This paper documents the meteorology of these monsoon floods, which occurred over two months. The paper will address three components of this complex event.

It will document the large scale meteorological forcing. Record rainfall in preceding months preconditioned the soil and river heights. The annual monsoon or wet season is such that major flooding is part of the background climatology. A major La Nina event coincided with the time of the flooding; and a number of the short-term heavy rainfall episodes were influenced by an active phase of the Madden Julian Oscillation.

It will describe the major synoptic weather systems involved, including the passage of upper level westerly troughs across the monsoon flow, monsoon surges, monsoon lows, inland troughs and trade easterly rainfall events. These are common systems in the Australian monsoon, but are not documented in the literature. The City of Brisbane flooding event was associated with an upper level baroclinic cut-off low, fed with moisture by the easterly tradewinds.

The paper will synthesise the major components of this two-month long flooding events into a schematic picture of different types of flooding event and into different types of metrological system.

TROPICAL MODES OF VARIABILITY

Jorgen S. Frederiksen [1] and Carsten S. Frederiksen [2]

[1] Centre for Australian Weather and Climate Research, CSIRO Marine and Atmospheric Research, Aspendale, Victoria, Australia

[2] Centre for Australian Weather and Climate Research, Bureau of Meteorology, Docklands, Victoria, Australia

Abstract:

The formation of intraseasonal oscillations and equatorially trapped waves such as Kelvin waves, equatorial Rossby waves, mixed Rossby-gravity waves, and eastward inertio-gravity waves is studied using a global two-level primitive equation instability model. It is found that the leading intraseasonal oscillation mode has a largely first internal mode structure in the tropics with more equivalent barotropic structure of the streamfunction in the extratropics including distinct Pacific-North American (PNA) and North Atlantic Oscillation (NAO) teleconnection patterns. The convectively coupled equatorial waves also have dispersion relations and properties consistent with those found in observational studies. The comparison between the observed tropical modes of variability and the theoretical modes is discussed. The changes in theoretical intraseasonal oscillation modes during the second half of the twentieth century are examined and related to observed changes in Australian winter rainfall.

Introduction

A large part of synoptic to sub-seasonal variability of the tropical atmosphere is due to equatorial waves including Kelvin waves (K), equatorial Rossby waves (ER), mixed Rossby-gravity waves (MRG), eastward inertio-gravity waves (EIG) and the Madden-Julian intraseasonal oscillation (MJO). The equatorially trapped waves play important dynamical roles in initiating tropical cyclones and hurricanes while the passage of the MJO can result in active and break phases of monsoonal circulations. Here we compare the properties of the MJO and equatorial waves in a theoretical study with a primitive equation model with those from observations. We also examine the changes in theoretical intraseasonal oscillation modes during the second half of the twentieth century and relate the changes in their growth rates and structures to observed changes in Australian winter rainfall.

Primitive equation instability model

The tropical modes of variability analysed in this study have been obtained using the two-level linearized primitive equation model employed in a series of studies by Frederiksen and Frederiksen (e.g., 1993, 2002, 2007, 2011) where further details of the methodology is presented. The model includes a generalized Kuo-type heating parameterization that incorporates closures for both convection and evaporation-wind feedback. In the first part of the study where the general properties of tropical modes are considered we use the global January 1979 basic state. In the second part of the study, where changes in intraseasonal variability during the 20th century are considered, July basic states for 1949-68, 1975-94 and 1997-2006 are employed, since the variability is most sensitive in southern winter season.

Convectively coupled equatorial waves

The instability study with an observed three dimensional (3D) basic state generates a wide range of growing modes with properties analogous to storm, blocks, teleconnection patterns and as well the class of convectively coupled equatorial waves and the MJO. Here we are primarily concerned with the tropical modes of variability. Fig.1 shows the frequency and period of the dominant equatorial waves as functions of zonal wavenumber for the 3D basic state (solid symbols) and the corresponding zonally averaged basic state (open symbols) for January 1979. For the 3D basic state the x-axis represents the dominant wavenumber with largest magnitude of the velocity potential (and baroclinic streamfunction). These theoretical results line up closely results with the spectra obtained from observations shown in Fig.2 of Wheeler et al. (2000). The properties of the theoretical convectively coupled equatorial modes also compare favourably with their results (Frederiksen 2002).

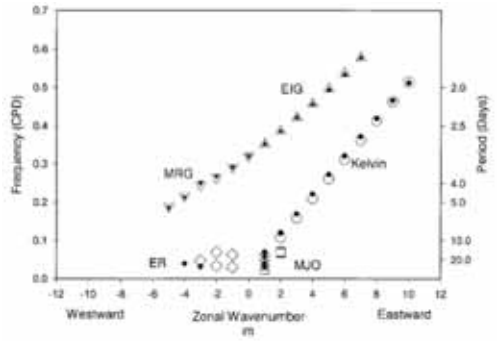

***Fig. 1**. Dispersion relations showing frequencies (cycles per day) and periods (days) of intraseasonal oscillations and equatorially trapped waves as functions of dominant zonal wavenumber* (m^*) *for the three-dimensional basic state (solid symbols) and of zonal wavenumber (m) for the zonally averaged basic state (open symbols). MJOs are denoted by squares, Kelvin waves (K) by circles, ER waves by diamonds, EIG waves by triangles and MRG waves by inverted triangles.*

Intraseasonal oscillation modes

Again, the properties of the theoretical intraseasonal oscillations are broadly similar to corresponding observational results (Frederiksen and Frederiksen 1993; Frederiksen 2002).

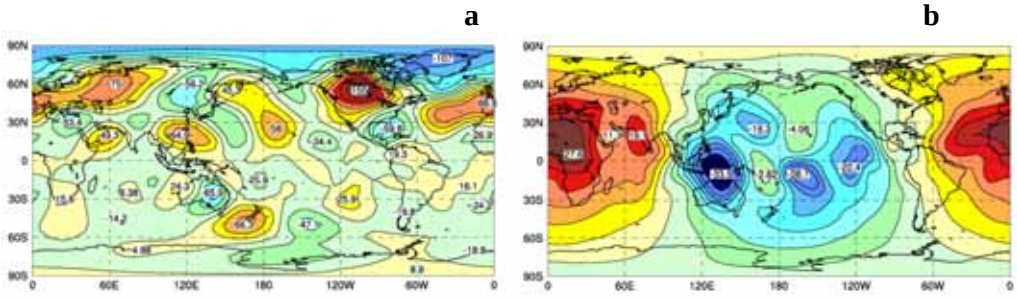

***Fig. 2**. (a) The global 500 hPa streamfunction and (b) the 300 hPa velocity potential for the leading intraseasonal oscillation mode, mode 66, for the January 1979 basic state.*

Fig. 2 shows the mean streamfunction ψ and the upper-level velocity potential $(-\chi)$ for mode 66, the dominant intraseasonal oscillation mode for the 3D basic state at a particular phase in its evolution and eastward propagation. During its evolution the theoretical mode shows strong PNA and NAO patterns in the extratropics at different phases. At the phase shown in Fig. 2a the negative phase of the NAO is particularly strong. This strong NAO pattern occurs 8 to 10 days after the tropical MJO convection is strongest over the Indian Ocean as has also been found in many observational studies (Frederiksen 2002). Also, from Fig. 2b, we see that the velocity potential has a largely zonal

wavenumber 1 envelope, as in observations, within which are embedded smaller scale structures. At the phase shown in Fig. 2b the convection is focused over Australia and the maritime continent.

Changes in tropical modes of variability

Instability theory may also be used to throw light on the causes of changing climate variability and rainfall such as has occurred over Australia during the second half of the 20th century. In particular, there has been a drying of southern Australia and a dramatic decrease in southwest Western Australian rainfall since the 1970s (Fig. 3); this has been explained to be caused by a significant reduction in the growth rate of storms that cross southern Australia and a southward deflection of some storms (Frederiksen and Frederiksen 2007, 2011). However, during this period parts of central Australia have seen and increase in rainfall, as shown in Fig. 3, and this is in turn associated with an increase in the growth rate of disturbances of tropical origin. In particular the growth rates of northwest cloud band and intraseasonal oscillations have increased during southern winter.

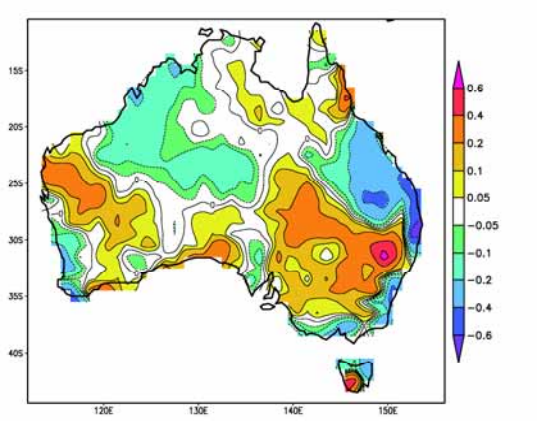

Fig. 3. *Trend from 1950 to 199 in Australian July rainfall (mm/month/year).*

First we consider the intraseasonal oscillations and their changing properties. Fig 4a shows the 300 hPa streamfunction of the fastest growing July intraseasonal oscillation mode for the time interval 1975-94 while Fig 4b shows the 300 hPa divergence in the Australian region at a particular time. The disturbance propagates eastward with a period of 35 days and has a growth rate of 0.19 day^{-1} or e-folding time of just over 5 days. A very similar intraseasonal oscillation mode, in term of structure and growth rate occurs for the time interval 1997-2006. We note however that for the earlier time interval of 1949-68 the growth rate is around 30% indicating an enhancement of tropical processes since the 1970s.

The faster growth since the 1970s of intraseasonal oscillations that have a wavetrain with large divergence crossing central Australia is consistent with the increased rainfall there as noted by Frederiksen and Frederiksen 2011. That study also noted there was an increase in the growth rate of northwest cloud band disturbances that cross central Australia in the latter two time intervals compared with the first. This increase is again consistent with the observed increase in rainfall there.

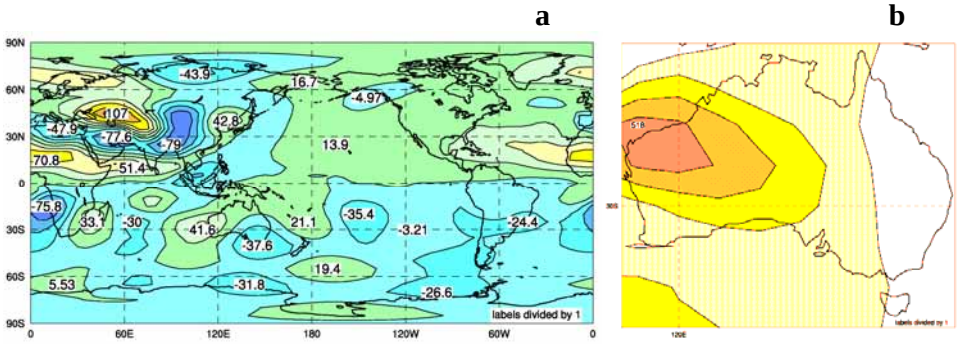

Fig. 4*. As in Fig. 2 but for (a) the global 300 hPa streamfunction and (b) the 300 hPa divergence in the Australian region for the leading intraseasonal oscillation mode, mode 35, for the July 1975-94 basic state.*

Discussion and conclusions

In this report, we have examined the generation mechanism and properties of theoretical analogues of tropical modes of variability. The theoretical modes have been found to compare closely with corresponding waves and oscillations obtained in observational analyses. In particular we have discussed the properties of intraseasonal oscillations and equatorially trapped waves such as Kelvin waves, equatorial Rossby waves, mixed Rossby-gravity waves, and eastward inertio-gravity waves. The theoretical results have been obtained using a global two-level primitive equation instability model. As in observations, the leading intraseasonal oscillation mode has a largely first internal mode structure in the tropics with more equivalent barotropic structure of the streamfunction in the extratropics including distinct PNA and NAO teleconnection patterns. Again, the convectively coupled equatorial waves have dispersion relations and properties comparable with those found in observational studies. The changes in theoretical intraseasonal oscillation and northwest cloud band modes during the second half of the twentieth century have been examined and related to observed changes in Australian winter rainfall.

References

Frederiksen, J.S. 2002. Genesis of intraseasonal oscillations and equatorial waves. *J. Atmos. Sci., 59*, 2761-2781.

Frederiksen, J.S. and Frederiksen, C.S. 1993. Monsoon disturbances, intraseasonal oscillations, teleconnection patterns, blocking and storm tracks of the global atmosphere during January 1979: Linear theory. *J. Atmos. Sci., 50,* 1349-1372.

Frederiksen, J.S. and Frederiksen, C.S. 2007. Interdecadal changes in Southern Hemisphere winter storm track modes. *Tellus, 59 A*, 599-617.

Frederiksen, J.S. and Frederiksen, C.S. 2011. Twentieth century winter changes in Southern Hemisphere synoptic weather modes. *Adv. Meteorol.,* Article ID 353829, 16 pp.

Wheeler, M., Kiladis, G.N. and Webster, P.J. 2000: Large-scale dynamical fields associated with convectively-coupled equatorial waves. *J. Atmos. Sci., 57,* 613-640.

INDIGENOUS SEASONAL UNDERSTANDING IN MONSOON AUSTRALIA: EXAMPLES FROM THE NORTHERN TERRITORY AND WESTERN AUSTRALIA

Emma Woodward[1]

[1]*CSIRO Ecosystem Sciences, Darwin, Northern Territory, Australia*

Introduction

Aboriginal peoples' knowledge of their environment is frequently rich, detailed and highly interconnected. In northern Australia, Indigenous understanding of the monsoon environment comprises many scales of understanding, where the meteorological, hydrological, biological and spiritual intertwine at multiple layers to create a knowledge system both unique and complementary to a western-science perspective.

This paper draws on the findings of four years work with six Aboriginal language groups to document Indigenous seasonal knowledge from across tropical Western Australia and the Northern Territory within a water resource planning context (see Jackson et al. 2011; Woodward et al. 2012). Some of the information was documented for the first time, and each set of observations has been captured in an Indigenous seasonal calendar. Information presented in the calendars includes the Indigenous seasons (ranging from 4 to 13 annual seasons), the plants and animals hunted and gathered through the annual cycle, their specific uses and techniques for collection and preparation, and the signs or ecological and meteorological indicators that inform resource use behaviour.

Specifically, the paper focuses on the knowledge of two language groups; the Gooniyandi from the Fitzroy River area in the Kimberley region of WA and the Ngan'gi from the Daly River region in the NT, to reveal the complexity and diversity of Indigenous seasonal knowledge from the Australian monsoon region.

Indigenous ecological knowledge

Indigenous knowledge that has allowed people to survive through an intimate understanding of their environment is frequently referred to as Indigenous ecological knowledge.

Indigenous ecological knowledge is thought of as '*…a cumulative body of knowledge and beliefs handed down through generations by cultural transmission about the relationship of living beings (including humans) with one another and with their environment*' (Berkes 1993). Indigenous knowledge of this kind is not static, but dynamic, changing with the environmental and social conditions of the group. Indigenous ecological knowledge is highly contextualised and localised with the detail relevant in a local context. The knowledge system often clearly reflects local connection to place, with the continual acquisition of knowledge generated by communities heavily reliant on natural resources.

In the monsoonal tropics of northern Australia diverse sets of Indigenous ecological knowledge, unique to each language group, persist and are currently used on a daily basis to make decisions including those related to resource use (i.e. hunting, fishing and gathering). Common to each language group is a detailed set of ecological indicators that act as cues for the targeting of specific resources, many falling into the category of phenological knowledge. Phenological knowledge is interesting because of its direct link to meteorological phenomena and climatic patterns.

Seasonal resource use indicators

Phenological indicators can be thought of as stable biological timepieces that respond to seasonal variation between years (Lantz and Turner 2003). Phenological events generally occur in consistent order, with the arrival of one event predicting the imminence of another. Phenological knowledge encompasses all biological seasonality, including the observation of life cycle changes in specific plant or animal species to indicate the timing of the onset of growth stages in other species, conceptions of time as they relate to seasonal change, and spiritual beliefs about cause and effect relationships of seasonal change (Lantz and Turner 2003). Phenological knowledge is a significant aspect of many Indigenous knowledge systems, given the typical reliance on subsistence resource use. Increasingly, phenological knowledge is attracting interest worldwide as a monitoring tool for environment change, specifically climate change (Guyot et al. 2006, McDonald et al. 1997).

In contrast to the Gregorian calendar, which follows pre-set calendar dates (for months and seasons), the seasons of the Gooniyandi and Ngan'gi calendars are defined by one or more indicative events, which herald the arrival of a new season. These events, or seasonal indicators, can be a combination of ecological, meteorological or metaphysical observations. For knowledgeable people, these key events indicate the availability of specific food resources. In the Ngan'gi calendar eight of the thirteen Indigenous seasons follow the lifecycle stages of the local Speargrass species (*Sorghum intrans*), and are therefore directly correlated to annual variability in rainfall (McTaggart et al. 2009).

The Ngan'gi seasonal calendar

The Ngan'gi seasonal calendar from the Daly River region of the NT includes the following seasonal resource use indicators:

- During the season known as Ngunguwe (which translates to 'mirage') it is very hot and humid with no rain. Mirages can be seen during the day and the Ghost Gum bark starts peeling, letting you know sharks are fat in the river The river is really low now and the depth of the river indicates it is a good hunting time for Stingray and Sawfish.

- Following the first rains of the wet season, Speargrass seeds begin to germinate and people know that the Bush Potato (Misyawuni) is available for gathering;

- The appearance of dragonflies (Ayiwisi) heralds the beginning of the dry season, and tell people it's a good time for Barramundi (Atyalmerr) fishing, and

- Shortly after the nor-westerly sea breeze begins to blow (a 'peaceful' wind that brings good fishing) the flowering of the Red Kapok (Yeninggisyi) indicates that it is time to collect Freshwater Crocodile eggs. In the following season but once the pods of the same tree turn brown and crack, the crocodile eggs are hatching and collection season has finished.

The Ngan'gi seasonal calendar has 5 seasons that fall within the wet season and 8 seasons that fall within the dry season. This is indicative of the diversity and extent of resource-related events that occur during the dry. During the wet period, access to hunting and fishing places is limited due to flooding or inundation, and animal species also disperse within the flooded landscape, making them more difficult to hunt. Less availability of food resources results in fewer phenological events, and fewer season names for this part of the seasonal calendar.

According to the Ngan'gi seasonal calendar, hunting and gathering of resources starts in earnest toward the end of the wet season with the collection of fruits during the season of Wudupuntyurrutu, when the river rises following heavy rains. During this time Saltwater Crocodile, Echidna and Rock Python are also actively hunted.

The dry season is coming when the Speargrass stalks start to die and turn a reddish colour while the big wet is subsiding. This season is known as Wurr wirribem filgarri, and is when people actively hunt for Prawns in the river and creeks.

The dry season has started when the wind blows from the east and Speargrass seeds have turned brown and start falling to the ground. This season is known as Wurr bengim miyerr. It is the Dragonflies that indirectly bring the wind in the early dry, as their arrival wakes the big Black Kangaroo (Agurri) that lives in the hills who then sings the wind, blowing it from the East. The dragonflies indicate to people that it's time to fish for Barramundi.

Wurr bengin derripal is a season name that literally translates to 'it's knocked the grass into a bent over position.' It refers to the times of the year when storms push the Speargrass over. It is still raining, and is a good time for harvesting Magpie Goose eggs, as there is still a fair amount of water around to support the floating goose nests. This time might be thought of as the late wet/early dry time. This time of the year is known to be good for Catfish, but not yet time for hunting other fish.
Resource collection starts to ramp up with the arrival of Wirirr marrgu. The Dry season is in full-swing, and the Speargrass is being burnt and black ash is on the ground. Dagum; the fog and dew that are present in the mornings, is seen now. The fog is a good sign to go fishing for Black Bream, Archer Fish, Mullet, Cherabin and Prawns.

The Gooniyandi seasonal calendar

According to the Goonyiandi, the rain, winds and storms that arrive in their country from four different directions are generated by four different snakes of four different skins or clan groups. These weather events are strongly tied to ecological observations and phenological knowledge that describes and reveals key resource events (Davis et al. 2011).
Rain, wind and river levels are explained by Gooniyandi as a complex cycle of linked events. For example:

- Barndiwiri is the first rain storm of the wet season. It is associated with the Jangala snake and arrives from the North. People know that this storm will make the rivers run.

- The flowers of Girndi, the Black Plum, fall to the ground with the first light rain of the wet season. The fruits grow in the initial wet season rains and the flickering of Fireflies at this time of the year (who share the same name as the plum) are said to 'cook' the fruit, making it ripe.

- Gooloowa is the rain that falls after the monsoons have finished and as Ngamari (female cold season) starts. Fish are said to shut their mouths when the Moongoowarla wind starts blowing from the East and the weather cools.

- As the wet season rains finish the wind changes direction and the Garrawoorda blows from the South. The water is high and this is a good time for catching Sawfish. The appearance of Red Dragonflies at this time also tells you Sawfish are fat.

- Wirayi are the boomerang-shaped clouds that can be seen at the end of the very hot weather of Barrangga season. Wirayi warn of a big storm coming. Manyboo are the white 'cotton wool' clouds that originate in the spring country during the middle of Yidirla, the wet season.

- Towards the end of the period of mild cold weather known as Girlinggoowa, Bambira the 'crocodile tree' flowers, signalling that Freshwater Crocodiles are laying eggs and it is time to go and collect them. Once the hot season of Barrangga arrives, the flowers are falling to the ground, the eggs have hatched and the collection season has finished.

Conclusion

The diversity of Indigenous monsoon understanding in northern Australia is driven by many factors including rainfall, temperature and the resulting vegetation and animal communities. However there are four factors that interconnect within each of the seasonal knowledge systems; a focus on resource use, knowledge of complex ecological indicators to facilitate resource collection, knowledge of meteorological phenomena and a strong metaphysical/spiritual understanding.

There is potential for Indigenous seasonal knowledge, maintained through continuous local observation of the environment, to be adopted in local monitoring for environmental and climatic change. Further investigation into how Indigenous knowledge might play a role in such monitoring and early detection of environment change over longer temporal scales, or multiple annual cycles, could be beneficial in the management of Australia's environment.

References

Berkes, F. 1993. Traditional ecological knowledge in perspective. *In: Traditional Ecological Knowledge: Concepts and Cases (ed.* J. T. Inglis*) pp.* 1–9*, UNESCO Canada/MAB, Ottawa.*

Davis, J., Street, M., Malo, H., Cherel, I. and Woodward, E. 2011. *Mingayooroo – Manyi Waranggiri Yarrangi. Gooniyandi Seasons* (calendar), *Margaret River, Fitzroy Valley, Western Australia*. http://www.csiro.au/en/Organisation-Structure/Divisions/Ecosystem-Sciences/Gooniyandi-Seasons-Calendar.aspx CSIRO Ecosystem Sciences, Darwin.

Guyot, M., Dickson, C., Paci, C., Furgal, C. and Man Chan, H. 2006. Local observations of climate change and impacts on traditional food security in two northern Aboriginal communities. *International Journal of Circumpolar* Health 65(5), 403-415.

Jackson, S., Finn, M., Woodward, E. and Featherston, P. 2011. Indigenous socio-economic values and river flows: Final Report. CSIRO Ecosystem Sciences, Darwin.

Lantz, T.C. and Turner, N.J. 2003. Traditional Phenological Knowledge of Aboriginal Peoples in British Columbia. *Journal of Ethnobiology* 23(2): 263-286.

McDonald, M., Arragutainaq, L. and Novalinga, Z. 1997. Voices from the Bay: Traditional Ecological Knowledge of Inuit and Cree in the Hudson Bay Bioregion. Canadian Arctic Resources Committee and Environmental Committee of Municipality of Sanikiluaq, Ottawa, Canada.

McTaggart, P., Yawulminy, M., Ariuu, C., Daning, D., Kamarrama, K., Ngulfundi, B., Warrumburr, M., Wawul, M. and Woodward, E. 2009. *Ngan'gi Seasons, Nauiyu – Daly River, Northern Territory*, Australia. http://www.csiro.au/en/Organisation-Structure/Divisions/Ecosystem-Sciences/Ngangi-Seasonal-Calendar.aspx CSIRO Ecosystem Sciences, Darwin.

Woodward, E., Jackson, S., Finn, M. and Marrfurra McTaggart, P. 2012. Utilising Indigenous seasonal knowledge to understand aquatic resource use and inform water resource management in northern Australia. *Ecological Management & Restoration* 13(1), 58-64.

A CONVECTIVE QUASI-EQUILIBRIUM VIEW OF OBSERVED MONSOON INTERANNUAL VARIABILITY

William R. Boos and John V. Hurley

Dept. of Geology and Geophysics, Yale University
New Haven, Connecticut, USA

Abstract

Idealized dynamical theories that employ a convective quasi-equilibrium (QE) treatment for the diabatic effects of moist convection have been used in theoretical studies of monsoons for the past couple decades, but only recently has the climatological mean thermodynamic structure of observed monsoons been shown to be consistent with a QE framework. That recent work is extended here through examination of the interannual variability of observed monsoons in a QE framework. Using two reanalysis products and two precipitation datasets, we examine linear relationships between seasonal anomalies of subcloud equivalent potential temperature (θ_{eb}) and precipitation in multiple monsoons. This approach provides a single, near-surface, thermodynamically relevant variable over both land and ocean, extending previous studies of monsoon variability that emphasized ocean surface temperatures. Positive precipitation anomalies in multiple monsoon regions are found to be associated with an enhanced meridional gradient of θ_{eb} equatorward of the mean precipitation maximum, as expected in idealized QE treatments of monsoons. However, enhanced precipitation in several monsoon regions is also associated with enhanced θ_{eb} local to and poleward of the monsoon precipitation maximum, in regions occupied by continental deserts. Shallow meridional circulations associated with these deserts are shown to covary with monsoon precipitation, and the variations in θ_{eb} over the dry interior of Australia are shown to precede variations in Australian monsoon rainfall by several months. Possible mechanisms for these relationships are discussed.

Introduction

Earth's seasonal cycle of insolation drives monsoon circulations only indirectly, with ocean and land surfaces absorbing most shortwave radiation before transferring the associated energy to the atmosphere via turbulent fluxes of sensible and latent heat. These surface heat fluxes are then redistributed through the troposphere by moist convection, so that a full understanding of the mean state and interannual variability of monsoons requires understanding how the diabatic effects of moist convection interact with the large-scale flow. Here we use a convective quasi-equilibrium framework to examine the interannual variability of monsoons in multiple regions.

Interannual variations in monsoon strength have long been associated with changes in land surface properties, but research in recent years has focused on sea surface temperature (SST) as a leading cause of monsoon variability. For example, Blanford (1884) suggested that heavy Himalayan snowfall led to Indian drought, and Charney (1975) argued that reductions in vegetation could increase land surface albedo and atmospheric subsidence in a positive feedback. But Blanford's hypothesized relation between Himalayan snow and Indian precipitation has proven inconsistent with observations (Robock et al., 2003), and the Sahel drought that motivated Charney's hypothesis is now thought to have been driven mainly by SST (Eltahir and Gong, 1996; Nicholson, 2000; Giannini et al., 2003). SST changes are now considered to be the leading cause of monsoon interannual variability (Yang and Lau, 2004), and rainfall in the Asian and Australian monsoons indeed covaries strongly with both the El Nino-Southern Oscillation and an east-west Indian Ocean SST dipole (Li et al., 2007; Taschetto et al., 2009; Saji et al., 1999; Webster et al., 1999).

Land surface processes presumably make some contribution to monsoon interannual variability, but hypotheses for the influence of soil moisture, surface albedo, and other surface characteristics have been difficult to test observationally and seem subject to substantial regional variability (e.g. Douville et al. 2001; Vernekar et al. 1995; Godfred-Spenning and Reason 2002; Yasunari 2011). One difficulty is that land surface properties must be combined with the SST field to obtain an estimate of horizontal gradients in a relevant thermodynamic variable. Land surface temperature, although well-observed, is largely unrelated to the strength of monsoon circulations, in which the phase changes of atmospheric water play a first-order role. A more relevant variable is moist entropy in the atmospheric boundary layer, which is defined over both land and ocean. Eltahir and Gong (1996) showed that high Sahel precipitation in 1958 was accompanied by a strong meridional entropy gradient, while weak Sahel precipitation in 1960 was accompanied by a weak entropy gradient. The present work, in many ways, simply extends the analysis of Eltahir and Gong (1996) across multiple monsoon regions and a longer time period.

The relevance of boundary layer moist entropy for monsoons can be found in theories for convective quasi-equilibrium (QE). Such theories posit that moist, precipitating convection does not act as a heat source that drives large-scale flow, but instead simply relaxes the atmosphere toward a state of convective neutrality (Arakawa and Schubert 1974; Emanuel et al. 1994). In a strict form of QE, changes in CAPE are assumed to be dynamically negligible so that temperatures within the convecting layer follow a moist adiabat tied to the entropy, or equivalent potential temperature of air below the base of cumulus clouds (θ_{eb}). This strict form of QE is theoretically attractive because it dramatically simplifies the vertical structure of the troposphere and ties it to a single near-surface variable, but it is clear that this is an oversimplification for many tropical atmospheric phenomena (Brown and Bretherton 1997). Nevertheless, strict forms of QE have been used in numerous theoretical studies of monsoons (Chou et al. 2001; Neelin 2007; Prive and Plumb 2007; Boos and Emanuel 2008). Monsoon dynamics takes a particular form under strict QE because convection in monsoons tends to occur in a narrow, large-scale ascent zone near the free-tropospheric temperature maximum; moist convection is suppressed in the subsiding branch of the circulation so that θ_{eb} is decoupled from free-tropospheric temperature there. Maxima of θ_{eb} and free-tropospheric temperature are thus coincident for monsoons in a QE framework, and the location of these maxima marks the poleward edge of the ascent branch of the thermally direct monsoon circulation, as in idealized theories for Hadley circulations (e.g. Lindzen and Hou 1988; Emanuel 1995; Prive and Plumb 2007).

It was recently shown that a QE framework decently describes the seasonal-mean state of many observed monsoons (Nie et al. 2010). In particular, maxima of θ_{eb} in many of Earth's regional monsoons are located in the same positions as maxima of upper-tropospheric temperature, T_u. This is true in South Asia, where the maxima of θ_{eb} and T_u are located over northwest India and Pakistan (Fig. 1a). Sharp horizontal gradients in θ_{eb} are coincident with topography there, suggesting that topography may prevent the mixing of dry, low-θ_{eb} desert air into the monsoon thermal maximum (e.g. Boos and Kuang 2010, Chakraborty et al. 2006). Maxima of θ_{eb} and T_u are also spatially coincident over Australia and southern Africa during austral summer (Fig. 1c, d), with the precipitation maximum located slightly equatorward of the thermal maximum, consistent with theory. In contrast, T_u in northern Africa is dominated by the South Asian thermal maximum (Fig. 1b), consistent with the idea that South Asian monsoon heating forces Rossby waves that warm and dry the troposphere over Africa (Rodwell and Hoskins 1996). The northern African monsoon does seem to perturb the T_u distribution, with the zonally elongated band of high θ_{eb} air over the Sahel being in quasi-equilibrium, perhaps, with the ridge of T_u that extends into the Atlantic near 15°N.

The goal of this work is to examine the covariation of monsoon precipitation with θ_{eb} on interannual time scales. This is an obvious next step now that the QE framework used in numerous theoretical studies has been shown to decently describe the climatological mean state of observed monsoons (Nie et al. 2010). This document constitutes a brief summary of results presented in greater detail in Hurley and Boos (2012) as well as Nie et al. (2010).

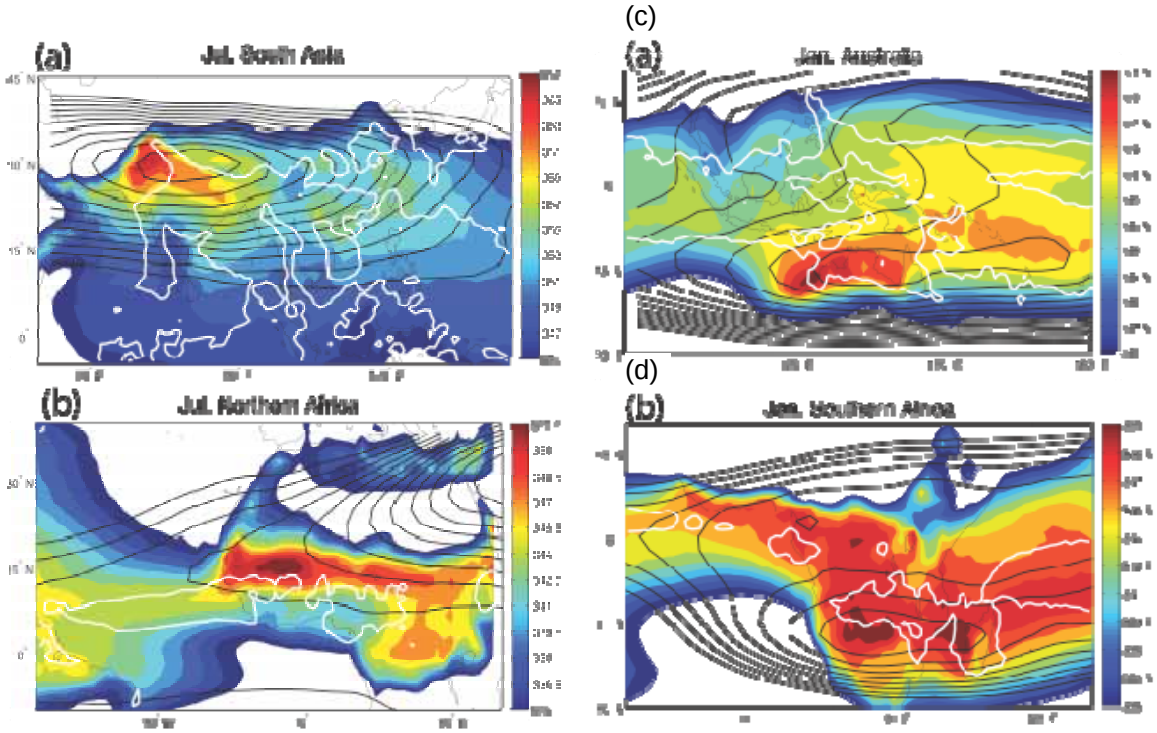

Fig. 1: *Evaluation of QE for the local summer mean state in (a) South Asia, (b) northern Africa, and (c) Australia, and (d) southern Africa. Colors show subcloud θ_e and black contours show saturation θ_e (i.e. a measure of temperature) averaged from 200 to 400 hPa. The white contour indicates the region that has precipitation greater than 6 mm day^{-1}. The saturation θ_e contours begin at (a) 345 K, (b) 340 K, and (c, d) 341 K with respective intervals of 1 K, 1 K, and 0.5 K. Reproduced from Nie et al. (2010).*

Data and Methods

Global distributions of θ_{eb} were calculated using data from the European Centre for Medium-Range Weather Forecasts Reanalysis-40 (ERA-40; Uppala et al. 2005) on a terrain-following level about 20 hPa above Earth's surface. Upper-tropospheric temperature and 700 hPa wind were also obtained from ERA-40. Precipitation was obtained from both the Global Historical Climatology Network (GHCN; Peterson and Vose 1997) and the Global Precipitation Climatology Project (GPCP; Adler et al. 2003). Precipitation was horizontally averaged over six geographic areas (e.g. the boxes in Fig. 2) chosen to reflect the interannual variability of regional monsoons and to generally be consistent with prior studies.

All analyses used three-month averaged time series for the full calendar year, except for analyses of spectral coherence which used monthly data. Three-month averages were taken over the standard seasonal periods of Dec.-Feb., March-May, June-Aug., and Sept.-Nov., and only minor sensitivity to the choice of these periods was found. Use of three-month averages reduces the signal from subseasonal variability, and use of data for the entire year allows the influence of changes in the length of the rainy season to be included in our results. We also removed the θ_{eb} variability linearly associated with the Nino 3.4 index as obtained from the National Oceanic and Atmospheric Administration. While study of variations of θ_{eb} related to the El Nino-Southern Oscillation (ENSO) might help in understanding the mechanisms by which monsoon precipitation interacts with that climate signal, we leave that task for future work and focus on less studied mechanisms that are at least linearly independent of one widely used ENSO index.

Brown and Bretherton (1997) found monthly values of θ_{eb} and T_u to have statistically significant autocorrelations at the 95% level for a representative time of four months and so reduced the number

of degrees of freedom in their monthly data by a factor of four. In assessing the statistical significance of our regression coefficients, we take the somewhat arbitrary but even more conservative approach of reducing our degrees of freedom by the same factor of four for three-monthly data. This makes correlation coefficients significant at the 95% level for a value of 0.3 for GHCN data and 0.4 for the shorter GPCP data.

Results and Discussion

Regression coefficients for GHCN precipitation anomalies regressed onto ERA-40 θ_{eb} anomalies (relative to the seasonal cycle) are shown in Fig. 2 for four monsoon regions. For all regions, positive precipitation anomalies are associated with positive continental θ_{eb} near and slightly poleward of the peak climatological precipitation. Some of the precipitation indices are also negatively related to θ_{eb} on the equator or in the opposite hemisphere (this is also the case for the North and South American monsoons, which are not shown). For example, enhanced Sahel precipitation is associated with a band of enhanced θ_{eb} that stretches across Africa near 20°N and also with reduced θ_{eb} over the Amazon basin and southern Africa (Fig. 2a). A qualitatively similar pattern is associated with precipitation in southern Africa (Fig. 2d). Australian monsoon precipitation is positively related to θ_{eb} over much of the Australian continent and is also associated with a zonal dipole of midlatitude θ_{eb} over the southern Indian Ocean (Fig. 2c). In all regions, continental variations in θ_{eb} are due mostly to variations in subcloud specific humidity, with changes in subcloud temperature having the opposite sign (not shown).

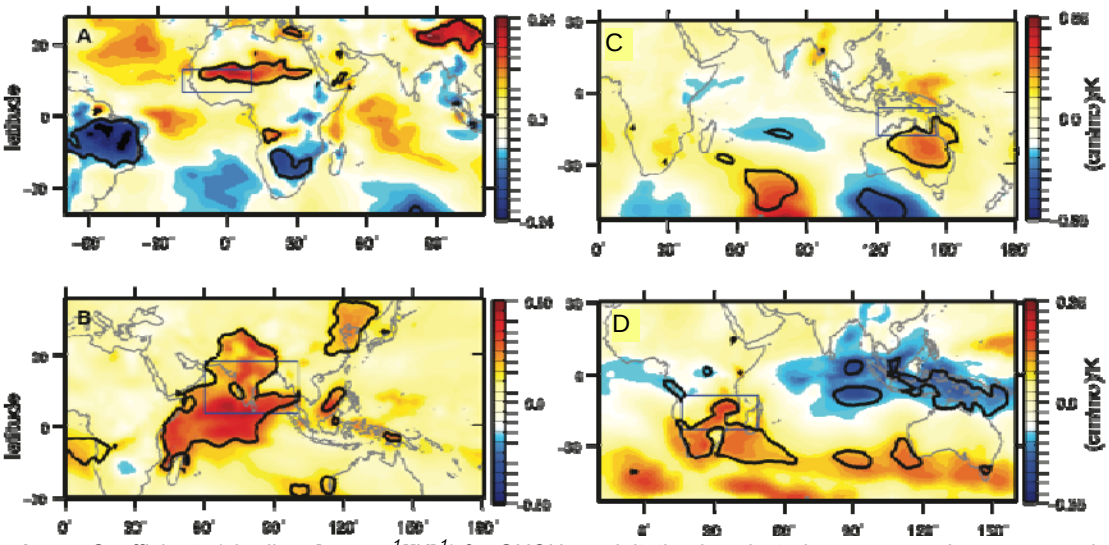

Fig. 2: *Coefficients (shading, [cm mo^{-1}][K]$^{-1}$) for GHCN precipitation in selected monsoon regions regressed onto ERA-40 θ_{eb} for 1958-2002 for (a) northern Africa, (b) South Asia, (c) Australia, and (d) southern Africa. Precipitation was averaged over the boxed regions, and thick black contours delineate regions where the coefficients are statistically significant at a 95% level.*

South Asia differs from other regions in that precipitation there is positively related to θ_{eb} over a comparatively extensive region that stretches from northern India to Madagascar (Fig. 2b). Finally, we note that over South Asia, enhanced precipitation seems to occur when the θ_{eb} field is uniformly elevated, without any discernable change in the meridional gradient (Fig. 2b). This is consistent with the idea that topography insulates the South Asian summer monsoon from the influence of adjacent deserts by preventing the intrusion of dry desert air into the monsoon thermal maximum (e.g. Chakraborty et al. 2006, Boos and Kuang 2010). In other words, topography not only help to create a strong mean summer monsoon in South Asia, but it may also suppress covariations between desert thermodynamics and monsoon rainfall.

A negative relationship between monsoon precipitation and θ_{eb} on the opposite side of the equator is consistent with the simple idea of enhanced monsoon precipitation occurring during years in which the meridional θ_{eb} gradient was enhanced between the summer and winter hemispheres, as suggested by Eltahir and Gong (1996). However, if that idea completely described monsoon interannual variability, then one would see monsoon precipitation covarying strongly with the amplitude of the climatological mean θ_{eb} maximum. Instead, precipitation seems to covary most strongly with θ_{eb} poleward of the climatological mean θ_{eb} maximum in Australia and both northern and southern Africa (compare Figs 1 and 2). The sites of these strong, positive regression coefficients are desert regions which have relatively low θ_{eb} in the climatological mean, so that these regression patterns signify a flattening of the meridional gradient on the poleward side of the climatological θ_{eb} maximum in Australia and both northern and southern Africa.

One hypothesis is that when θ_{eb} is elevated poleward of the climatological θ_{eb} maximum, the equatorward advection of low-θ_{eb} air into that maximum is reduced (assuming negligible change in horizontal winds). But one would then expect to see the amplitude of the θ_{eb} maximum increase during years of enhanced precipitation, and such a pattern is notably absent from Fig. 2. An alternate hypothesis is that the association of monsoon rainfall with θ_{eb} in adjacent deserts involves dynamics not represented in the simple framework that relates θ_{eb} and T_u to a deep, first-baroclinic circulation; all of the idealized QE theory for monsoons discussed above is phrased in terms of such first-baroclinic mode dynamics (Emanuel 1995; Chou et al. 2001; Prive and Plumb 2007; Boos and Emanuel 2008). Deserts are known to be the sites of shallow, thermally direct circulations confined to the lower troposphere. These shallow circulations consist of near-surface poleward flow that extends beyond the primary monsoon precipitation maximum and terminates near the peak subcloud potential temperature maximum (θ_b, not θ_{eb}; Fig. 3). Shallow flow associated with the Saharan heat low has been studied for decades in connection with the mid-tropospheric African easterly jet (Burpee 1972; Thorncroft and Blackburn 1999), but shallow heat-low flow was only recently identified in the peak summer climatologies in Australia and southern Africa (Nie et al. 2010). Regression of monsoon precipitation onto 700 hPa flow over Australia shows that enhanced precipitation occurs when outflow from the heat low weakens (Fig. 4). Combined with the regression coefficients for θ_{eb}, this shows that Australian monsoon precipitation is enhanced when the Australian continental interior is cooler and moister and the associated heat low circulation is weaker. While further work is needed to explore the significance of these changes in shallow flow, this at least raises the possibility that first-baroclinic mode theory may not completely explain the observed interannual variability of monsoons.

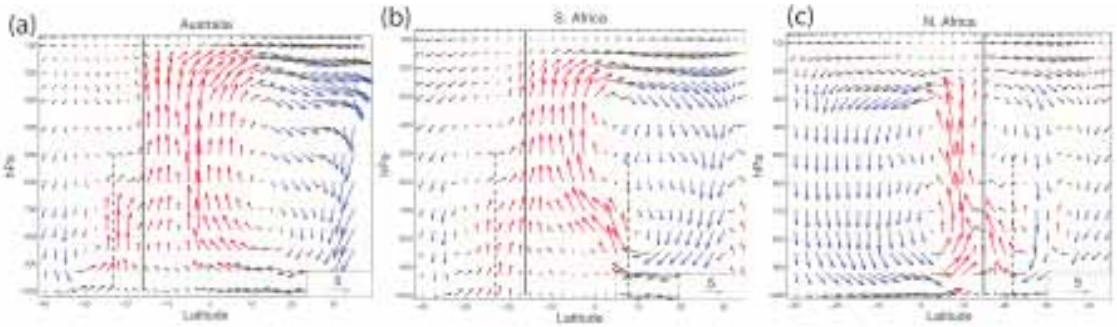

Fig. 3: *ERA-40 meridional and vertical wind for (a) Australia in Jan., 120-140°E, (b) southern Africa in Jan., 15-35°E, (c) northern Africa in July, 20°W-20°E. Upward and downward motion with amplitude larger than 0.02 Pa s^{-1} is in red and blue, respectively. Note the deep ascent equatorward of the peak subcloud θ_e (marked by vertical solid line) and the shallow ascent at higher latitudes near the peak low-level θ (marked by vertical dashed line). Vertical velocities amplified 80 times for clarity. From Nie et al. (2010).*

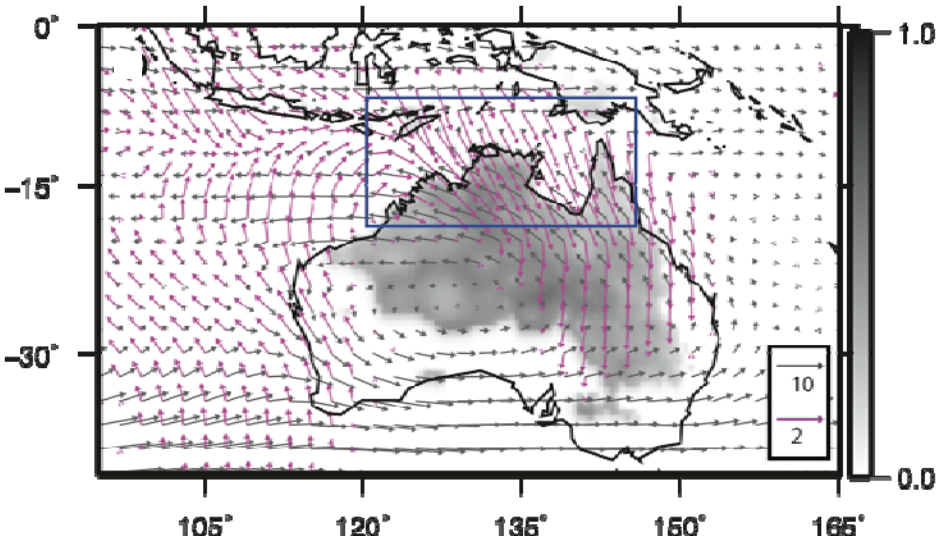

Fig. 4: *Shading shows coefficients ([cm mo^{-1}][cm mo^{-1}]$^{-1}$) for the regression of GHCN precipitation on precipitation horizontally averaged over northern Australia (the boxed region). Vectors show the Dec.-Feb. climatological wind (grey vectors, m s^{-1}) and the coefficients of precipitation regressed on the 700 hPa horizontal wind (magenta vectors, [cm mo^{-1}][m s^{-1}]$^{-1}$). Shading is plotted only for coefficients statistically significant at the 95% level, and magenta vectors are plotted only where either the regression coefficient for the zonal or meridional wind is significant at the 95% level.*

While contemporaneous relationships between monsoon precipitation and θ_{eb} are interesting because they help in understanding the mechanisms responsible for monsoon variations, an antecedent relationship between these variables could be of practical utility in forecasting seasonal rainfall. Here we present a brief analysis of the temporal phase of the relationship between Australian monsoon rainfall and θ_{eb}. Coherence and phase spectra were computed for the Australian precipitation index and θ_{eb} averaged over a region that includes continental Australia (120-150°E, 0-42°S). To assess possible sensitivity to the time period and the precipitation data set, we computed results for the regionally-averaged ERA-40 θ_{eb} paired with three precipitation time series: GPCP for 1979-2002, GHCN for 1979-2002, and GHCN for 1958-2002. All three combinations showed statistically significant coherence between precipitation and θ_{eb} over a range of interannual time scales (Fig. 5a). The phase spectrum shows that θ_{eb} leads precipitation at these interannual time-scales by several months, and that this phase lag is statistically distinct from zero for periods of 1.5 to 3 years. This does not establish variations in desert θ_{eb} as a cause of rainfall variations, but it does indicate that it may nevertheless be useful in predictions.

The results presented herein are a brief summary of those contained in Hurley and Boos (2012) as well as Nie et al. (2010). Work is in progress to better understand covariations of monsoon precipitation and θ_{eb}, using both idealized numerical models and observations collected in monsoon regions and their adjacent deserts.

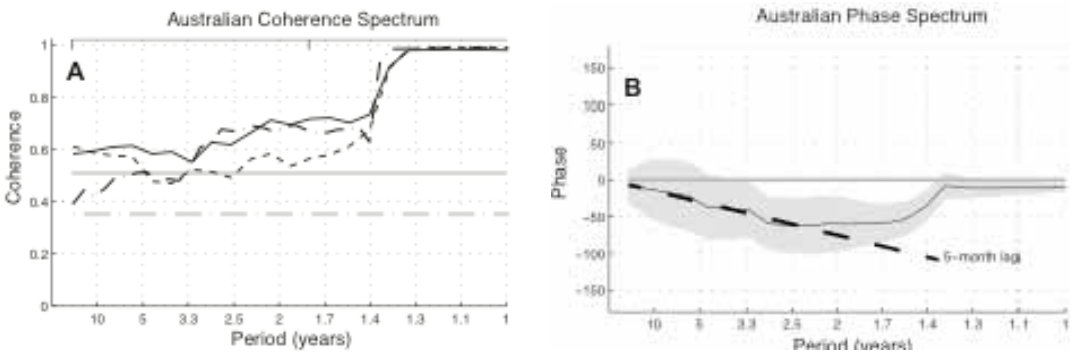

Fig. 5: *Cross-spectral analysis of precipitation (averaged 120-146°E, 5-20°S) and θ_{eb} (averaged 120-150°E, 0-42°S). (a) Coherence for ERA-40 θ_{eb} and: GPCP precipitation for 1979-2002 (solid black line), GHCN precipitation for 1979-2002 (dashed line), and GHCN precipitation for 1958-2002 (dash-dot black line). Horizontal grey lines indicate the 95% significance level for 1979-2002 (solid) and 1958-2002 (dash-dot). (b) Phase for GPCP precipitation and ERA-40 θ_{eb}, with horizontal grey line indicating zero phase angle and θ_{eb} leading precipitation for negative phase angles. Grey shading indicates a 95% bias-corrected confidence interval and the dashed line indicates a 5-month phase lag.*

References

Adler, R. F., and Coauthors, 2003: The version-2 global precipitation climatology project (GPCP) monthly precipitation analysis (1979-present). *J. Hydrometeorology*, **4,** 1147-1167.

Arakawa, A. and Schubert, W.H. 1974: Interaction of a cumulus cloud ensemble with large- scale environment .1. *J. Atmos. Sci.*, **31,** 674-701.

Boos, W.R. and Emanuel, K.A. 2008: Wind-Evaporation Feedback and the Axisymmetric Transition to Angular Momentum-Conserving Hadley Flow. *J. Atmos. Sci.*, **65,** 3758-3778.

Boos, W.R. and Kuang, Z. 2010: Dominant control of the South Asian monsoon by orographic insulation versus plateau heating. *Nature*, **463,** 218-222.

Brown, R G. and Bretherton, C.S. 1997: A test of the strict quasi-equilibrium theory on long time and space scales. *J. Atmos. Sci.*, **54,** 624-638.

Burpee, R. 1972: The origin and structure of easterly waves in the lower troposphere of North Africa. *J. Atmos. Sci.*, **29**, 77–90.

Chakraborty, A., Nanjundiah, R. and Srinivasan, J. 2006: Theoretical aspects of the onset of Indian summer monsoon from perturbed orography simulations in a GCM. *Ann. Geophys.*, **24**, 2075–2089.

Charney, J.G. 1975: Dynamics of deserts and drought in the Sahel. *Q. J. R. Meteorol. Soc.*, **101,** 193-202.

Chou, C., Neelin, J.D. and Su, H. 2001: Ocean-atmosphere-land feedbacks in an idealized monsoon. *Q. J. R. Meteorol. Soc.*, **127,** 1869-1891.

Douville, H., Chauvin, F. and Broqua, H.2001: Influence of soil moisture on the Asian and African monsoons. Part I: Mean monsoon and daily precipitation. *J. Climate*, **14,** 2381- 2403.

Eltahir, E.A.B. and Gong, C. 1996. Dynamics of the wet and dry years in West Africa. *J. Climate*, **9,** 1030-1042.

Emanuel, K.A., Neelin, J.D. and Bretherton, C.S. 1994: On large-scale circulation in convecting atmospheres. *Q. J. R. Meteorol. Soc.*, **120,** 1111-1143.

Emanuel, K.A. 1995: On thermally direct circulations in moist atmospheres. *J. Atmos. Sci.*, **52,** 1529-1534.

Giannini, A., Saravanan, R. and Chang, P. 2003: Oceanic forcing of Sahel rainfall on interannual to interdecadal time scales. *Science*, **302,** 1027-1030.

Godfred-Spenning, C.R. and Reason, C.J.C. 2002: Interannual variability of lower- tropospheric moisture transport during the Australian monsoon. *Int. J. Climatol.*, **22,** 509-532.

Hurley, J.V. and Boos, W.R. 2012: Interannual variability of monsoon precipitation and subcloud equivalent potential temperature. In review at *J. Climate*.

Li, Y., Lu, R.Y. and Dong, B.W. 2007: The ENSO-Asian monsoon interaction in a coupled ocean-atmosphere GCM. *J. Climate*, **20,** 5164-5177.

Lindzen, R.S. and Hou, A.Y.1988: Hadley circulations for zonally averaged heating centered off the equator. *J. Atmos. Sci.*, **45,** 2416-2427.

Neelin, J. D. 2007: Moist dynamics of tropical convection zones in monsoons, teleconnections and global warming. *The Global Circulation of the Atmosphere*, T. Schneider, and A. H. Sobel, Eds., Princeton University Press.

Nicholson, S. 2000: Land surface processes and Sahel climate. *Rev. Geophysics*, **38**, 117–140.

Nie, J., Boos, W.R. and Kuang, Z.M. 2010: Observational Evaluation of a Convective Quasi-Equilibrium View of Monsoons. *J. Climate*, **23**, 4416-4428.

Peterson, T.C. and Vose, R.S. 1997: An overview of the global historical climatology network temperature database. *Bulletin of the American Meteorological Society*, **78,** 2837-2849.

Prive, N.C. and Plumb, R.A. 2007: Monsoon dynamics with interactive forcing. Part I: Axisymmetric studies. *J. Atmos. Sci.*, **64,** 1417-1430.

Robock, A., Mu, M.Q., Vinnikov, K. and Robinson, D.2003: Land surface conditions over Eurasia and Indian summer monsoon rainfall. *J. Geophys. Res.-Atmospheres*, **108**.

Rodwell, M.J. and Hoskins, B.J. 1996: Monsoons and the dynamics of deserts. *Q. J. R. Meteorol. Soc.*, **122,** 1385-1404.

Saji, N.H., Goswami, B.N., Vinayachandran, P.N. and Yamagata, T.1999: A dipole mode in the tropical Indian Ocean. *Nature*, **401**, 360-363.

Taschetto, A.S., Ummenhofer, C.C., Sen Gupta, A. and England, M.H. 2009: The effect of anomalous warming in the central Pacific on the Australian monsoon. *Geophys. Res. Lett.*, **36**, L12704, doi:10.1029/2009GL038416.

Thorncroft, C. and Blackburn, M. 1999: Maintenance of the African easterly jet. *Q. J. R. Meterol. Soc.*, 125, 763–786.

Uppala, S.M. and Coauthors, 2005: The ERA-40 re-analysis. *Q. J. R. Meteorol. Soc.*, **131,** 2961-3012.

Vernekar, A. D., Zhou, J. and Shukla, J.1995: The effect of Eurasian snow cover on the Indian Monsoon. *J. Climate*, **8,** 248-266.

Yang, S. and Lau, K.M. 2004: Interannual variability of the Asian monsoon. *Asian Monsoon*, B. Wang, Ed., Springer-Praxis, 259-293.

Yasunari, T. 2011: Role of Vegetation in the Monsoon Climate System. In Chang, C.-P., Y. Ding, N.-C. Lau, R. H. Johnson, B. Wang, and T. Yasunari, eds., *The Global Monsoon System: Research and Forecast*, World Scientific Publishing Co. Pte. Ltd., pp. 583–595.

Webster, P.J., Moore, A.M., Loschnigg, J.P. and Leben, R.R. 1999: Coupled ocean-atmosphere dynamics in the Indian Ocean during 1997-98. *Nature*, **401**, 356-360.

SOME ASPECTS OF PREDICTION AND DIAGNOSIS OF THE ONSET OF THE AUSTRALIAN MONSOON USING ACCESS

Noel Davidson, Gary Dietachmayer, Kamal Puri, Elizabeth Ebert, Tony Hirst, Lawrence Rikus, Peter Steinle and Kevin Tory

Centre for Australian Weather and Climate Research, A partnership between the Australian Bureau of Meteorology and CSIRO, Melbourne, Australia
n.davidson@bom.gov.au

Background

With the implementation of the Australian Community Climate and Earth System Simulator, ACCESS (Puri et al. 2012), and its competitive performance in operational forecasting over midlatitudes, it becomes important to assess the skill over the tropics for short to medium timescales, 0-10 days. Standard metrics for verification are not ideal over the tropics, where critical features are precipitation, changes in the large-scale tropical circulation, and changes in the low level flow. In particular we would like to evaluate prediction of (a) significant tropical weather events, like Monsoon Onset, and (b) skill in prediction of tropical rainfall. The current study addresses the first of these questions.

Onset is often characterized by a sudden strengthening and deepening in tropical westerly winds, which are overlain by upper tropospheric easterlies (eg, Drosdowsky, 1996). However, many onsets are also preceded by up to a 7-day pre-conditioning period of enhanced vertical motion and moistening (Davidson et al., 2007). Critical components of the summer monsoon are the clouds (diabatic heat sources) which drive the large-scale divergent circulation that is the Monsoon. Thus a key to monsoon events is the triggering and maintenance of widespread convection. Various physical mechanisms have the potential to influence the onset of the Australian monsoon and convective outbreaks over the tropics generally. They include extratropical-tropical interaction (Lim and Chang, 1981, Keenan and Brody, 1988, Davidson et al., 2007), intra-tropical interactions (Davidson and Hendon, 1989), and the Madden-Julian Oscillation (MJO) (Hendon and Liebmann, 1990, Wheeler and Hendon, 2004). There is compelling evidence that all these processes may at times be important (e.g., Hung and Yanai, 2004), and may even be inter-related but operate on different timescales. For example the annual change in solar insolation and land-sea contrast provide a mechanism for longer-term pre-conditioning and forcing of the monsoon. The important role of the MJO at intraseasonal timescales is described in a number of studies. On much shorter timescales, the influence of evolving midlatitude weather systems appears to play at least a modulating role. As an illustration of the latter mechanism, the upper-level flow during a number of onsets is shown in Fig.1. Evidence of a propagating Rossby wave can be seen as a series of troughs and ridges extending from the southwest Indian Ocean into the Australian tropics. Note also that the wave structures are very similar to the local circulation patterns documented for enhanced cloudy phases of the monsoon by Keenan and Brody (1988). Their composites suggest that enhanced cloudiness exists in the northeast to southeast flow on the equatorward side of the trough-ridge couplet.

Extratropical-tropical Interaction during Onset of the Monsoon

Based on analysis of a number of onsets, Davidson et al. (2007) suggested that monsoon onset is regularly associated with major cyclogenesis events over the southwest Indian Ocean in the presence of a subtropical jet over the eastern Indian Ocean. The proposed mechanism for extratropical-tropical interaction is northeastward Rossby wave propagation from the cyclogenesis region into the tropics at upper levels. At these levels, westerly winds extend to nearly 10^0S and provide a favourable

background flow for such propagation. The process eventually results in the amplification of an equatorward-extending midlatitude upper trough and tropical ridge, which appears to provide favourable conditions for the development of widespread tropical convection and the underlying monsoon trough.

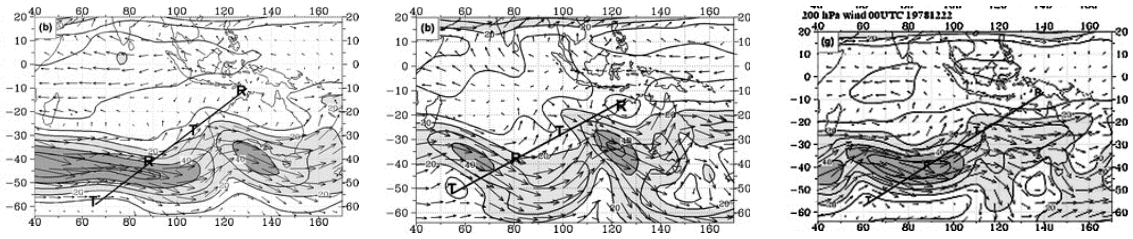

Fig. 1: *Wind fields at 200 hPa prior to onset in the seasons of 1978-79 (WMonex), 1986-87 (AMEX) and 1992-93 (Toga-Coare). Contour interval 10 ms^{-1} with light and dark shadings for winds greater than 20 ms^{-1} and 40 ms^{-1} respectively. Ts and Rs indicate where the troughs have deepened and the ridges built.*

To test this hypothesis, the influence of high-latitude cyclogenesis on the tropical circulation was investigated with the aid of an idealized, dry, three-dimensional, baroclinic-wave channel model. The initial state consisted of (a) a zonally-constant baroclinic region centered on 40^0S, from which the high-latitude cyclogenesis developed, (b) a weak monsoon trough at 15^0S, and (c) a subtropical jet at 25^0S. The major findings from the simulations were: 1. There is evidence of northeastward Rossby wave propagation from the cyclogenesis region towards low latitudes. 2. Consistent with theoretical studies, the subtropical jet plays a key role by providing a favorable westerly background flow for group propagation into the tropics. 3. High-latitude cyclogenesis in the presence of a subtropical jet can influence the meridional location, zonal structure, vorticity and divergence in the monsoon trough. 4. Vorticity and divergence changes are consistent with enhancement of the monsoon trough (increases in low level cyclonic vorticity) and the potential for triggering of a large-scale convective outbreak (changes in upper level divergence). We then ask: Can such processes be seen in the real and model atmospheres?

Monsoon Onset during the 2010-2011 Season

Figure 2 shows from ACCESS-G analyses, time-height sections of zonal wind, vertical motion and relative humidity during the period 1 November 2010 to 31 January 2011. A clearly-defined onset of persistent, deep monsoon westerly winds is evident around 12 December 2010. As in other years, moistening and increased ascent is analysed during the days prior to the development of westerly winds. In addition, bursts in upper level westerly winds are evident prior to onset, during the transition season (the six weeks prior to onset), as midlattude troughs penetrate to low latitudes. These are usually associated with moistening (right panel) and rainfall. Interestingly it is after one of these events that upper level easterly winds become established over the tropics, a number of days prior to onset. This structure is again consistent with the observed relationship between enhanced tropical cloudiness and the large-scale circulation (Keenan and Brody, 1988), and with the structure of a propagating Rossby wave at upper levels.

Prediction of Onset by ACCESS-G

Historically models have shown limited skill in prediction of monsoon events, possible because of (a) limitations with resolution, initialization and moist physics, and (b) inability to adequately represent the processes described above. Figure 3 shows a comparison of time-height sections of zonal winds obtained from ACCESS-G 3-day, 5-day and 10-day forecasts. These should be compared with the analysed time series in the left panel of Fig.2. There are clearly some phase and amplitude differences, particularly as the lead times increase, but there is generally good agreement between the time series for these space and time scales.

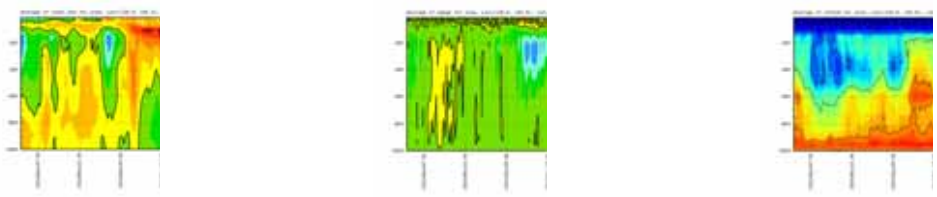

***Fig. 2**: 2010-2011 onset: Time-height sections of (a) zonal wind, (b) vertical motion, and (c) relative humidity, for the zone 15^0S – 5^0S, 110^0E – 145^0E from the ACCESS-G analyses, for the period 1 November 2010 to 31 January 2011. Contour intervals are respectively 4 ms^{-1}, 0.01 hPa/s and 5%.*

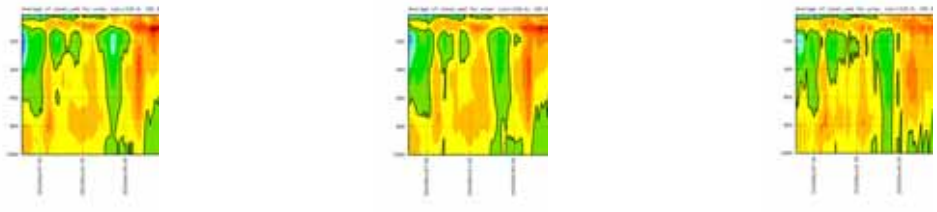

***Fig. 3:** Time-height sections from 3-day, 5-day and 10-day ACCESS-G forecasts of zonal wind for the domain 5^0S-15^0S, 110^0E-145^0E, for the period 1 November 2010 to 31 January 2011. Westerly winds are positive. Contour interval is 4ms^{-1}.*

As an illustrative example of an onset forecast from ACCESS-G, Fig.4 shows time-height sections of zonal wind, vertical motion and relative humidity from the 10-day ACCESS-G forecast from base time 00UTC, 6 December 2010. Recalling that in this year Onset was near 12 December, ACCESS-G shows encouraging skill at forecasting the rapid and large-scale changes in relative humidity, ascent and monsoon westerlies from 6 days prior to onset. The monsoon is not forecast to be strong or deep enough, but the prediction provides very valuable guidance on the changes that were later observed.

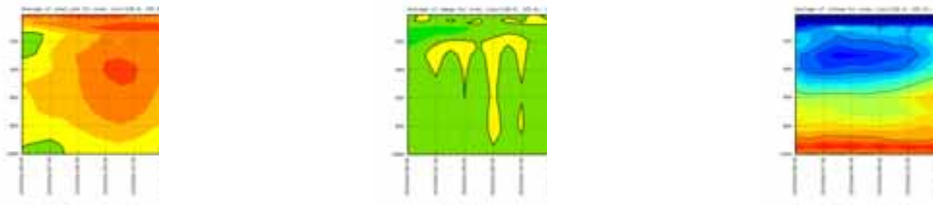

***Fig. 4.** Time-height sections of (a) zonal wind, (b) vertical motion, and (c) relative humidity, for the zone 15^0S – 5^0S, 110^0E – 145^0E from the ACCESS-G 10-day forecast from base time 00UTC 6 December 2010. Data points are every 12 hours. Contour intervals as in Fig. 2.*

Figure 5 shows the 200 hPa initial and 48-hour forecast wind field from base time 00UTC 6 December 2010. The development of large amplitude, long waves is clearly evident over the Indian Ocean and Australian longitudes. As part of this development, the amplifying ridge over low latitudes, with associated developing easterly winds on its northern flank are evident. The mechanism requires further quantification, but as in previous studies, evidence suggests that such extratropical-tropical interactions play an important role during onset of the Australian monsoon.

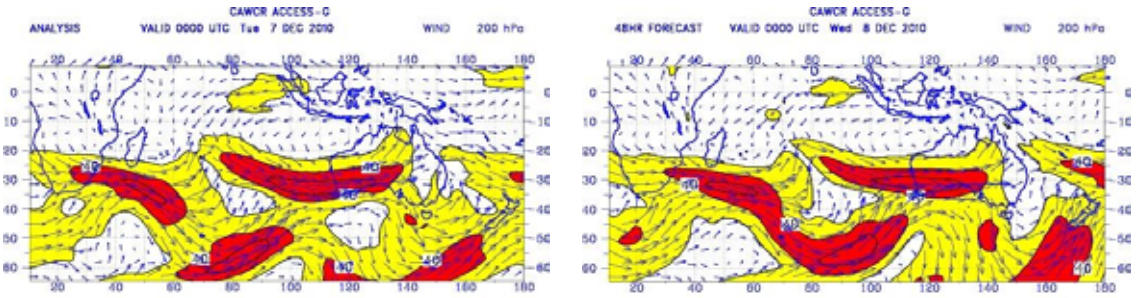

Fig. 5. *Initial condition and 48-hour forecast of 200 hPa wind field from the ACCESS-G, 10-day forecast from base time 00UTC 6 December 2010. Units are ms^{-1}.*

Summary

The Onset of the Australian Monsoon is characterized by a sequential increase in moistening, vertical motion and eventually development of low-level monsoon westerlies. The onset process can take of the order of 7 days to fully complete. Extratropical-tropical interaction seems to occur during onset and this takes the form of propagating Rossby waves at upper tropospheric levels over the Indian Ocean into the deep tropics. This region is particularly favourable for such events, since (a) high-latitude cyclogenesis is a regular occurrence, and (b) pre-existing polar front and subtropical jet structures assist with the propagation of waves into the tropics. Idealized simulations suggest that such waves can potentially influence the structure of the Monsoon and development of widespread convection.

From the exceedingly limited forecast sample analysed here, ACCESS-G, with its 4D-VAR initialization and improved resolution and physics, has shown encouraging skill at prediction of circulation changes over the tropics, and in particular Onset. The model appears to forecast the evolving extratropical and tropical flows in a similar way to what is seen in the analyses. Further work on prediction and diagnosis of the Monsoon is planned.

References

Davidson, N.E., Tory, K.J., Reeder M.J. and Drosdowsky, W.L. 2007: Extratropical-tropical interaction during onset of the Australian Monsoon: Re-analysis diagnostics and idealized dry simulations. *J. Atmos. Sci.*, 64, 3475-3498.

Davidson, N.E. and Hendon, H.H. 1989: Downstream development in the Southern Hemisphere monsoon during FGGE/WMONEX. *Mon. Wea. Rev.*, 117, 1458-1470.

Drosdowsky, W. 1996; Variability of the Australian summer monsoon at Darwin: 1957–1992. *J. Clim.*, 9, 85–96.

Hendon, H.H. and Liebmann. B. 1990: The Intraseasonal (30–50 day) Oscillation of the Australian summer monsoon. *J. Atmos. Sci.*, 47, 2909–2924.

Hung, C.-W. and Yanai, M. 2004: Factors contributing to the onset of the Australian summer monsoon. *Quart. J. Roy. Meteor. Soc*., 130, 739-758.

Keenan, T.D. and Brody, L.R. 1988: Synoptic-scale modulation of convection during the Australian summer monsoon. *Mon. Wea. Rev*: 116, 71–85.

Lim, H. and Chang, C.-P. 1981: A theory for midlatitude forcing of tropical motions during winter monsoons. *J. Atmos. Sci*., 38, 2377–2392.

Wheeler, M.C. and Hendon, H.H. 2004: An All-Season Real-Time Multivariate MJO Index: Development of an Index for Monitoring and Prediction. *Mon. Wea. Rev.*, 132, 1917–1932.

MODULATION OF MONSOON ACTIVITY BY TROPICAL PACIFIC VARIABILITY AND CLIMATE MODEL FIDELITY APOLOGIES

Andréa S. Taschetto, Yue Li, Nicolas C. Jourdain and Alexander Sen Gupta

Climate Change Research Centre, ARC Center of Excellence for Climate Systems Science, University of New South Wales, Sydney, Australia
a.sengupta@unsw.edu.au

This project will look at the fidelity of the Indian and Australian monsoon systems in the CMIP5 models and factors influencing their inter-annual variability. In particular, we examine different flavours of ENSO and their influence on the Australian monsoon and the relationships between the Indian and Australian monsoons that make up the Tropospheric Biennial Oscillation.

Numerical experiments have demonstrated that the location of maximum interannual variability in the tropical Pacific can result in large differences in the Pacific-Australian monsoon teleconnection (Taschetto et al. 2009). In the observational record there is a clear shortening and intensification of the Australian monsoon in Warm Pool El Nino years, even if the total monsoon rainfall remains close to normal (fig.1). These changes are mediated through changes to the Walker circulation and the generation of a Gill-Matsuno-type disturbance (Taschetto et al. 2010, 2009). Here we examine the fidelity of cold-tongue and warm pool ENSO events in the CMIP5 climate models (Taschetto et al. submitted). The CMIP5 models capture the observed asymmetry in the intensity between the warm and cold events (i.e. El Niños are stronger than La Niñas), and between the two types of El Niños, i.e. Cold Tongue (CT) El Niños are stronger than Warm Pool (WP) El Niños, although the strength of the latter is overestimated. However, CMIP5 models fail to reproduce the asymmetry between the two types of La Niñas, i.e. simulated CT (WP) events are generally stronger (weaker), in disagreement with the observations. While the timing of the peak of ENSO events are generally well reproduced in the models, the duration of most types of ENSO extend for too long.

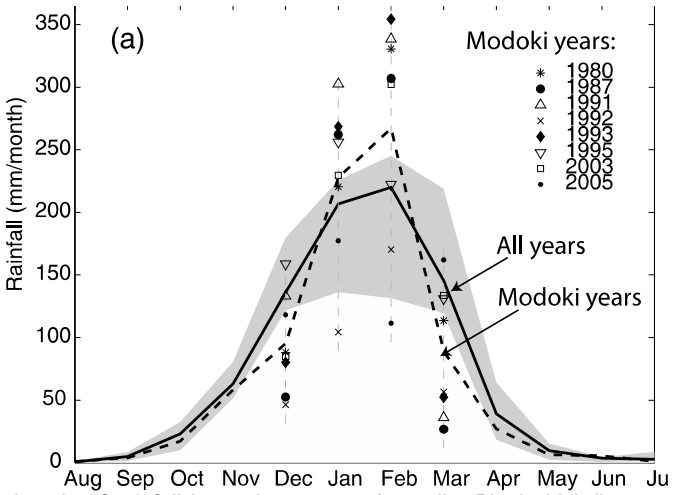

Fig. 1 *Observed annual cycle of rainfall in north- western Australia. Black thick line represents the climatology and the thick dashed line indicates the anomalous behavior during El Nino Modoki years. Individual monthly December to March values for Modoki events are highlighted with different symbols. Values outside the grey shaded area are significant at the 95% level based on a Monte Carlo test.*

We also examine the Indian-Australian monsoon seasonality and the transitions that make up the Tropospheric Biennial Oscillation (Li et al. 2012). In particular, we examine if there is any enhanced predictability associated with the in-phase Indian-Australian and out of phase Australian-Indian and

Indian-Indian monsoon transitions in a number of observational datasets and in the CMIP climate models. Only the transition from a strong (weak) Indian monsoon to a strong (weak) Australian provides significantly enhanced predictability across the observations and most of the CMIP models. Predictabilities for other transitions are variable both across observational products and the climate models.

References

Li, Y., Jourdain, N., Taschetto, A.S., Ummenhofer, C.C., Ashok, K. and Sen Gupta, A. 2012. Evaluation of monsoon seasonality and the tropospheric biennial oscillation transitions in the CMIP models. *Geophysical Research Letters*, doi:10.1029/2012GL053322. http://www.agu.org.wwwproxy0.library.unsw.edu.au/pubs/crossref/pip/2012GL053322.shtml (Accessed October 2, 2012).

Taschetto, A.S., Sen Gupta, A., Jourdain, N., Santoso, A., Ummenhofer, C.C. and England, M.H. 2012. Cold tongue and warm pool ENSO events in CMIP5: mean state and future projections. *Journal of Climate*, submitted.

Taschetto, A.S., Ummenhofer, C.C., Sen Gupta, A. and England, M.H. 2009. Effect of anomalous warming in the central Pacific on the Australian monsoon. *Geophys. Res. Lett.*, **36**, doi:200910.1029/2009GL038416.

Taschetto, A.S., Haarsma, R.J., Sen Gupta, A., Ummenhofer, C.C., Hill, K.J. and England, M.H. 2010. Australian Monsoon Variability Driven by a Gill–Matsuno-Type Response to Central West Pacific Warming. *J. Climate*, **23**, 4717–4736.

RELATIONSHIP BETWEEN THE AUSTRALIAN AND MARITIME CONTINENT MONSOON AND THE EL NIÑO SOUTHERN OSCILLATION IN REANALYSIS DATA AND THE CMIP3/CMIP5 SIMULATIONS

Nicolas C. Jourdain[1], Alexander Sen Gupta[1,2], Andrea S. Taschetto[1,2], Caroline C. Ummenhofer[3], Aurel F. Moise[4], Karumuri Ashok[5]

1 Climate Change Research Centre, University of New South Wales, Sydney, NSW, Australia
2 ARC Centre of Excellence for Climate System Science, NSW, Sydney, NSW, Australia
3 Department of Physical Oceanography, Woods Hole Oceanographic Institution, Woods Hole, USA
4 Centre for Australian Weather and Climate Research, Bureau of Meteorology, Melbourne, Australia
5 Centre for Climate Change Research, Indian Institute of Tropical Meteorology, Pune, India

Introduction

The Australian and Maritime Continent (Neale and Slingo, 2003) monsoon occurs in austral summer (December to March, DJFM). Contrary to popular understanding, the Australian and Maritime Continent monsoon does not appear to be primarily driven by land-ocean contrast (Yano and McBride, 1998; Chao and Chen, 2001). Australian monsoon rainfall tends to be weak during El Niños (Holland, 1986). The positive phase of the IOD (that peaks in SON) also tends to weaken the following Australian/Maritime continent monsoon (Cai et al., 2005).

On longer timescales, the impact of climate change on the monsoon system is a major concern. Climate change may directly affect the monsoon in two compensating ways: 1- warmer SSTs enable more evaporation and tend to increase the monsoon strength 2- SSTs warm more in the equatorial region than in the Tropics, which tends to weaken the monsoon circulation. These two mechanisms are tightly linked to possible change in SST global modes of variability, in particular ENSO (El Niño Southern Oscillation) and the IOD (Indian Ocean Dipole).

Over the last few years, the ability of general circulation models (GCMs) to realistically simulate the Indo-Pacific monsoon and its teleconnections has been analyzed in the context of the Coupled Model Intercomparison Program 3 (CMIP3), contributing to the Intergovernmental Panel on Climate Change (IPCC) Fourth Assessment Report (IPCC, 2007). While the link between ENSO and the Australian monsoon rainfall is rather well captured by the CMIP3 models (Colman et al., 2011), the ENSO-rainfall relationship is poorly captured near Papua-New Guinea (Cai et al., 2009). These authors have suggested that the ENSO-rainfall relationship is affected by the so called "cold tongue bias" where SST is too cold along the equator, and positive SST anomalies extend too far West during El Niño events (with a significant impact on the Maritime Continent rainfall). In the CMIP3 ensemble, there is no model consensus on how interannual variability of tropical Australian precipitation will change in future climate (Moise et al., 2012). By contrast, a clear increase of future monsoon rainfall has been found over the Maritime Continent (Smith et al., 2012).

Here, we evaluate the Australian and Maritime Continent monsoon and its teleconnections to ENSO in the CMIP simulations. We perform a combined analysis of simulations from 24 CMIP3 models and from 35 models taking part in the new Coupled Model Intercomparison Program 5 (CMIP5). Results from 7 atmospheric reanalyses are also included.

Datasets

We use monthly precipitation averaged in over North Australia, land only, North of 20S (LAUS) and monthly precipitation averaged over the entire Maritime Continent, including over the ocean (AMAR: 100E-150E,20S-5N). In addition, the standard NINO34 index is used to describe ENSO. In this work, all the diagnostics related to the interannual variability of an index are made after removal of the trend (linear least mean square fit) and of the climatological seasonal cycle.

The observational rainfall products used in this paper are: CMAP, GPCP, GPCC, AWAP, and APHRODITE. The 3 last rainfall datasets are bases on stations, and provide land-only rainfall. We use HadISST as SST observations. We also use 7 reanalyses: NCEP-NCAR-I, NCEP-DOE-II, NCEP-CFSR, ERA40, ERAinterim, JRA25, and MERRA.

We analyze 24 CMIP3 and 35 CMIP5 simulations based on the historical simulations (called *20C3M* in CMIP3 and *historical* in CMIP5). The simulations start approximately in 1850 and end approximately in 2000 and 2005 for CMIP3 and CMIP5 respectively. The CMIP3 models and experiments have been widely described in the literature, and more details can be found in Randall et al. (2007). Information regarding CMIP5 institutions and expanded model names is available on http://cmip-pcmdi.llnl.gov/cmip5. Where we present multi-model means information, we first average across ensemble members of a given model, before averaging across the models. We also use a limited number of CMIP5 simulations in a future greenhouse gas and aerosols emission scenario. We use the representative concentration pathway rcp8.5 (Moss et al., 2010). This scenario corresponds to a radiative forcing by approximately 8.5 $W.m^{-2}$ higher in 2100 than during the pre-industrial period. This is the most extreme scenario used to constrain the CMIP5 simulations in the sense that energy and industry CO_2 emissions increase continuously until 2100.

Results

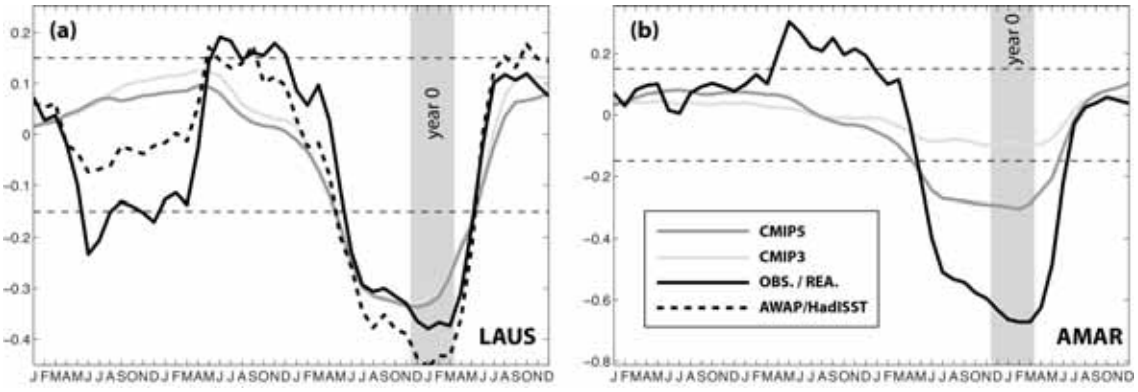

Fig. 1 *(a) Lag correlation between DJFM LAUS at year 0 and lagged monthly NINO34. (b) Same with AMAR instead of LAUS. The multi-observation/reanalyses mean is in solid black, the CMIP5 multi-model mean in dark gray, and the CMIP3 multi-model mean in light gray. The reference dataset for LAUS (i.e. AWAP) is shown in dashed black.*

Concerning LAUS, both the CMIP3 and the CMIP5 simulations show a moderate anti-correlation (-0.3) to NINO34 (Fig. 1-a), i.e. an Australian monsoon occurring during an El Niño event tends to be weaker than normal. This anti-correlation is significant at the 90% level for most of the CMIP3 and CMIP5 models (see upper quartiles), and is slightly under-estimated as compared to long observation time series (r=0.45 for AWAP).

Expanding the region used to define the Australian monsoon, by including the Maritime Continent (land and ocean), we find stronger correlations in the observations, reaching ~0.7 in the multi-observation/reanalysis mean (Fig. 1b). Such strong anti-correlations are generally not reached in CMIP simulations, with a multi-model mean of -0.1 and -0.3 for the CMIP3 and the CMIP5 models respectively (Fig. 1-b). The CMIP5 models thus have better skills to capture the AMAR-ENSO relationship, and more than 25% of CMIP5 models give anti-correlations that reach the range of reanalysis. Looking at the SST response to ENSO (not shown), it is clear that most models that reproduce the observed AMAR-ENSO concomitant anti-correlation also simulate a realistic ENSO pattern along the equator, with a cold anomaly in the climatological warm pool region (i.e. approximately at the location of the Maritime Continent). This result is not surprising for this maritime region where convection is triggered by warm SSTs.

Future projections

Based on the model skill to reproduce the Indo-Pacific monsoon and its link to ENSO (not shown), we select 10 models to analyze change in monsoon rainfall from 1850 to 2100 in the rcp8.5 emission scenario (Fig. 2). A majority of the models do not show any trend in LAUS or AMAR rainfall over the 20th century. At the end of the 21st century, 7 of the 10 models produce 10 to 20% more monsoon rainfall over Australia than at the end of the 19th century. The picture is not so clear over the Maritime Continent, where only 4-5 models produce a significant increase of monsoon rainfall (~10%), and two models produce less rainfall.

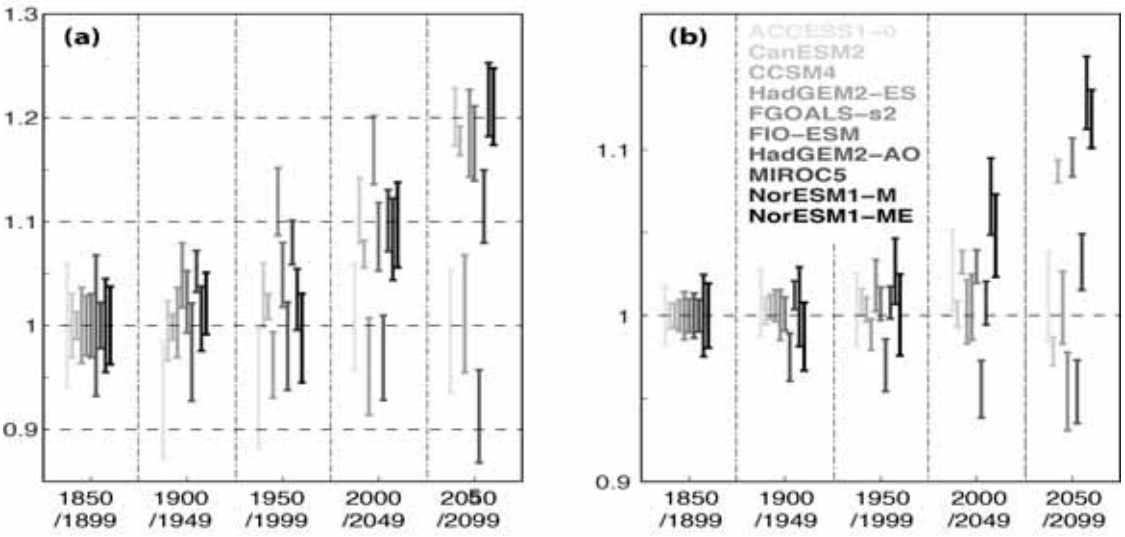

Fig. 2 *Relative increase of 50-year monsoon rainfall (i.e. divided by the 1850-1899 mean) for LAUS (a) and AMAR (b) in 10 CMIP5 models.*

Conclusion

A majority of CMIP5 models are able to approximately represent the part of the Australian monsoon variance that is related to ENSO (20% in the observations). It is not the case over the Maritime Continent. Further investigations suggest that this is partly due to the wrong SST response to ENSO North of Papua-New Guinea, and partly due to mesoscale processes associated with narrow island and mountains in the Maritime Continent.

Acknowledgment

This study was made in the context of the ARC project DP110100601. We acknowledge the World Climate Research Programme's Working Group on Coupled Modelling, which is responsible for CMIP, and we thank the climate modeling groups for producing and making available their model output, observations, or reanalyses. The U.S. Department of Energy's Program for Climate Model Diagnosis and Intercomparison (PCMDI) provided coordinating support and led development of software infrastructure in partnership with the Global Organization for Earth System Science Portals. We thank the Australian National Computational Infrastructure (NCI) for help in the download process.

References

Adler, R., Huffman, G., Chang, A., Ferraro, R., Xie, P., Janowiak, J., Rudolf, B., Schneider, U., Curtis, S., Bolvin, D., et al. (2003). The version 2 global precipitation climatology project (GPCP) monthly precipitation analysis (1979-present). J. Hydrometeorol., 4(6):1147--1167.

Cai, W., Hendon, H. H. and Meyers, G. (2005). Rainfall Teleconnections with Indo-Pacific Variability in the WCRP CMIP3 Models. J. Climate, 18:1449--1468.

Colman, R. A., Moise, A. F. and Hanson, L. I. (2011). Tropical Australian climate and the Australian monsoon as simulated by 23 CMIP3 models. J. Geophys. Res., 116(D10):D10116.

Chao, W. and Chen, B. (2001). The origin of monsoons. J. Atmos. Sci., 58(22):3497--3507.

Holland, G.J. (1986). Interannual variability of the Australian summer monsoon at Darwin: 1952-82. Mon. Wea. Rev., 114(3):594--604.

Moise, A.F., Colman, R.A. and Brown, J.R. (2012). Behind uncertainties in projections of Australian tropical climate: Analysis of 19 CMIP3 models. J. Geophys. Res., 117(D10):D10103.

Neale, R. and Slingo, J. (2003). The maritime continent and its role in the global climate: A GCM study. J. Climate, 16(5):834--848.

Randall, D.A., Wood, R.A., Bony, S., Colman, R., Fichefet, T., Fyfe, J., Kattsov, V., et al. (2007). Cilmate Models and Their Evaluation. In: Climate Change 2007: The Physical Science Basis. Contribution of Working Group I to the Fourth Assessment Report of the Intergovernmental Panel on Climate Change. Cambridge University Press, Cambridge, United Kingdom and New York, NY, USA.

Smith, I.N., Moise, A.F. and Colman, R.A. (2012). Large-scale circulation features in the tropical western Pacific and their representation in climate models. J. Geophys. Res., 117(D4):D04109.

Yano, J.I. and McBride, J L. (1998). An aquaplanet monsoon. J. Atmos. Sci., 55(8):1373--1399.

INTRASEASONAL VARIABILITY OF THE AUSTRALASIAN MONSOON

Matthew Wheeler and John McBride

Centre for Australian Weather and Climate Research,
Bureau of Meteorology, Melbourne, Victoria, Australia

Introduction

This presentation will focus on material contained in our recently revised book chapter Wheeler and McBride (2011). This book chapter describes the intraseasonal climate and weather variability of the ‘‘Australasian monsoon’’ region comprising northern Australia, Indonesia, New Guinea, the surrounding seas, and the near equatorial southwest Pacific. The chapter includes a summary of existing published work on intraseasonal variability (ISV) as well as some new calculations to fill in what we felt were the main knowledge gaps. The full text and figures of the chapter are available from http://cawcr.gov.au/staff/mwheeler/abstracts/ISVbook.WM11.pdf. The topics covered in the chapter are: the seasonal cycle of the background flow; broadband intraseasonal behaviour (bursts and breaks); broadband intraseasonal behaviour (spectral analysis); meteorology of the bursts and breaks; characteristics and influence of the Madden-Julian oscillation (MJO); 1983/1984 and 1987/1988 case studies; MJO influence on monsoon onset; other modes and sources of ISV; modulation of tropical cyclones; extratropical-tropical interaction; and, prediction. Below we provide some of the key figures followed by the conclusions in full.

Review and Results

Fig. 1 provides an indication of the importance of ISV relative to the seasonal cycle and interannual variability. The amplitude of ISV is as high or higher than that of these other frequency bands, and almost all occurrences of monsoon onset align with an intraseasonal event.

Fig. 2 shows the strong coherence between convection (OLR or rain) and wind in the intraseasonal frequency range. The near 180° phase relationship between OLR and wind indicates that on the intraseasonal time scale (like for the seasonal time scale), enhanced convection occurs simultaneously with westerly wind anomalies.

The most important source of ISV in the Australasian monsoon is the MJO. Fig. 3 demonstrates the average impact of the MJO on rainfall and circulation in the region during summer. Fig. 4 shows that the association of the MJO with the monsoon varies greatly each year. For example, in 1987/88 we estimate that 58% of the intraseasonal variation of the monsoon was associated with the MJO, but the value was only 9% for 1982/83. Fig.5 shows the relationship between the MJO and monsoon onset. Monsoon onset occurs preferentially in the half cycle of the MJO defined by Phases 4-7 of the Wheeler-Hendon Realtime Multivariate (RMM) index.

Fig. 6 shows the composite structure of perhaps the next most important mode of ISV in the region; the n=1 equatorial Rossby wave. It is characterised by westward propagation of circulation cells on either side of the equator.

Finally, Fig. 7 demonstrates the relationship between the MJO and tropical cyclones (TCs). Over the Indian Ocean the modulation is as strong as 4 to 1. That is, a TC is about 4 times more likely to occur during the favourable phases of the MJO (Phases 2, 3, and 4) compared to the un-favourable MJO

phases (Phases 7, 8, and 1). This modulation has been exploited for multi-week TC activity prediction by Leroy and Wheeler (2008).

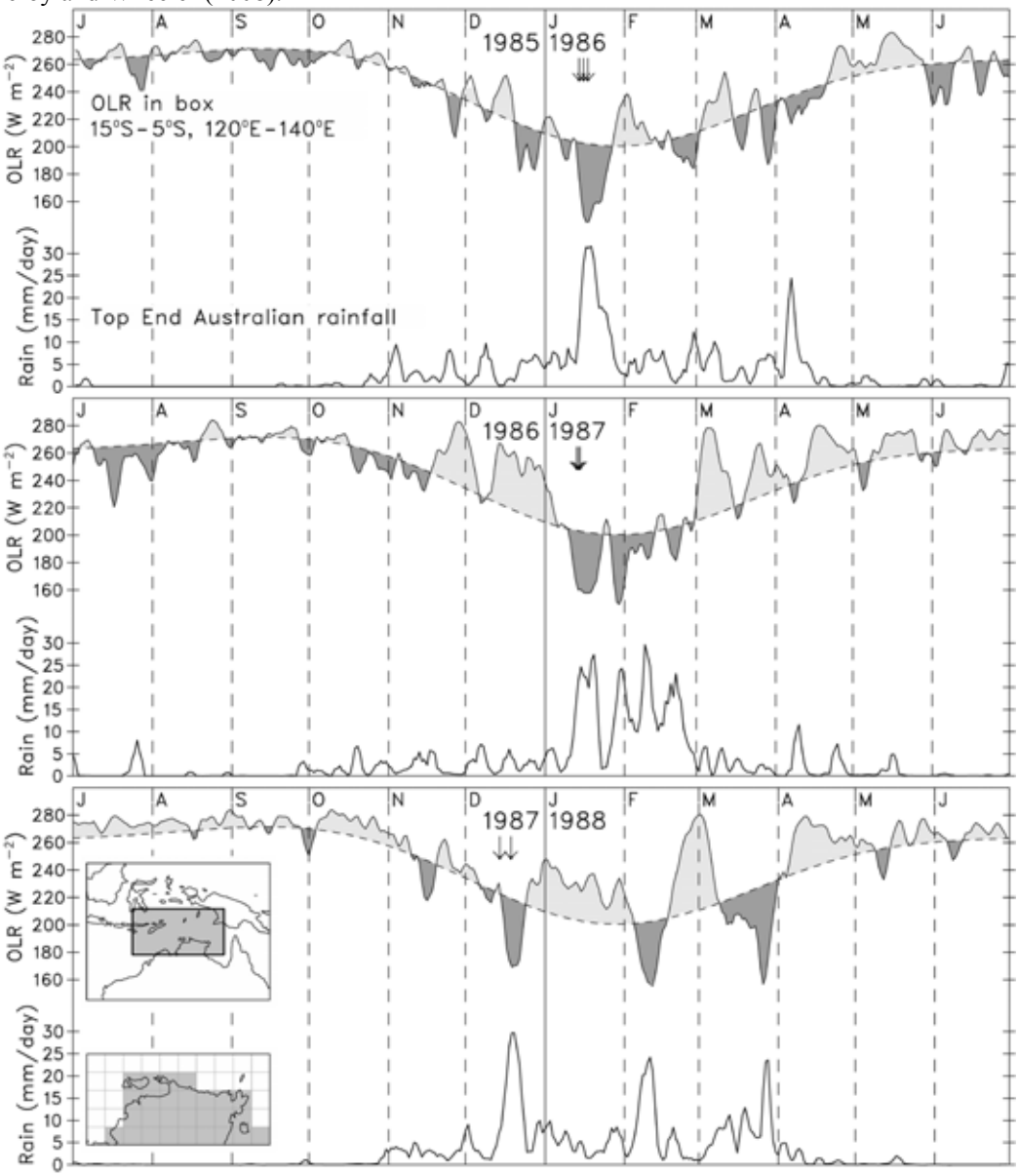

Fig. 1. *Intrinsic intraseasonal structure of the monsoon as revealed by a 3-day running mean time series of NOAA satellite-observed OLR, averaged for the box 15°S to 5°S and 120°E to 140°E, and Australian "Top End" rainfall, averaged for all available Australian Northern Territory stations north of 15°S. Dashed line (for the OLR) shows the climatological seasonal cycle created by taking the mean and first three harmonics of the 1979 to 2001 climatology. Dark/light shading (for the OLR) are indicative of times of anomalously active/inactive convection. Also shown, by arrows above the OLR curve, are the monsoon onset dates as defined by Hendon and Liebmann (1990a), Drosdowsky (1996), and Hung and Yanai (2004). Key maps for the areas used for the OLR and rainfall are shown on the bottom left.*

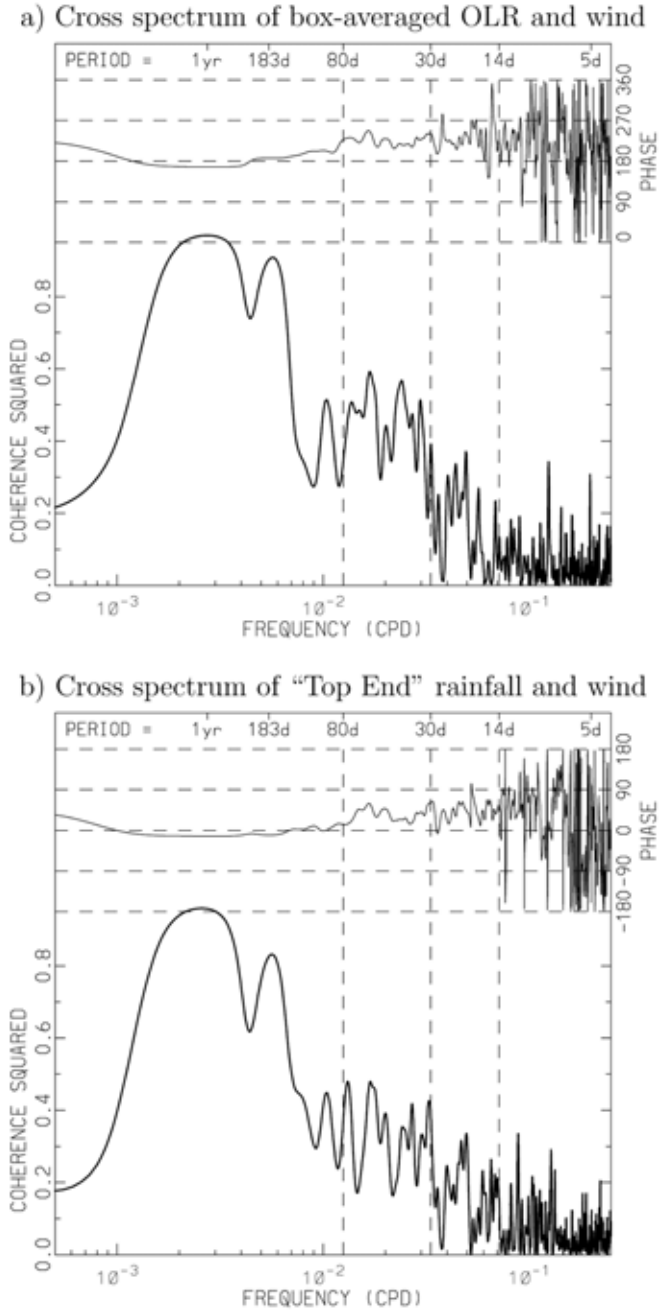

Fig. 2. *(a) Coherence-squared and phase between multi-year time series (using all days of the year) of OLR and 850-hPa zonal wind both averaged for the box 15°S to 5°S and 120°E to 140°E (same box as in Fig.1). Multiple passes of a 1-2-1 filter were applied to the co- and quadrature-spectra before computing the phase and coherence resulting in an effective bandwidth of 2.5x10^{-3} cpd. A 90° phase relationship means that OLR is leading the wind by a quarter cycle. (b) As in (a), except between "Top End" averaged rainfall (see box in Fig.1) and 850-hPa zonal wind averaged over the box 15°S to 10°S and 130°E to 135°E.*

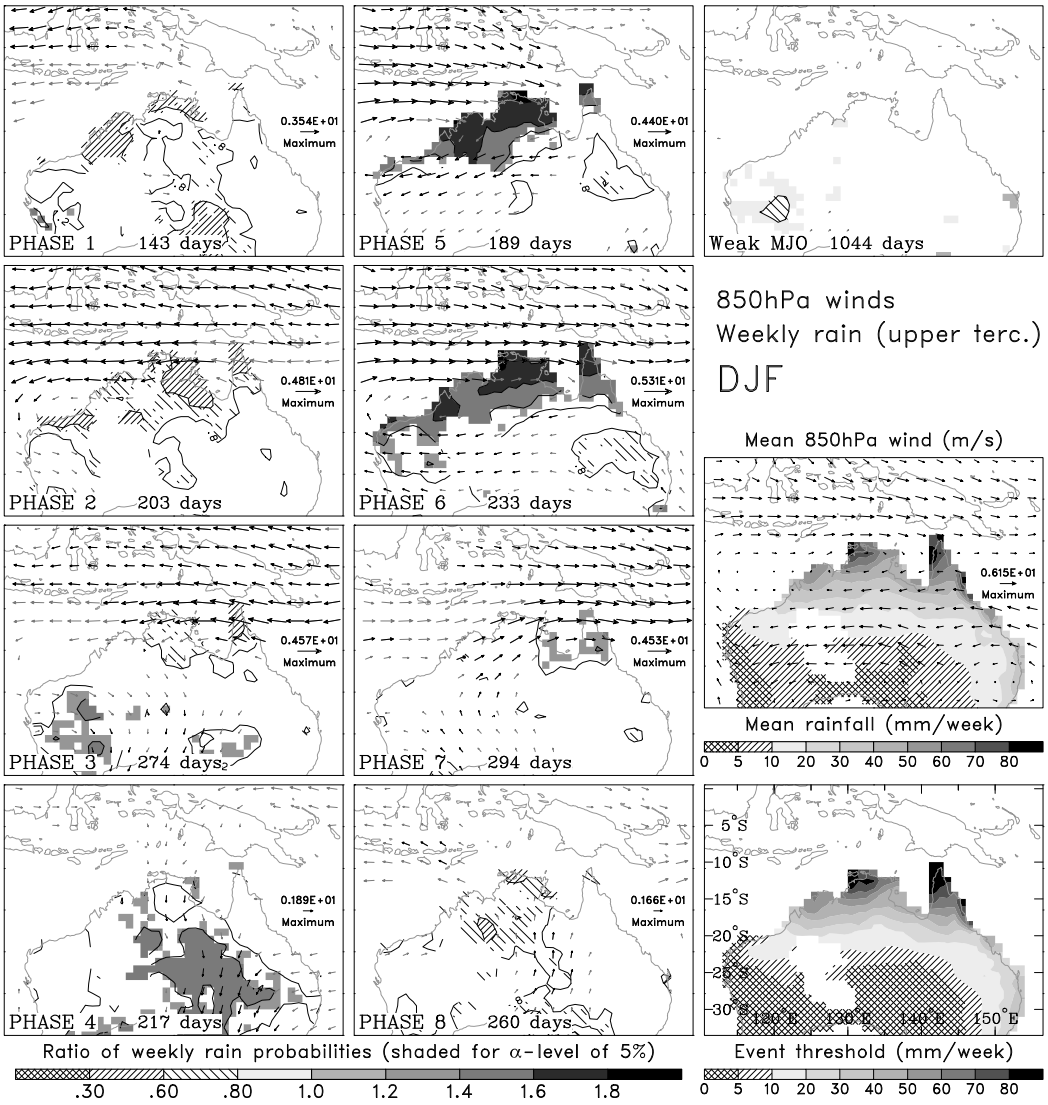

Fig. 3. *Left and middle columns: MJO composites of weekly rainfall probabilities (contours and shading, available over Australia only) and 850-hPa wind anomalies (vectors, available over entire domain) for the December-January-February (DJF) season. Rainfall probabilities refer to the chance of weekly rainfall exceeding the upper tercile, expressed as a ratio with the mean probability (nominally 33%). Contour levels are provided in the key with the 1.0 contour ommitted. Shading/hatching varies with each contour, but is only provided where the signal is determined to be locally significant at the 5% level. For the winds, black vectors are determined to be significant at the 5% level, and grey vectors at the 20% level, with the magnitude of the maximum vector in each panel provided; Top-right panel: as above, except for the Weak MJO category; Mid-right panel: climatological DJF mean winds (vectors) and mean rainfall (shading). The vector length in the mean plot is scaled to be exactly half that of the vectors in the MJO composite plots; Bottom-right panel: threshold for an upper tercile weekly rainfall event. Adapted from Wheeler et al. (2009).*

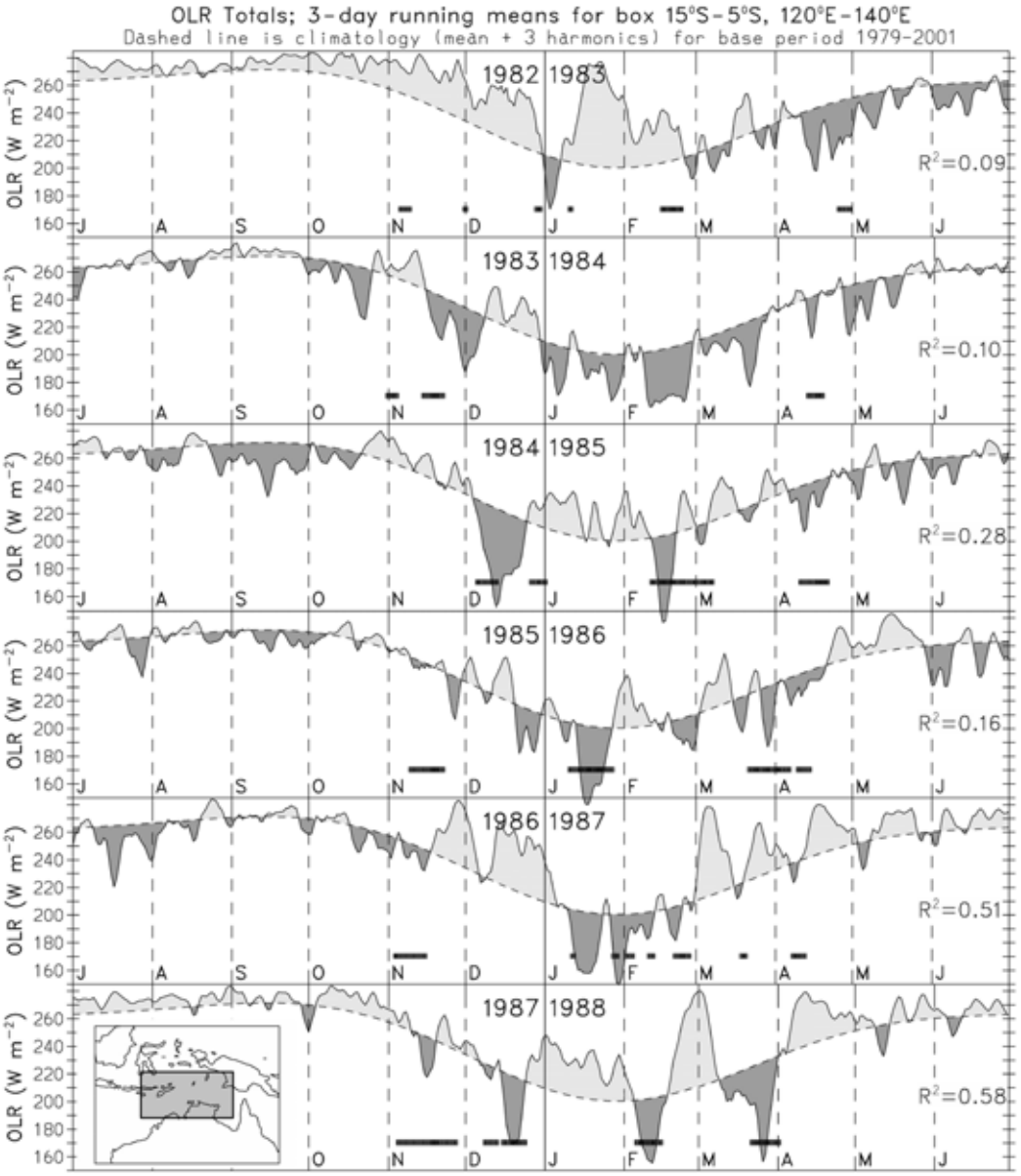

Fig.4. *As in Fig. 1, except showing OLR series only and showing a solid bar when the phase of the MJO, as defined by the Wheeler-Hendon (2004) Real-time Multivariate MJO (RMM) index, was in either Phase 4, 5, or 6, for the months of November through April only. Also given are the squares of the multiple correlation coefficients between the OLR anomaly time series and the RMM1 and RMM2 values calculated for the November through April months.*

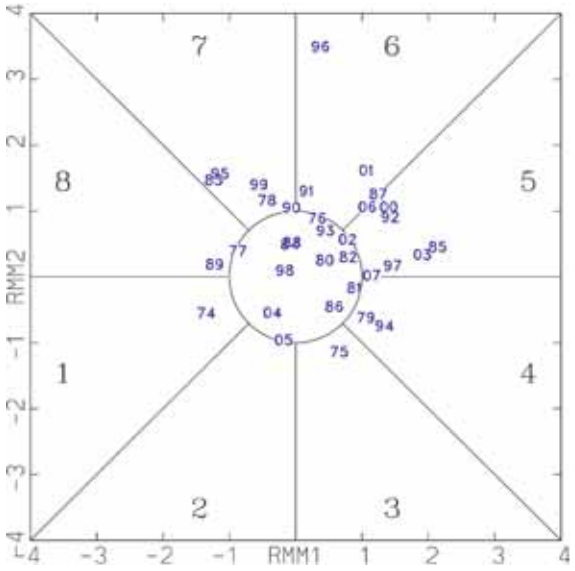

Fig. 5. *(RMM1,RMM2) phase space points (as marked by the double-digit numbers) for the days on which the monsoon was defined to onset, based on the daily deep-layer mean zonal wind, at Darwin, Australia. The number plotted refers to the monsoon year, being that of the nearest December. The monsoon dates are defined and taken (with updates) from Drosdowsky (1996), covering all wet seasons from 1974/75 to 2007/08.*

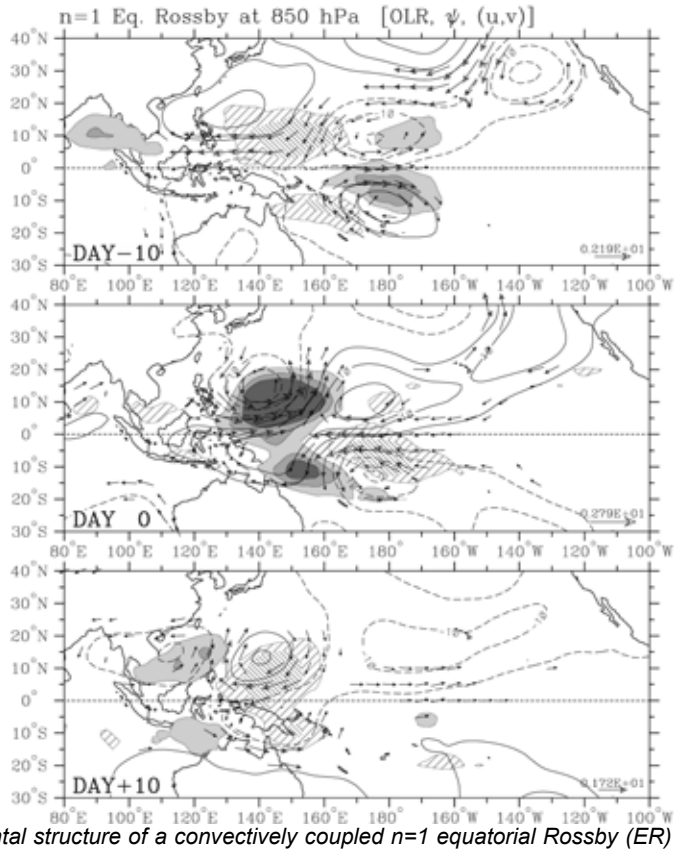

Fig. 6. *Typical horizontal structure of a convectively coupled n=1 equatorial Rossby (ER) wave over a sequence spanning 21 days, as computed using lagged regression based on a two standard deviation anomaly in the ER wave filtered OLR series at 10^{o}S, 150^{o}E. Shading/cross-hatching show the negative/positive OLR anomalies at the levels of -15, -10, -5, 5, and 10 W m^{-2}. Contours are streamfunction at the 850 hPa level, having an interval of 5×10^{5} m^{2} s^{-1}, with negative contours dashed and the zero contour omitted. Vectors are the 850-Pa wind anomalies, plotted only where the local correlation of either wind component is statistically significant at the 99% level. [Reproduced from Wheeler et al. (2000).]*

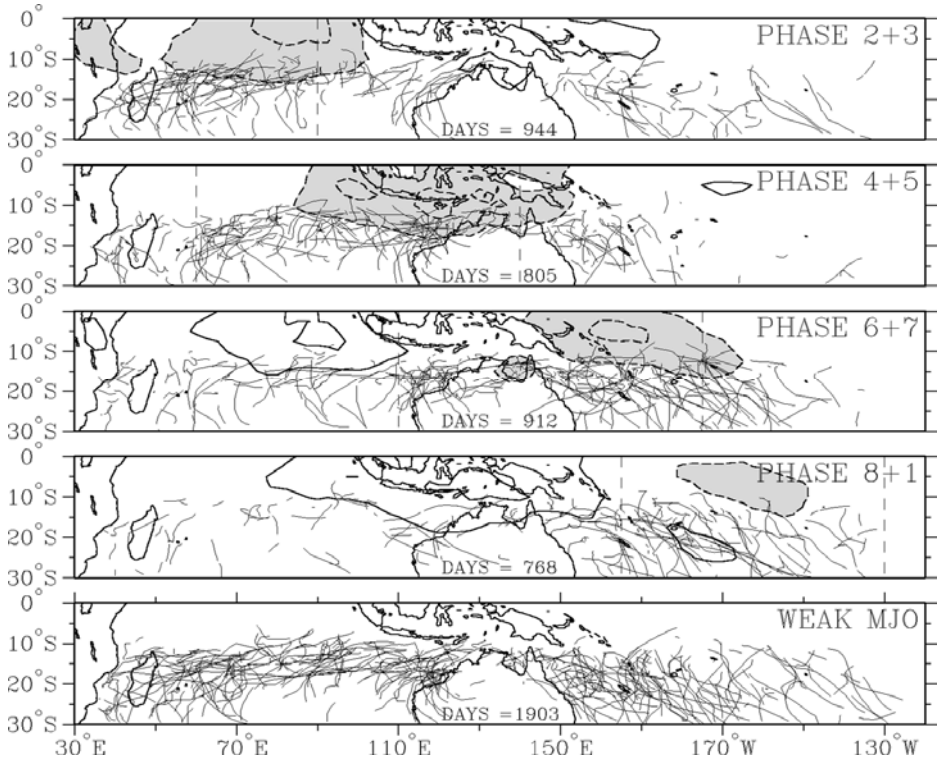

Fig. 7. *Tropical cyclone (TC) tracks (defined using a threshold of estimated central pressure of 995 hPa) stratified according to the phase of the MJO as described by the RMM index of Wheeler and Hendon (2004). November through April data used for years from 1974 to 2003. "Weak MJO" refers to days when the amplitude of the (RMM1,RMM2) vector is less than 1.0. The number of days counted within each of the MJO categories is provided. Also shown (with contours and shading) is the composite OLR anomaly for the corresponding MJO phases: Contour interval is 10Wm^{-2}, with negative contours dashed, the zero contour omitted, and values less than -10Wm^{-2} shaded.*

Conclusions

Based on our review of the literature and additional analysis, the following key points can be made:

1) Compared to other frequency bands, to the seasonal cycle, and to other regions of the globe, the intraseasonal frequency range has large amplitude in the Australasian monsoon. Consequently, the presence of ISV appears necessary for many of the defining characteristics of the monsoon, for example, the monsoon's sudden onset, its breaks, and deep westerly bursts.

2) Frequency-only power spectra of most monsoon parameters (excluding rainfall) show a robust signature of the MJO, but are otherwise predominantly 'red', with no spectral gap between intraseasonal and higher frequencies with which to distinguish them. There is, however, high coherence between monsoon parameters (e.g. zonal wind versus rain) at intraseasonal scales, particularly beyond a period of 20 days which is not seen at higher frequencies. This high coherence provides a dynamical distinction for the intraseasonal frequency range.

3) The phase of the zonal wind versus rain cross-spectra demonstrates the similarity in structure between the seasonal cycle and ISV. That is, both frequency bands share the useful, and traditional, concept of a two-state system: viz. wet-westerlies versus dry-easterlies. This disappears at higher frequencies and provides a further point of distinction for the intraseasonal frequency range.

4) Convection studies over northern Australia have revealed that while the large-scale monsoon bursts involve more rain, the individual convective cells within the bursts are generally less intense than their counterparts in the breaks.

5) The MJO is the strongest mode of ISV within the Australasian region, with a discernible impact on many aspects of the monsoon. For rainfall, the greatest MJO-associated anomalies occur over far northern Australia and the seas to its north, with new research showing a relatively smaller signal over the islands of Sumatra, Borneo, Java, Sulawesi, and New Guinea owing to the complications of topography and the diurnal cycle.

6) Using the framework of the Wheeler-Hendon (RMM1, RMM2) measure of the MJO, the influence of the MJO on the ISV can be quantified. The case studies of the 1983/84 and 1987/88 summers reveal large differences. The 1987/88 season was characterized by three large amplitude intraseasonal events which corresponded to cycles of the MJO. In contrast the 1983/84 summer had a similar level of ISV activity, but with no strong MJO signal.

7) There have been a number of studies of the influence of the MJO on monsoon onset with conclusions ranging from "no MJO influence" to "a one-to-one correspondence with MJO passage". We discuss the methodologies of each of these. Using the (RMM1, RMM2) framework we show onset almost always occurs across Wheeler-Hendon Phases 4-7, which can be interpreted as the locally-active half of the MJO cycle. Thus it appears that while the planetary-scaled MJO is limiting monsoon onset to be within its active half-cycle lasting for a few weeks, the actual day of onset is set by other, shorter timescale phenomena.

8) Other well-defined modes of ISV also exist and have an impact in the region. Of particular note are the convectively-coupled Kelvin and n=1 ER waves, both of which can be identified in plots of total fields in some illustrative cases. Many cases of the sometimes westward propagation of large-scale convection over the region can be identified with ER waves.

9) Besides that accounted for by the above-mentioned modes of tropical ISV, there is still much variance in the intraseasonal band. Given its close correspondence to the red spectrum of a lag-1 autoregressive model, some of this variance appears best described as simply a consequence of the continuum of scales from 'weather' to 'climate'. An isolated TC, for example, given its large amplitude, will project significantly onto the intraseasonal frequencies.

10) The intrusion of disturbances and energy from the extratropics is yet another source of ISV in the Australasian monsoon. Likewise, there is an influence of the region's tropical ISV on the extratropics.

11) The intraseasonal modulation of TCs provides an interesting avenue for our dynamical understanding and application for extended-range TC forecasts.

12) The increased understanding of ISV in the Australasian monsoon has led to a new era of application work focusing on ISV prediction, with many ISV prediction products now available.

References

Drosdowsky, W. 1996. Variability of the Australian summer monsoon at Darwin: 1957- 1992. *J. Climate*, 9, 85-96.

Hendon, H.H. and Liebmann, B.1990a. A composite study of onset of the Australian summer monsoon. *J. Atmos. Sci*., 47, 2227-2240.

Hung, C.-W. and Yanai, M. 2004. Factors contributing to the onset of the Australian summer monsoon. *Quart. J. Roy. Meteor. Soc*., 130, 739-758.

Leroy, A. and Wheeler, M.C. 2008. Statistical prediction of weekly tropical cyclone activity in the Southern Hemisphere. *Mon. Wea. Rev.*, 136, 3637-3654.

Wheeler, M.C. and Hendon, H.H. 2004. An all-season real-time multivariate MJO index: Development of an index for monitoring and prediction. *Mon. Wea. Rev.*, 132, 1917-1932.

Wheeler, M.C., Hendon, H.H., Cleland, S., Meinke, H. and Donald, A. 2009. Impacts of the Madden-Julian oscillation on Australian rainfall and circulation. *J. Climate*, 22, 1482-1498.

Wheeler, M., Kiladis, G.N. and Webster, P.J. 2000. Large-scale dynamical fields associated with convectively coupled equatorial waves. *J. Atmos. Sci.*, 57, 613-640.

Wheeler, M.C. and McBride, J.L. 2011. Australasian monsoon. In: W.K.M. Lau and D.E. Waliser (eds), *Intraseasonal Variability in the Atmosphere-Ocean Climate System* (2nd edition). Springer, pages 147-198.

VARIATIONS OF MJO ACTIVITY AND THE AUSTRALIAN SUMMER MONSOON IN OBSERVATIONS AND SIMULATIONS WITH ECHAM6

Jonathan Schubert[1] Harry H. Hendon[2] Christian Jakob[1]

Monash University[1], Melbourne Vic
Centre for Australian Weather and Climate Research[2], Melbourne Vic.

Introduction

Interannual variations of global MJO activity, as measured for instance by the mean variance of the Wheeler and Hendon (2004) MJO index, are of interest because of their possible role for variations of the Australian summer monsoon rainfall. For instance, Hendon et al. (1999) showed that years of strong global MJO activity tended to be years of below normal summer monsoon rainfall, although cause and effect were not elucidated. Nonetheless, because MJO activity appears to not be strongly related to ENSO or other tropical SST variations (see also Slingo et al. 1999), variability of the MJO would appear to be a source of unpredictability of the Australian summer monsoon.

The purpose of the present study is to investigate the robustness of these earlier studies using longer data records and a more subjective index of MJO activity (i.e. Wheeler and Hendon 2004). Furthermore many of models used to explore MJO variability in these earlier studies were extremely deficient in the simulation of the MJO (e.g. Slingo et al. 1996). Thus, we will also explore the reproducibility of MJO activity in an ensemble of AMIP-simulations using the ECHAM6 LR (T63L47) model, which is generally regarded as having an above average simulation of the MJO. We will further explore the sensitivity of MJO activity to mean state variations in tropical SST and convection using the coupled runs based on ECHAM6 (i.e., the MPI--ESM). Finally, we will make inferences about changes of MJO activity in a future climate by examining the behaviour in the 4xCO2 run of the MPI-ESM.

Data

MJO activity is diagnosed using OLR and winds from NCEP reanalyses. SST is monitored with the Reynolds OI analyses. Observed data covers the period 1979-2008, which is also the period for which we have the three member ensemble of the AMIP integrations from ECHAM6. The historical run from the coupled version of ECHAM6 (MPI-ESM) spans 1850-2000. To be compatible with the observed and AMIP records, we use three 30-years periods from the last 90 years of the run. Similarly, the 4xCO2 runs from MPI-ESM span 150 years, but here we sample behaviour in three 30-year segments.

The capability of the ECHAM models to simulate the MJO is summarized by the east-west ratio of the power in the MJO time and space scales (zonal wavenumbers 1-3 with periods 30-90d). The observed ratios for OLR and U850 are 3.0 and 3.9, respectively. For the AMIP runs, the ratios are 1.6 and 1.8, for the historical runs they are 1.9 and 1.8, and for the 4xCO2 run they are 2.4 and 2.6. In summary, the uncoupled model simulates a modestly realistic spectral peak in the MJO band. Coupling improves the simulation slightly. Interestingly, the best simulation of the MJO is produced in the 4xCO2 run. We speculate that this increased MJO activity in the 4xCO2 run is due to the mean state change in that run, whereby relatively stronger SST warming in the equatorial eastern Pacific promotes an expanded "warm pool" upon which the MJO can develop and propagate.

Interannual Variations of the MJO and the Monsoon

Hereafter, we diagnose MJO activity following Wheeler and Hendon (2004). We define the MJO index (MJOI) as the mean value over the austral summer season of the sum of the squares of PC1 and PC2 from the EOF analysis of combined fields of OLR, U850 and U200. The MJO index was computed separately for observations and for each model run. Note that we use intraseasonally filtered input data, in contrast to Wheeler and Hendon (2004) who used minimal time-filtering.

We assess the relationship of MJO activity with SST variations associated with ENSO by correlation of the MJOI averaged over the Nov-Mar season with Nino3 SST. For observation this correlation is ~-0.2 (ie higher activity is favored by La Nina condition) where as in the AMIP and historical runs the correlation is 0.14 and 0.16, respectively, suggesting that El Nino promotes stronger MJO activity in the ECHAM models. However, these correlations are weak, and the general conclusion is that MJO variability is largely independent of ENSO.
This apparent lack of reproducibility of year-to-year variations MJO activity in the AMIP runs is confirmed by an estimate of the SST-forced variability, which is the ratio of the variance of the ensemble mean MJOI to the total variance of the MJOI. This ratio for the three-member AMIP run is less than 10%, confirming that the variability of MJO activity is largely unrelated to imposed boundary forcing by tropical SST.

Although the seasonal mean MJO activity appears to be largely unrelated to SST variations, the variability is associated with mean state changes of convection. We demonstrate this by regressing seasonal mean anomalies of SST and OLR onto the MJOI. The results for observations and the three model runs are shown in Fig. 1. For observations, enhanced MJO variability occurs in years when enhanced convection occurs in the western Pacific and is suppressed over the Australian summer monsoon, confirming the earlier results of Hendon et al. (1999). The weak association with La Nina is seen in the SST anomaly, although the SST anomalies are not deemed to be significant. The interpretation of this result is that MJO activity is favored by an eastward extension of mean convection from the western Pacific into the central Pacific and a decreased of convection in the off-equatorial Australian summer monsoon, thereby promoting the eastward propagation of he MJO along the equator.

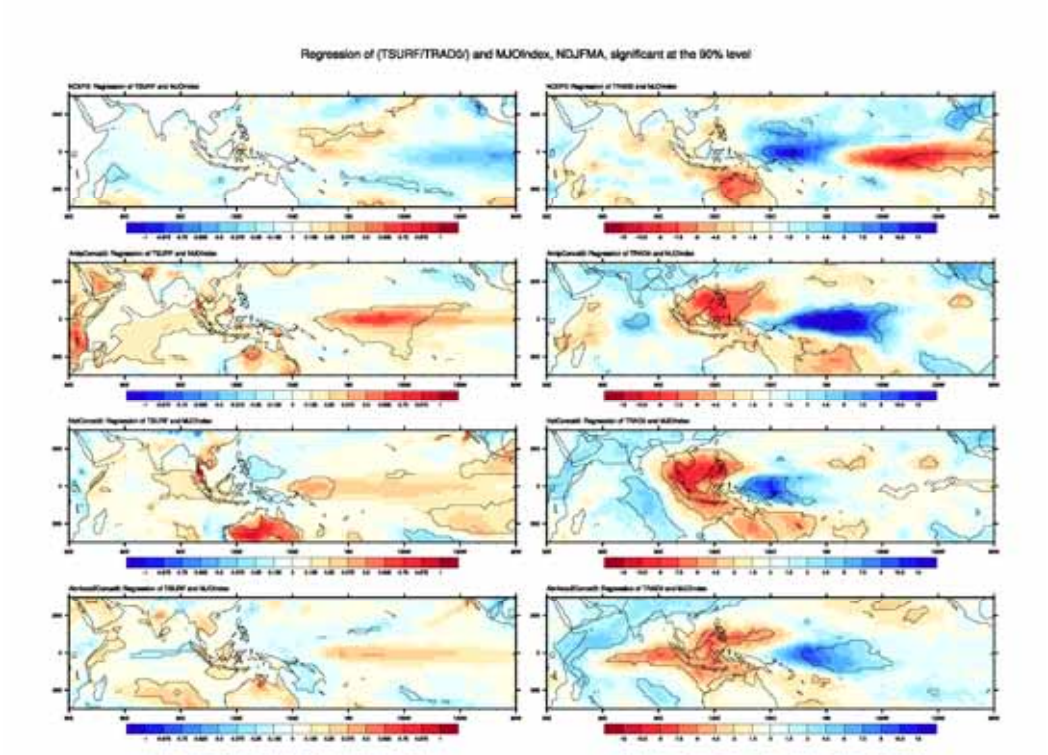

Fig. 1 *Regression of seasonal mean (Nov-Mar) anomalies of SST (left column, deg C) and OLR (right column, W/m2; note scale is inverted) onto the MJOI. Anomalies are scaled for a 1 standard deviation of the MJOI. Significant anomalies at the 90% level are encircled by the solid contours. Top row is observations. Second row is AMIP run. Third row is coupled historical run. Bottom row is 4xCO2 run.*

The AMIP run shows a somewhat similar pattern of anomalous mean state convection (second row of Fig. 1), but the region of enhanced convection is shifted further east in the Pacific. The SST anomaly that promotes this shift in mean convection is more akin to El Nino rather than La Nina, which appears to be a fundamental bias of the uncoupled model. In the coupled run, the pattern of anomalous convection associated with enhanced MJO variability is more similar to the observed than in the AMIP run. Interestingly, the interannual variability of the MJO in the 4xCO2 run is also associated with a shift of mean convection further into the central Pacific as in the AMIP run. However, this sensitivity in the 4xCO2 run probably reflects the mean-state change due to the response to CO2 so that the anomalous MJO behaviour is operating on a mean state that has convection shifted into the central Pacific.

Conclusion

Interannual variations of the MJO activity are shown to be weakly related to SST variations in both observations and model simulations. However, in the model runs enhanced MJO activity is promoted by an El Nino-like conditions where as in observations MJO activity is promoted by La Nina like conditions. In both model and observed, the MJO is promoted by an eastward expansion of the warm pool convection, although we can not determine cause and effect but clearly the mechanism for this to happen is different in the model and observations. In both the coupled run and the observations, enhanced MJO activity is associated with decreased Australian monsoon rainfall, which confirms earlier studies and emphasizes the role of the MJO for promoting unpredictability of summer monsoon rainfall. In the 4xCO2 run, this relationship of increased MJO activity with decreased summer monsoon convection disappears, presumably because the mean state change in the 4xCO2 run acts to shift the mean MJO activity into the central Pacific, thereby de-sensitizing the simulated variations MJO to convection in the monsoon.

References

Hendon, H.H., Zhang, C. and Glick, J.D. 1999: Interannual variation of the MJO during austral summer. J. Clim., 12 , 2538-2550.

Slingo, J.M. and Coauthors, 1996: Intraseasonal oscillations in 15 atmospheric general circulation models: Results from an AMIP diagnostic subproject. Climate Dyn., 12, 325-357.

Slingo, J.M., Rowell, D.P., Sperber, K.R. and Nortley, F.1999: On the predictability of the interannual behaviour of the Madden-Julian Oscillation and its relationship with El Niño. Quart. J. Roy. Meteor. Soc., 125, 583-609.

Stevens, B. and co-authors, 2012: The atmospheric component of the MPI-M Earth System Model: ECHAM6. J. Geophys. Res. (in press).

Wheeler, M.C. and Hendon, H.H. 2004: An all season real-time multivariate MJO index: Development of an Index for monitoring and prediction. Mon. Wea. Rev., 132, 1917-1932.

AN UNPRECEDENTED INTRASEASONAL LEEUWIN CURRENT WARMING EVENT IN FEBRUARY-MARCH 2011

Ming Feng[1], Michael McPhaden[2], Shang-Ping Xie[3], Jan Hafner[3]*

[1]CSIRO Marine and Atmospheric Research, Underwood Avenue, Floreat 6014 Western Australia, Australia

[2]Pacific Marine Environmental Laboratory, NOAA, USA

[3]University of Hawaii, Honolulu, Hawaii, USA

At the climax of the 2010-2011 *La Niña*, the Leeuwin Current, a poleward flowing eastern boundary current off the west coast of Australia, was unseasonably strong and transported anomalous amount of warm water southward along the coast, increasing the upper ocean heat content (sea level) and causing unprecedented sea surface temperature anomalies of more than four times the typical interannual variations in February – March 2011. The unseasonable occurrence of the Leeuwin Current was forced by easterly wind anomalies in the equatorial western Pacific through oceanic teleconnection, as well as by low sea level pressure anomalies off the west coast of Australia through atmospheric teleconnection of the *La Niña* condition in the Pacific.

Both satellite and shelf mooring observations revealed that peak surface temperatures of 27-29°C, 5°C warmer than its summer climatology, occurred off the mid west coast of Australia during a 2-week period in late February – early March 2011. This peak warming event had caused widespread coral bleaching and fish kills, as well as other ecological implications. The peak warming appeared to be induced by an intraseasonal variation of alongshore winds off the west coast of Australia. The alongshore wind anomalies not only caused the surge of the Leeuwin Current transport, but also reduced the latent heat release in the region, both contributing to the peak of the warming event.

IMPACT OF THE MJO ON THE WA MARINE ENVIRONMENT DURING THE MONSOON

Andrew G. Marshall and Harry H. Hendon

Centre for Australian Weather and Climate Research, Bureau of Meteorology, Melbourne, VIC, Australia

Introduction

The near-equatorial surface westerly wind anomalies produced by the Madden-Julian Oscillation (MJO) generate downwelling Kelvin waves and upwelling Rossby waves that propagate along the equator in the Pacific and Indian oceans. Upon reaching the eastern Indian Ocean boundary, a component of the downwelling equatorial Kelvin waves becomes coastally trapped and propagates south-eastward along the Sumatra and Java coasts towards northern Australia; it has been suggested that these coastal waves may appear down the Western Australian (WA) coast within a few weeks after their generation in the Indian Ocean, thereby modulating the southward flowing Leeuwin Current that is trapped along the WA coast. However, the gaps in the island chains south of Java suggest that a direct transmission of the Kelvin wave is unlikely. Here we explore intra-seasonal variations in sea surface height and surface current along the WA coast to better understand how the MJO signal in currents, SST, and sea level gets onto the west Australian coast. Understanding the impact of intra-seasonal variability on the WA marine environment is important for fisheries and other marine ecosystems that are sensitive to the variations in mixing, temperature and transport by the Leeuwin current.

Model and Data Description

The primary data used in this study are the daily upper ocean analyses provided by the POAMA (Predictive Ocean Atmosphere Model for Australia) Ensemble Ocean Data Assimilation System (PEODAS) (Yin et al. 2011) for the period 1980-2010. The horizontal resolution of the PEODAS analysis is 0.5 degree latitude by 2 degree longitude. In order to detect the finer detail of variations in currents and sea surface height along the WA coast we use data from the Bluelink reanalysis (BRAN) version 2.1 (0.1 degree horizontal grid) available for 1992-2006, derived from an integration of the Ocean Forecasting Australia Model that assimilates observations using the Bluelink Ocean Data Assimilation System (Oke et al. 2008).

For monitoring sea level variations associated with the Leeuwin Current, we use the daily record of GLOSS/CLIVAR sea level observations at Fremantle, on the south west coast of Australia (115.73°E, 32.05°S), obtained from the University of Hawaii Sea Level Center for the period 1985-2009. We also make use of daily 850hPa wind data from the NCEP/NCAR global reanalysis 1 for 1980-2010 (Kalnay et al. 1996) and SST data from the high resolution (0.25 degree grid) Reynolds OI AVHRR analysis, available for 1982-2010. For all data we calculate anomalies relative to the annual climatology based on each available period.

The state of the MJO is depicted using the Real-time Multivariate MJO (RMM) index, which captures the large-scale structure of the MJO in zonal wind and convection along the equator (Wheeler and Hendon 2004). Here we use the same 8 phases as defined by Wheeler and Hendon (2004), with the MJO deemed to be in an active cycle when the RMM index amplitude is greater than 1.5 standard deviations. We also focus on the November-April extended austral summer period when the MJO is strongest and shifted into the Southern Hemisphere, and thus when the MJO is most likely to influence intra-seasonal variability on the WA coast.

Impact of the MJO on the Indian Ocean and NW Australian shelf

A direct impact of the MJO circulation on the surface of the Indian Ocean is via the surface heat flux anomalies, which we show as composites for the MJO over phases 2, 4, 6 and 8 (left hand column Fig. 1). Heat flux anomalies in the central part of the basin are in quadrature with zonal wind stress anomalies (not shown), thus suggesting a primary role of the surface shortwave radiation variation by the MJO convection for producing the surface heat flux variation there. Focusing on the northwest (NW) shelf of Australia, the variation in anomalous heat flux acts to heat the surface in phases 8, 1 and 2; this is due primarily to increased insolation during the suppressed convective phase of the MJO. Associated with this positive heat flux anomaly into the ocean are subsequent positive peaks in SST at about a ¼ of a cycle later (phases 1-4; middle column). One half cycle later, the converse evolution of surface heat flux (cooling) and development of negative SST anomalies on the NW shelf can be clearly seen.

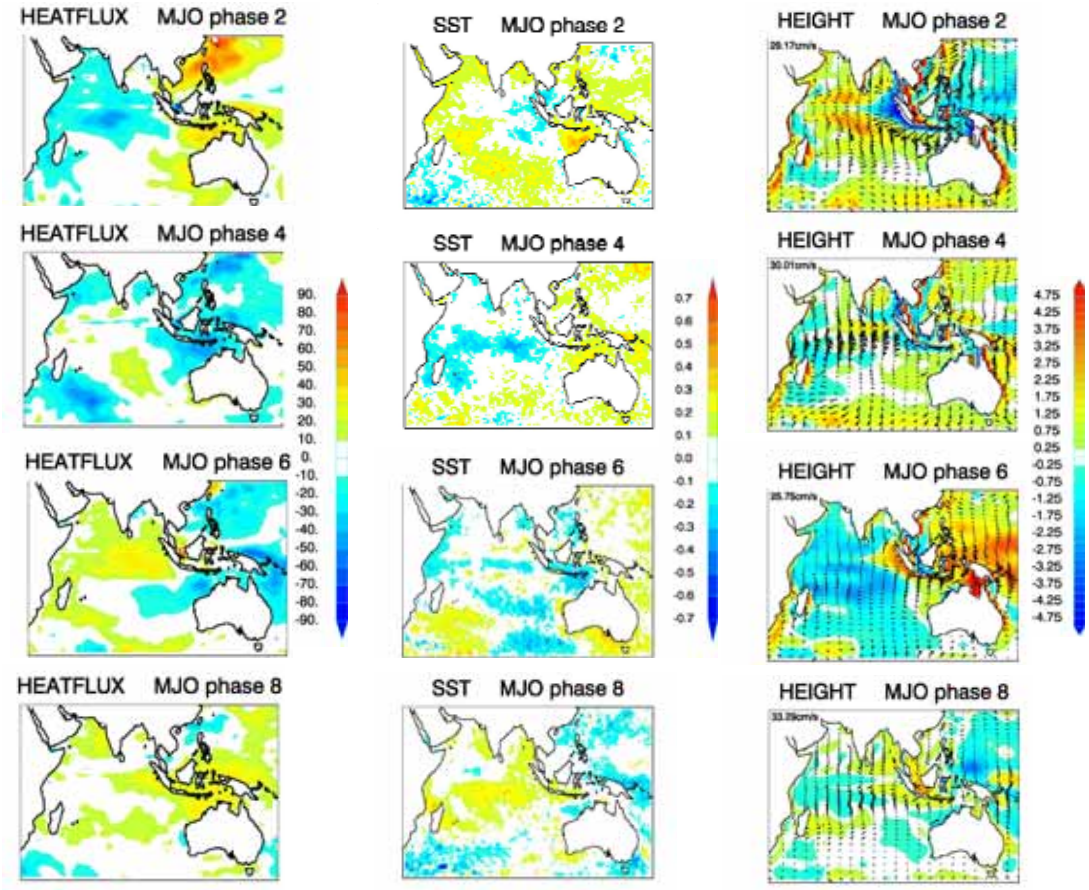

***Fig. 1**: Composite total heat flux (left column; W/m^2), SST (middle column; K) and sea surface height (right column; cm) anomalies for phases 2, 4, 6 and 8 of the MJO over the November-April season. Surface current anomaly vectors are also plotted (right column; cm/sec) and scaled by the sine of latitude; the magnitude of the strongest equatorial current anomaly is printed in the upper left corner of each panel.*

The evolution of the dynamical response of the upper ocean is explored using composite sea surface height and current anomalies (Figure 1, right column). Ekman transport acts in response to the MJO wind stress forcing in the tropics, with surface current anomalies diverging away from the equator in phases 8, 1 and 2 in association with the MJO easterly anomalies. Conversely, when MJO westerlies occur over the Indian Ocean one half cycle later, the surface current anomalies are seen to converge on the equator (phases 4-6). This results in positive surface height anomalies in a narrow strip along

the equator that are carried eastward as a downwelling Kelvin wave and arrive at the eastern Indian Ocean boundary by phase 6. As the MJO continues to evolve in its lifecycle through phases 6-8, a component of the downwelling equatorial Kelvin waves becomes coastally trapped and propagates southeast along the Indonesian coastline, raising the sea surface height there. However, there is no evidence that these coastally trapped Kelvin waves get across the Timor Sea onto the WA coast. Rather, MJO easterlies over the Maritime Continent in phases 1-3 (not shown) appear to drive Ekman transport that converges onto the NW shelf (Fig. 1). Positive height anomalies that concurrently appear on the NW shelf suggest a link between MJO easterlies north of Australia and intra-seasonal SST variability on the NW shelf.

In order to better understand and quantify the heat sources that contribute to MJO-driven temperature variability on the NW Australian shelf, we estimate the heat budget for the top 50m averaged over the box region bound by coordinates 115-130°E and 12-20°S according to the equation:

$$\frac{\partial T}{\partial t} = \frac{Q}{\rho C_p H} - (u\frac{\partial T}{\partial x} + v\frac{\partial T}{\partial y}) - w\frac{\partial T}{\partial z}$$

The right hand side of the equation represents the total heat flux forcing (first term), horizontal advection of heat into the mixed layer (second term), and vertical advection of heat (third term). The total heat flux (Q) is scaled by the specified depth of the mixed layer (here we assume H=50m) and the volumetric heat capacity of seawater (ρCp). Figure 2 (left panel) shows relative contributions between the three terms in addition to the total temperature variation (∂T/∂t) calculated over the top 50m of the ocean and the scaled temperature anomaly (dashed curve), as a function of MJO phase.

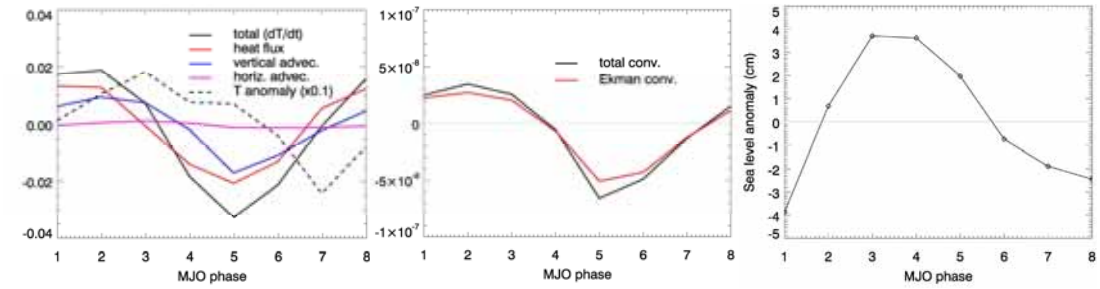

***Fig. 2**: Left panel: Heat budget decomposition (K/d) for the top 50m on the NW Australian shelf (115-130°E, 12-20°S); heat flux (red), horizontal advection (pink), and vertical advection (blue) plotted against total temperature variation (solid black; K/d) and scaled temperature anomaly (dashed black; × 0.1K). Middle panel: Ekman convergence and total convergence (s^{-1}) on the NW Australian shelf. Right panel: composite Fremantle sea level anomaly (cm). All shown as a function of MJO phase.*

The largest contributors to intra-seasonal temperature variations on the NW shelf are heat flux and vertical advection; horizontal advection has little impact. The heat flux and vertical advection terms are almost in phase and reach a maximum in MJO phases 1-2 and a minimum in phase 5. MJO zonal wind stress anomalies also exhibit peak easterly strength over the NW shelf in phase 2 and peak westerly strength in phase 5 (not shown); these results suggest that vertical advection on the shelf is driven by Ekman transport in response to the MJO zonal wind anomalies. We demonstrate the role of Ekman transport on the NW Australian shelf in Fig. 2 by comparing the total convergence with the estimated Ekman convergence; Ekman transport accounts for most of the convergence on the NW shelf and varies as a function of MJO phase consistent with vertical advection of heat.

Impact of the MJO on the WA coast

Composite anomalies of sea level measurements at Fremantle as a function of MJO phase suggest that the MJO variability on the NW shelf is transmitted along the WA coast, with peak sea level occurring in phases 3-4 (Fig. 2). We elucidate the dynamical relationship between Fremantle sea level and the MJO signal on the NW Australian shelf with lag-correlations of sea surface height, surface currents and surface wind stress with Fremantle sea level, filtered to 30-90d, in Fig. 3. High sea level at Fremantle at lag 0d is associated with increased surface height and southward currents down the WA coast. The increased surface height signal first appears on the NW shelf about 12 days prior to the sea level peak, coincident with surface easterlies and southward Ekman transport onto the shelf. Thereafter, southward surface currents extend down the WA coast concurrently with increased sea surface height and consistent with an increased southward transport by the Leeuwin current; the timing of this southward transport supports a coastal wave mechanism triggered by the piling up of warm water and associated sea level rise on the NW shelf.

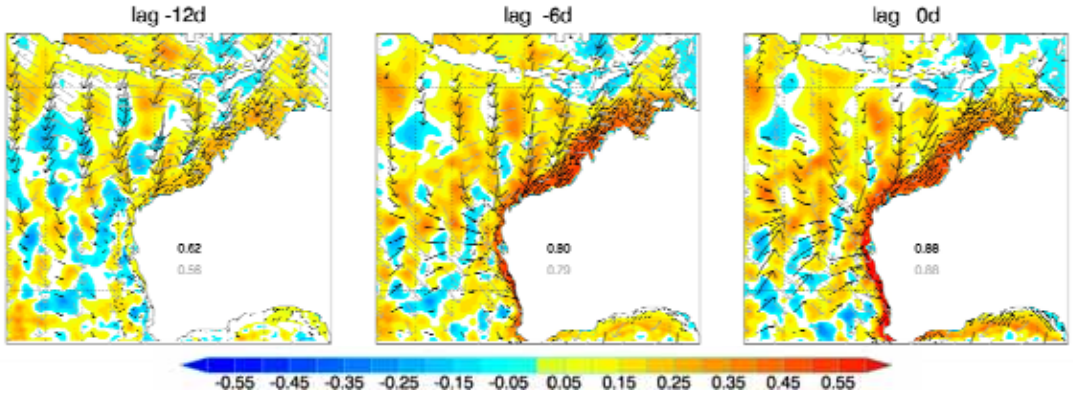

***Fig. 3**: Fremantle sea level lag-correlation with sea surface height (shaded), surface currents (black vectors), and surface wind stress (grey vectors) at lags of -12d, -6d and 0d, filtered to 30-90d. Shading and vectors are represented at the 0.05 significance level. The magnitude of the maximum plotted vector is printed on each Australian map for PEODAS currents (black text) and wind stress (grey text).*

Conclusions

Anomalous mixed layer heating on the NW shelf in the suppressed/easterly phase of the MJO is driven roughly equally by increased anomalous heat flux into the ocean and anomalous Ekman-induced downwelling. Conversely, anomalous mixed layer cooling on the NW shelf in the convective/westerly phase of the MJO is driven by both decreased heat flux into the ocean and Ekman-induced upwelling. The piling up of warm water and associated sea level rise on the NW shelf triggers a coastal trapped wave that propagates southward along the WA coast and raises sea level at Fremantle in MJO phases 3-4. The MJO signal in Fremantle sea level appears not to originate as an equatorial wave, but rather is directly forced by the MJO on the NW shelf. Considering our ability to predict the MJO to 4 weeks lead time in the current version of the POAMA seasonal prediction system, future work should explore the application of MJO forecasts to management of the WA marine environment.

References

Oke, P.R., Brassington, G.B., Griffin, D.A. and Schiller, A. 2008. The Bluelink Ocean Data Assimilation System (BODAS). *Oc. Model., 20*, 46-70.

Wheeler, M.C. and Hendon, H.H. 2004. An all-season real-time multivariate MJO index: Development of an index for monitoring and prediction. *Mon. Wea. Rev., 132*, 1917-1932.

Yin, Y., Alves, O. and Oke, P.R. 2011. An ensemble ocean data assimilation system for seasonal prediction. *Mon. Wea. Rev., 139*, 786-808.

IMPACT OF THE MJO ON THE GULF OF CARPENTARIA DURING THE MONSOON

Eric C. J. Oliver[1,2] and Keith R. Thompson[2]

[1]Institute for Marine and Antarctic Studies, University of Tasmania, Hobart, Tasmania, Australia
[2]Department of Oceanography, Dalhousie University, Halifax, Nova Scotia, Canada

Introduction

The Madden-Julian Oscillation (MJO) is an atmospheric phenomenon but the associated precipitation, convection, and wind anomalies also interact with the ocean surface. Broad scale patterns of intraseasonal sea level anomalies have been detected worldwide (Fu 2003) and are largely driven by surface wind stress. Oliver and Thompson (2010) found that sea level from many ocean regions, including the equatorial Pacific, the west coast of the American continent, the Gulf of Carpentaria and the northeastern Indian Ocean, have significant correlations with the MJO. Sea level and circulation in the Gulf of Carpentaria have been shown to be related to the MJO during the Australian-Indonesian monsoon season (Oliver and Thompson 2011) and these results are reviewed here as well as a discussion on the predictability of Gulf of Carpentaria sea level.

Data

Six-hourly fields of surface winds were obtained from the NCEP/DOE Reanalysis 2. Hourly time series of sea level were obtained from three tide gauge locations around the Gulf of Carpentaria: Groote Eylandt was obtained from Australian Baseline Sea Level Monitoring Project; Karumba and Weipa were obtained from Maritime Safety Queensland, Queensland Government, Australia. The MJO is characterised using the real-time bivariate index of Wheeler and Hendon (2004) and daily values were obtained from the Government of Australia Bureau of Meteorology

Intraseasonal sea level, wind and MJO variability during the Monsoon

The prevailing winds over the Gulf of Carpentaria are strongly linked to both the local trade winds and the Australian-Indonesian monsoon. The background flow in this region is dominated by the southeasterly trade winds which peak in July. During Austral Summer the Australian-Indonesian monsoon causes reversal of the mean flow and predominantly northwesterly winds (see Forbes and Church (1983)). The Madden-Julian Oscillation has been shown to be strongly related to bursts and breaks (e.g., modulations) of the Australian-Indonesian monsoon (Hendon and Liebmann 1990; Wheeler and McBride 2005).

To examine the relationship between the MJO index and average wind over the Gulf of Carpentaria we calculated the coherence between these two variables as a function of frequency. The coherence reaches a peak for both zonal and meridional wind components over the intraseasonal band, defined as periods between 30 and 90 days (not shown, see Oliver and Thompson (2011) henceforth OT11). Zonal wind has the highest coherence with the MJO (between 0.5 and 0.7 across the intraseasonal band). Directional dependence was explored by looking at the average coherence over the intraseasonal band between the MJO and wind projected onto various wind directions (not shown). The intraseasonal coherence peaks for westerly to northwesterly winds (or easterly to southeasterly). Using a barotropic ocean circulation model (see OT11 for model details) it has been shown that the

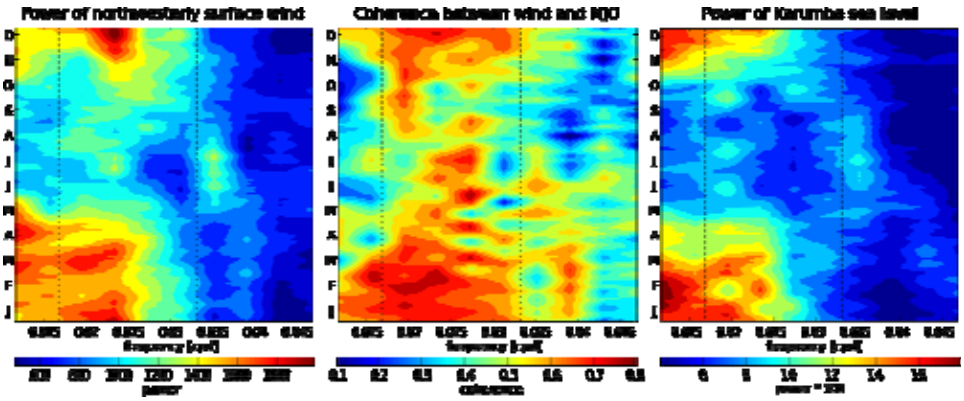

***Fig. 4**: Seasonal variation of the spectral density of the northwesterly surface wind over the Gulf (left), the coherence between the wind and the MJO index (centre), and the spectral density of observed sea level at Karumba (right). Vertical lines indicate periods of 30 ad 60 days.*

Gulf responds most strongly to wind in the northerly to northwesterly (or, equivalently, the southerly to southeasterly) direction. Therefore, sea level in the Gulf of Carpentaria is expected to respond strongly to MJO-related wind stress during the monsoon.

The seasonal variation of the spectral properties of the wind and the MJO was explored by calculating evolutionary spectra using 180 day subsets of the wind time series with successive blocks shifted by one day. The seasonal cycle of spectral density was then calculated by averaging across years for each day of the year. The seasonal variation of the northwesterly wind spectrum (Fig. 1, left panel) shows that the energy is relatively high over the intraseasonal band during Austral Summer which coincides with the Australian-Indonesian monsoon. This time of year also corresponds to relatively high coherence between the wind and the MJO (Fig. 1, centre panel) consistent with previous work (Salby and Hendon 1994; Zhang and Dong 2004).

The coherencies between the MJO and the sea level from the Gulf of Carpentaria tide gauges show peaks between 0.6 and 0.7 over intraseasonal time scales (not shown). The seasonal cycle in the spectral density of sea level at the three tide gauges, calculated in the same way as for wind, shows the same cycle as the wind (Fig. 1, right panel) indicating the expected sea level-wind-MJO.

Impact of the MJO on sea level and circulation

Sea level and depth-averaged circulation in the Gulf of Carpentaria were predicted from a barotropic numerical ocean model (POM, see OT11 for model details) over the 1979 to 2009 period and the domain is bounded by 120°E, 146°E, 20°S and 3°S. The model slightly underpredicts the observed intraseasonal sea level at the tide gauge locations however the root mean square (RMS) errors between observed and predicted sea levels are lower than the RMS amplitude of the model predictions indicating that the model has some predictive skill. Correlations between observed and predicted sea level, after filtering out variability on time scales longer than 120 days, are generally above 0.7 indicating that the predictions capture the intraseasonal variability well. The model also reproduces the seasonal modulation of intraseasonal sea level variability (e.g., such as that shown in Fig. 1, right panel).

The dependence of observed wind and sea level on the MJO was examined by compositing based on its phase. Composites of zonal wind show the passage of a convergence region at the surface associated with the movement of active MJO-related convection over the Maritime Continent. This leads to anomalous easterlies over the Maritime Continent at the equator when the convective centre is over the Indian Ocean (phases 1-3) and anomalous westerlies when it is over the Pacific Ocean (phases 6-7). The Gulf of Carpentaria, just south of the Maritime Continent, experiences anomalous

northwesterlies during phases 6-7 with set-up of coastal sea level evident at all three tide gauges and anomalous southeasterlies during phases 1-3 with set-down at all three stations (see arrows in lower left of panels in Fig. 2).

The composites of model predicted sea level and depth-averaged current anomalies based on MJO phase are also shown in Fig. 2 and are consistent with sea level set-up and set-down respectively. For example, the phase 7 (2) composite of depth averaged currents exhibits a cyclonic (anticyclonic) gyre centred in the Gulf of Carpentaria and strong eastward (westward) flow through the Torres Strait. As the MJO performs a cycle the composites pass through a quiescent state (phase 8), followed by the set-down pattern (phase 1-3), and then another quiescent state (phase 4-5), before returning to the set-up pattern (phases 6-7).

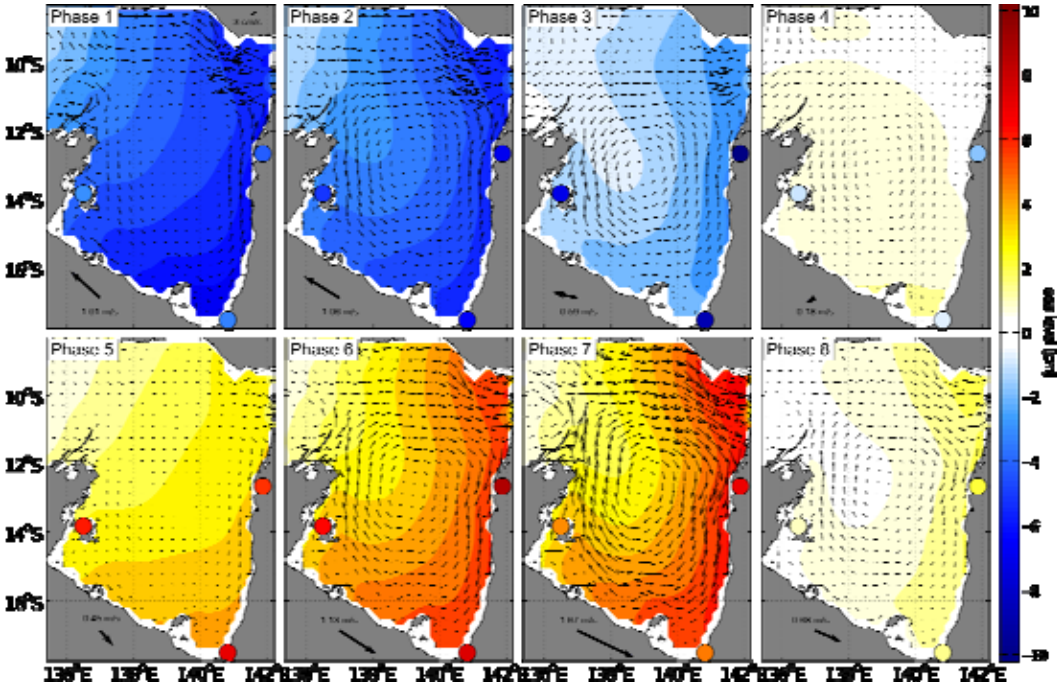

***Fig. 5**: Composites of sea level (colours), depth-averaged currents (small arrows), and surface wind (large black arrow in lower left of each panel) associated with the eight phases of the MJO index. The coloured circles and contours show the composites of observed and model predicted sea level respectively. A current speed of 3 m/s is indicated in the top right of the first panel.*

Predictability

The potential predictability of the MJO-related sea level setup in the Gulf of Carpentaria is now explored using a simple statistical prediction model following Oliver (2012). We relate the sea level series from the Karumba tide gauge (η_t) and the MJO index (first and second components denoted $I_{1,t}$ and $I_{2,t}$ respectively) using a lagged linear regression model

$$\eta_{t+k} = \sum_{d=0}^{D} \beta_{1,d} I_{1,t-d} + \beta_{2,d} I_{2,t-d} + \varepsilon_t$$

where t is a time index, k is a future prediction time, the β are regression coefficients and ε_t is an error term. The model includes $I_{1,t}$ and $I_{2,t}$ at all lags d from 0 to D. In practice the inclusion of so many lags provides an overfit model and in this study we only include lags 0 and 8 days. The model is applied for November through March only, the period for which the MJO-sea level connection is strongest. The model is trained on the first half of the time period and validation statistics are calculated over the second half of the period.

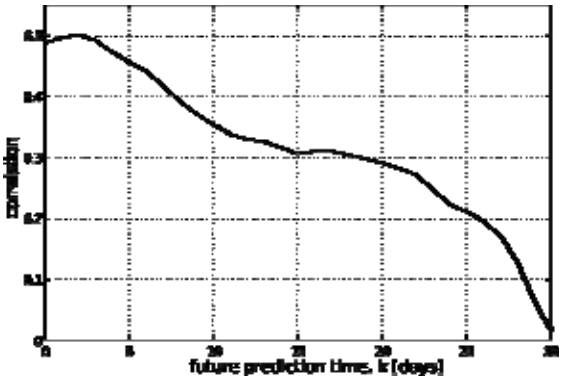

Fig. 6: *Potential predictability of sea level at Karumba from the MJO index as measured by the correlation between the sea level series and the lagged linear regression model as a function of future prediction time* k.

The correlation between η_t and the statistical model prediction, over the validation period, as a function of future prediction time k is shown in Fig. 3. The correlation is ~0.5 instantaneously ($k = 0$ days). The correlation at future prediction times drops slowly, reaching zero at about $k = 30$ days. However, after 20 days the correlation has only dropped by half indicating that in this time period the model can still account for some (~10%) of the variability. These correlation values may seem low but it should be kept in mind that the sea level record was not filtered and so retains variability on time scales outside the intraseasonal band.

Conclusions

We have used a barotropic circulation model to show that intraseasonal sea level and depth-averaged circulation variations in the shallow waters of the Gulf of Carpentaria are dominated by wind setup due to MJO-related surface wind stress. The influence of the wind stress on sea level and circulation is strongest during Austral Summer when the MJO influences the occurrence of bursts and breaks in the Australian-Indonesian monsoon. The sea level signal at the head of the Gulf was shown to be predictable given historical MJO values and predictions of the future MJO index (e.g., Rashid et al. (2011)) may lead to better forecast skill for sea level and circulation in the Gulf of Carpentaria on intraseasonal time scales. Future work may focus on (i) the use of future projections of the MJO index to predict intraseasonal variability in the Gulf of Carpentaria and (ii) an examination of the secondary effects of the intraseasonal variations in the Gulf of Carpentaria (e.g., chlorophyll-a variability).

References

Forbes, A. and Church, J. 1983. Circulation in the Gulf of Carpentaria II. Residual currents and mean sea level. Australian Journal of Marine and Freshwater Research, 34, 11-22.

Fu, L. 2003. Wind-forced intraseasonal sea level variability of the extratropical oceans. Journal of Physical Oceanography, 33, 436-449.

Hendon, H. and Liebmann, B. 1990. The Intraseasonal (30-50 day) Oscillation of the Australian Summer Monsoon. Journal of the Atmospheric Sciences, 47, 2909-2924.

Oliver, E. 2012.Response of sea level and circulation in the Gulf of Thailand to local forcing related to the Madden-Julian Oscillation. Submitted to Ocean Dynamics.

Oliver, E. and Thompson, K. 2010. Madden-Julian Oscillation and sea level: Local and remote forcing. Journal of Geophysical Research, 115, C01003.

Oliver, E. and Thompson, K. 2011. Sea level and circulation variability of the Gulf of Carpentaria: Influence of the Madden-Julian Oscillation and the adjacent deep ocean. Journal of Geophysical Research, 116, C02019.

Rashid, H.A., Hendon, H.H., Wheeler, M.C. and Alves, O. 2011. Prediction of the Madden-Julian oscillation with the POAMA dynamical prediction system. Climate Dynamics, 36, 649-661.

Salby, M. and Hendon, H. 1994.Intraseasonal behavior of clouds, temperature, and motion in the Tropics. Journal of the Atmospheric Sciences, 51, 2207-2224.

Wheeler, M.C. and Hendon, H. 2004. An all-season real-time multivariate MJO index: Development of an index for monitoring and prediction. Monthly Weather Review, 132, 1917-1932.

Wheeler, M.C. and McBride, J.L. 2005.*Intraseasonal Variability in the Atmosphere-Ocean Climate System, chap. Australian-Indonesian Monsoon. pp*125-173. Springer.

Zhang, C. and Dong, M. 2004.Seasonality in the Madden-Julian Oscillation.Journal of Climate, 17, 3169-3180.

ASIAN-AUSTRALIAN MONSOON NWP WITH THE METUM

Sean Milton, Stuart Webster, Prince Xavier, Gill Martin, Martin Willett, Ann Shelly, Jane Mulcahy, and Julian Heming.

Met Office, Exeter, UK

Introduction

The Global Monsoon system represents major climatic anomalies impacting both regional climate and local weather systems in the tropics and subtropics and determining water availability for millions of people. A key requirement for successful forecasts is the ability to predict precipitation across a range of space and timescales from individual squalls, thunderstorms and cyclones embedded within the monsoon flow, to the sub-seasonal variability that modulates the higher frequency weather through the active and break cycles. Monsoons also exert a global influence on the atmospheric circulation and weather worldwide through remote teleconnections (Rodwell and Hoskins (1996), Trenberth et. al. (2006)). This paper discusses the performance of the Met Office Unified Model (MetUM) prediction system at short (1-5 days) and medium-range (6-15 days) NWP timescales for the Asian and Australian monsoon systems. We also highlight the use of MetUM NWP predictions in a seamless prediction framework (Senior et. al. (2010), Brown et. al. (2012)), as a means of identifying the source of model systematic errors in key (moist) physical processes and the role this approach plays in potentially improving longer-range predictions. Sensitivity of the monsoons to physical processes at climate timescale with MetUM is discussed in Martin et. al. (2012).

Increasingly, there is recognition that the monsoons and other tropical variability are complex coupled ocean-atmosphere-land phenomena (Webster (2006)). In addition to exploring the more traditional model resolution, numerics and parametrization sensitivity there is also active research into "convective permitting" resolutions (4km-1km) and the role of increasing Earth-System (E-S) complexity in providing benefits at weather timescales. The E-S complexity builds upon developments originally for climate predictions and includes (i) coupled ocean-atmosphere interactions (Johns et al. (2012)), linking the global atmospheric and ocean forecasting efforts at the Met Office, and (ii) prognostic aerosols, including interactions with cloud. Inclusion of these important physical interactions may ultimately improve NWP predictions and provide new capability (e.g. air quality forecasts). In the short-term we recognise that forecast skill may deteriorate as we try to understand the interactions in a fully coupled system with more degrees of freedom than traditional NWP. Development of coupled ocean-atmosphere and aerosol data assimilation/initialisation will also be important components to be addressed in the future.

MetUM NWP performance in Asian-Australian Monsoon

MetUM is a unified modelling system (Brown et. al., 2012) with essentially the same atmospheric dynamical core and physical parameterisations used for global weather and climate prediction (see Walters et. al. (2011) for details of the latest global atmosphere configurations). For coupled prediction across timescales the atmosphere model (MetUM) is coupled to the NEMO ocean model, the CICE sea-ice model, the JULES land surface model, and a representation of aerosols is currently provided by the CLASSIC aerosol scheme and in future by the UKCA-MODE aerosol scheme. MetUM is also used for regional mesoscale/convective scale prediction over the UK. A 1.5km regional model version is operational over the UK. This model is "convection permitting" and the convection is explicitly resolved rather than parameterised. These resolutions are also used in research mode in other regions of the globe to try and understand the multi-scale nature of organised

convection and its interactions with the large scale flow (e.g. CASCADE project (Holloway et. al., 2012)). Some preliminary results are presented in this paper for the Asian Monsoon below.

Asian Monsoon in Met Office and ECMWF NWP - diagnosing systematic error sources.

The Met Office (MetUM) and ECMWF (IFS) modelling systems show very different error growth with forecast range. MetUM suffers from a "dry" monsoon bias which shows a weakening of the low-level Monsoon circulation and an anticyclone forming over India early in the forecast range (Fig. 1(f)) with an enhanced divergent circulation at 200hPa that retards the tropical easterly jet in the Indian Ocean (Fig.1(h)). There are also large errors in the divergent winds with convergence at low levels into the region of excessive precipitation in the Indian Ocean (Fig. 1(f)) and divergence aloft (Fig. 1(h)). The precipitation shows a growing wet bias over the equatorial Indian Ocean, a dry bias over India itself and a further wet bias over the Himalayas (Fig. 1(c) and (d)). This systematic error is very robust, develops quickly within a few days of initialisation and also forms the major systematic bias seen at longer climate timescales (see Martin et. al (2012) - this volume). A more detailed examination of the time variability of the precipitation shows that over the oceans rain is too frequent and the model fails to capture suppressed periods but also the extremes. This has implications for intra-seasonal variability (see next section and Kim et. al (2011)).

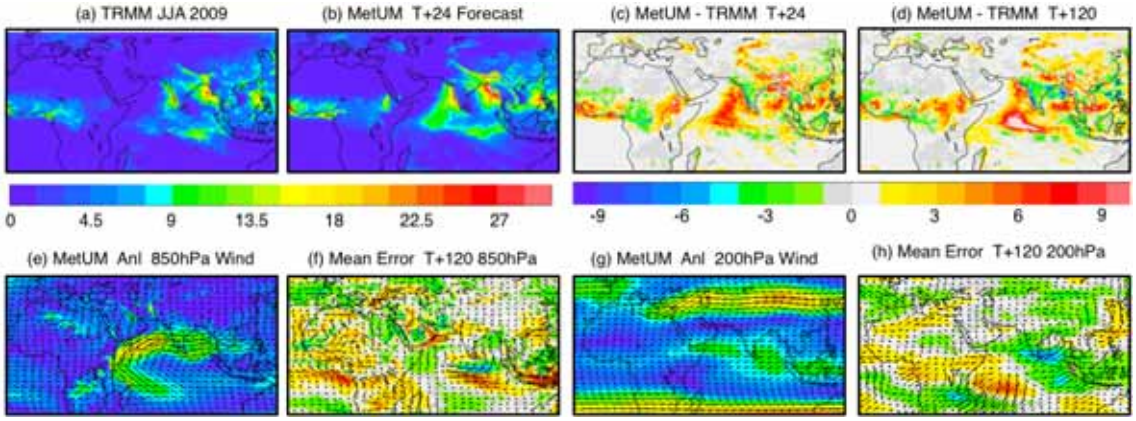

Fig. 1: *JJA 2009 Asian monsoon precipitation and circulation in observations/analyses and MetUM forecasts. Panels (c),(d),(f) and (h) show model errors.*

In contrast, the ECMWF model operational at this time showed a "wet" Monsoon with low level flow that increases in strength and excessive precipitation over the Indian Monsoon (not shown). Again this error structure is seen across all prediction timescales and a variety of model resolutions (pers. comm. M.Rodwell). It is interesting that two state-of the art operational NWP models with very similar physical parameterisations and dynamical cores show such divergent behaviour at short ranges which also match the longer term climate-drift in each model. In order to uncover the source of systematic error growth we are studying this "wet" and "dry" monsoon in these two models in more detail. We are following the approach of using very short-range physical tendencies to study the time-mean budgets of heat and momentum, but also considering the time evolution of tendencies and model short-range error to attempt to map the covariance of forcing to error growth. Initial focus is on the low level monsoon flow and the PV evolution under the influence of diabatic and frictional tendencies.

High Resolution Modelling of the Asian Summer Monsoon - Convective Scale.

The uncertainty around the physics and dynamics of multi-scale convection and how to parametrize it, remain fundamental barriers to model improvements. As part of the EMBRACE project (EU FP7) we have begun to assess the impact of model resolution on the simulation of the Asian summer monsoon and investigate whether high-resolution convection permitting simulations reduce the systematic

errors typical in coarser resolution parameterised convection simulations. Ultimately, the aim is to use the high resolution simulations (assuming they are of sufficient quality), combined with observations, to further our understanding of the monsoon and motivate improvements to the convection parameterisation. This builds on the development of the 1.5km UK version of MetUM for operational weather prediction and also on the work of the CASCADE project exploring convective scale modelling for tropical flows over Africa and the warm pool region (e.g. Holloway et. al. (2012)).

Four limited area models (LAMs) have all been run directly inside an N512 (25km) GA4.0 version of MetUM. These LAMs have resolutions of 1.5km, 4km, 24km and 120km and all span the same region (see Fig 2). All four LAMs have been run for the same time period, are all initialised using the same global model analysis flow fields and are all forced at their lateral boundaries by the same driving model data (N512 global). The configuration of these simulations enables a clean assessment of horizontal resolution.

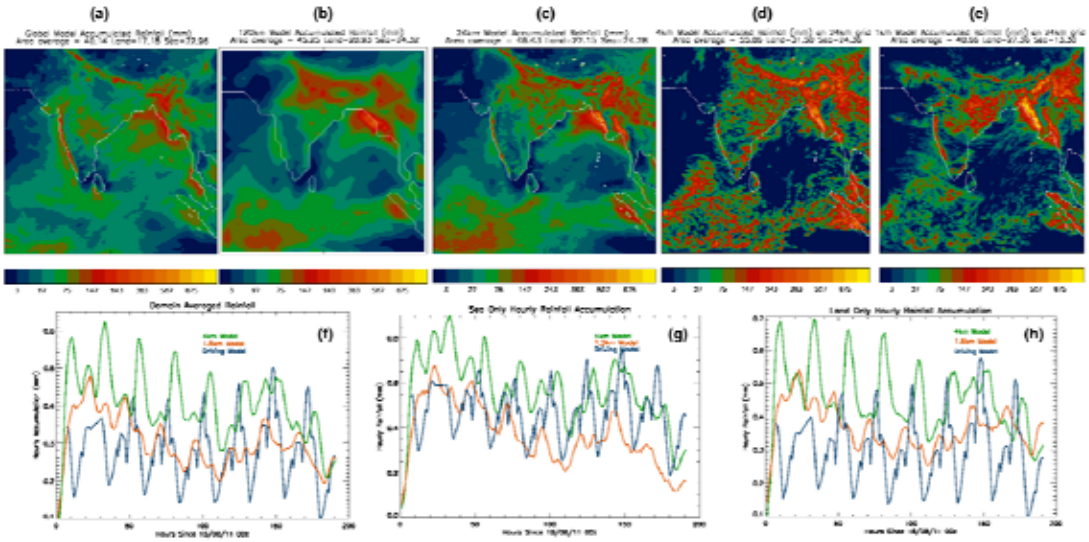

Fig 2. *Precipitation accumulations for 20th-26th August 2011 (top panels) for (a) Driving Model (N512-25km global) and LAM runs at a variety of resolutions (b) 120km, (c) 24km, (d) 4km and (e) 1.5km. Bottom panels show the time series of domain averaged hourly precipitation 18th-26th August for (f) Full domain (g) Ocean (h) Land.*

The N512 global model, which provides the LBC data for the four LAMs, is kept as close to reality as possible by reinitialising every 6 hours with successive Met Office operational analyses. The data used to create the LBCs is output hourly from the global model. In contrast to the global model, the LAMs are all free running, and so after they are initialised the only two ways in which they "feel reality" are through the LBC data and also through the daily updating of their SSTs from OSTIA analyses. The LAMs can therefore all spin up/down towards their preferred climate state. Initialised 18th August 2011, 00z, results are shown for 20th 00z through to 26th 00z (Fig. 2). This period was chosen as it was anomalously wet over central India. The parameterised convection runs have very similar domain averaged precipitation (Fig. 2 (a),(b) and (c)). In contrast the 4km model rainfall clearly looks excessive (Fig. 4(d) and (f)), whereas the 1.5km rainfall domain average is more similar to the driving model (Fig. 2(f)). The 1.5 km model is relatively dry in Southern India with a clear rain shadow downstream of the western Ghats (Fig. 2(e)). The 1.5km and 4km models have large areas of ocean where rainfall is suppressed compared to the parameterised models, where precipitation is widespread over the ocean basins. However, for the domain averages, the 4km actually has larger ocean precipitation than the driving global model (Fig.2(g)), showing that where it is raining the events are more intense. The 1.5km model has less domain averaged precipitation over the ocean of all model simulations and less in the equatorial Indian Ocean (Fig. 2 (e) and (g)), which is a key bias in the global forecasts with parameterised convection (Fig.1). Over land the diurnal cycle range in the 1.5km model is much less than in the driving model. The driving global model shows a clear

(unrealistic) minimum during the night (<0.2mm/hr). Interestingly, the 4km has a different diurnal cycle to the 1.5km model with maximum daytime precipitation a few hours earlier. These are preliminary results and work is underway to contrast with more detailed observations and examine the vertical diabatic heating profiles in the parameterised and resolved convection (S.Webster pers. comm.).

Work has also started on short (1-2 year) global AMIP style climate simulations at N1024 (12km) resolution with both parameterised convection and convection permitting set-ups (M.Roberts pers. comm.). In addition to studying the local impacts of convection this will hopefully allow study of the teleconnections and intra-seasonal varaiability associated with improved diurnal cycle and very different diabatic heating profiles in the convection permitting runs.

Australian Monsoon, MJO, and Equatorial Waves in MetUM.

The basic state errors in the Australian monsoon bear some similarity to those in the Asian summer monsoon. The mean precipitation in day 1 and day 5 forecasts for DJF 2010/11 show a deficit of rainfall over the land in northern Australia and excessive precipitation over the oceans (Fig. 3). This very clear land-sea contrast in the model is still not well understood. There is considerable inter-annual variability in these biases, although the character of too little (much) precipitation over land (ocean) is still evident. Despite these errors in the basic state the MetUM NWP forecasts showed some remarkable predictability of the extremes encountered over Australia during DJF 2010/11 associated with the active La Nina. The Queensland-Brisbane floods were well predicted by the global model (Fig. 3 (e-g)) as was Tropical cyclone Yasi which hit the Queensland coast on 3 February 2011. Further convective scale (~1-2km) modelling of the Brisbane floods with MetUM as part of the CAWCR/ACCESS efforts has shown the models ability to capture the most extreme rainfall both spatially and temporally (K.Puri, pers comm). At seasonal timescales the DJF 2010/11 anomalies in precipitation, closely linked to the La Nina, were captured in GLOSEA4 predictions made in November 2010 (A.Scaife, pers. comm.).

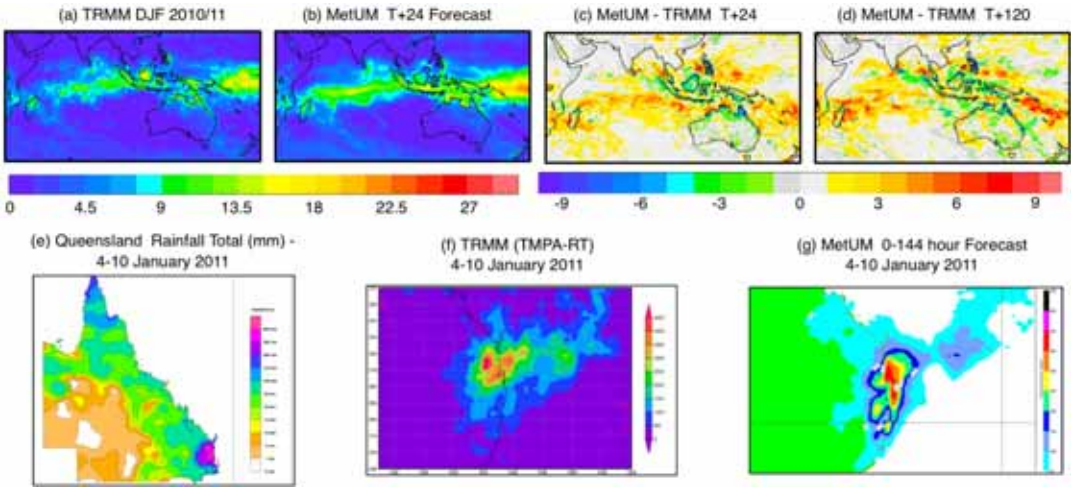

***Fig. 3**: DJF 2010/11 Australian monsoon precipitation in observations and MetUM forecasts. Top panels show the seasonal mean TRMM and MetUM forecasts and errors. Bottom panels show the accumulated precipitation for the Queensland-Brisbane flooding event of January 2011.*

Despite these successes the MetUM, in common with many other NWP and climate models, has difficulty in modelling the phase, amplitude and propagation of the MJO and monsoon intra-seasonal variability. The MJO is the major mode of intra-seasonal variability in the Australian Indonesian region and closely linked to both onset of the Australian Monsoon system and its intra-seasonal variability in the form of active-break cycles (Wheeler and McBride (2005)). At forecast ranges out to 15 days the MetUM MOGREPS system shows good predictability of the MJO in both ensemble mean

and control forecast out to 10 days ahead and is very competitive with predictions from the other major NWP centres (Gottshalck et. al., 2010). Beyond 10 days the predictability of all models begins to decline and at seasonal and climate timescales MetUM has traditionally had a poor representation of MJO structure and predictability (e.g. Fig. 4(a)). However, the MJO has shown a strong sensitivity to aspects of the convective parametrization. A number of changes to convection between GA2.0 and GA3.0 science versions (Walters et. al. (2011)) gave a modest improvement in the MJO (Fig.4). Further research in collaboration with University of Reading (N. Klingaman and S.Woolnough) has shown that an increase in entrainment (1.5 times current values) gives a marked improvement in the MJO variability with a decline in westward propagating signals and an increase in the amplitude at MJO frequencies and wave-numbers (Fig. 4). Sensitivity studies have shown this is linked particularly to increased entrainment at mid-tropospheric levels and is probably linked to moisture feedbacks and the responsiveness of the model to environmental humidity fluctuations (Xavier (2012)). Further research is required to investigate MJO predictability at medium-range timescales with these revised model formulations. More detailed research of the physical processes (e.g. vertical diabatic heating profiles) at a range of prediction timescales is currently being undertaken as part of the MJO-YOTC model intercomparison project (Petch et. al., 2011).

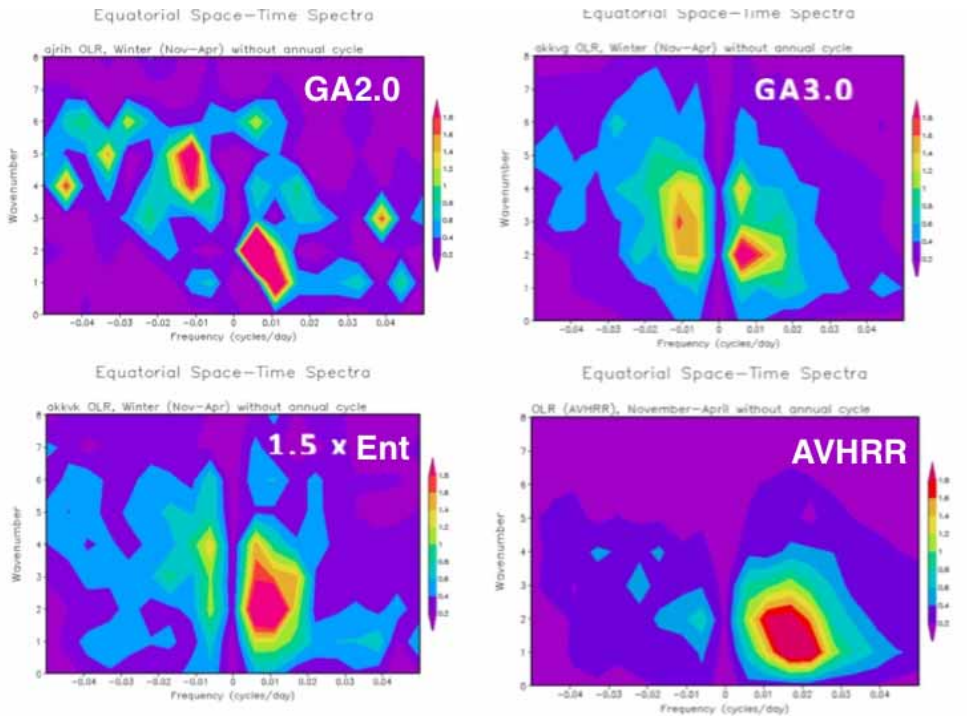

Fig 4: *Wavenumber-Frequency spectra of OLR showing MJO scales for boreal winter (Nov-Apr) from AMIP simulations of MetUM with (a) GA2.0 atmospheric model formulation, (b) GA3.0, (c) GA3.0 including 1.5 times entrainment in the convective parameterisation (d)*

Another important aspect of tropical variability at synoptic and sub-seasonal timescales is the representation of equatorial convectively coupled waves in atmospheric models (Wheeler and Kiladis (1999), Yang et. al. (2009), Frierson et. al.(2011)). There is a huge range of behaviours in climate and NWP models (see Lin et. al. (2006) for comparison of climate models in IPCC AR4). MetUM has shown a poor representation of equatorial waves in recent HadGEM climate versions (Yang et. al. (2009) and Fig.5) and in NWP where the signal of the waves in the analysis reduces in amplitude by over half within a few days of the forecast. As part of the global model development a revised dynamical core, ENDGAME, is under test at the Met Office. ENDGAME represents an evolution of the existing "New Dynamics", and part of the change to formulation involves an iterative step for the semi-implicit semi-Lagrangian dynamics. This results in more accurate departure points, reduced off centring and a scheme which is more implicit (approaching Crank-Nicholson). An emerging property

of this new scheme is that model variability is enhanced across a broad range of space and timescales, with improved transient eddy kinetic energies and more stratospheric gravity wave activity in higher resolution NWP versions at 25km and below. Of interest here are the equatorial waves, and in particular the Kelvin waves which show a 20% increase in strength and closer agreement to observations (Fig. 5). A similar increase in Kelvin Wave activity occurs when the CAPE timescale for convection is reduced The aim is to implement ENDGAME into version GA5.0 of MetUM in 2013.

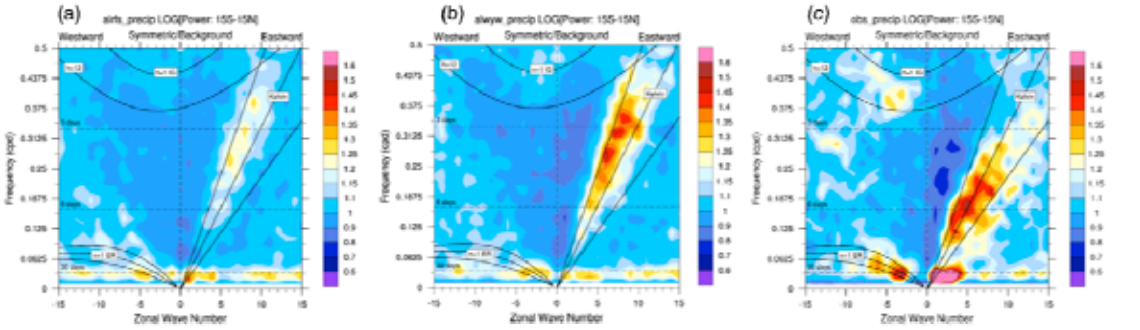

Fig 5: *Wavenumber-frequency spectra of tropical precipitation for (a) New Dynamics version of MetUM, (b) development version of ENDGAME dynamical core, and (c) GPCP observations. Theoretical dispersion relationships are also shown overlaid.*

Seamless model development and Monsoon NWP Predictions

Benefits of a Unified Model framework for accelerating model developments are that short-range NWP predictions allied to detailed observations can help identify the sources of model systematic errors, but also that Earth-System complexity developed for climate prediction can more easily be imported into an NWP framework. Examples are outlined below.

Coupled ocean-atmosphere predictions at weather timescales.

Johns et al. (2012) describe recent research to evaluate coupling the ocean and atmosphere on NWP timescales. At this early research stage we have taken the N216L85 (~60km resolution) atmosphere and the ORCA025L75 NEMO ocean initialised independently and coupled them together and run for 15 days. This is the same modeling system recently implemented for operational seasonal prediction in GLOSEA5. Initials results are promising, with the NWP verification scores for the coupled system very competitive and for some tropical scores actually outperforming the atmosphere only runs. Benefits are also seen for the ocean forecasting with the coupled system showing improvements in SST scores compared to the global (FOAM) ocean only forecasts.

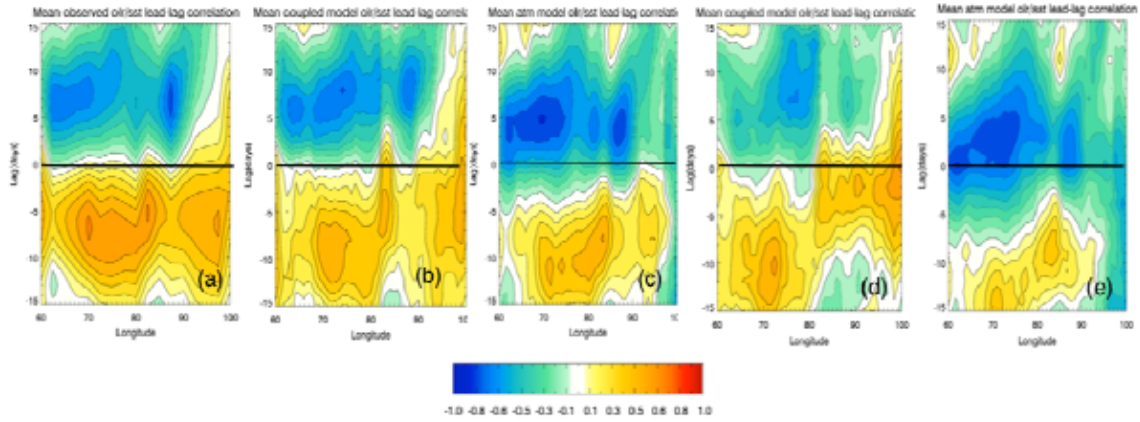

Fig 6: *Lead-lag relationship between SST and OLR across the Indian Ocean for (a) Observations (OSTIA & NOAA OLR) (b) Coupled model at day 1 (c) Atmosphere control at day 1 (d) Coupled model at day 5 and (e) Atmosphere control at day 5 over YOTC E and F MJO cases (Oct 2010-Jan 2011)*

We also see an improved coupled representation of the phase relationship between SST's and convection in the Tropics where anomalously warm SST's are observed to lead enhanced convection by ~5-10 days and anomalously cool SST's are led by enhanced convection by ~5-10 days (Fig. 6(a)). The phase lag relationship is emulated in day 1 atmosphere control forecasts but quickly drifts to a state where SST's and convection are co-located (Fig.6(e) - day 5). In this atmosphere only configuration, MJO related fluxes can have no influence on the SST, so convection adjusts to a location where SST is favourable and results in an in-phase relationship between OLR and SST anomalies. This trend is illustrated in the day 5 forecast, where peak correlations are at lag 0. However, the coupled model demonstrates an ability to reproduce the observed lagged relationship at day 5, with some spatial/temporal variation (Fig 6(d)), and continues to maintain the lagged relationship (though weaker) right through to day 15 (not shown).

Aerosols in Weather Prediction - Monsoon Impacts.

Finally, we briefly mention the efforts to assess the benefits of prognostic aerosols for NWP prediction. Mineral dust is already part of the global operational NWP system (currently implemented as a tracer only). Research is ongoing to assess the impacts of other aerosol species (sea-salt, biomass burning and anthropogenic aerosols) at NWP timescales, initialising using the MACC aerosol initial states generated at ECMWF. We are engaged in a collaborative project, SAPRISE, sponsored by the UK academic community (NERC) and involving Indian partners at NCMRWF to look at the impacts of aerosols on Monsoon precipitation. The impacts of dust and black carbon on the Asian Monsoon have been active research areas in recent years. For example, Lau et. al. (2006) advance one hypothesis, suggesting increased tropospheric heating due absorbing aerosols leading to an "elevated heat pump" mechanism over the Himalayas in spring and enhanced monsoon circulations. Our preliminary results show both the direct and indirect impacts of aerosol forcing impacts on both the monsoon precipitation and circulation in complex ways, although the indirect impacts appear to be larger. More research is required to quantify the exact mechanisms and dynamical responses.

Summary

Predicting the Asian-Australian Monsoon system across weather and climate timescales remains a challenging problem. Many systematic model errors are robust and difficult to diagnose and improve. The combination of a new generation of convection permitting simulations, improved Earth Observations, field experiments (e.g. DYNAMO/CINDY) and novel diagnostic techniques hold promise for real progress in the next few years. For MetUM we are attempting to pull together all of these strands in collaboration with UK Universities and International collaborators (CAWCR, NCMRWF, KMA, NIWA etc.) to improve the MetUM model for all prediction timescales. Results have been shown here from model developments to convection and the dynamical core (ENDGAME) which impact intra-seasonal monsoon/MJO variability and convectively coupled equatorial waves. Further research is exploring the role of increased Earth-System complexity due to ocean-atmosphere interactions and aerosols. At NWP timescales both of these are showing significant and in some cases beneficial impacts on NWP forecasts.

References

Brown, A.R., Milton, S., Cullen, M., Golding, B., Mitchell, J. and Shelly, A. (2012): Unified Modelling and Prediction of Weather and Climate: A 25-Year Journey. *BAMS*, DOI:10.1175/BAMS-D-12-00018.I.

Frierson, D., M, Kim, D., Kang, I-S., Li, M-I. and Lin, J. (2011): Structure of AGCM-Simulated Convectively Coupled Kelvin Waves and Sensitivity to Convective Parameterization, JAS, 68, 26-45.

Gottschalck, J., Wheeler, M., Weickmann, K., Vitart, F., Savage, N., Lin, H., Hendon, H., Waliser, D, Sperber, K., Nakagawa, M., Prestrelo, C., Flatau, M. and Higgins, W. (2010): A framework for

assessing operational Madden–Julian Oscillation forecasts: A CLIVAR MJO working group project. BAMS, 91, 1247-1258, doi:10.1175/2010Bams2816.1.

Holloway, C.E., Woolnough, S.J. and Lister, G.M.S. (2012) Precipitation distributions for explicit versus parameterized convection in a large-domain high-resolution tropical case study. Quarterly Journal of the Royal Meteorological Society. ISSN 1477-870X doi: 10.1002/qj.1903.

Johns, T.C., Shelly, A., Rodriguez, J.M., Copsey, D., Guiavarc'h, C. and Sykes, P., 2012. Report on extensive coupled ocean-atmosphere trials on NWP (1-15 day) timescales. PWS key deliverable report. Available from the Met Office and on the Met Office collaboration Wiki.

Daehyun, K., Sobel, A.H., Maloney, E.D., Frierson, D.M.W. and Kang, I-S. 2011: A Systematic Relationship between Intraseasonal Variability and Mean State Bias in AGCM Simulations. *J. Climate*, **24**, 5506–5520.

Lau, K.M., Kim, M.K., and Kim, K.M. (2006): Asian summer monsoon anomalies induced by aerosol direct forcing: the role of the Tibetan Plateau. Climate Dynamics, 26, 855-864.

Lin, J. and co authors (2006): Tropical Intraseasonal Variability in 14 IPCC AR4 Climate Models. Part I: Convective Signals. J.Climate, 19, 2665.

Martin, G. And co-authors (2012): Understanding and evaluation of monsoon processes in the MetUM. In this volume.

Petch, J., Waliser, D., Jiang, X., Xavier, P. and Woolnough, S. 2011: A global model intercomparison of the physical processes associated with the Madden-Julian oscillation. GEWEX News, August 2011, pages 3-5.

Rodwell, M.J. and Hoskins, B.J. (1996): Monsoons and the dynamics of deserts. Quart. J. Roy Meteorol. Soc., 122, 1385-1404.

Senior, C.A. and co-authors (2011): Synergies between numerical weather prediction and general circulation climate models. In The Development of Atmospheric General Circulation Models ed. L.Donner, W.Schubert and R.Somerville, Cambridge University Press, 76-116.

Trenberth, K., Hurrell, J.W. and Stepaniak, D.P. (2006): The Asian Monsoon: Global Perspectives. Pp 67-87, Chapter 2 of "The Asian Monsoon" edited by Bin Wang, Springer-Praxis.

Walters, D.N. (2011). The Met Offi1ce Unif1ied Model Global Atmosphere 3.0/3.1 and JULES Global Land 3.0/3.1 con1figurations. Geoscientific Model Development, 4(4): 919- 941.

Webster, P.J. (2006): The coupled monsoon system. Pp 3-66, Chapter 1 of "The Asian Monsoon" edited by Bin Wang, Springer-Praxis.

Wheeler, M. and Kiladis, G.N. (1999): Convectively Coupled Equatorial Waves: Analysis of Clouds and Temperature in the Wavenumber-Frequency Domain. JAS, 56, 374-399.

Wheeler, M.C. and McBride, J.L. (2005). Australian-Indonesian monsoon. In "Intraseasonal Variability in the Atmosphere-Ocean Climate system", Eds W.K.M. Lau and D.E. Waliser, Pub. Praxis. Springer, pp.1–50.

Xavier, P. K. (2012): Intraseasonal convective moistening in CMIP3 models, J. Clim., 25, 2569-2577

Yang, G-Y, Slingo, J. and Hoskins, B. (2009): Convectively Coupled Equatorial Waves in High-Resolution Hadley Centre Climate Models. J.Climate, 22 ,1897-1919.

RECENT ACTIVITIES OF GLOBAL MODEL DEVELOPMENT AT JMA FOR PREDICTION OF MONSOONS

Masayuki Nakagawa

Numerical Prediction Division, Japan Meteorological Agency
1-3-4 Otemachi, Chiyoda-ku, Tokyo 100-8122, JAPAN
E-mail: m-nakagawa@met.kishou.go.jp

Introduction

The Japan Meteorological Agency (JMA) operates several numerical weather prediction (NWP) models to meet various kinds of requirements on weather forecasting. The suite of the NWP models covers a wide temporal range of forecast periods from a few hours to two seasons providing a seamless sequence of products for the public.

The supercomputer system at JMA has been upgraded in June 2012, and now in operation. Theoretical peak performance of the new system, HITACHI SR16000/M1, is about 30 times higher than its predecessor, HITACHI SR11000, and is more than 800 TFLOPS.

Taking advantage of advanced computational resources, JMA plans to upgrade its numerical weather prediction system. This paper describes the upgrade plans for the operational Global Spectral Model (GSM) particularly upgrades affecting prediction of monsoons.

Outline of the global NWP system

The specifications of GSM are summarized in Table 1. GSM has 60 layers up to 0.1 hPa. The vertical resolution is higher in the lower atmosphere for better simulation of the planetary boundary layer processes. In the horizontal, prognostic variables are spectrally discretized with a truncation wave number of triangular 959 (TL959). The corresponding transform grids are spaced by about 0.1875 degree corresponding to about 20 km with the reduced Gaussian grid. The time integration is based on a two-time level, semi-implicit semi-Lagrangian scheme. A vertically conservative semi-Lagrangian scheme (Yoshimura and Matsumura 2003) is adopted. For the precipitation schemes, the cumulus convection scheme proposed by Arakawa and Schubert (1974) with modifications by Moorthi and Suarez (1992), Randall and Pan (1993) and Pan and Randall (1998) and a prognostic cloud water scheme similar to that of Smith (1990) are implemented.

Enhancement of number of vertical layers

The number of vertical levels of GSM is planned to be enhanced from sixty to one hundred as shown in Fig. 1. The topmost level of the model is going to be raised from 0.1 hPa to 0.01 hPa and the vertical resolution will be increased in the whole forecast domain. The number of layers in the troposphere will be increased from 35 to 59. The higher vertical resolution is expected to improve representation of atmospheric vertical structure and atmospheric processes particularly that in boundary layer which is important in monsoon prediction by numerical weather prediction models. Raising model topmost level enables to use satellite data channels better that have sensitivity for middle atmosphere on data assimilation.

Table 1: Framework of GSM.

Grid size/ Number of grids	0.1875 deg. / 1920 (equator) – 6 deg. / 60 (closest to pole) x 960 (TL959)
Vertical levels/ Top	60 / 0.1 hPa
Forecast range (initial time)	84 hours (00, 06, 18 UTC), 216 hours (12 UTC)
Time step	600 sec.
Vertical diffusion	Stability (Richardson number) dependent, local formulation
Gravity wave drag	Longwave scheme (wavelengths > 100 km) mainly for stratosphere Shortwave scheme (wavelengths appr. 10 km) only for troposphere
Planetary boundary layer	Mellor and Yamada level-2 turbulence closure scheme Similarity theory in bulk formulae for surface layer
Treatment of sea surface	Climatological sea surface temperature with daily analyzed anomaly Climatological sea ice concentration with daily analyzed anomaly
Land surface	Simple Biosphere (SiB) model
Radiation	Two-stream with delta-Eddington approximation for shortwave Table look-up and k-distribution methods for longwave
Convection	Prognostic Arakawa-Schubert cumulus parameterization
Cloud	Prognostic cloud water, cloud cover diagnosed from moisture and cloud water
Analysis	4D-Var

At the same time, three changes will be introduced to improve mesosphere climatology and upper boundary condition: (1) refinement of upper absorbing layer by adding 2nd-order linear horizontal diffusion in the divergence equation and adjusting 4th-order linear horizontal diffusion to reduce the effect of reflection in the troposphere from a upper boundary; (2) upgrade of the climatic value of ozone used in the radiation scheme; and (3) enhancement of dumping by Rayleigh friction to make mesosphere temperature climatology closer to SPARC. In addition, longwave radiation scheme will also be revised to use two-stream approximation based on Li and Fu (2000) to improve representation mainly in the middle atmosphere.

Preliminary experiment shows that increasing the model vertical resolution reduces area covered by marine stratocumulus represented by diagnostic stratocumulus scheme (Kawai and Inoue 2006) in GSM near the west coast of continents.

Coupling of an ocean mixed-layer model

Atmosphere-ocean interaction plays important role in monsoon. The coupling of an ocean model to GSM has been studied and evaluated for tropical cyclone (TC) events. The ocean model coupled was the Meteorological Research Institute Community Ocean Model (MRI.COM; Tsujino et al., 2009). The ocean mixed layer scheme of Noh and Kim (1999) was adopted in the ocean model.

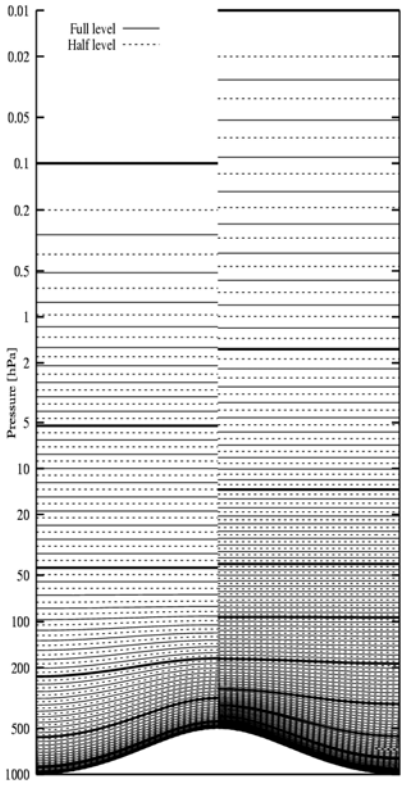

***Fig. 1**: Distribution of vertical layers of GSM. Left: current, right: planned.*

Preliminary experiments with the coupled model were carried out for several TC events to assess the impact of the coupling on TC forecasts. Fig. 2 shows the results for the case of Typhoon Morakot in 2009. The coupled model reproduced its TC intensity level that corresponded closely to analysis values by considering sea surface cooling caused by the passage of the typhoon, while the operational model overestimated the development of the typhoon. Medium-range forecast experiments were also conducted to investigate the impact of the coupling on overall forecast skill. The results suggested that skill was sensitive to the accuracy of the initial oceanic field, and that the present coupled model had a tendency toward increased cold bias in both lower atmospheric temperatures and SST for medium-range forecasts. More research is necessary to address bias and improve forecast skill.

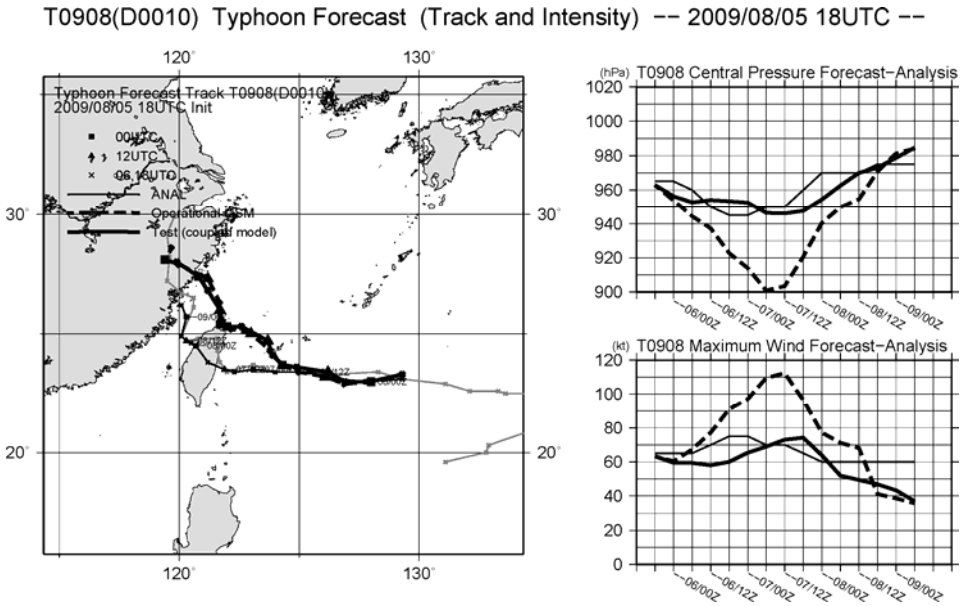

***Fig. 2**: Predicted track (left), central pressure (top right) and maximum wind speed (bottom right) of typhoon Morakot (T0908). The initial time of the forecast is 18 UTC 5 August 2009. The solid line, broken line and thin solid line indicate forecast by coupled model, that by operational model and the analyzed best track, respectively.*

Summary

JMA plans to enhance the number of vertical layers of GSM from 60 to 100 and to raise the topmost level from 0.1 hPa to 0.01 hPa. The higher vertical resolution is expected to improve representation of atmospheric vertical structure and atmospheric processes, which leads to better prediction of monsoons. Coupling of an ocean mixed-layer model to GSM has been studied and found to improve the TC intensity forecast, though more research is necessary to reduce bias.

To further improve the accuracy of GSM, JMA is developing the model continuously. In addition to the developments mentioned above, the diagnostic marine stratocumulus scheme is going to be upgraded to reduce excessive lower cloud cover over land. Climatic value of aerosol and absorption coefficient for water vapor used in the radiation scheme are planned to be renewed. Non-orographic gravity wave drag parameterization will be implemented to improve climatologies in the middle atmosphere. Upgrade of Simple Biosphere model is under development.

References

Arakawa, A. and Schubert, W. H. 1974: Interaction of a cumulus cloud ensemble with the large-scale environment, Part I. *J. Atmos. Sci.*, **31**, 674-701.

Kawai, H. and Inoue, T. 2006: A simple parameterization scheme for subtropical marine stratocumulus. *SOLA*, **1**, 017–020.

Li, J. and Fu, Q. 2000: Absorption approximation with scattering effect for infrared radiation. *J. Atmos. Sci.*, **57**, 2905-2914.

Moorthi, S. and Suarez, M.J. 1992: Relaxed Arakawa-Schubert: A parameterization of moist convection for general circulation models. *Mon. Wea. Rev.*, **120**, 978-1002.

Noh, Y. and Kim, H.J. 1999: Simulations of temperature and turbulence structure of the oceanic boundary layer with the improved near-surface process. *J. Geophys. Res.*, 104 (C7), 15621–15634.

Pan, D.-M. and Randall, D. 1998: A cumulus parameterization with a prognostic closure. *Quart. J. Roy. Meteor. Soc.*, **124**, 949-981.

Randall, D. and Pan, D.-M. 1993: Implementation of the Arakawa-Schubert cumulus parameterization with a prognostic closure. *Meteorological Monograph/The representation of cumulus convection in numerical models*, **46**, 137-144.

Smith, R.N.B. 1990: A scheme for predicting layer clouds and their water content in a general circulation model. *Quart. J.Roy. Meteor. Soc.*, **116**, 435-460.

Tsujino, H., Motoi, T., Ishikawa, I., Hirabara, M., Nakano, H., Yamanaka, G., Yasuda T. and Ishizaki, H. 2009: Reference Manual for the Meteorological Research Institute Community Ocean Model (MRI.COM) Version 3. *Technical Reports of the Meteorological Research Institute*, **59**.

Yoshimura, H. and Matsumura, T. 2003: A Semi-Lagrangian Scheme Conservative in the Vertical Direction. *CAS/JSC WGNE Res. Act. in Atmos. and Ocea. Modelling*, **33**, 319-320.

DEVELOPMENTS WITHIN THE ACCESS NWP SYSTEMS

Peter Steinle on behalf of the Earth System Modelling Research Program

Centre for Australian Weather and Climate Research, A partnership between the Australian Bureau of Meteorology and CSIRO, Melbourne, Australia
p.steinle@bom.gov.au

There have been two major advances in the Numerical Weather Prediction (NWP) systems based on the Australian Community Climate and Earth System Simulator, ACCESS (Puri et al. 2012) during the last 18 months. These are the operational implementation of an upgraded operational (APS1) global system and the development of a convective scale research system. A brief review of the performance of these two systems during summer over Northern Australia will be presented.

The APS1 global system contains an upgrade in resolution to N320 (481 latitude points, 640 longitude points) and 70 vertical levels from the previous system, APS0 which had a resolution of N144 (217x288 points), 50 levels. The atmospheric model upgrades include significant improvements to the parameterization of various physical processes, in particular a new prognostic cloud scheme, PC2 (Wilson et al 2008) is used. Other revisions include changes to the boundary layer (Edwards et al. 2011), radiation (Manners et al. 2008) and convection. Higher resolution (4km and 1.5km) models account for the advection of rainfall. In addition, the assimilation was upgraded to include the use of soundings from the *Infrared Atmospheric Sounding Interferometer (IASI, Pavelin et al., 2008, Hilton et al., 2009)* aboard the Metop-A instrument and GPS radio-occultation from the Constellation Observing System for Meteorology, Ionosphere, and Climate (COSMIC) satellites (Rennie 2008, 2010). These changes have combined to provide a gain of approximately 24 hours in the forecast skill in the tropics, and major gains in the skill of some tropical cyclone forecasts.

The development of the convective scale system is to support the use of radar data within NWP systems and is part of the Strategic Radar Enhancement Project. There are a significant number of issues with convective scale NWP and radar data. First and foremost the space and time scales of features captured by radars require a high resolution assimilation system – a 12km system with 4dVAR will perform an analysis at 36km, neither of which are suitable for capturing anything but the broadest of scales from a single radar. These scales also have very limited predictability so a latency of around 8 hours or so is not appropriate. Another consideration is the highly nonlinear relationships between model variables associated with clouds and precipitation, and so the variational assimilation of cloud or precipitation features requires a very accurate background which is difficult given the highly patchwork coverage offered by the Bureau's radars. These issues have been addressed by developing a system that uses a 1.5km grid to provide the resolution, 3 hourly 3dVAR to reduce the latency and latent heat nudging (Jones and Macpherson, 1997) to initialize the precipitation. The nudging compares radar and gauge quantitative precipitation estimates with model forecasts each time step (50s) to obtain a vertically integrated estimate of latent heating deficit or surplus. The latent heating profile in the model is then scaled accordingly. However, the nudging provides only a small gain in accuracy for a few hours. This limited effect is thought to be partly due to errors in the model's rainfall distribution, as well as the inherent limitations of latent heat nudging. The rainfall distribution for the 1.5km model has too little light rain and too much heavy rain, although the overall patterns appear reasonable. The deficiencies of the 1.5km model are however much less than the existing operational systems which exhibit excessive amounts of light rain, and usually under-forecast heavy rain, although at times they can also produce excessive heavy rain, comparable to that of the higher resolution models.

It will be shown that the main value of the high resolution assimilation comes from the higher frequency assimilation-forecast cycle. This is not surprising as 3 hour 3dVAR without satellite sounding data is generally inferior to 6 hour 4dVAR with satellite data. While the rainfall data is able to provide some compensation for the deficiencies of the high resolution assimilation systems, the incomplete coverage, and inherent differences between modelled and observed precipitation distributions limit the value of radar data. In addition assimilation over small domains excludes many observations that could assist scales of similar size to the domain, but these scales may be accurately analysed by the larger scale nesting system. However, by comparing forecasts that would be available at a given time, the advantage of the high resolution system for short term precipitation forecasting is clear.

References

Edwards J.M., McGregor, J.R., Bush, M.R. and Bornemann. F.J. 2011: "Assessment of numerical weather forecasts against observations from Cardington: seasonal diurnal cycles of screen-level and surface temperatures and surface fluxes". *Q. J. R. Meteorol. Soc.* 137: 656–672.

Hilton, F., Atkinson, N., English S.J. and Eyre, J.R. 2009: "Assimilation of IASI at the Met Office and assessment of its impact through observing system experiments", *Q. J. R. Meteorol. Soc.,* 135: 495-505.

Jones, CD and Macpherson, B.1997: "A Latent Heat Nudging scheme for the Assimilation of Precipitation Data into an operational Mesoscale Model." *Met Apps*, 4:269-277.

Manners, J., Thelen, J.C., Petch, J., Hill, P. and Edwards, J.M. 2008: "Two fast radiative transfer methods to improve the temporal sampling of clouds in numerical weather prediction and climate models", *Q. J. R. Meteorol. Soc.,* 135: 457-468.

Pavelin, E.G., English, S.J. and Eyre, J.R. 2008: "The assimilation of cloud-affected infrared satellite radiances for numerical weather prediction", *Q. J. R. Meteorol. Soc.,* 134: 737-749.

Puri, K., Dietachmayer, G., Steinle, P., Dix, M., Rikus, L., Logan, L., Naughton, M., Tingwell, C., Xiao, Y., Barras, V., Bermous, I,. Bowen, R., Deschamps, L., Franklin, C., Fraser, J., Glowacki, T., Harris, B., Lee, J., Le, T., Roff, G., Sulaiman, A., Sims, H., Sun, X., Sun, Z., Zhu, H., Chattopadhyay, M. and Engel, C. 2012: "Implementation of the initial ACCESS Numerical Weather Prediction system", *Aust. Met. Oc. Journal,* submitted.

Rennie M. 2008: "The assimilation of GPS radio occultation data into the Met Office global model". *Met R&D Technical Report 510* (available via the Met Office website), Met Office, UK.

Rennie M. 2010. "The Impact of GPS Radio Occultation Assimilation at the Met Office." *Q. J. R. Meteorol. Soc.* 136: 116–131.

Wilson, D.R., Bushell, A.C., Kerr-Munslow, A.M., Price J.D. and Morcrette, C.J. 2008: "PC2: A prognostic cloud fraction and condensation scheme. I: Scheme description". *Q. J. R. Meteorol. Soc.,* 134: 2093-2107.

ACCESS SHORT-RANGE RAINFALL PREDICTION IN THE AUSTRALIAN TROPICS

Beth Ebert

CAWCR Weather & Environmental Prediction

Introduction

Numerical weather prediction (NWP) models are the main source of objective guidance used by forecasters in predicting temperature, wind, and rainfall out to seven days. For quantitative precipitation forecasts (QPFs) in particular, it is well known that the models tend to be less accurate in the tropics than in mid-latitudes. This is because tropical rainfall is dominated by convection, where the detailed rain location and timing are highly uncertain.

Improvements in our ability to model tropical rainfall in the 1-7 day range seem to be hard to achieve. While verification of the QPFs from the Bureau's previous generation of NWP models (GASP and LAPS) showed gains in mid-latitude rain prediction skill from 1996 to 2009, only small improvements were evident in the tropics (Ebert *et al.* 2003, Ebert 2009a). Initial comparisons of ACCESS and GASP/LAPS rainfall performance showed that the ACCESS modelling system produced better rainfall forecasts than the older models (Ebert 2009b). However, that study did not differentiate seasonal or regional performance.

Here ACCESS QPFs from the operational (APS0) version of the ACCESS global, regional, and Australian models (ACCESS-G, -R, -A, respectively) are systematically verified in the Australian tropics (defined here as 10°-20°S, 115°-150°E) during two wet seasons, November-March 2010-11 and 2011-12. The primary reference data come from the Bureau's operational 0.25° daily rain gauge analysis (Weymouth *et al.* 1999) and apply to land areas only. Additional reference data include the TRMM 3B42 0.25° multi-satellite precipitation estimates (Huffman *et al.* 2007). To better delineate QPF performance for different convective regimes, the verification results are stratified for paired phases of the Madden Julian Oscillation (MJO) as defined by Wheeler and Hendon (2004), as well as for the five wet season regimes of Pope *et al.* (2009). Due to page limits, only a small subset of results are shown here.

Visual comparison - example of 26 Dec 2010

An example of ACCESS QPFs is shown in Fig. 1 for rain falling on 26 December 2010. This event occurred during an extended active monsoon period, with some parts of the Top End receiving a two-week total accumulation in excess 400mm. The daily rainfall shown here is typical for the active monsoon period. The models show different levels of detail. The 5-day forecast from ACCESS-G is fairly smooth since the model grid is about 80 km, the ACCESS-R forecast (37 km) contains greater detail, and the ACCESS-A model (11 km) shows finer structure still. All models predicted an area of heavy rain centred on or just north of the Top End. Interestingly, only ACCESS-G predicted the area of enhanced convection over the Gulf of Carpentaria.

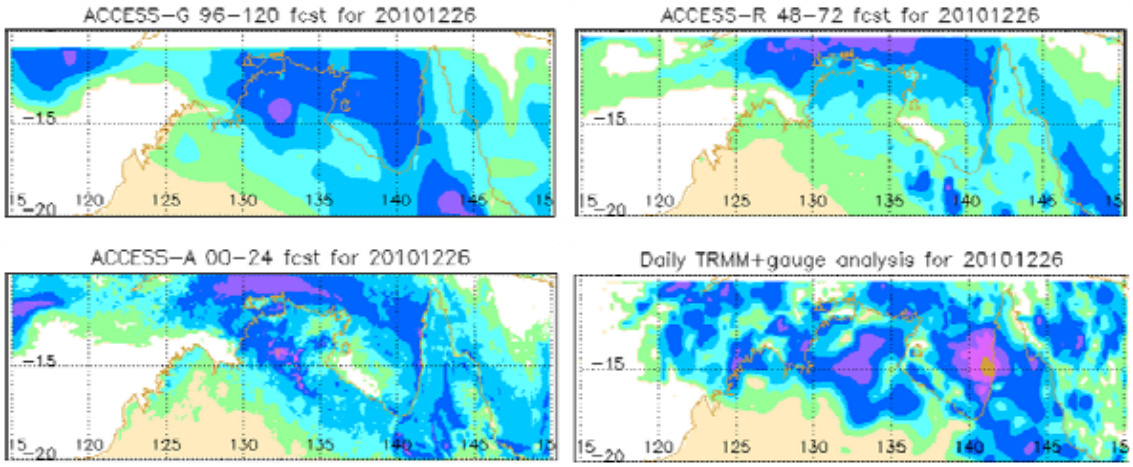

***Fig. 1**. Forecast and observed 24h rainfall accumulations for 26 December 2010.*

ACCESS QPF performance as a function of rain intensity

Figure 2 shows the dependence of ACCESS QPF performance on the rain intensity for three model versions and lead times, all verified on their native model grids. The performance is remarkably similar for these forecasts (note that coarser resolution and shorter lead times are both advantageous). The frequency bias (FBI) indicates that all models under-predict the frequency of heavier rain rates. The probability of detection (POD) decreases from near perfect detection for rain/no rain to about 10% for heavy rain exceeding 50 mm d^{-1}, even though the false alarm ratio is 70-85% for the heaviest rain. This evidence, along with the equitable threat score (ETS) indicate the difficulty that ACCESS has in predicting the occurrence of heavy rain.

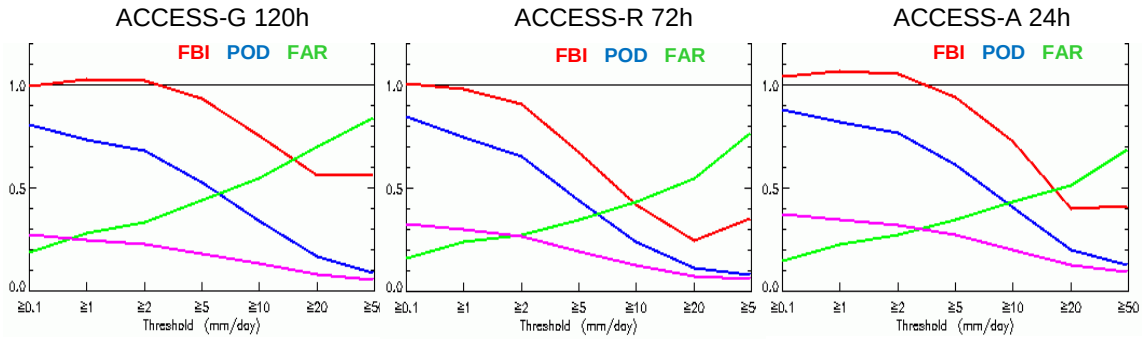

***Fig. 2.** Categorical verification scores for (a) ACCESS-G 5-day forecasts, (b) ACCESS-R 3-day forecasts, and (c) ACCESS-A 1-day forecasts as a function of rain threshold (land only).*

ACCESS QPF performance as a function of regime

The time series of forecast and observed daily rain volume over the tropical land area is shown in Fig. 3. The ACCESS model captures both the timing and the amplitude of the rainfall. The degree to which 5-day forecasts can successfully predict the amount of tropical rainfall is quite remarkable. A negative bias in rain amount is evident, particularly for ACCESS-R.

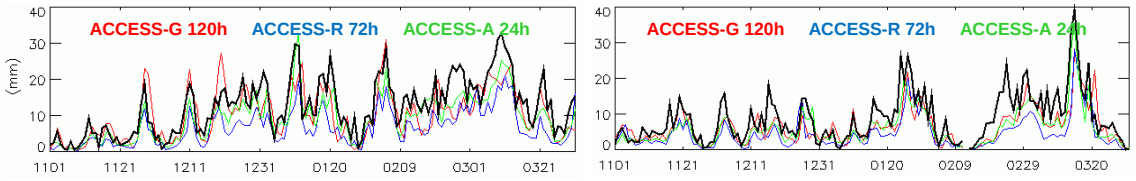

***Fig. 3**. Observed and forecast daily rain volume (km^3) over land for the 2010-11 (left) and 2011-12 (right) wet seasons.*

Table 1 shows the observed and forecast rain volume observed and for these forecasts, stratified by paired MJO phases. MJO phases 1 and 2 normally correspond to dryer than average conditions in summer, while phases 5 and 6 are wetter than normal and are usually associated with the active monsoon period (Wheeler *et al.* 2009). In 2010-11 and 2011-12 Phases 5 and 6 had the greatest rain volume, but surprisingly the second wettest regime corresponded to MJO phases 1 and 2. As seen in Fig. 3, the ACCESS model underestimated the rain volume in all regimes, with ACCESS-R having the largest bias.

The ability of ACCESS-G forecasts to predict the grid-scale occurrence of moderate rainfall exceeding 10 mm d^{-1} is shown in Fig. 4. The errors are due partly to underestimation of moderate rain frequency (Fig. 2), but mainly to imprecise forecasts of the rain pattern. In the first three days of the forecast, rain in MJO phases 5 and 6 is predicted most skilfully and the model forecasts are more accurate than a 1-day persistence forecast. At medium ranges rain in MJO phases 7 and 8 is the most predictable.

Table 1. Observed and forecast rain volume over land (km^3) as a function of MJO phase.

MJO Phase	**All** (n=302)	**1,2** (n=30)	**3,4** (n=47)	**5,6** (n=69)	**7,8** (n=46)
Observed	12.9	14.4	11.1	15.5	11.9
ACCESS-A 24h forecast	9.7	8.7	7.7	12.0	8.4
ACCESS-R 72h forecast	7.1	7.1	5.5	8.8	6.0
ACCESS-G 120h forecast	9.7	9.6	8.9	12.5	9.9

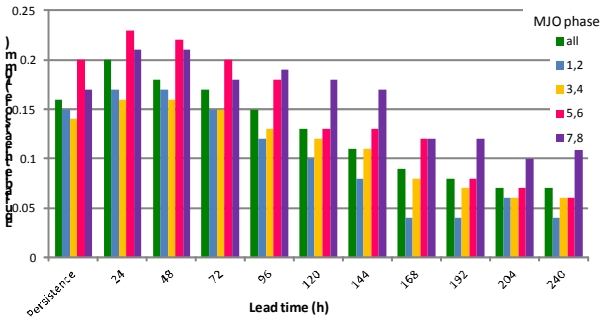

***Fig. 4.** Equitable threat score for rain exceeding 10 mm d^{-1} for ACCESS-G and 24h persistence forecasts (land only) as a function of forecast lead time.*

Discussion

Much more extensive analysis of these verification results will be done in the near future to better quantify tropical rainfall prediction skill and guide future ACCESS model improvements. Comparisons will be made against other global models including ECMWF and GFS, and against the Poor Man's Ensemble. Diagnostic spatial verification approaches will be used to characterise the sources of error and estimate spatial scales for which useful skill exists. This study will provide a

benchmark of QPF accuracy against which recent (APS1) and future (APS2 and beyond) improvements in the ACCESS model can be measured.

Acknowledgments

The author would like to thank Harry Hendon for suggesting that the ACCESS performance be stratified as a function of MJO phase.

References

Ebert, E. 2009a: Precipitation intercomparison over Australia. *Report of the twenty-fifth session of the CAS/JSC WGNE, Offenbach, Germany, 2-6 November 2009*.

Ebert, E. 2009b: Heavy rain forecasts using the ACCESS model. *Proc. 3rd CAWCR Modelling Workshop: Modelling and Understanding High Impact Weather, 30 Nov-2 Dec 2009.*

Ebert, E.E., Damrath, U., Wergen W. and Baldwin, M.E. 2003: The WGNE assessment of short-term quantitative precipitation forecasts. *Bull. Amer. Met. Soc.*, **84**, 481-492.

Huffman, G. J. and Coauthors, 2007: The TRMM Multisatellite Precipitation Analysis (TMPA): Quasi-global, multiyear, combined-sensor precipitation estimates at fine scales. *J. Hydrometeor*, **8**, 38-55.

Pope, M., Jakob, C. and Reeder, M.J. 2009: Regimes of the North Australian wet season. *J. Climate*, **22**, 6699-6715.

Weymouth, G., Mills, G.A., Jones, D., Ebert, E.E. and Manton, M.J. 1999: A continental-scale daily rainfall analysis system. *Aust. Met. Mag.*, **48**, 169-179.

Wheeler, M.C. and Hendon, H.H. 2004: An all-season real-time multivariate MJO index: Development of an index for monitoring and prediction. *Mon. Wea. Rev.*, **132**, 1917-1932.

Wheeler, M.C., Hendon, H.H., Cleland, S., Meinke, H. and Donald, A.2009: Impacts of the Madden–Julian Oscillation on Australian rainfall and circulation. *J. Climate*, **22**, 1482-1498.

CHALLENGES IN MONSOON FORECASTING AT DARWIN

Craig Earl-Spurr

Although the classically accepted definitions of the monsoon relate to the seasonality of prevailing winds, colloquially the monsoon refers simply to the accompanying rainfall phenomena. As such it is necessary to be able to distinguish between subtle differences in a variety of patterns that may match the scientific definitions but that can lead to far more pronounced differences in observed weather. It follows that in order to produce an accurate and meaningful forecast, an integral part of the operational forecasters role is the ability to recognise and interpret these local influences on monsoon variability. Focussing on Northern Australia, and in particular Darwin, this talk will discuss local conceptual models of the monsoon and its influences.

UNDERSTANDING AND EVALUATION OF MONSOON PROCESSES IN THE METUM

Gill Martin

Met Office Hadley Centre, FitzRoy Road, Exeter, UK

With contributions from Stephanie Bush, Nicholas Klingaman, Richard Levine, Sean Milton, Andrew Turner, and members of the joint Met Office/NCAS-Climate Monsoon Working Group.

Introduction

The monsoons are complex phenomena whose simulation has proved a challenge for modellers for several decades. Many studies have shown sensitivity to convection and boundary layer parametrisation (e.g. Mukhopadhyay et al. 2010 and references therein; Hong 2010 and references therein), cloud microphysics and land surface properties (e.g. Douville et al. 2001; Yasunari et al. 2006), as well as model resolution (e.g. Kim et al. 2008). Idealised sensitivity experiments have shed light on the major forcing regions, such as orographic forcing from the Himalayas and the Tibetan plateau (e.g. Boos and Kuang 2010) and the western Ghats (e.g. Wang and Chang 2012), land-sea contrasts between the Indian peninsula and the surrounding ocean, and sea surface temperature forcing from the Arabian Sea, Bay of Bengal and the equatorial Indian Ocean (Levine and Turner 2012).

Here we highlight a number of monsoon studies which are being done using the MetUM, which is a Unified Modelling framework where the same physical configuration can be used across a range of spatial and temporal scales. The MetUM has benefitted from the synergy between NWP and climate modelling in many past model developments, e.g. Martin et al. (2010) showed how the seamless model development approach was used to improved tropical performance.

Typical monsoon systematic errors

Climatology

Typical South Asian monsoon systematic errors in a climate configuration of the MetUM, HadGEM1, were described by Ringer et al. (2006) and include excessive rainfall over the equatorial Indian Ocean and the Himalayan foothills and underestimation of rainfall over the Indian peninsula. These biases were reduced in the HadGEM2 configuration through the seamless modelling approach (Martin et al. 2010), although their basic pattern still remains. Many of these biases are common to other GCMs (e.g. Sperber et al. 2012). Generally, the South Asian summer monsoon circulation is simulated better than the rainfall, although at low-levels there is excessive divergence of the monsoon flow at the western Indian coast, an anti-cyclonic bias over India, excessive flow along the Himalayan foothills, and anomalous easterly flow across the equatorial Indian Ocean. In East Asia, typical model systematic errors include a weak intensity of the North Pacific subtropical high pressure region associated with anomalously weak southerly inflow and an underestimation of rainfall over eastern China and Korea (Boo et al. 2011). In West Africa, in coupled atmosphere-ocean models the rainfall tends to be biased to the south and underestimated over the Sahel, related to warm sea surface temperature (SST) biases in the Gulf of Guinea, while many atmosphere-only models fail to reproduce the seasonal north-south movement of the rain band even when forced by realistic SSTs

(Vellinga et al. 2012). Over Australia, monsoon rainfall over the northern land areas tends to be underestimated while that over the surrounding sea is overestimated.

Fig. 1 shows how the systematic errors in South Asian summer monsoon rainfall in the MetUM persist from daily forecast timescales to climate simulations. Similar consistency is found for the monsoon circulation errors. The biases develop within the first few days of simulation, suggesting that they are a direct impact of parameterisations and not due to non-linear feedback processes operating on longer time-scales. This provides the potential for reducing these systematic biases through improved parametrisation of physical processes in the model (see Milton et al. in this volume).

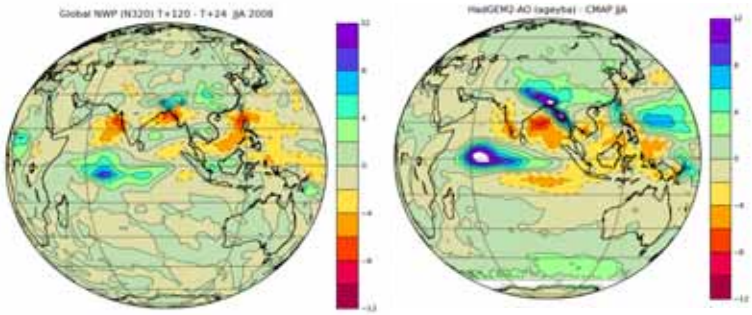

***Fig. 1**: 5-day (left) and climatological (30-year mean; right) rainfall errors in June, July, August (JJA) from the MetUM.*

Interannual Variability

Monsoons exhibit significant interannual variability that models struggle to capture (e.g. Annamalai et al. 2007). Many of the monsoon systems are strongly linked to El Nino Southern Oscillation (ENSO) but models are unable to simulate correctly either ENSO teleconnections or ENSO itself. This can affect both the monsoon climatology and amplitude of interannual variability and the response to individual events, even in seasonal hindcasts. For example, in 1997, seasonal coupled model hindcasts from the GloSea4 system (Arribas et al. 2011) simulated warm El Nino SST anomalies that extended too far west, leading to anomalous ascent over warm SSTs which pushed into the Maritime Continent, shifting the anomalous subsidence west of where it was observed (Fig. 2). This resulted in poor simulation of the rainfall anomaly pattern in that year. Generally, models are more successful in simulating the dynamical response of the monsoons to ENSO than the regional changes in rainfall. This is probably due to the larger-scale nature of the typical indices involved (e.g. the dynamical monsoon index proposed by Webster and Yang 1992).

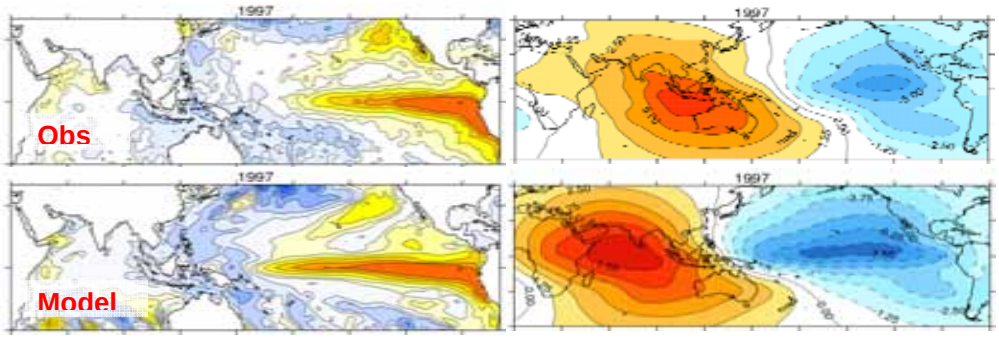

***Fig. 2**: Observed (top) and modelled (bottom) SST (left) and 200 hPa velocity potential (right) anomalies in JJA from seasonal coupled model hindcasts.*

Intraseasonal variability

Evaluation of monsoon sub-seasonal variability has focused on the total sub-seasonal variance in precipitation across the global monsoon domain, links to the eastward-propagating Madden-Julian oscillation (MJO), the northward propagation of organised convection from the tropical Indian Ocean

to the Indian subcontinent, and the length of monsoon wet and dry spells. Total sub-seasonal precipitation variance has been deficient in all development versions of HadGEM3, associated with a weak MJO that fails to propagate. The lack of sub-seasonal variance constrains the probability distribution function of daily rainfall in all monsoon regions toward the mean. Consistent with a poor MJO, active and break events propagate only weakly northwards from the equator to India (in coupled models); the dearth of active events may be responsible for the low number of monsoon depressions in the model (e.g. Krishnamurthy and Shukla 2007). In all monsoon regions, the auto-correlation of daily, grid-point rainfall is far too long compared with satellite observations, suggesting that the model becomes "stuck" in particular regimes and cannot switch between active and break monsoons. This may point to errors in local land-surface↔precipitation feedbacks. Such findings are common to other models, such as those used in CMIP5.

Sensitivity studies to understand model errors

SST biases

Since monsoons develop in response to the seasonal variations in meridional temperature gradient between land and ocean, monsoon simulations are subject to SST biases which develop in coupled atmosphere-ocean models. The Indian Ocean is a particular problematic region, with many models showing biases in SST, evaporation, precipitation and air-sea coupling. Models also often exhibit warm SST biases in the Gulf of Guinea which weaken the West African Monsoon and limit its northward progression, while persistent equatorial cold SST biases in the Pacific, affecting ENSO, are also common.

Northern Arabian Sea cold SST biases are common amongst CMIP3 and CMIP5 models (Levine et al. 2012), and appear to be driven by common atmospheric mechanisms during winter. Applying idealised SST anomalies, based on coupled model biases in different regions, to observed SSTs in atmosphere-only experiments with a prototype climate configuration, HadGEM3, shows that the persistence of the northern Arabian Sea cold SST bias into summer significantly weakens simulated monsoon rainfall in the early part of the South Asian summer monsoon season (Fig. 3, and Levine and Turner 2012). However, a cold SST bias which also occurs in HadGEM3 (and in several other models) over the equatorial Indian Ocean counteracts this weakening during the rest of the season by enhancing the meridional temperature gradient.

Examining the development of these SST biases in initialised coupled seasonal hindcasts reveals that the interaction between the biases in these two regions varies with the lead time of the hindcast. In simulations initialised in spring, the cold Arabian Sea SST bias does not have time to develop, leaving the equatorial SST bias (which develops in response to excessive rainfall there) to strengthen the monsoon through the enhanced meridional temperature gradient. Thus, in seasonal hindcasts initialised in May, the monsoon rainfall is enhanced over and above that of the both the coupled climate configuration and the observations.

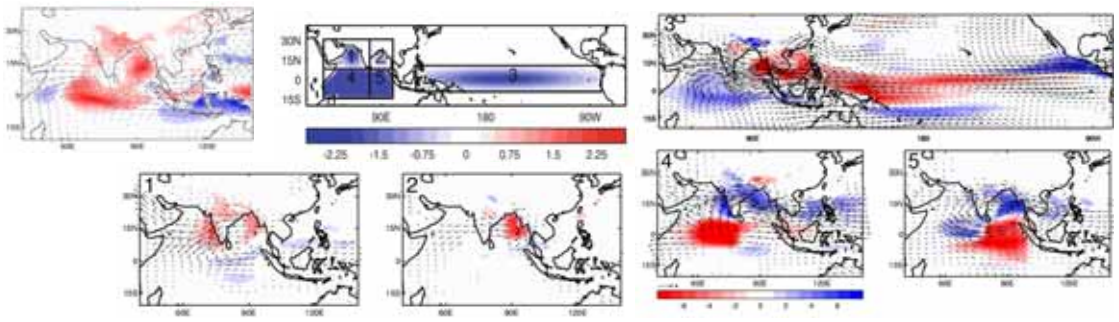

Fig. 3: *Top left: differences in monsoon rainfall (shaded) and 850 hPa horizontal winds (vectors) between atmosphere-only and coupled configurations of HadGEM3 in JJAS; Top middle: SST anomalies based on HadGEM3 coupled model SST biases and applied in AMIP experiments; Subsequent panels: the effect of applying coupled model style SST anomalies on rainfall (colours) and 850hPa wind (vector) anomalies. Scales are shown below panel labelled "4". The numbers correspond to the regional SST anomalies (top middle) which are applied individually.*

Role of convection parametrisation

The development of a cold SST bias in the western equatorial Indian Ocean is related to a persistent positive rainfall bias in this region in the atmosphere component. Targeted application of changes to parameters in the convection scheme illustrates how changes in convection intensity in this region affect the rainfall pattern in the surrounding regions. We find that the response of the South Asian monsoon precipitation and 850 hPa circulation in a prototype HadGEM3 AMIP-style run to increasing the convective entrainment rate profile by a factor of 1.5 globally is of opposite sign in the western equatorial Indian Ocean (WEIO) from that in the western equatorial Pacific (WEP) (Fig. 4, top left panel). The increased rainfall resulting from this change in the WEP region is unexpected and could result from feedbacks between this and other regions. However, we find that the response to making this change only in the specific regions of interest is similar in pattern (though smaller in magnitude) to the response when the entrainment rate is increased globally (Fig. 4, top panels). The reasons for the opposite responses in the two regions are still under investigation. However, the experiments reveal the influence of changing the parametrisation in one region on the rainfall and circulation in surrounding regions, such as around the Indian peninsula, Indonesia and over the western Pacific.

Such studies also suggest that the distribution of convective intensity, both spatially and temporally, can influence the climatological amount and spatial distribution of rainfall. Although observations of rainfall intensity on sub-daily timescales are scarce, examination of the impact of changing convection scheme parameters on the spectrum of rainfall intensities produced by the model every timestep provides insight into these relationships. Fig. 4 (lower panels) shows the change in the deep convective rainfall intensity spectrum in the WEIO region when the entrainment parameter is increased. The frequency of high intensity rainfall events is reduced and replaced by an increased frequency of more moderate intensity events which make a greater contribution to the mean precipitation, although the latter itself is reduced. Similar changes in the rainfall intensity spectrum are seen in the WEP region, although the mean precipitation is increased overall.

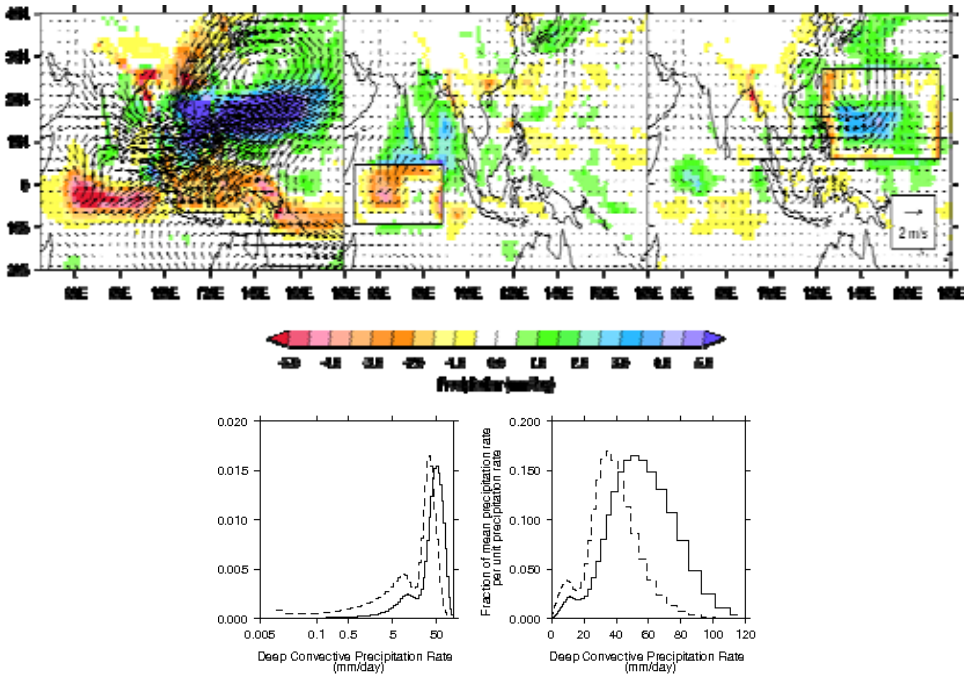

Fig. 4: *Top panels: The response of south Asian JJAS precipitation and 850 hPa circulation in a HadGEM3 GA3.0 AMIP style run to increasing the convective entrainment rate profile by a factor of 1.5. Left: the response when the entrainment rate is increased globally. Middle and right: The response when the entrainment rate is increased only in a region of interest, such as the Western Equatorial Indian Ocean (middle) or Western North Pacific (right).*

Lower panels: Histograms showing how increased entrainment alters frequency and amount of deep convective precipitation at different rates. The histograms include every time-step for July and August and every grid point over an area in the WEIO (50 - 90E, 10S - 5N). Solid line: control; dashed line: increased entrainment experiment. Left: The fraction of the total number of points and timesteps with a given precipitation rate. Right: The contribution of a given precipitation rate to the mean precipitation rate, per unit precipitation rate. The area of each bar is proportional to the amount of precipitation accumulating at that rate.

More radical sensitivity experiments include progressively removing the land of the Indian peninsula in order to investigate the influence of the convection scheme behaviour over land on the regional systematic biases. In common with many other models, the MetUM struggles to represent the timing of the diurnal cycle of rainfall over land, with the peak in precipitation and outgoing longwave radiation occurring several hours too early and a lack of rainfall in the evening. Successively saturating, flooding, and then removing the land area of the Indian peninsula results in increased rainfall over the "peninsula" region and more continuous convection throughout the day. There is also a response to removing the orography of the western Ghats, and this response is largely independent of the change to the land surface conditions. This implies that the orography determines the spatial distribution of the rainfall over the peninsula while the land surface conditions affect the amount of rain, mainly through changes in the diurnal variation of surface fluxes.

Studies with high resolution models which explicitly represent convection show improved representation of the diurnal cycle with convection peaking later in the day (e.g. Kendon et al. 2012). New nested model runs with increased horizontal resolution up to 1.5km over India, and with the convection parametrisation switched off, are underway in order to increase our understanding of the role of the parametrisation deficiencies on the monsoon biases and potentially improve the representation of convective processes in lower resolution models (see Milton et al. in this volume).

Role of the land surface

Although the basic drivers of the South Asian and West African monsoon systems are similar (i.e. the seasonal reversal of the land-sea temperature contrast and the resulting inflow of warm, moist air from the tropical ocean onto the landmass), the West African monsoon shows an additional significant dependence of rainfall on soil moisture on the seasonal timescale (Douville et al. 2001). The West African monsoon onset is characterised by an abrupt shift of the rain band from around 5º N through most of June (the pre-onset phase) up to 10º N in early July. Estimates of the date of the northward shift of the monsoon rain band have been made in the two ensembles of prototype HadGEM3 runs used by Comer and Best (2012). In the former ensemble, soil moisture evolves according to the model's prognostic equations. In the latter, soil moisture is prescribed at every timestep so that it does not vary across the members of that ensemble. When soil moisture is prescribed, there is a clear reduction in the spread of dates, and they are clustered towards the start of the control range. The earlier (on average) onset date will produce a northward shift in the average rain band through July. Preliminary work suggests that the earlier onset may be attributed to drier soils in the prescribed soil moisture runs promoting a stronger meridional circulation.

Several studies (e.g. Osborne et al., 2004; McCarthy et al., 2012) have demonstrated significant impacts on tropical climate from vegetation changes in both the tropics and the mid-latitudes. We have examined the influence of changes in land cover resulting from the interactive terrestrial carbon cycle in the HadGEM2 Earth System configuration (HadGEM2-ES) on the present-day simulation and future projections of the South Asian summer monsoon (Martin and Levine 2012). When interactive vegetation is included, the persistent dry bias over India described above is associated with an increase in the bare soil fraction in this region, as well as in other regions such as the Sahel and Saudi Arabia. This generates a large increase in the atmospheric dust loading, which affects the radiation balance in the region. Experiments where this radiative feedback is removed have shown that the radiative effect of the increased dust contributes to a further increase in the dry bias in the seasonal mean Indian rainfall (Fig. 5, left), and that this dominates any other response to the vegetation distribution.

In the absence of radiative effects of changes in dust, a response to changes in the vegetation distribution over Eurasia can be discerned (Fig. 5, right). In a similar manner to previous work (e.g. Turner and Slingo 2011), we find that changes in tree cover over northeast Eurasia are associated with changes in snow cover which generate a dynamical response in the South Asian summer monsoon through their effects on the development of the meridional temperature gradient.

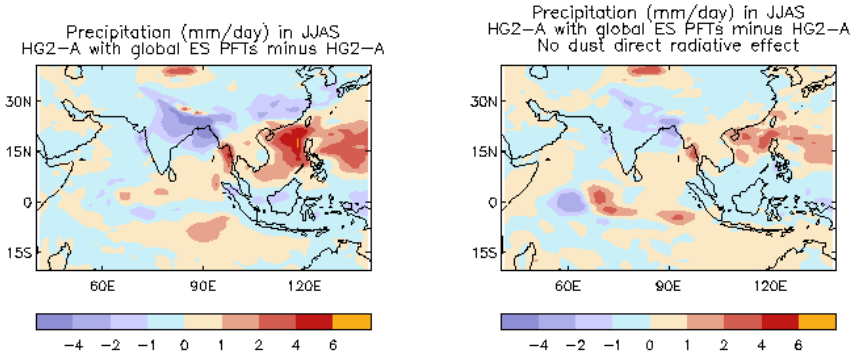

Fig. 5: *Changes in JJAS precipitation between (a) HadGEM2-A with and without the vegetation distribution from -ES, (b) as (a) but without the direct radiative effect of dust.*

Role of orographic forcing

Boos and Kuang (2010) showed that the strength of the South Asian monsoon is dependent on Himalayan orography, rather than elevated heating over the Tibetan Plateau. Their model study

suggested that, although Tibetan plateau heating locally enhances rainfall along its southern edge, the large-scale South Asian summer monsoon circulation is otherwise unaffected by removal of the plateau, provided that the narrow orography of the Himalayas and adjacent mountain ranges is preserved. However, the MetUM (in common with several other current models) produces excessive rainfall along the Himalayan foothills, and it is likely that this error is related to the underestimation of rainfall over the Indian peninsula.

The interaction between the Himalayan wet bias and the Indian dry bias has been examined in Regional Climate Model (RCM) experiments, which use the same model physics as the global climate model. Experiments have been run at approximately 50km resolution for different domains surrounding the Indian subcontinent. Significant improvements are found when excluding the Himalayas from the RCM domain, with rainfall moving from the Himalayas towards central India (Fig. 6, left). A consistent result is obtained in the RCM with the standard domain when smoothing the steep gradients of the southern slopes of the Himalayas, which reduces low-level convergence (Fig. 6, right). This suggests the model may have problems reacting to steep slopes. Excessive rainfall over the Himalayas may be emphasized by the apparent difficulty for model convection to develop over central India. Work is ongoing to understand the errors near steep Himalayan and western Ghats orography, including the sensitivity to horizontal resolution and the potential lack of mesoscale convective systems generated over the western Ghats and propagating towards central India.

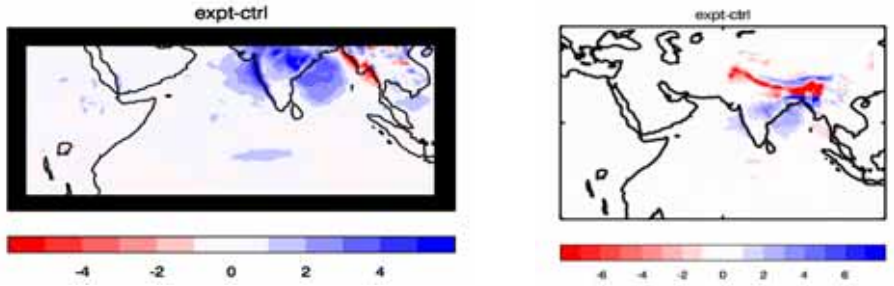

Fig. 6: *The impact on JJAS rainfall (mm/day) of (left) excluding the Himalayas from the RCM domain, and (right) smoothing the mean and sub-gridscale orography of the Himalayan region.*

Future projections

There is still much uncertainty in future projections of monsoon rainfall (e.g. Turner and Annamalai 2012). Inter-model spread amongst CMIP3 models for future projections of summer monsoon precipitation over the Indian region is larger than the mean precipitation increase. Contributions to the CMIP3 inter-model spread of various aspects of monsoon simulations have been shown to arise from differences in model formulation, such as different types of atmospheric convection schemes and differences in resolution. Uncertainty in multi-model future projections may arise from missing or incorrect representation of processes in models (such as convection) and from common model biases (e.g. in SST).

Model projections for future monsoons indicate generally small positive changes in monsoon rainfall. Models also predict warming of Arabian Sea surface temperatures of a similar order to the magnitude of typical climate model biases in this region (Levine and Turner 2012). HadGEM2 time-slice experiments have shown that a cold base state in the Arabian Sea can limit future rainfall increases both in absolute and relative terms (Levine et al. 2012). Analysis of CMIP5 RCP8.5 scenario runs shows that, while averaged over all CMIP5 models the mean early monsoon rainfall does not change much in the future, the spread of future rainfall change amongst models with small Arabian Sea SST biases is considerably larger during the early monsoon than for models with large Arabian Sea SST biases. This is consistent with future SST warming on top of a warmer mean state inducing larger changes in moisture fluxes through the non-linear Clausius-Clapeyron relationship. Therefore, it is possible that climate models with relatively large cold biases in the Arabian Sea are potentially underestimating the impact of greenhouse gas forcing and associated surface warming on the

monsoon. Similarly any models with warm Arabian Sea SST biases may overestimate increases of monsoon rainfall in future climate scenarios as a result of excessive acceleration of evaporation.

Summary

Representing monsoon systems, their variability and their response to climate change is an on-going challenge for modelling groups. Models share common biases in climatology and variability of the monsoons, and many of the errors are forced locally (in time and space), although some are related to biases elsewhere (e.g. the extratropical vegetation distribution, ENSO) or which occur in different seasons (e.g. Arabian Sea SST cold bias). Systematic errors develop rapidly (within 2 weeks for the atmosphere and the first month for SSTs), and models show only a small sensitivity to model resolution until sufficiently high resolution is reached that processes such as convection start to be represented explicitly. Future challenges include reducing coupled model SST biases (which affect the monsoon climatology, variability and teleconnections, even in seasonal forecasts), improving the representation of flow and rainfall over steep orography, and improving the representation of convective processes including diurnal variations, convective organisation, vertical distribution of diabatic heating, feedbacks on large-scale clouds and radiation, and interactions with the land surface.

References

Annamalai, H., Hamilton, K. and Sperber, K.R. 2007. The South Asian Summer Monsoon and Its Relationship with ENSO in the IPCC AR4 Simulations. *J. Climate, 20,* 1071–1092. doi: http://dx.doi.org/10.1175/JCLI4035.1

Arribas, A., Glover, M., Maidens, A., Peterson, K., Gordon, M., MacLachlan, C., Graham, R., Fereday, D., Camp, J., Scaife, A.A., Xavier, P., McLean, P., Colman, A. and Cusack, S. 2011. The GloSea4 Ensemble Prediction System for Seasonal Forecasting. *Mon. Weath. Rev., 139,* 1891-1910.

Boo, K.-O., Martin, G.M., Sellar, A., Senior, C.A. and Byun, Y.-H. 2011. Evaluating the East Asian monsoon simulation in climate models. *J. Geophys. Res., 116*, D01109, doi:10.1029/2010JD014737.

Boos, W.R. and Kuang, Z. 2010. Dominant control of the South Asian monsoon by orographic insulation versus plateau heating. *Nature, 463,* 218-222, doi:10.1038/nature08707

Comer, R. and Best, M. 2012. Revisiting GLACE: Understanding the Role of the Land Surface in Land-Atmosphere Coupling. *J Hydrometeorol*, in press.

Douville, H., Chauvin, F. and Broqua, H. 2001. Influence of soil moisture on the Asian and African monsoons. Part I: Mean monsoon and daily precipitation. *J. Climate., 14*, 2381-2403

Hong, S.-Y. 2010. A new stable boundary-layer mixing scheme and its impact on the simulated East Asian summer monsoon. *Q. J. R. Meteorol. Soc., 136*, 1481–1496. doi: 10.1002/qj.665

Kendon, E.J., Roberts, N.M., Senior, C.A. and Roberts, M.J. 2012. Realism of rainfall in a very high resolution regional climate model. *J. Climate,* doi: 10.1175/JCLI-D-11-00562.1

Kim, H.-J., Wang, B. and Ding, Q. 2008. The global monsoon variability simulated by CMIP3 coupled climate models. *J. Climate, 21*, 5271–5294, doi:10.1175/2008JCLI2041.1

Krishnamurthy, V. and Shukla, J. 2007. Intraseasonal and Seasonally Persisting Patterns of Indian Monsoon Rainfall. *J. Climate, 20,* 3-20. doi: http://dx.doi.org/10.1175/JCLI3981.1

Levine, R.C. and Turner, A.G. 2012. Dependence of Indian monsoon rainfall on moisture fluxes across the Arabian Sea and the impact of coupled model sea surface temperature biases. *Clim. Dyn. 38*, 2167-2190, DOI: 10.1007/s00382-011-1096-z

Levine, R.C., Turner, A.G., Marathayil, D. and Martin, G.M. 2012. The role of northern Arabian Sea surface temperature biases in CMIP5 model simulations and future projections of Indian summer monsoon rainfall. *Submitted to Climate Dynamics.*

Martin, G.M., Milton, S.F., Senior, C.A., Brooks, M.E., Ineson, S., Reichler, T. and Kim, J. 2010. Analysis and Reduction of Systematic Errors through a Seamless Approach to Modelling Weather and Climate. *J Clim., 23*, 5933-5957, DOI:10.1175/2010JCLI3541.1

Martin, G.M. and Levine, R.C. 2012. The influence of dynamic vegetation on the present-day simulation and future projections of the South Asian summer monsoon in the HadGEM2 family. *Earth Syst. Dynam. Discuss., 3,* 759-799, doi:10.5194/esdd-3-759-2012

McCarthy, M.P., Sanjay, J., Booth, B.B.B., Krishna Kumar, K., and Betts, R.A. 2012. The influence of vegetation on the ITCZ and South Asian monsoon in HadCM3. *Earth Syst. Dynam., 3,* 87-96, doi:10.5194/esd-3-87-2012.

Milton, S., Webster, S., Xavier, P., Willett, M., Shelly, A. and Martin, G. 2012. Asian-Australian Monsoon NWP with the UM. *Proceedings of the 6th Annual CAWCR Workshop on Understanding and Prediction of Monsoon Weather and Climate.*

Mukhopadhyay, P., Taraphdar, S., Goswami, B.N.and Krishnakumar, K. 2010. Indian Summer Monsoon Precipitation Climatology in a High-Resolution Regional Climate Model: Impacts of Convective Parameterization on Systematic Biases. *Weather Forecasting, 25*, 369–387, doi: http://dx.doi.org/10.1175/2009WAF2222320.1

Osborne, T.M., Lawrence, D.M., Slingo, J.M., Challinor, A.J., and Wheeler, T.R. 2004. Influence of vegetation on the local climate and hydrology in the tropics: sensitivity to soil parameters, *Clim. Dyn., 23*, 45–61, doi:10.1007/s00382-004-0421-1.

Ringer, M.A., Martin, G.M., Greeves, C.Z., Hinton, T.J., James, P.M., Pope, V.D., Scaife, A.A., Stratton, R.A., Inness, P.M., Slingo, J.M. and Yang, G.-Y. 2006. The physical properties of the atmosphere in the new Hadley Centre Global Environment Model, HadGEM1. Part II: Aspects of variability and regional climate. *J. Climate, 19*, 1302-1326.

Sperber, K.R., Annamalai, H., Kang, I.-S., Kitoh, A., Moise, A., Turner, A., Wang, B. and Zhou, T. 2012. The Asian summer monsoon: an intercomparison of CMIP5 vs. CMIP3 simulations of the late 20th century. *Clim. Dyn.* (submitted)

Turner, A.G. and Annamalai, H. 2012. Climate change and the South Asian summer monsoon. *Nature Clim. Change, 2,* 587–595, doi:10.1038/nclimate1495.

Turner, A.G. and Slingo, J.M. 2011. Using idealized snow forcing to test teleconnections with the Indian summer monsoon in the Hadley Centre GCM. *Clim Dyn, 36,* 1717-1735, doi:10.1007/s00382-010-0805-3.

Vellinga, M., Arribas, A. and Graham, R. 2012. Seasonal forecasts for regional onset of the West African monsoon. *Clim. Dyn*. (accepted)

Wang, Z. and Chang, C.-P. 2012. A Numerical Study of the Interaction between the Large-Scale Monsoon Circulation and Orographic Precipitation over South and Southeast Asia. *J. Climate, 25*, 2440–2455. doi: http://dx.doi.org/10.1175/JCLI-D-11-00136.1

Webster, P.J. and Yang, S. 1992. Monsoon and ENSO: selectively interactive systems. *Q. J. R. Meteorol. Soc., 118,* 877–926. doi:10.1002/qj.49711850705

Yasunari, T., Saito, K. and Takata, K. 2006. Relative Roles of Large-Scale Orography and Land Surface Processes in the Global Hydroclimate. Part I: Impacts on Monsoon Systems and the Tropics. *J Hydrometeor., 7,* 626–641, doi: http://dx.doi.org/10.1175/JHM515.1

SIMULATION OF ASIAN-AUSTRALIAN MONSOON BY ACCESS COUPLED MODELS

Harun A. Rashid

Centre for Australian Weather and Climate Research, a partnership between CSIRO and the Bureau of Meteorology, Melbourne, VIC, Australia

Harun.Rashid@csiro.au.

The large-scale monsoons play a prominent role in the global energy and hydrological cycles. The monsoons are characterized by seasonal reversals of regional winds, accompanied by substantial changes in rainfall, in tropical-subtropical latitudes. Examples of the large-scale monsoons are the Asian-Australian monsoon, African monsoon, and the North and South American monsoons. The physical processes involved in the formation of monsoons are complex, due in part to nonlinear interactions between the dynamical and thermodynamical processes across many space and time scales. Given the importance of monsoons to the atmosphere-ocean general circulation, as well as to regional economies, it is imperative that the state-of-the-art coupled general circulation models (CGCMs) simulate the large-scale monsoons with reasonable accuracy. However, monsoon simulations have been found to be one of the most challenging aspects of climate simulation in successive generations of CGCMs. While the recent CGCMs show an improved performance, the progress has been slow and has come about through painstaking analyses of observations and model simulations, leading to improved parameterizations of the physical processes.

In this presentation, we analyse the performance of two versions of the ACCESS coupled model, ACCESS1.0 and ACCESS1.3, in simulating the Asian-Australian monsoon using the simulations contributed to CMIP5 archive. We compare the simulated winds, precipitation, and surface temperatures with observations. The seasonal means of these variables, as well as their annual variations, are examined under the present-day climate. It is found that both ACCESS models simulate the spatial distributions of Australian monsoon precipitation reasonably well. However, there are also significant dry biases in both models in the Australian monsoon region (defined as the region enclosed by 120^{o}E–150^{o}E and 20^{o}S–10^{o}S). In AMIP-style simulations, however, the two models show differing characteristics, with ACCESS1.0 showing a dry bias throughout the monsoon region, whereas ACCESS1.3 showing a wet (dry) bias in the eastern (western) part of the region. The precipitation bias is largest along the coast in both models. There is a warm temperature bias over the region, consistent with the largely dry precipitation bias.

The precipitations in both ACCESS models are too low over the South Asian monsoon region (defined here as the region enclosed by 70^{o}E–100^{o}E and 5^{o}N–30^{o}N). In addition, there is a large wet precipitation bias in the western equatorial Indian Ocean, which is somewhat smaller in coupled simulations than in AMIP simulations. This wet precipitation bias to the south-west of the monsoon region appears to be related to the dry bias over the monsoon region, presumably through its modulation of the regional Hadley Cell. The western Indian Ocean wet bias may also be associated with the dry bias over the maritime continent through the local Walker circulation. As for the Australian monsoon, there is a warm bias over the South Asian monsoon region, which is consistent with the dry precipitation bias there. Additionally, the annual cycles of simulated precipitation and surface air temperatures in both monsoon regions show a good correspondence with the respective observed annual cycles. The lower and upper tropospheric horizontal winds over both monsoon regions have also been analysed in both models.

In summary, the large-scale features of the Asian-Australian monsoon are reasonably well simulated in both ACCESS models. However, as is commonly found in other CGCMs, there are biases in simulated precipitation, winds, and temperatures. In general, the simulated precipitation is too low

compared with observations. This and other model biases will be discussed in more detail in the presentation.

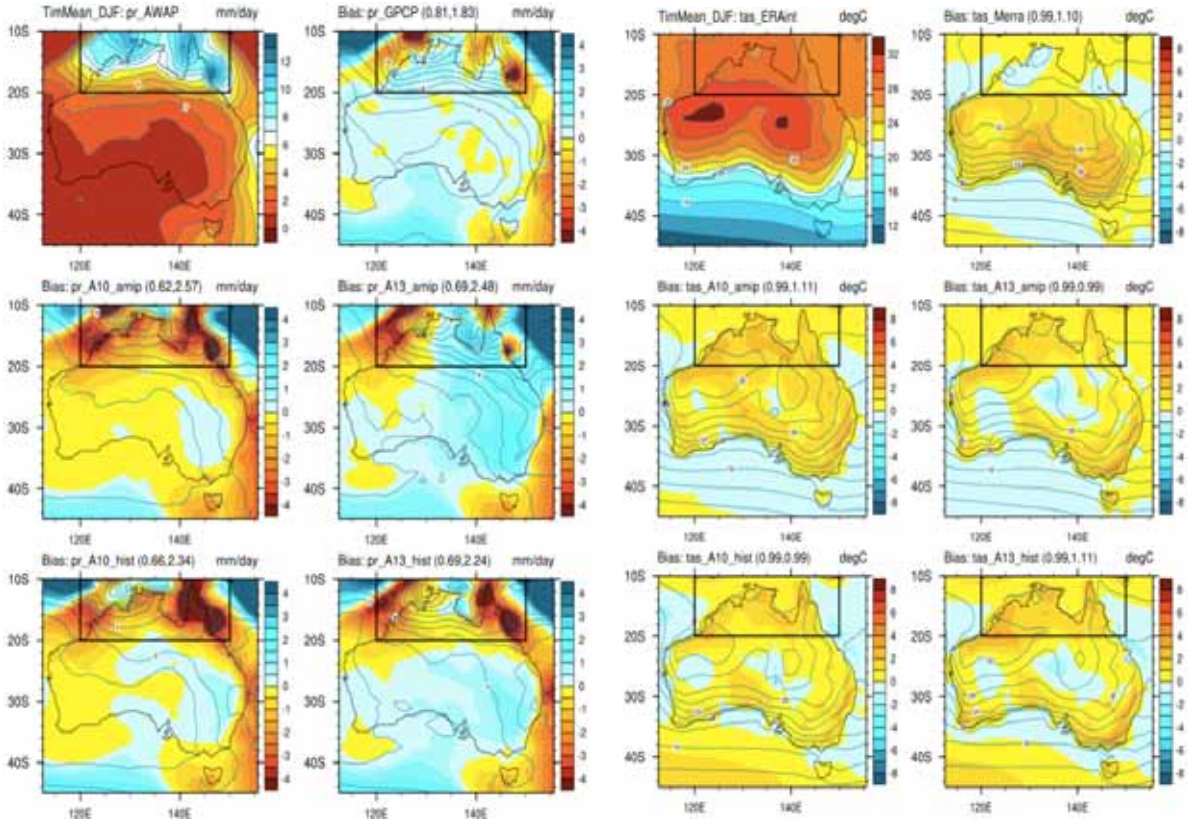

Fig. 1. *Seasonal mean (DJF) precipitations (mm/day) from observations and model simulations. a) AWAP, b) GPCP, c) ACCESS1.0 AMIP, d) ACCESS1.3 AMIP, e) ACCESS1.0 Historical, and f) ACCESS1.3 Historical simulation. The shades in b-f represent the departures of mean precipitation from AWAP precipitation (a). The contours in all panels show the full values.*

Fig. 2. *As in Fig. 1, but for seasonal mean (DJF) surface air temperatures (^{o}C). a) ERA-Interim, b) Merra, c) ACCESS1.0 AMIP, d) ACCESS1.3 AMIP, e) ACCESS1.0 Historical, and f) ACCESS1.3 Historical simulation.*

THE REPRESENTATION OF SUMMER-TIME RAINFALL IN NORTH-WEST AUSTRALIA BY ACCESS1.3

Duncan Ackerley[1], Gareth Berry[1], Christian Jakob[2] and Michael Reeder[1]

[1]Monash Weather and Climate, Monash University, Clayton, Victoria, Australia
[2] ARC Centre of Excellence for Climate System Science, School of Mathematical Sciences, Monash University, Clayton, Victoria, Australia

Australian summertime rainfall has been shown to be increasing in the north-west of the continent (Smith 2004). Despite this well documented increase in rainfall, numerous competing hypotheses as to the cause of the increase still remain with no overall consensus. Modelling work has been undertaken to explore the current (and possible future) trend in north-west Australia (NWA) rainfall but a detailed assessment of the rainfall generation processes on daily to sub-daily time scales has yet to be undertaken. These daily to sub-daily time scales have been shown to be important when considering the rainfall generation mechanisms over NWA.

In this study we assess the capability of the Australian Community Climate and Earth System Simulator version 1.3 (ACCESS1.3) general circulation model to represent the processes that lead to summer-time rainfall production in NWA. The model is forced using the Atmospheric Model Intercomparison Project (AMIP, Gates et al. 1999) boundary conditions from 1979 to 2008. The model underestimates the amount of rainfall during summer (December-January-February, DJF) throughout much of NWA (Fig. 1). This rainfall deficit in ACCESS1.3 can at least be partially attributed to a low-level south-easterly wind bias that transports relatively dry air from the Australian continent into NWA instead of relatively moist air flow from the Coral Sea and the Gulf of Carpentaria that can be seen in the ERA-Interim reanalysis data (see Fig. 2). Low-level air-flow from the north and east (such as the Coral Sea) has been shown to be the dominant moisture source for rainfall over inland NWA (Berry et al. 2011) and so the south-easterly bias is likely to be a contributing factor to the dry bias.

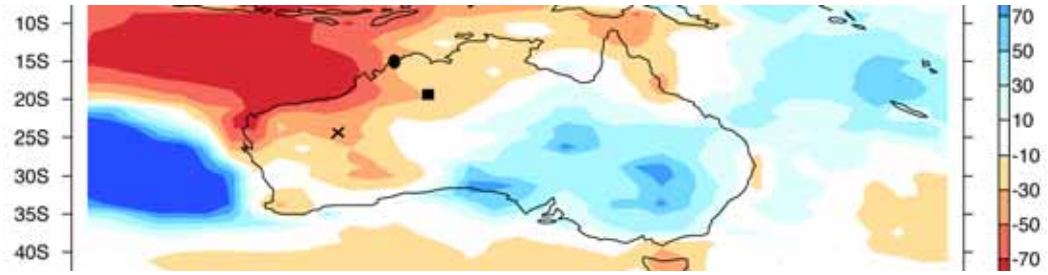

***Fig. 1**: The difference in DJF-mean rainfall for ACCESS1.3 relative to the Climate Prediction Centre (CPC) Merged Analysis of Precipitation (CMAP) dataset (1979/80 – 2007/08). The circle indicates the location of Mitchell Plateau; the square denotes Rabbit Flat and the 'X' for the grid point close to the nocturnal peak in rainfall.*

Inland rainfall in NWA also displays a distinct diurnal cycle that varies from the coast inland. Rainfall tends to occur during the afternoon at the coast but has a preference to occur overnight inland. This nocturnal rainfall preference inland is influenced by both the diurnal cycle of convergence in and around the NWA heat-low and also the availability of moisture (Berry et al. 2011; Spengler et al. 2005).

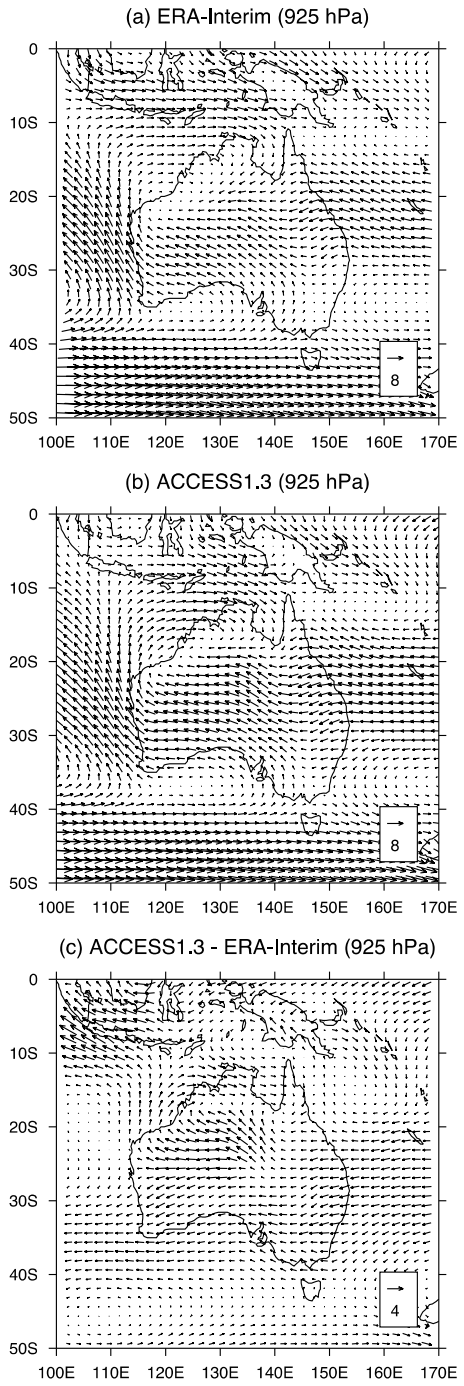

Fig. 2: *Wind vectors (m s^{-1}) averaged over all DJFs from 1979/80 – 2007/08 at 925 hPa from (a) the ERA-Interim reanalysis dataset, (b) ACCESS1.3 and (c) the difference ((b) minus (a)).*

The composited, 3-hourly rainfall accumulation from the Bureau of Meteorology's pluviographs at Mitchell Plateau (dot in Fig. 1, coastal site) and Rabbit Flat (square in Fig. 1, inland site) can be seen in Figs 3(a) and (b) (denoted by the dashed black lines, respectively). The afternoon (nocturnal) peak in rainfall at Mitchell Plateau (Rabbit Flat) can be seen clearly in Figs 3(a) and (b). Overlaid are the 3-hourly composited rainfall accumulations for ACCESS1.3 at the nearest model grid point to the pluviograph sites (blue lines). Both sites indicate that the rainfall occurs mainly around midday in the model, which is too early at both sites. The problem is more obvious at Rabbit Flat (Fig. 3(b)) where

the rainfall has a tendency to occur overnight, but in ACCESS1.3 the peak rainfall still occurs around midday. This premature triggering of rainfall in regions associated with convection is not unusual in general circulation models (Stratton and Stirling 2011). Despite this, the model does capture a nocturnal peak in rainfall; however it is displaced to the south and west of the location in the real world. The 3-hourly composited rainfall accumulations for ACCESS1.3 within the modelled 'Nocturnal Peak' are plotted as the amber line in Fig. 3(b) (location denoted by the 'X' in Fig. 1). This shows that while the model has the location of the nocturnal rainfall in the wrong place, the dynamical processes leading to nocturnal rainfall are represented by ACCESS1.3 in some capacity. The cause of this displacement is likely to be the result of the erroneous low-level airflow over the NWA region. More details will be given in the presentation and will be included in a forthcoming paper (Ackerley et al., in prep.).

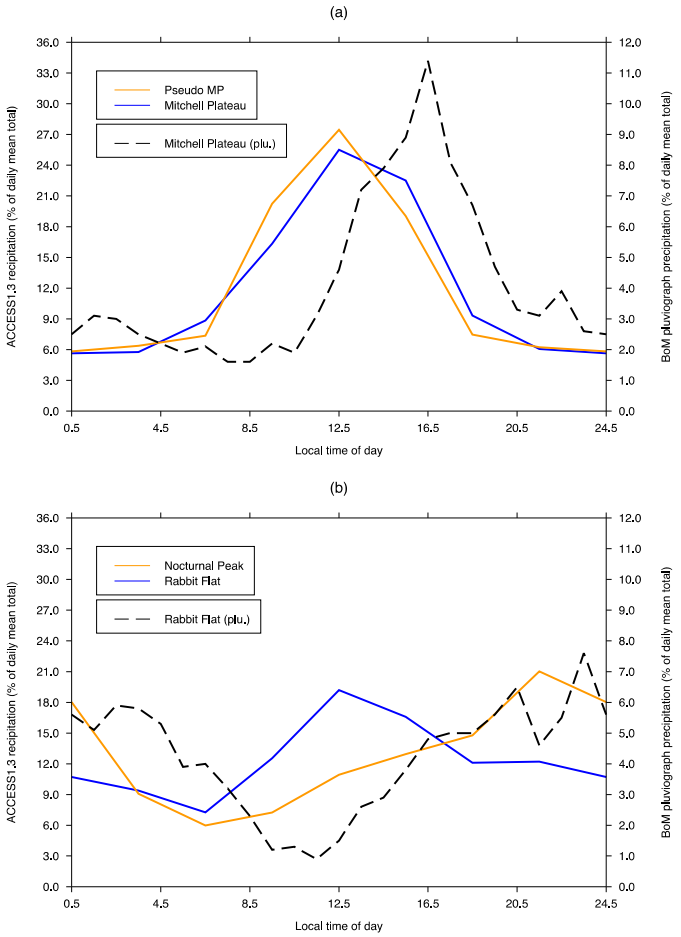

***Fig 3**. Composited 3-hourly, DJF rainfall at (a) the BoM pluviograph site at Mitchell Plateau (black, dashed line) and the nearest corresponding model grid point (blue line) and (b) for the BoM pluviograph site at Rabbit Flat (black, dashed line) and the nearest corresponding model grid point (blue solid line). Also plotted in (b) is the composited 3-hourly DJF rainfall close to the centre of ACCESS1.3's nocturnal rainfall peak in NWA (amber, solid line). ACCESS1.3 data averaged over 1979/80-2007/08.*

Acknowledgments

CMAP Precipitation data provided by the NOAA/OAR/ESRL PSD, Boulder, Colorado, USA, from their Web site at http://www.esrl.noaa.gov/psd/. ERA-Interim data were obtained from the European Centre for Medium-Range Weather Forecasts.

References

Ackerley, D., Berry, G., Jakob, C. and Reeder, M.J. The processes that lead to summertime rainfall in north-western Australia in the ACCESS1.3 GCM.

Berry, G., Reeder, M.J. and Jakob, C. 2011. Physical mechanisms regulating summertime rainfall over north-western Australia. *J. Clim., 24,* 3705-3717.

Gates, W. L. et al. 1999. An Overview of the Results of the Atmospheric Model Intercomparison Project (AMIP I). *Bull. Amer. Meteor. Soc., 80,* 29-55.

Smith, I. 2004. An assessment of recent trends in Australian rainfall. *Aust. Meteorol. Ocean. Journal, 53,* 163-173.

Spengler, T., Reeder, M.J. and Smith, R.K. 2005. The dynamics of heat lows in simple background flows. *Q. J. R. Meteorolo. Soc., 131,* 3147-3165.

Stratton, R. A. and Stirling, A.J. 2011. Improving the diurnal cycle of convection in GCMs. *Quart. J. Roy. Meteor. Soc., 138,* 1121-1134.

INTRASEASONAL MOISTURE BUDGET IN ACCESS MODEL

Hongyan Zhu[1], Harry Hendon[1], Martin Dix[2] and Zhian Sun[1]

[1] CAWCR, Bureau of Meteorology, Australia.
hzhu@bom.gov.au, h.hendon@bom.gov.au and z.sun@bom.gov.au
[2] CAWCR, CSIRO, Australia.
Martin.Dix@csiro.au

The intraseasonal moisture budget is analysed in ACCESS model simulations that have produced reasonable representations of eastward-propagating intraseasonal wind and precipitation variability. The goal of the study is to improve our understanding of the role that convection and dynamic processes play in the development and evolution of the tropical organized convection, in order to improve the simulation of intraseasonal variability in our global prediction models.

Breaking the vertical moistening profile into components associated with each of the elements of the model physics shows that parameterized convection tends to dry the troposphere and that large scale vertical advection moistens the troposphere. These two tendencies roughly balance each other; large scale precipitation dries the upper troposphere due to precipitation and moistens the lower troposphere due to evaporation; the total moisture tendency is asymmetric relative to the maximum precipitation, corresponding to the recharge and discharge process of organized convection in the Tropics. This moistening before and drying after the maximum precipitation is consistent with the large-scale horizontal advection of moisture.

The column-integrated intraseasonal moisture budget is analysed and the role of zonal and meridional moisture horizontal advection on the recharge-discharge mechanism of organized convection will be discussed in details.

HIGH-RESOLUTION SIMULATIONS OF CONVECTION OVER THE MARITIME CONTINENT

Todd Lane, Muhammad Hassim, and Simon Caine

School of Earth Sciences and ARC Centre of Excellence for Climate System Science, The University of Melbourne, Melbourne, Australia

The convection in the Maritime Continent region is characterised by a variety of scales and regimes, ranging from locally forced systems with a strong diurnal cycle though to large-scale propagating systems like the MJO. The locally forced systems can arise due to land and sea breeze circulations, orographic uplift, and other geographically forced circulations like gravity waves. Most of these processes occur on the mesoscale and are therefore poorly resolved by all but the highest resolution models. Indeed, it is well known that models with parameterized convection have difficulty simulating the diurnal cycle of convection in the maritime continent and unresolved mesoscale processes are one likely reason. However, even high-resolution convection-permitting models, which can resolve coastal boundaries and mesoscale phenomena, still possess errors and biases.

In this presentation convection-permitting simulations over parts of the maritime continent region are used to investigate some of the important processes governing the behavior of convection under conditions that promote a strong diurnal cycle. We identify some systematic errors in very high-resolution models, as well as highlight some important features of coastally forced convection.

PROCESSES OF MJO INITIATION OVER THE INDIAN OCEAN

Chidong Zhang

RSMAS, University of Miami

Abstract

One of the least understood aspects of Madden-Julian Oscillation (MJO) is the processes that lead to its convective initiation over the Indian Ocean. There are several competing hypotheses on this. This talk discusses these hypotheses in the context of preliminary results from the CINDY/DYNAMO field campaign of 2011-12. The two consecutive MJO events in October and November 2011 and their apparent connection through upper-level circulation re-catalyzes the debate on convective initiation of the MJO. Convective initiation of the MJO have been viewed as a self-sustained process (as described by the "discharge-recharge" paradigm) as well as a consequence of large-scale upstream forcing as a remnant of the previous MJO event or lateral forcing be extratropical perturbations. CINDY/DYNAMO observations and forecast experiments provide new insights to this issue. Among others, possible roles in MJO initiation may come from the ITCZ, downward zonal momentum transport, shallow to deep convective transition, deepening of the moist layer, the Maritime Continent, dry vs. moist advection. Preliminary results from an observational denial experiment did not show influences on MJO forecast skill by in situ information from within the Indian Ocean and suggests the necessity of large-scale circulation to MJO initiation. Regional modeling case studies indicate that even with heavy forcing at the lateral boundaries and low-boundary, deficiencies in cumulus parameterization schemes can easily stop the MJO from being initialized, suggesting the critical role of local convection to MJO initiation. These and other conflict results highlight our lack of understanding of the most fundamental processes of convective initiation of the MJO. Finally, potential advancement in gaining such understanding by using the CINDY/DYNAMO observations is discussed.

LINKING IMPROVED MJO SIMULATIONS TO THEORETICAL UNDERSTANDING

Eric D. Maloney

Department of Atmospheric Science
Colorado State University
Fort Collins, Colorado, USA
emaloney@atmos.colostate.edu

Introduction and Theory

Recent research has argued that strong mutual interactions between tropospheric moisture and convection are fundamental to the dynamics of the Madden-Julian oscillation (MJO). If the tropical atmosphere is assumed to be characterized by a state of weak temperature gradients (WTG, a very good assumption at timescales characterized by the MJO), then gravity waves are not allowed. Under such conditions, a class of disturbances called moisture modes becomes dominant, which have recently been proposed as an explanation for the MJO (e.g. Raymond and Fuchs 2009; Maloney et al. 2010). Understanding the maintenance and propagation dynamics of moisture modes is tantamount to understanding the maintenance and propagation of tropospheric moisture anomalies, which support tropical convection anomalies.

Given that temperature tendency can be ignored to first order in such a framework, the vertically-integrated moist static energy (MSE) budget becomes an equation for vertically-integrated moisture tendency, and hence a powerful tool for understanding MJO dynamics. In my presentation, I will show recent examples of how the vertically-integrated MSE budget has been used in recent modeling and observational results to understand basic MJO dynamics (Maloney 2009; Sobel et al. 2010; Maloney et al. 2010; Kiranmayi and Maloney 2011; Andersen and Kuang 2012). These studies have argued that the MJO is a moisture mode destabilized by wind-evaporation and cloud-radiative feedbacks and propagated eastward through horizontal advection. Essentially, for an MJO moisture anomaly to grow or be sustained convection must either itself lead to moistening of the column, or sources of moist entropy such as surface evaporation feedbacks or cloud-radiative feedbacks must overcome convective moisture discharge to create a positive moisture tendency. These conditions are typically referred to as “negative gross moist stability” or “negative effective gross moist stability,” respectively (Raymond et al. 2009). The lessons learned from these analyses have recently been applied to the development of an idealized semi-empirical model of the MJO that succinctly explains destabilization and propagation mechanisms, as well as scale selection (Sobel and Maloney 2012a,b).

Improving MJO Simulations

Learning from this recent MJO theory, it is argued that the ability of a general circulation model to correctly simulate the MJO is likely to strongly depend on the model’s ability to simulation realistic interactions between convection and tropospheric moisture. Climate models traditionally have convection parameterizations that are far too insensitive to free tropospheric dryness (e.g. Derbyshire et al. 2004). In particular, entrainment of dry air into rising convective plumes effectively stifles parcel buoyancy in nature, but is often a process poorly simulated in model. Therefore, increasing the realism of convection-free tropospheric humidity interactions is one important factor in improving the realism of model MJO simulations.

I discuss in my presentation the results from two recent manuscripts that provide examples of how improving convective sensitivity to free tropospheric humidity, as well as other modifications,

engender stronger model intraseasonal variability (Hannah and Maloney 2011; Benedict et al. 2012). In Hannah and Maloney (2011), a version of the NCAR Community Atmosphere Model 3 (CAM3) is used to show that inclusion of a minimum entrainment threshold, which effectively increases the amount of convective entrainment of environmental air in dry atmospheres, is effective at improving intraseasonal variability. However, it is also shown that such changes have a demonstrable effect on the tropical mean state, producing a colder and drier troposphere. It is also shown by Hannah and Maloney (2011) that the mean tropical diabatic heating profile becomes more bottom-heavy with inclusion of a minimum entrainment threshold, which implies that convection becomes less efficient at discharging moisture from the column. Such behavior produces interesting changes in the vertically-integrated MSE budget, which will be discussed further below and in the presentation.

Benedict et al. (2012) use a version of the GFDL Atmosphere Model 3 to show that modifications to the triggering assumptions and convective closure substantially improve intraseasonal variability in the model. Model parameters that are varied include the closure assumption, a trigger based on low-level vertical velocity, convective entrainment, the amount of condensate evaporation that goes into downdrafts, and the amount of condensate evaporation that goes into the environment. The models with strongest intraseasonal variability implement a requirement on the low-level vertical velocity as a convective trigger or use an entrainment-based dilution of CAPE in the convective closure. It is shown that model versions with improved intraseasonal variability, as in Hannah and Maloney (2011), are associated with a more bottom-heavy mean diabatic heating profile. The results of Hannah and Maloney (2011) and Benedict et al. (2012) both indicate that models that produce more realistic intraseasonal variability are associated with a more bottom-heavy diabatic heating profile.

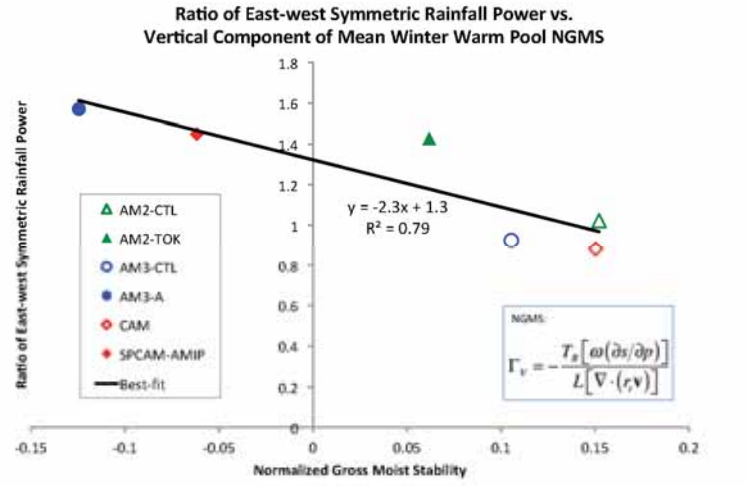

Fig. 1: *East-west power ratio versus gross moist stability (GMS) calculated for three pairs of models with good and bad MJO simulations. From Jim Benedict.*

Process-Oriented Diagnosis

Process-oriented diagnostics based on the MSE budget can be used to determine whether such changes to the heating profile explain the preference for stronger MJO activity in these models. A quantity called gross moist stability (GMS) describes how efficiently convection and associated large-scale circulations export MSE (moisture under WTG theory) from the column per unit convective activity. Convective activity can be represented based on column-integrated moisture convergence, precipitation, or some other quantity. GMS is small or negative where shallow convection drives a large amount of low-level moisture convergence but net condensation is small, and larger where deep convection drives low-level moisture convergence, but larger amounts of condensational drying in the column. Stratiform heating profiles produce strong positive GMS, indicating that a large amount of

moisture is discharged from the column during periods of stratiform heating (e.g. Peters and Bretherton 2006). Figure 1 compares GMS between three model pairs (GFDL AM2, AM3, NCAR CAM3/SP-CAM), one each with a weak MJO and one with a strong MJO. The models with stronger MJOs have much lower or negative GMS, indicating that convection in these models is not very efficient at discharging column moisture or even moistens the column, making it easier to maintain moisture anomalies that support MJO convection. For the case of reduced but not negative GMS, processes such as wind-evaporation feedbacks and cloud-radiative feedbacks can more easily destabilize the model MJO. These and other process-oriented diagnostics will be explained during the presentation.

References

Andersen, J.A., Kuang, Z. 2012: Moist Static Energy Budget of MJO-like Disturbances in the Atmosphere of a Zonally Symmetric Aquaplanet. *J. Climate*, **25**, 2782–2804.

Benedict, J.J., Maloney, E.D., Sobel, A.H., Frierson, D.M. and Donner, L.J. 2012: Tropical intraseasonal variability in Version 3 of the GFDL Atmosphere Model. *J. Climate*, in press.

Derbyshire, S.H., Beau, I., Bechtold, P., Grandpeix, J.-Y., Piriou, J.-M., Redelsperger, J.-L. and Soares, P.M.M. 2004: Sensitivity of moist convection to environmental humidity. *Quart. J. Roy. Meteor. Soc*., **30**, 3055–3079.

Hannah, W.M. and Maloney, E.D. 2011: The role of moisture-convection feedbacks in simulating the Madden-Julian oscillation. *J. Climate*, **24**, 2754-2770.

Landu, K. and Maloney, E .D. 2011: The intraseasonal moist static energy budget in reanalysis data. *J. Geophys. Res*., **116**, D21117, doi:10.1029/2011JD016031.

Maloney, E.D. 2009: The moist static energy budget of a composite tropical intraseasonal oscillation in a climate model. *J. Climate*, **22**, 711-729.

Maloney, E.D., Sobel, A.H. and Hannah, W.M. 2010: Intraseasonal variability in an aquaplanet general circulation model. *J. Adv. Modeling. Earth. Sys*, **2**, Art. #5, 24 pp.

Peters, M.E. and Bretherton, C.S. 2006: Structure of tropical variability from a vertical mode perspective. Theor. Comp. Fluid. Dyn., doi:10.1007/s00162-006-0034-x.

Raymond, D.J. and Fuchs, Z. 2009: Moisture modes and the Madden-Julian Oscillation. *J Climate*., **22**, 3031–3046.

Raymond, D. J., Sessions, S., Sobel, A.H. and Fuchs, Z. 2009: The mechanics of gross moist stability. *J. Adv. Model. Earth Sys.*, **1**, doi:10.3894/JAMES.2009.1.9.

Sobel, A.H. and Maloney, E.D. 2012a: An idealized semi-empirical framework for modeling the Madden-Julian oscillation. *J. Atmos. Sci*., in press.

Sobel, A.H. and Maloney, E.D. 2012b: Moisture modes and the eastward propagation of the MJO. *J. Atmos. Sci.*, in press.

Sobel, A.H., Maloney, E.D., Bellon, G. and Frierson, D.M. 2010: Surface fluxes and tropical intraseasonal variability: a reassessment. *J. Adv. Model. Earth Syst.*, Vol. 2, Art. #2, 27 pp., doi:10.3894/JAMES.2010.2.2.

SIMULATION AND PREDICTION OF THE MJO AND ITS TELECONNECTIONS USING POAMA

Andrew G. Marshall, Debra Hudson, Matthew C. Wheeler, Harry H. Hendon and Oscar Alves
Centre for Australian Weather and Climate Research, Bureau of Meteorology, Melbourne, VIC, Australia

Introduction

The Bureau of Meteorology's dynamical Predictive Ocean Atmosphere Model for Australia (POAMA), which was originally designed for forecasting on the seasonal timescale, has been upgraded to version 2 (POAMA-2) with enhancements made to the data initialisation and ensemble generation strategy to better suit forecasting at multi-week lead times. The new POAMA-2 system is designed to fill the gap in current prediction capability between weather forecasts and seasonal outlooks for Australia. One of the main targets of this research has been to improve our understanding of the climate drivers that influence intra-seasonal climate variability and forecast skill. This paper summarises our evaluation of the simulation of the Madden-Julian Oscillation (MJO; e.g. Madden and Julian 1994) and its influence on rainfall prediction in POAMA-2.

The MJO exerts an important influence on weather and climate in many parts of the globe, especially in Australia during the summer monsoon (Wheeler et al. 2009). The MJO consists of large-scale coupled patterns in atmospheric circulation and deep convection that propagate eastward over the equatorial Indian and western Pacific oceans with a period of 30-90 days. The state of the MJO is depicted using the bivariate Real-time Multivariate MJO (RMM) index, which captures the large-scale structure of the MJO in zonal wind and convection along the equator. The RMM index is obtained from a combined EOF analysis of equatorially-averaged (15°N-15°S) outgoing longwave radiation (OLR), 850hPa zonal wind, and 200hPa zonal wind anomalies (Wheeler and Hendon 2004). Here, we assess the capability of POAMA-2 to (i) predict the RMM index, (ii) simulate rainfall associated with the MJO including teleconnections to Australian climate, and (iii) predict global and regionall rainfall associated with the MJO on intra-seasonal timescales.

Model and Data Description

POAMA-2 uses the Bureau of Meteorology unified atmospheric model version 3 and the Australian Community Ocean Model version 2. Initial conditions are provided by separate data assimilation schemes for the ocean, land and atmosphere components of the global coupled model; for POAMA-2 these include an ensemble ocean data assimilation system (Yin et al. 2011) and an atmosphere/land initialisation system (Hudson et al. 2011). Full details of the model components are given in Wang et al. (2011). A coupled breeding technique is used to produce perturbed initial conditions that are consistent with both the ocean and atmosphere at the initial time of the forecasts. The perturbations are generated using the coupled ocean-atmosphere model and then rescaled to represent forecast uncertainty due to sensitivity to initial condition errors. This new strategy represents a significant milestone in our development of the POAMA forecast system for intra-seasonal prediction.
The POAMA-2 hindcast framework consists of a 33-member ensemble of 9 months duration initialized on the 1st, 11th and 21st of each month between 1980 and 2010. We utilise the first 6 weeks of precipitation, OLR and zonal wind data for hindcasts initialized on the 1st of the month. Hindcast anomalies are formed relative to the hindcast model climatology, which is a function of both start month and lead time, and thus a first-order linear correction for model mean bias is made. We define a lead time of one week as the mean of the first week of each hindcast. Global rainfall anomaly simulations and predictions are verified against the Climate Prediction Centre Merged Analysis of

Precipitation pentad dataset (CMAP), and the observed RMM index is calculated using NCEP/NCAR reanalysis data.

Prediction of the MJO

Figure 1 illustrates the skill in predicting the daily RMM index for POAMA-2 (solid) and for the previous version of the model, POAMA-1.5 (dashed). For this analysis we use data output from 1980-2006; a period that is common to both models. We score the daily ensemble mean RMM index for each model using root-mean-square error (RMSE), which is calculated as a function of forecast start month for lead times out to 35 days. For a climatological forecast of the bivariate RMM anomaly index the RMSE=√2, and thus forecasts are typically deemed to be skilful for RMSE< √2. However Fig. 1 shows the approach to √2 at long lead time is slow; POAMA-2 predicts the large-scale structure of the MJO out to about 4 weeks with a 1-week improvement in skill compared to POAMA-1.5 for lead times beyond about 2 weeks. We attribute this improvement in skill largely to the improved spread-error relationship in the POAMA2 ensemble.

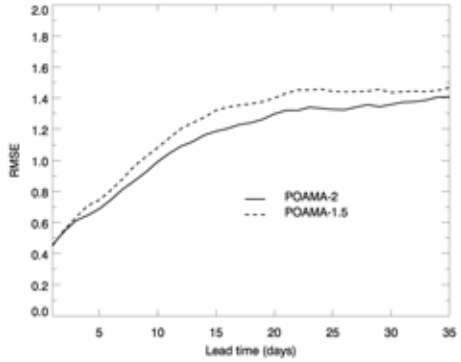

***Fig. 1**: Root-mean-square error of the predicted RMM index for the ensemble mean POAMA-2 (solid) and POAMA-1.5 (dashed) forecast as a function of lead time (days).*

Simulation of MJO rainfall

We assess the ability of POAMA-2 to reproduce the broad-scale spatial structure of MJO rainfall on intra-seasonal timescales. Figure 2 shows composite maps of weekly-mean rainfall based on the 8 phases of the MJO lifecycle defined by Wheeler and Hendon (2004), for observations and POAMA-2. Model composites are formed using lead times 3-6 weeks so as to be independent of initial conditions and model spin-up, and we combine adjacent MJO phase pairs corresponding to the convectively active phase of the MJO over the Indian Ocean (2/3), Maritime Continent (4/5), western Pacific (6/7), and Western Hemisphere (8/1). We present composite MJO-rainfall anomalies in Fig. 2 for November-April when the MJO is strongest and shifted into the Southern Hemisphere.

POAMA-2 reproduces the observed broad-scale characteristics of each MJO phase with reasonable fidelity over the Indian and western Pacific Ocean (Indo-Pacific) region, including over northern Australia. The model also captures some features of the MJO's impact on tropical rainfall away from the Indo-Pacific region, with anomalous drying (wet conditions) over parts of Brazil and equatorial Africa in phases 4/5 (8/1). A notable deficiency, however, is the underestimation of the magnitude of the rainfall anomaly over the eastern Indian Ocean by up to 50%, which is particularly evident in phases 2/3 and 6/7 when the rainfall anomaly peaks over this region. The POAMA-2 representation of MJO rainfall shown here is similar to that of POAMA-1.5 (Marshall et al. 2011), which is not surprising given that the atmospheric models in POAMA-2 and POAMA-1.5 are similar.

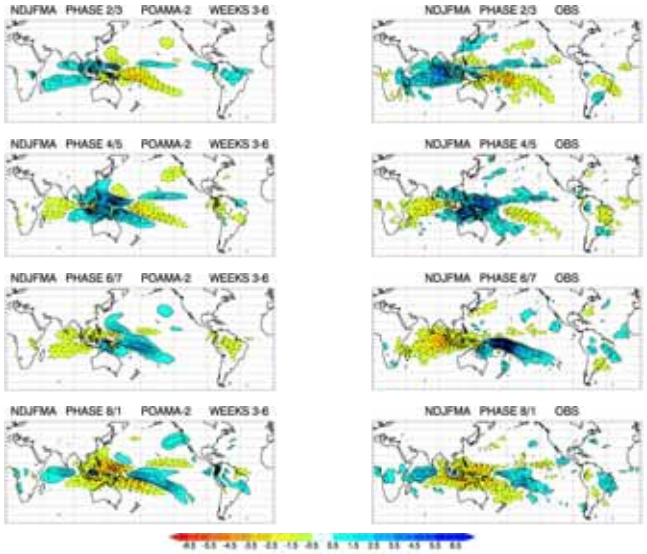

***Fig. 2**: Rainfall anomaly composite maps for MJO phases 2/3, 4/5, 6/7, and 8/1 over the period November-April for POAMA-2 hindcasts at lead times of 3-6 weeks (left column) and for observations (right column).*

Prediction of MJO rainfall

We finally turn our attention to the ability of POAMA-2 to predict rainfall at intra-seasonal timescales in association with the MJO. Probabilistic verification for the second fortnight (comprising the average of forecast weeks 3 and 4) for November-April start times is shown in Fig. 3 using the Relative Operating Characteristic (ROC) for rainfall in the upper tercile for forecasts with and without an MJO event in the initial conditions. There are 73 cases where the MJO is strong at the initial time (RMM index ≥ 1 standard deviation, in any phase) and 35 cases where it is weak (RMM index < 1). The ROC score measures the ability of the forecasting system to discriminate between events and non-events, thereby providing information on forecast resolution. In Fig. 3, ROC scores greater than 0.5 indicate forecast skill better than climatology.

The high ROC scores across the equatorial Pacific for both strong and weak MJO cases owe their existence to the high predictability of rainfall associated with the El Niño-Southern Oscillation (ENSO), which is largely independent of the presence or absence of the MJO in the initial condition. Elsewhere, POAMA-2 shows a larger and more cohesive spatial coverage of ROC scores greater than 0.6 over parts of the Indo-Pacific (extending into the North Pacific), North Atlantic Ocean, and eastern Australia when the MJO is strong at the initial time, compared with when the MJO is weak at the initial time. The MJO is known to have a strong direct impact over the Indo-Pacific, and thus we expect the MJO to be important for intra-seasonal prediction over this region. Atmospheric teleconnections of the MJO are known to modulate local climate over eastern Australia and the North Atlantic Ocean, and thus the MJO also appears to be a source of intra-seasonal rainfall predictability over these extra-tropical regions; this is a key result in the development of POAMA-2 for intra-seasonal prediction. We further note that the ROC skill for predicting MJO-rainfall over these tropical and extra-tropical regions is considerably higher and more spatially cohesive for POAMA-2 than for POAMA-1.5 (not shown) in the second fortnight, consistent with the vast improvement in predicting the MJO index in POAMA-2 (out to 4 weeks) compared with POAMA-1.5 (3 weeks; Fig. 1).

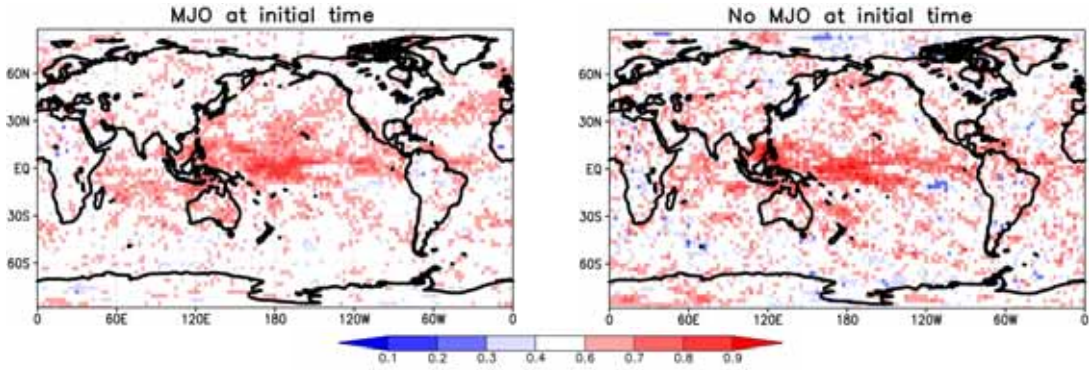

Fig. 3: *ROC scores of the probability that precipitation averaged over days 15-28 is in the upper tercile for Nov-Apr forecast start months for cases with an MJO in the initial conditions (left) and with no MJO in the initial conditions (right).*

Conclusions

The new POAMA-2 intra-seasonal forecast system demonstrates improved skill compared to POAMA-1.5 in predicting the MJO by about 1 week lead time. Prediction of the large-scale structure of the MJO out to 4 weeks in POAMA-2 (Fig. 1), combined with effective simulation of MJO rainfall across the Indo-Pacific in November-April (Fig. 2), translate into improved intra-seasonal prediction of rainfall anomalies in the second fortnight of the forecast when the MJO is strong at the initial time, compared with when the MJO is weak at the initial time. These improvements predominantly occur over parts of the Indo-Pacific, North Atlantic Ocean, and eastern Australia (Fig. 3), and thus the MJO contributes to intra-seasonal prediction skill for rainfall over these regions. POAMA-2 also shows improved skill for predicting MJO-rainfall compared with POAMA-1.5 with the introduction of perturbed initial conditions using coupled breeding. We are now focusing our attention on the MJO in the next version of POAMA, which will be based on the ACCESS model.

References

Hudson, D., Alves, O., Hendon, H.H. and Wang, G. 2011. The impact of atmospheric initialisation on seasonal prediction of tropical Pacific SST. *Clim. Dyn., 36*, 1155-1171.

Madden, R.A. and Julian, P.R. 1994. Observations of the 40–50 day tropical Oscillation - a review. *Mon. Wea. Rev., 122*, 814-837.

Marshall, A.G., Hudson, D., Wheeler, M.C., Hendon, H.H. and Alves, O. 2011. Assessing the simulation and prediction of rainfall associated with the MJO in the POAMA seasonal forecast system. *Clim. Dyn., 37*, 2129-2141.

Wang, G., Hudson, D., Yin, Y., Alves, O., Hendon, H., Langford, S.,Liu, G. and Tseitkin, F. 2011. POAMA-2 SST skill assessment and beyond. *CAWCR Res. Letters*, *6*, 40-46.

Wheeler, M.C. and Hendon, H.H. 2004. An all-season real-time multivariate MJO index: Development of an index for monitoring and prediction. *Mon. Wea. Rev., 132*, 1917-1932.

Wheeler, M.C., Hendon, H.H., Cleland, S., Meinke H. and Donald, A. 2009. Impacts of the Madden–Julian Oscillation on Australian Rainfall and Circulation. *J. Clim., 22*, 1482-1498.

Yin, Y., Alves, O. and Oke, P.R. 2011a. An ensemble ocean data assimilation system for seasonal prediction. *Mon. Wea. Rev.*, *139*, 786-808.

TROPICAL CYCLONES IN POAMA

Kay Shelton[1], Andrew Charles[2], Harry Hendon[1] and Yuriy Kuleshov[2]

[1]Centre for Australian Weather and Climate Research – A Partnership between the Bureau of Meteorology and CSIRO, GPO Box 1289 Melbourne, VIC 3001 Australia.
[2]National Climate Centre, Bureau of Meteorology, GPO Box 1289 Melbourne, VIC 3001

Abstract

The Bureau of Meteorology (BoM) is developing dynamically-based seasonal predictions of tropical cyclone (TC) activity for the Australian and South Pacific regions. The fully-coupled global climate model (GCM) on which these predictions are based is the Predictive Ocean-Atmosphere Model for Australia (POAMA). A new objective TC identification and tracking scheme, developed within BoM and designed for use with relatively coarse GCMs, is applied to the 30-member 31-year POAMA hindcast ensemble. Using this technique, it is confirmed that tropical cyclone-like disturbances are present within the POAMA hindcast. The structure of these disturbances resembles those identified in other GCMs. The geographic distribution of genesis locations and the tracks of the disturbances are similar to those for observed TCs. The seasonal and interannual variability of the TC-like disturbances in POAMA is consistent with observations; however, too few disturbances are present in the Australian region. The modulation of the geographic distribution of the TC-like disturbances by the El Niño-Southern Oscillation is also consistent with observations. The results reported in this paper serve as a foundation for the provision of predictions of seasonal TC activity using POAMA.

Introduction

Outlooks of tropical cyclone (TC) activity for an upcoming TC season (November-April in the Southern Hemisphere) provide governments and organisations with a basis for guidance on how disaster management resources might best be allocated to respond to possible TC encounters. The Australian Bureau of Meteorology (BoM) has been issuing such outlooks for the Australian region since the start of the 2009/2010 TC season, and for the South Pacific region since the start of the 2010/2011 TC season. These outlooks have evolved over time from initially providing the predicted number of tropical cyclones, to now (http://www.bom.gov.au/climate/ahead/tc.shtml) providing the probability of exceeding the long-term mean activity along with a measure of confidence (skill) in this prediction. The predictions of TC activity provided by BoM are generated using an empirical model which exploits the historical relationship between observed tropical cyclone activity since the 1969/1970 TC season and the seasonal (3-month) mean of i) the equatorial sea surface temperature (SST) in the Niño 3.4 region (5°N-5°S, 170°W-120°W) and ii) the Southern Oscillation Index (SOI), for the July-September (JAS) period ahead of the TC season. The science behind this prediction scheme has a long history, dating back to pioneering work by Neville Nicholls in the 1970s. Nicholls (1979) first noted the possibility of using equatorial SSTs and the SOI to predict TC activity in the Australian region. More recent studies have demonstrated the correlations of the JAS Niño 3.4 SST index and the SOI with TC season activity, for the period 1969/1970-2005/2006, are both ~0.68 (Kuleshov et al., 2009), although higher correlations are found when the August-October season is used. Thus, the El Niño-Southern Oscillation (ENSO) can explain approximately 50% of the interannual variability in TC season activity.

The strong correspondence of equatorial SSTs and the SOI with TC activity in the Australian and South Pacific regions has been repeatedly noted in the literature (e.g. Nicholls, 1979; Hastings, 1990; Kuleshov et al., 2008; Ramsay et al., 2008) and has been utilised for generating TC activity predictions (Kuleshov et al., 2009; Chand et al., 2010; Werner and Holbrook, 2011). Preliminary verification of such predictions has revealed the limitations of the relationship. While this may not be

entirely surprising given the limited extent to which variability in TC activity can be attributed to ENSO, the result has been exaggerated by changes in the nature of ENSO throughout the historical period used to train the empirical prediction schemes. Changes in the nature of ENSO and its impacts on the large-scale environment challenge the historical TC-ENSO relationship on which current prediction schemes are based.

An alternative to the above statistical approach is to use dynamical predictions from coupled global climate models (GCM), which can produce one (or several) realization(s) of the evolution of the global ocean-atmosphere climate system for several months ahead. Such predictions implicitly include changes in the climate as these changes are captured by the environmental analyses used to initialize the model. Such models are comprised primarily of the fundamental basic equations which also govern the real atmosphere-ocean system. It then follows that by identifying and tracking TC-like disturbances in GCM realizations for the period of the TC season, predictions of the TC season activity can be made that account for variations in the climate.

As part of the Pacific-Australia Climate Change Science and Adaptation Planning (PACCSAP) Program, BoM is developing dynamically-based seasonal TC activity predictions using the Predictive Ocean-Atmosphere Model for Australia (POAMA). The ability of POAMA to simulate TCs and provide useful predictions of TC activity is evaluated by investigating the representation of TCs and their geographic, seasonal and interannual variability in the model's hindcast for the 1980-2010 period.

Tropical cyclone identification

The version of POAMA used in this study is the current operational seasonal version, referred to as POAMA 2.4 (hereafter P24). A full description of this model can be found, for instance, in Langford et al. (2011). The P24 system is comprised of an ensemble of 30 members and a hindcast which spans the 31-year period 1980-2010. For the purpose of the current study, only the ensemble of realizations initialized on the 1 October each year are used. These realizations each provide nine months of daily global atmospheric environmental fields at a resolution of approximately 2.5° x 2.5°.

The tropical cyclone identification and tracking method utilised in this study is the "Okubo-Weiss-Zeta" (OWZ) scheme described in Tory et al. (2012b, 2012c). In brief, this scheme identifies regions of low deformation vorticity (using the diagnostic OWZ parameter) at the 850- and 500-hPa levels which are vertically coherent and are sustained for an appreciable duration. Where such regions occur in the presence of small vertical wind shear and large lower tropospheric humidity, the local environment is considered conducive to imminent tropical cyclogenesis. For a tropical cyclone to be declared: i) the OWZ parameter must have exceeded certain thresholds at both the 850- and 500-hPa levels, ii) the areal coverage of vertically coherent OWZ parameter must exceed a certain size over the ocean, iii) certain lower tropospheric humidity thresholds must be exceeded in this area, iv) the vertical wind shear in this area must not exceed a threshold and v) this area must persist, meeting all other criteria, for at least 48 hours.

To apply this methodology to the P24 system, the low resolution environmental fields are bilinearly interpolated to 1° x 1° grids. The P24 data introduce a complication when applying the OWZ scheme: low-level humidity fields are required by the scheme, preferably at the 950- or 925-hPa levels, however the P24 hindcast archive is available at the surface and at 850 hPa. Following examination of P24 humidity fields at both 850 hPa and the surface, and comparison with a very limited sample of P24 model output at 950 hPa, the surface humidity fields are selected to provide the required fields for the OWZ scheme. The threshold values for the various parameters used in the application of the OWZ scheme to P24 data are identical to those used by Tory et al. (2012a) to evaluate tropical cyclone variability in a variety of GCMs. The OWZ scheme is applied to the nine-month daily P24 data for each ensemble member and year individually. The resulting statistics regarding the identified TC-like

disturbances in each of the 30 members are then averaged together to give ensemble mean statistics for each year.
The TC-like disturbances identified in P24 are compared with observations of TCs in the Southern Hemisphere in the dataset prepared by the National Climate Centre, BoM, for the same 31-year period of the P24 hindcast. Tropical cyclogenesis for observed TCs is defined as the first time the central pressure is ≤ 995 hPa.

To investigate the interannual variability in P24 TCs, the phase of ENSO is determined individually for each member of the ensemble and each TC season using that member's Niño 3.4 region SST anomaly (where the anomaly is defined relative to the climatological ensemble mean value). A positive (negative) ENSO event is declared when the three-month mean SST anomaly exceeds 0.5°C (-0.5°C) for five continuous months. For observations, the ENSO phase for the TC seasons is defined using the 5VAR index, following Kuleshov et al. (2009).

Tropical cyclones in POAMA

The OWZ technique identifies TC-like disturbances throughout the nine-month period for all of the P24 hindcast ensemble members. The structure of these TC-like disturbances (not shown; hereafter referred to as "model TCs") resemble those in other studies using relatively coarse GCMs (e.g. Bengtsson et al., 1995; Vitart et al., 1997).

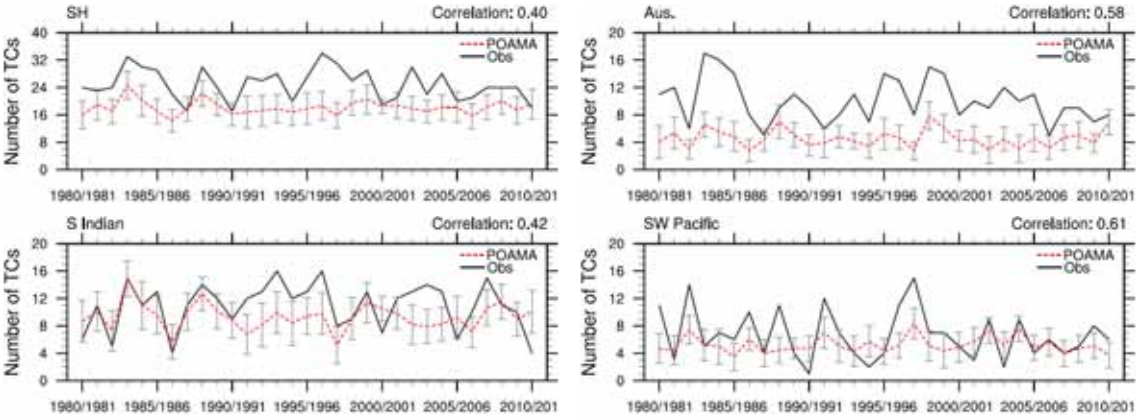

***Fig. 1**: Time series of the annual number of TCs in the (top left) Southern Hemisphere, (top right) Australian Region, (bottom left) South Indian Ocean and (bottom right) south-west Pacific Ocean, from observations (solid line) and P24 ensemble mean (dashed line). The grey bars indicate ± 1 standard deviation in the P24 ensemble mean based on the 30-member ensemble. The correlation between the observations and P24 ensemble mean is shown above each panel.*

Figure 1 presents a comparison of the P24 ensemble mean annual total (October-June) of model TCs over the 31-year hindcast period with the observed annual total (July-June) of TCs over the same period. The time series are shown for the Southern Hemisphere (SH) and three sub-regions: the South Indian Ocean (SIO; 30°E-90°E), the Australian region (AR; 90°E-160°E) and the south-west Pacific Ocean (SWPac; 160°E-120°W). The number of model TCs in the SH is less than observed and the interannual variability is small, which is partly an artifact of ensemble averaging. The overall number of model TCs in the SIO compares well with observations, however the numbers in the SWPac and AR are less than observed, especially for the AR. The observed number of TCs in the AR is outside the range of 1 standard deviation in the P24 ensemble for almost every year, suggesting a systematic deficiency in the model (or in the applicability of the OWZ scheme) in this region. The consistency in interannual variability between P24 and observations is encapsulated in the correlation between the two time series. For the AR and SWPac, the two time series vary similarly, with correlations of ~0.6, while the SIO is much lower, near 0.4. Despite the relatively poor variability of model TCs in the

SIO, the first 10 years of the time series show a high degree of similarity in both variability and in actual number of TCs. This feature requires further investigation.

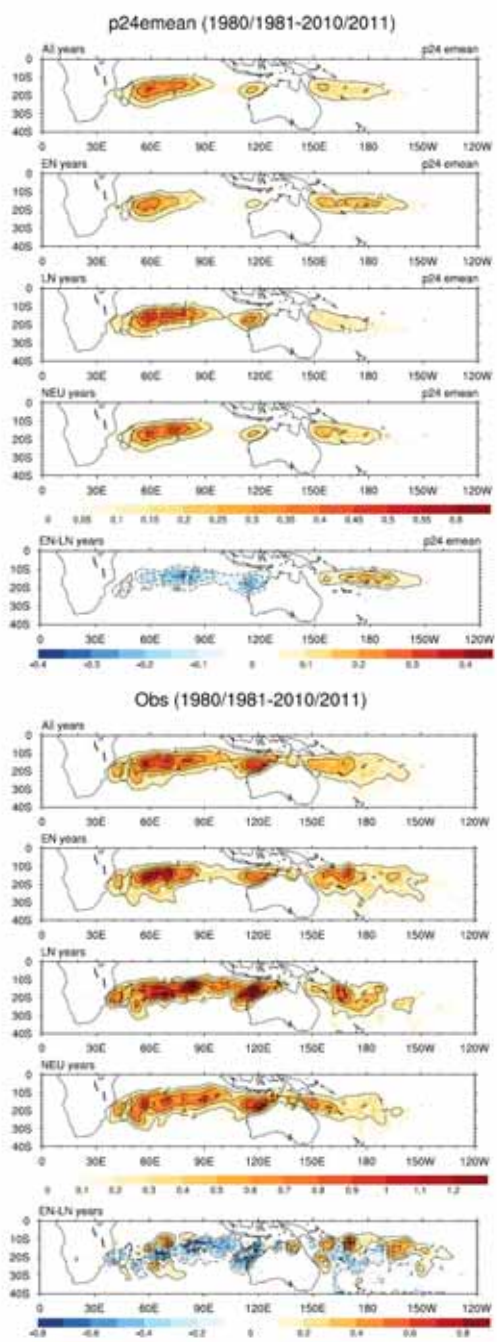

***Fig. 2**: Tropical cyclone track density (number of TCs per 2° x 2° grid box per season) for (left) observations and (right) P24 ensemble mean. Climatological track density is shown in the top panels, followed by those for El Niño years, La Niña years and neutral years; the difference between El Niño and La Niña years shown at the bottom. Note the colour scales and contour intervals differ for the observations and P24 plots. For the difference plots, positive values are solid contours; negative are dashed; the zero-line is omitted. The contour interval for the difference plots is 0.1 for observations and 0.05 for P24. For all other plots, the contour interval is 0.2 for observations and 0.1 for P24.*

Figure 2 shows the climatological TC track density in the Southern Hemisphere for observations and the P24 ensemble mean, along with the track density for each ENSO phase and the difference between the warm and cool phases (El Niño minus La Niña). The climatological model TC tracks (top right) show similar features to those of observations (top left), with maxima in western SIO and off the west and east coasts of Australia in the AR. The overall track density for P24 is less than that of observations, and this is most evident in the AR and SWPac, consistent with there being too few model TCs in these regions (as highlighted in Fig. 1). The influence of ENSO on the model TC geographic distribution shows similarities with observations: the track density in the SIO and western region of the AR is higher in La Niña (LN) that El Niño (EN); the areal coverage of model TC tracks is larger in EN than LN in the eastern portion on the AR and SWPac, and the track density id shifted further equatorward in EN compared to LN. The EN-LN difference maps (bottom panels) summarise these points.

Overall, the model TCs in the P24 system, identified using the OWZ scheme, exhibit a geographic and interannual variability that are consistent with observations. This result is a promising foundation for the ultimate goal of providing seasonal TC activity predictions based on POAMA. Future work on the project will include calibration of the model TC activity for the AR and SWPac, as well as trying to gain a better understanding of the drivers of interannual variability of observed TCs in these regions and how well these drivers are represented in POAMA.

References

Bengtsson, L., Botzet, M. and Esch, M. 1995. Hurricane-type vortices in a general circulation model. *Tellus A*, *47*, 175–196.

Chand, S.S., Walsh, K.J.E. and Chan, J.C.L. 2010. A Bayesian regression approach to seasonal prediction of tropical cyclones affecting the Fiji region. *J. Climate*, *23*, 3425–3445.

Hastings, P.A. 1990. Southern Oscillation influences on tropical cyclone activity in the Australian/south-west Pacific region. *Int. J. Climatol.*, *10*, 291–298.

Kuleshov, Y., Qi, L., Fawcett, R. and Jones, D. 2008. On tropical cyclone activity in the Southern Hemisphere: Trends and the ENSO connection. *Geophys. Res. Lett.*, *35*, L14S08.

Kuleshov, Y., Qi, L., Fawcett, R. and Jones, D. 2009. Improving preparedness to natural hazards: Tropical cyclone prediction for the Southern Hemisphere. In: *Advances in Geosciences*, (J. Gan, Ed.), (Singapore: World Scientific Publishing), pp. 127–143.

Langford, S., Hendon, H.H. and Lim, E.-P. 2011. Assessment of POAMA's predictions of some climate indices for use as predictors of Australian rainfall. *CAWCR Technical Report*, *031*, 60 pp.

Nicholls, N. 1979. A possible method for predicting seasonal tropical cyclone activity in the Australian region. *Mon. Wea. Rev.*, *107*, 1221–1224.

Ramsay, H.A., Leslie, L.M., Lamb, P.J., Richman, M.B. and Leplastrier, M. 2008. Interannual variability of tropical cyclones in the Australian region: role of large-scale environment. *J. Climate*, *21*, 1083–1103.

Tory, K.J., Chand, S.S., Dare, R.A. and McBride, J.L. 2012a. An assessment of a model-, grid- and basin-independent tropical cyclone detection scheme in selected CMIP3 global climate models. *J. Climate*, (Accepted).

Tory, K.J., Chand, S.S., Dare, R.A. and McBride, J.L. 2012b. The development and assessment of a model-, grid- and basin-independent tropical cyclone detection scheme. *J. Climate*, (Accepted).

Tory, K.J., Dare, R.A., Davidson, N.E., McBride, J.L. and Chand, S.S. 2012c. The importance of low-deformation vorticity in tropical cyclone formation. *Atmos. Chem. Phys. Discuss.*, *12*, 17539–17581.

Vitart, F., Anderson, J.L. and Stern, W.F. 1997. Simulation of interannual variability of tropical storm frequency in an ensemble of GCM integrations. *J. Climate*, *10*, 745–760.

Werner, A. and Holbrook, N.J. 2011. A Bayesian forecast model of Australian region tropical cyclone formation. *J. Climate*, *24*, 6114–6131.

DYNAMICAL PREDICTION OF EXTREME AUSTRALIAN MONSOON IN 2010-11

Eun-Pa Lim, Harry Hendon, Guo Liu and Griffith Young

Centre for Australian Weather and Climate Research, The Bureau of Meteorology, Melbourne VIC 3000 Australia

Historically, in contrast to the Australian pre-monsoon rainfall that has strong relationship with El Nino-the Southern Oscillation (ENSO) promoted by air-sea coupling, the monsoon rainfall has a much weaker relationship with ENSO as the background winds in austral summer tend to offset the anomalous winds caused by the teleconnection. Consequently, the Australian monsoon rainfall has intrinsically less predictability than the pre-monsoon rainfall, and in general it is difficult to be predicted with good skill by both statistical and dynamical forecast system (Hendon et al. 2012).

Nevertheless, 2010-11 extreme Australian monsoon rainfall was skilfully predicted by the Bureau of Meteorology's dynamical seasonal forecast system, the Predictive Ocean and Atmosphere Model for Australia (POAMA) at up to 3-4 month lead times (Fig. 1). Therefore, in this study we have attempted to investigate the source of the predictability and prediction skill by conducting some dynamical model experiments that were designed to assess the sensitivity of prediction skill to realistic atmosphere, land and ocean initial conditions. Our results suggest that much of the summer rainfall over northern Australia was likely to be driven by the anomalous sea surface conditions associated with the 2010-11 strong La nina and its oceanic teleconnection to the Leeuwin current. In addition, the wet soil condition prepared by extreme rainfall in the pre-monsoon season appears to have played a role in promoting the monsoon rainfall.

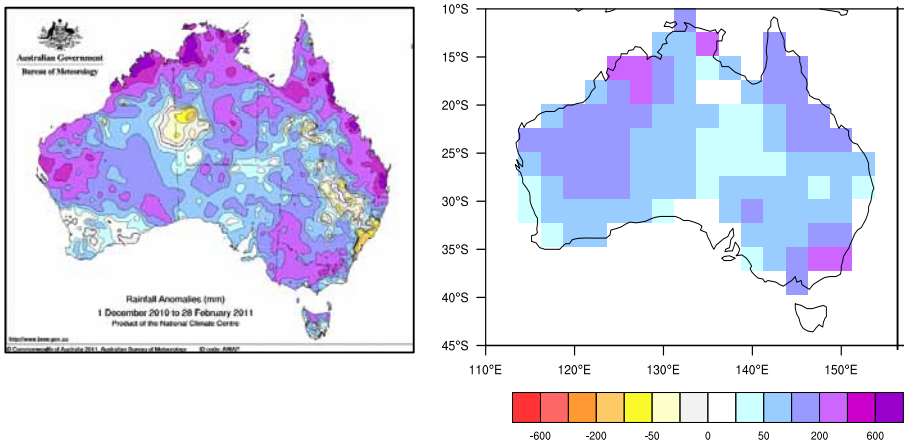

***Fig. 1**: Rainfall anomaly of December-January-February (DJF) in 2010-11 in the observation (left) and in 1 month lead forecasts of POAMA. The color shading indicates rainfall anomaly in mm per season.*

References

Hendon, H., Lim E.-P. and Liu, G.2012: The role of Air–Sea Interaction for Prediction of Australian Summer Monsoon Rainfall. *J. Climate*, 25, 1278-1290

PREDICTION OF NORTH AUSTRALIAN WET SEASON ONSET AND INTRA-SEASONAL VARIABILITY IN POAMA

Wasyl Drosdowsky and Matthew Wheeler

Centre for Australian Weather and Climate Research,
Bureau of Meteorology, Melbourne, Australia

Introduction

Currently seasonal climate outlooks issued by the National Climate Centre of the Bureau of Meteorology consist of probabilistic forecasts of total seasonal rainfall. Northern Australia is characterised by a monsoon climate, and for many agricultural and pastoral purposes, the timing of rainfall, and especially the start of the wet season (suitably defined) is generally a more important and useful parameter.

The onset and variability of wet season rainfall is examined on two different time scales. Firstly we examine the long range prediction of onset, in a probabilistic sense at up to three months lead time. At shorter time scales we examine the predictability of intra-seasonal variability within the wet season. At present there is no operational forecast of either of these parameters. Lo *et al* (2007) developed a prediction system for the onset of the wet season using logistic regression with antecedent SOI as the predictor. The large scale state of the tropical atmosphere is monitored using the Real-time Multi-variate MJO (RMM) indices describing the MJO. However these indices, being global in scale, do not always reflect the local conditions over northern Australia. This intra-seasonal variability of the wet season is monitored locally using OLR averages over various regions.

While various wet season onset definitions have been proposed, we use that of Lo *et al* (2007). Wet season onset is defined to have occurred when a threshold rainfall accumulation of 50 mm is reached from 1st September.

Observational Data and Onset

Rainfall data used in this study are the daily analyses from the Australian Water Availability Project (AWAP) at 1 x 1 degree resolution, over the period 1960 to 2009.
The median onset date (Fig. 1a) occurs first in late October over the western Top End around Darwin in the north, on the northeast Queensland coast, and over southeast Queensland. The concept of an onset is perhaps less applicable in the last two regions in which there is no real dry season, with some rainfall along the east coast during the winter season.. The median onset is progressively later further inland away from these locations, generally occurring before 1st December for locations north of 18°S over Western Australia (WA) and the Northern Territory (NT) and everywhere east of 145°E and later for locations further south/west.

There is significant inter-annual variability in the onset dates as shown by the inter-quartile range (Fig. 1b), with lowest variability in the same areas as earliest onset, and with highest variability over the inland areas. Much of the interannual variability is due to the El Nino Southern Oscillation, (ENSO) and this strong dependence on ENSO was the basis for the statistical forecast scheme of Lo *et al* (2007).

Rainfall over Australia has shown major trends over the past 50 years, with marked decline over the southwest and parts of the southeast in winter. In the tropical regions, there has been a strong increase in summer (DJFM) rainfall over northern Australia, especially WA and the western Top End, but little change in the spring transition period during which onset occurs over much of northern Australia. Consequently, a strong trend, of over 50 days in 50 years (Fig. 1c), towards earlier onset is evident over parts of WA and southern NT where mean onset typically occurs during December and January. In Central Australia near Alice Springs the trend has been -1.5 days per year, or 75 days earlier over the 1960 to 2009 period. In the north and east where onset occurs during the spring months of October and November the trend is mixed, but generally weak at less than 10 days over 50 years. This significant trend towards earlier onset over the interior of Western Australia and the southern parts of the Northern Territory which may confound statistical predictions of onset in these regions.

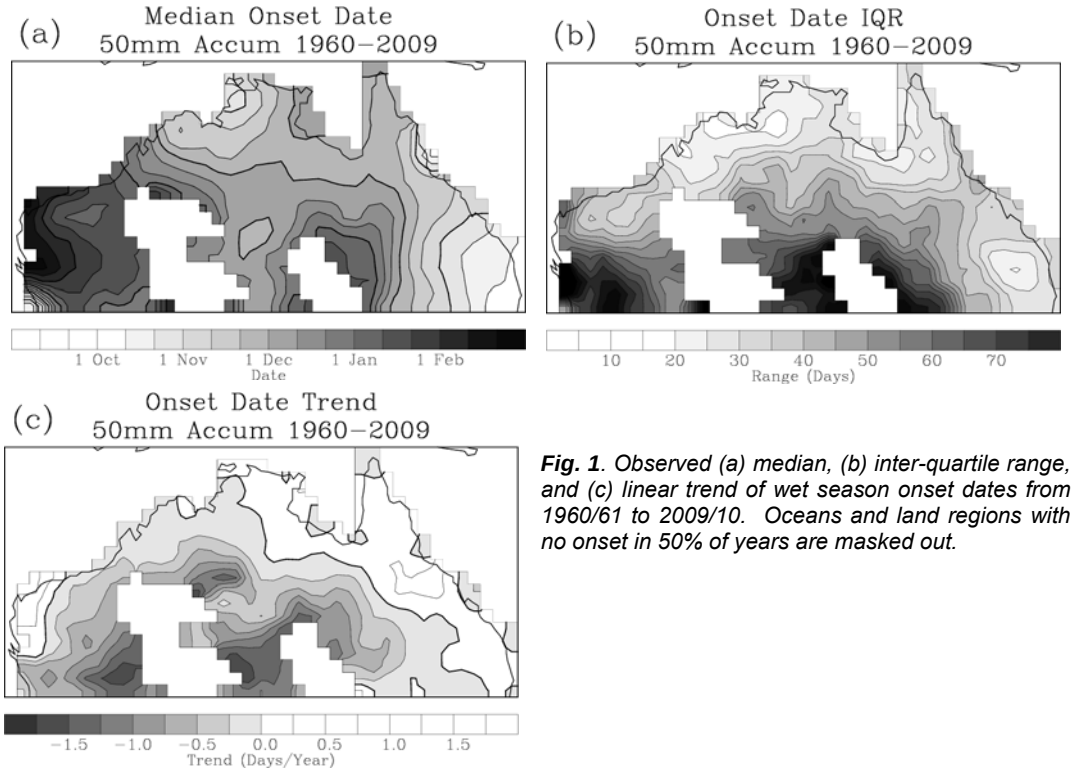

***Fig. 1**. Observed (a) median, (b) inter-quartile range, and (c) linear trend of wet season onset dates from 1960/61 to 2009/10. Oceans and land regions with no onset in 50% of years are masked out.*

Model Data and Onset.

The POAMA model is in a state of constant development and refinement. The first operational version for seasonal prediction (P15b) ran til November 2011, when it was replaced with the current version P24. A parallel version M24 has been developed for intra-seasonal prediction. P24 uses the same basic atmospheric model as P15b, but has three different configurations; P24a has an alternative parameterization of shallow convection physics, P24b has explicit bias ("flux") correction of SST during model integration, while P24c is identical to P15b. The P24 suite has an improved ocean data assimilation scheme and ensemble generation system compared to P15b.

The ensemble generation system uses a single atmospheric state, and 10 perturbed ocean states for each of the three model configurations (total of 30 forecasts) initialised on 1st of each month (hindcasts) and 1st and 15th of each month (real-time forecasts), and run out to 9 months. Hindcasts are available for 50 years from 1960 to 2009, while real-time forecasts available from

September 2009. For lead 0 forecasts (starting on September 01) the latest possible onset date is therefore 270 days or approximately the end of May, while for a three month lead (starting June 01) the latest onset would be the end of February. This is the longest lead time considered in this study.

Onset date is calculated in the same manner as for the observed data. Figure 1a shows that the observed wet season onset over most of northern Australia occurs between early October and late December. Lim *et al* (2009) showed that the earlier version of POAMA (P15b) had dry bias in springtime (SON) rainfall over parts of the tropics, including northern Australia. This is also a feature of all three variants of P24, and consequently there is strong late bias in the modelled onset dates. Figure 2 shows the cumulative probability that onset has occurred by a certain date, for the observed data, and for each lead time for one model configuration (P24a in this case) for a grid point over the western Top End near Darwin.. The onset date in the model is similar for all lead times ie there is consistency between successive model runs, and the distribution of modelled onset dates is similar to that of observed, but with a large late bias in the model, due to the models dry spring bias.

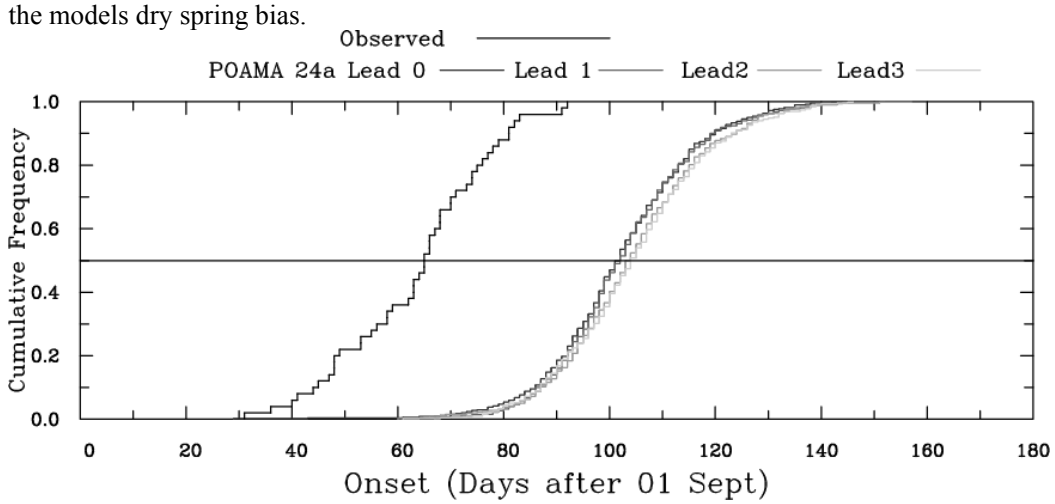

***Fig. 2**. Cumulative probability of onset occurring by given date, for observations and for P24a at leads of 0 to 3 months for gridpoint near Darwin.*

Probability of early onset for each model configuration is determined for each year in the hindcast period by simply counting the number of early onsets, relative to the appropriate climatology to remove the effect of the dry bias, in the 10 ensemble members for that model configuration. These probabilities are also combined for a 30 member multi-model ensemble (MME).

Skill of the 50 probabilistic hindcasts of wet season onset is calculated for each model, and for the combined MME. Three measures of skill are assessed: the percent correct at each grid point, the Brier Skill Score (relative to climatology) at each grid point, and the overall reliability and resolution of the forecasts through the attributes diagram.

The MME shows skill over most of northern Australia at all lead times, with the "percent correct" exceeding 50% over most of the region and exceeding 70% over about a third of the Northern Territory and parts of Queensland. Brier skill score is also positive over the region, with values up to 30% over the Top End and on Cape York Peninsula. The forecasts also exhibit a high degree of reliability, as shown by the attributes diagram, which uses data aggregated from all land gridpoints north of 30°S.

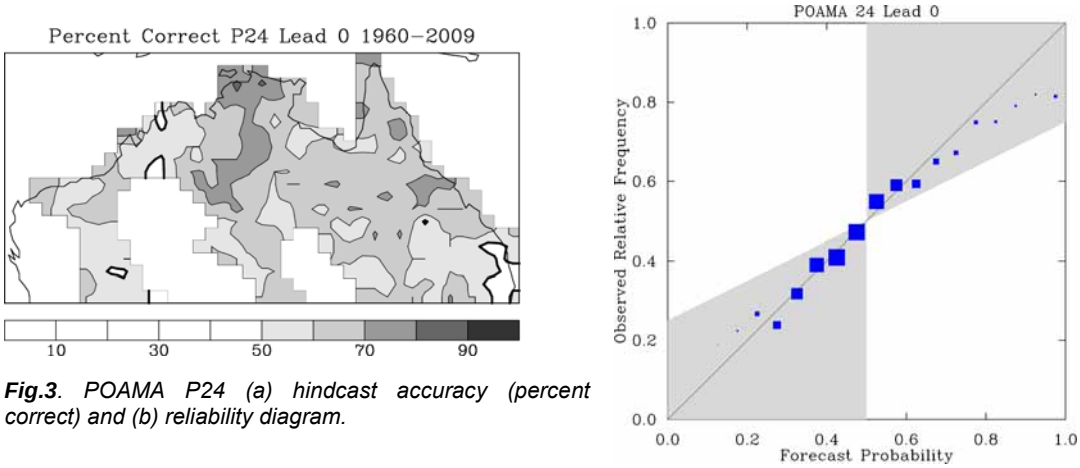

***Fig.3**. POAMA P24 (a) hindcast accuracy (percent correct) and (b) reliability diagram.*

Intra-seasonal Variability

Intra-seasonal forecasts are examined for OLR anomalies area averaged over a box covering northern Australia and adjacent ocean areas. This area has been monitored for some time and regarded as a good proxy of monsoon activity. The new version of POAMA (M24) is used for this study. This version features improved intialisation of ensemble members, but is only run for a shorter lead time of four months, and at present has a much shorter hindcast record than the P24 version.

For this version 36 hindcasts per year have been performed for a thirty year period from 1980 to 2009. Hindcasts are initialised on the 1st, 11th and 21st of each month, and run out to at least 120 days (4 months). Real time forecasts have been performed once a week (each Thursday) since August 2011.

Aggregated over all hindcasts, POAMA shows skill over climatology at all lead times out to at least 35 days, and over persistence at all lead times beyond 2 days.

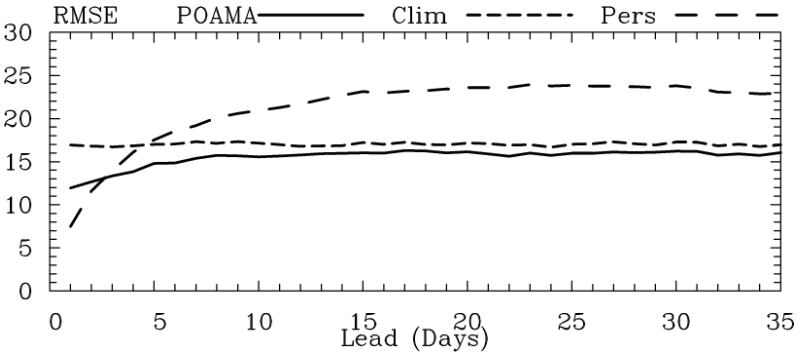

***Fig.4.** Hindcast skill of POAMA M24 for OLR anomalies in box 5S-17.5S, 120E-150E*

References:

Lo, F., Wheeler, M.C., Meinke, H. and Donald, A. 2007: Probabilistic forecasts of the onset of the north Australian wet season. Mon. Wea. Rev., 135, 3506-3520.

Lim, E.-P., Hendon, H.H., Hudson, D., Wang, G. and Alves, O. 2009: Dynamical forecast of inter-El Nino variations of tropical SST and Australian spring rainfall. Mon. Wea. Rev., 137, 3796-3810.

POAMA SEA SURFACE TEMPERATURE FORECAST SKILL IN THE WESTERN TROPICAL PACIFIC OCEAN

Aurel Griesser[1]

Centre for Australian Weather and Climate Research, Melbourne, Australia

The Australian Bureau of Meteorology currently produces a range of operational seasonal forecast products, such as seasonal ENSO outlooks (http://www.bom.gov.au/climate/enso/) and sea surface temperature (SST)-related products for the Great Barrier Reef region (Spillman 2011), as well as various experimental products (http://poama.bom.gov.au/poama2.shtml). Further SST-related products tailored to the western tropical Pacific Ocean are currently being developed, and in support of this effort, a skill assessment is being undertaken.

The seasonal forecast system Predictive Ocean and Atmosphere Model for Australia (POAMA) is a dynamical global atmosphere-ocean coupled system with 33 ensemble members (Wang et al. 2008; Zhao and Hendon 2009; Lim et al. 2009; Hudson et al. 2011). The data assimilation system (POAMA Ensemble Ocean Data Assimilation System, PEODAS; Yin et al. 2011) is also coupled. The current version of POAMA is run weekly.

The skill assessment documented herein examines deterministic skill based on the bias-corrected forecast ensemble mean SST anomaly, looking at correlation coefficient and mean absolute error (MAE). The mean absolute error is the average (over time) of the magnitude of the difference between the forecast SST anomaly and the observed SST anomaly. The region of interest is the western tropical Pacific Ocean, specifically including the Marshall Islands in the north, East Timor in the west, the Line Islands of Kiribati in the east, and Fiji, Tonga, Niue and Vanuatu in the south (25°S to 20°N, 120°E to 150°W). The skill is assessed based on POAMA's monthly hindcast data-set over the period 1982 to 2010. Reynolds OISST (Reynolds et. al. 2002) is used as the verification dataset (observations).

Figure 1 shows the anomaly correlation coefficient and MAE calculated over the period 1982 to 2010 at each grid cell in the western tropical Pacific Ocean region, for January and July at lead times of one month (the second month of the forecast). Correlation coefficient values are generally above 0.7 over the western end of the cold tongue, during January over most of the region lying to the north of the equator, and in July over a large part of the region south of the equator (i.e., it is higher in the winter hemisphere). Low correlation coefficient values (below 0.4) are found in the Coral and Arafura Seas during January, and north of Papua New Guinea in the southern Philippine Sea during July. MAE is high (above 0.4°C) within three degrees latitude of the equator to the east of 150°E during July, and south of approximately 15°S during January, regions which do not correspond with low correlation coefficients. However, the region of high MAE along the equator is also a region of relatively high inter-annual variability compared with the surrounding ocean: normalising the error by the local variance results in a much more uniform error field (not shown).

Taken together, the four panels of Fig. 1, as well as equivalent panels for other months (not shown), suggest that there is a significant degree of spatial and temporal variation in forecast skill over the western tropical Pacific Ocean.

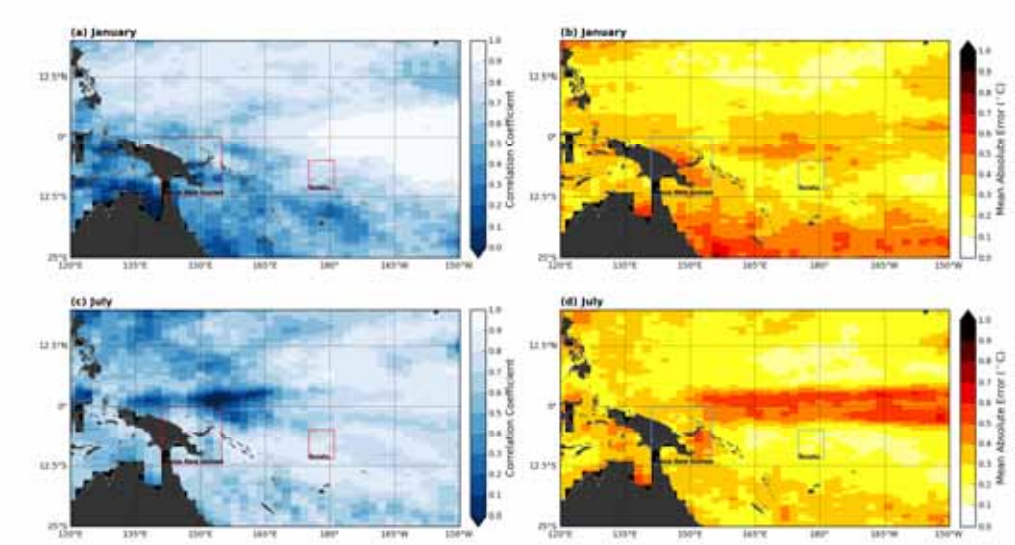

***Fig. 1**. Anomaly correlation coefficient of POAMA hindcasts at lead time one month, calculated over 1982 to 2010 for January (a), and July (c), and mean absolute error calculated over the same period for January (b) and July (d).*

In order to examine in more detail the annual variation in skill, SSTA indices were created by averaging the SST anomaly over various regions loosely based on the exclusive economic zones of the countries in the region: two such regions are shown in Fig. 1, labelled Papua New Guinea and Tuvalu. These regions contain 130 and 36 ocean grid cells respectively. Based on Fig. 1 (and equivalent figures for other months, not shown), the Tuvalu index should have relatively low mean absolute error and high correlation coefficient (suggesting overall good skill), while the Papua New Guinea index is defined over an area of lower correlation and higher mean absolute error (therefore, lower skill). For these two indices, the correlation coefficient and the mean absolute error were calculated for each month, for lead times zero to three, over 1982 to 2010. Calculated over these 29 years, a correlation coefficient value of 0.37 is statistically significant at the 5% level.

Figure 2 shows the correlation coefficient and mean absolute error as a function of forecast start month and lead time for the Papua New Guinea and Tuvalu indices. The correlation coefficient tends to decrease with lead time and the mean absolute error tends to increase. The correlation coefficients of both indices are above 0.7 for most of the first three months of the forecasts (lead times zero, one, and two). Mean absolute error during the first forecast month (lead time zero) is generally below 0.2°C for both indices, with some exceptions. The mean absolute error of the Papua New Guinea index increases faster with lead time than that of the Tuvalu index. By the fourth forecast month (lead time three), the Papua New Guinea index as forecast by POAMA was often more than 0.3°C different than in observations (OISST): for coral reef bleaching, where thermal tolerance levels are of order 1°C, this discrepancy could become significant.

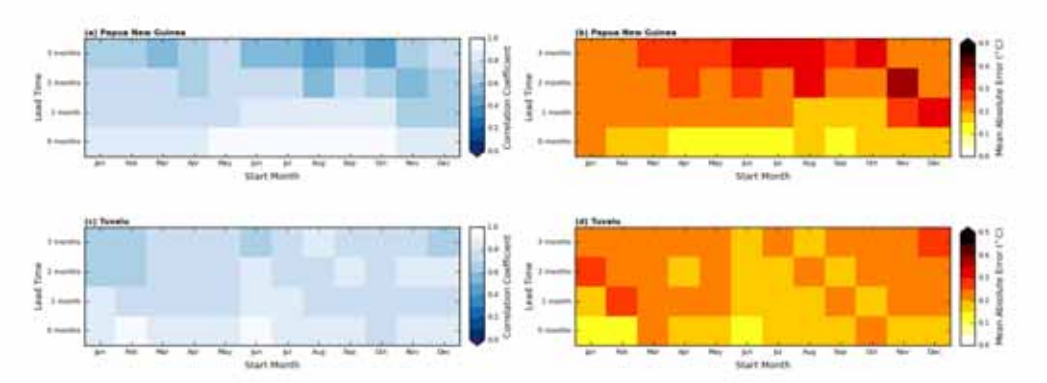

Fig. 2. *Anomaly correlation coefficient (calculated over 1982 to 2010) of index Papua New Guinea (a), and index Tuvalu (c), and mean absolute error calculated over the same period for index Papua New Guinea (b) and index Tuvalu (d).*

The SST indices will be used in probabilistic skill assessments, and in the development of appropriate country-specific forecast products based on SST (e.g. degree heating weeks) for various Pacific Ocean island nations. The spatial and temporal variations in skill shown in Figs 1 and 2 should be considered carefully when developing forecast products and accompanying documentation.

Conclusions

- There exists considerable spatial and temporal variation in forecast skill over the western tropical Pacific Ocean.
- Correlation coefficient of SST anomaly is above 0.7 over large regions of the western tropical Pacific Ocean, generally higher in the winter hemisphere.
- Over large parts of the western tropical Pacific Ocean, POAMA's SST forecasts over the second forecast month (lead time one month) have a mean absolute error of less than 0.4°C.

References

Hudson, D.A., Alves, O. Hendon, H.H. and Wang, G. 2011: The impact of atmospheric initialisation on seasonal prediction of tropical Pacific SST. *Climate Dynamics*, **36**, 1155–1171.

Lim, E.-P., Hendon, H. H., Hudson, D., Wang, G. and Alves, O. 2009: Dynamical Forecast of Inter–El Niño Variations of Tropical SST and Australian Spring Rainfall. *Monthly Weather Review*, **137**, 3796–3810.

Reynolds, R.W. et al. 2002. An improved in situ and satellite SST analysis for climate. *Journal of climate,* **15**, 1609-1625.

Spillman, C.M. 2011: Operational real-time seasonal forecasts for coral reef management. *Journal of Operational Oceanography*, **4**, 13–22.

Wang, G., Alves, O., Hudson, D., Hendon, H., Liu, G. and Tseitkin, F. 2008: SST skill assessment from the new POAMA-1.5 system. *BMRC Research Letters*, 8, 2–6.

Yin, Y., Alves, O. and Oke, P.R. 2011. An Ensemble Ocean Data Assimilation System for Seasonal Prediction. *Monthly Weather Review*, **139**, 786–808.

Zhao, M. and Hendon, H.H. 2009: Representation and prediction of the Indian Ocean dipole in the POAMA seasonal forecast model. *Quarterly Journal of the Royal Meteorological Society*, **135**, 337–352.

APPLICATION OF SEASONAL PREDICTION ON SUGAR CANE

Roger C. Stone[1], Yvette Everingham[2], and Torben Marcussen[1]

1. University of Southern Queensland, West Street, Toowoomba, Queensland, Australia, 4350.
2. James Cook University, 1 James Cook Drive, Douglas, Townsville, Queensland, Australia, 4811.

Abstract

Climate forecasting has the potential to have immense value for the Australian sugar industry, especially in regards to the provision of timely warning of excessive rainfall occurring during the critical harvest periods of autumn/early winter and spring/early summer. While statistical climate forecasting approaches have been demonstrated to provide modest skill and value for sugar industry management decisions, key issues in regards to provision of longer lead times and also for those decisions related to harvesting in autumn/early winter remain a problem. Development and application of fully coupled ocean-atmosphere model seasonal (and intra-seasonal) climate forecast systems offer major opportunity for improved management decisions and industry cost savings, especially for those periods for which statistical forecast systems have not proven useful. Integration of recently developed dynamical seasonal climate forecast systems with cane and sugar growth simulation models would also provide considerable value to the sugar industry in terms of the provision of more accurate forecasting of potential yield and commercial cane sugar (CCS) for this industry.

Introduction

Queensland produces 90% of the Australian sugar crop, most of it for export. This equates to a mean value of approximately 32 million tonnes of cane and 5 million tonnes of raw sugar (in a 'normal climate year'). To produce this amount of sugar there are approximately 4000 cane farms, 24 sugar mills and 6 bulk storage ports making Queensland Sugar Limited the 3rd largest sugar supplier in the world. Climate extremes, especially excessive rain during the harvest period (June to November) can result in massive losses for the entire industry – from the farm production component through to the milling component and especially through to the marketing and export component.

In 2010, one component alone of the sugar industry suffered losses of many hundreds of millions of dollars due to excessive rain (due to the developing and continuation of the major La Niña event of that year) occurring through the entire harvest period with subsequent yield downgrading and inability to harvest many crops due to wet weather and flooding. Appropriate climate forecasting systems, especially those that have the capability to be integrated into sugar production yield models and core decision systems are urgently required to be developed and included at various stages of the management cycle in the sugar industry.

Linking seasonal climate forecasting to management decisions

Management issues associated with the entire value chain in sugar production are remarkably complex and extend across a number of spatial and temporal scales (Everingham et al. 2002) (Fig 1). Figure 1 provides just an example of the range of management decisions associated with the various components of sugar industry management: with this example for the Queensland sugar industry. A key message from this diagram is that more simple and general climate forecast output may not be relevant to many aspects of sugar industry planning and management. Instead, more targeted climate (and weather) forecast information needs to be considered and developed if weather and climate forecast output is to meet the challenges faced by this industry. Furthermore, components of the sugar industry involved in milling and (especially) export planning and forward selling have a critical need for forecast information of total yield values for the Queensland sugar crop. Integrated statistical climate-yield forecast systems have been trialled with modest results obtained so far. The key challenge remains in determining the capability and value in developing a fully integrated coupled ocean-atmosphere modelling system(s) that can be integrated with state-of-the art crop (sugar production) modelling systems.

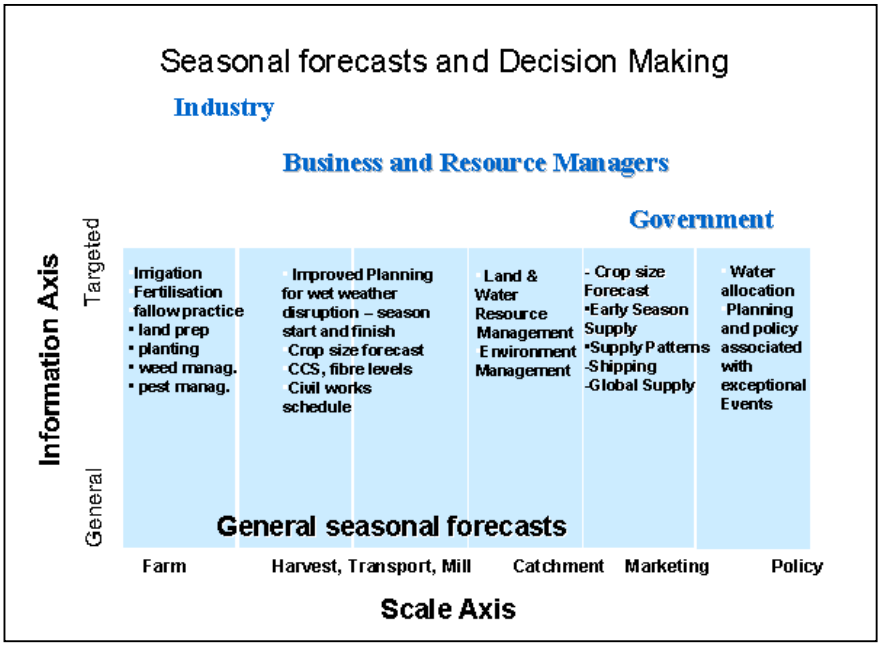

***Fig. 1**: The relationships between scale, information content, and decision-makers in defining relevant systems and the systems approach to applying seasonal forecasts for the Queensland sugar industry (after Hammer, 2000; Everingham et al., 2002; Stone and Meinke, 2005).*

Until recently, the most applied seasonal climate forecast systems were statistically derived and these have provided useful but modest application and benefits to the sugar industry (Stone and Meinke, 2005). In an example for the critical harvesting period of October-November, relationships between the SOI 'phases' (Stone et al. 1996) and the likelihood of rainfall in the upper quartile for a mill region in Northern Queensland ('Macknade Mill') are provided (Fig. 2). Statistically significant values are highlighted in green. Indeed, statistical forecasting systems have provided useful information for many years for many sugar regions due to the strong influence of El Niño/Southern Oscillation for most sugar growing regions, especially for the spring/early summer period.

	lead		SOI	32032 Macknade				
period	(mths)	response	period	Neg	Pos	Fal	Ris	Neu
on	0	rainfall	aug/sep	**0.05**	**0.47**	0.10	0.23	0.22
on	1	rainfall	jul/aug	**0.00**	**0.46**	0.30	0.32	0.21
on	2	rainfall	jun/jul	**0.00**	**0.56**	0.13	0.26	0.16
on	3	rainfall	may/jun	**0.00**	0.41	0.25	**0.43**	**0.10**
on	4	rainfall	apr/may	**0.06**	0.32	0.21	0.39	0.19
on	5	rainfall	mar/apr	0.13	0.29	**0.06**	0.38	0.30
on	6	rainfall	feb/mar	0.23	0.29	0.13	0.25	0.30

***Fig.2**: Example of forecasting rainfall probability values likely to fall in the 'upper quartile' - Macknade Sugar Mill, North Queensland associated with the SOI 'phases' (values shaded in green are statistically significant at p=.05).*

However, there remain critical and key requirements for seasonal or similar forecasts related to (what is referred to in the industry) as 'early season supply management' which involves the need for an indication of excessive rainfall for the May to July period in any year. This means a requirement for seasonal climate forecast systems for the 'predictability gap' of the southern hemisphere autumn which remains somewhat problematic with current statistical systems. Additionally, a particularly critical need for the sugar industry is the provision of climate forecast systems with increased lead times that will enable more effective tactical and strategic planning for all segments of the sugar industry.

Finally, development of a fully integrated yield production model incorporating crop simulation model input (eg 'APSIM/Canegrow') integrated with climate forecast systems is critically required. Some success has been obtained utilising statistical seasonal climate forecast systems. A more recent development has been through a project that seeks to fully integrate a number of coupled ocean-atmosphere models with sugar production simulation models through an ensembles approach. This approach is involving the Bureau of Meteorology's POAMA/ACCESS system together with the UK Met Office and/or ECMWF seasonal forecast outputs downscaled to local regions. Details of the progress being made in this new development will be provided.

References

Everingham, Y.L., Muchow, R.C., Stone, R.C., Inman-Bamber, G., Singels, A. and Bezuidenhout, C.N. 2002. Enhanced risk management and decision-making capability across the sugarcane industry value chain based on seasonal climate forecasts. *Agric. Systems 74, 3*, 459-477.

Hammer, G.L. 2000. A general systems approach to applying seasonal climate forecasts. In: *Applications of Seasonal Climate Forecasting in Agricultural and Natural Ecosystems: The Australian Experience* (eds. G.L. Hammer, N. Nicholls, and C. Mitchell), 51-66. Dordrecht, The Netherlands: Kluwer Academic Publishers.

Stone, R.C., Hammer, G.L. and Marcussen, T. 1996. Prediction of global rainfall probabilities using phases of the Southern Oscillation Index. *Nature 384*, 252-255.

Stone, R.C. and Meinke, H. 2005. Operational seasonal forecasting of crop performance. *Phil. Trans. Roy, Soc. B 360*, 2109-2124.

DYNAMICAL SEASONAL TYPHOON PREDICTION WITH THE JMA/MRI-CGCM AND ITS LINKAGE OF ASIAN MONSOON PREDICTION

Toshiyuki Nakaegawa

Abstract

Dynamical seasonal predictions of the inter-annual variability of typhoon genesis in the western North Pacific (WNP) during the active typhoon season from June to October are investigated. The physical mechanisms of the predictability are discussed in relevant to the predictability of Asian Monsoon circulation. Seven-month integrations for 28 years starting from late April using seasonal prediction system of the Japan Meteorological Agency (JMA) were performed according to the protocol of the Climate-system Historical Forecast Project under the CLIVAR Working Group on Seasonal to Inter-annual Prediction. The ensemble size is 10 and initial conditions are prepared with the JMA analyses for atmosphere and ocean respectively. The horizontal resolution of atmospheric and ocean general circulation models are about 180 km and 1 degree respectively. The inter-annual variability of the number of typhoon genesis is not well predictable deterministically, but is well so in the latter half period. This fact suggests the difficulty in predicting the inter-annual variability of the Monsoon trough activities because most typhoons are formed in or near the trough. In contrast, the good deterministic skill in predicting the inter-annual variability of the mean location of typhoon genesis is found. This stems from the predictability of the inter-annual variability of the atmospheric circulation as a part of Asian Monsoon system in the WNP influenced by ENSO. The inter-annual variability of the Asian Monsoon indices representing a latitudinal shift of the atmospheric circulation in the WNP is better predicted than that of the Asian Monsoon indices representing a longitudinal shift in this experiment. This difference in predictability among these Asian Monsoon indices provides a physical mechanism for the difference in predictability between the mean latitude and longitude regarding the inter-annual variability of typhoon genesis. Probabilistic predictions also demonstrate the good predictabilities of the mean location of typhoon genesis for tercile-based categories. Therefore, both deterministic and probabilistic predictions using the seasonal prediction system provide useful in genesis about the mean location of typhoon genesis.

IMPACT OF ASIAN AND NON-ASIAN ANTHROPOGENIC AEROSOLS ON 20TH CENTURY ASIAN SUMMER MONSOON

Tim Cowan[1,2] and Wenju Cai[1]

[1]CSIRO Marine and Atmospheric Research,
Aspendale, Victoria, Australia.
[2]Climate Change Research Centre, University of New South Wales,
Sydney, New South Wales, Australia.

Abstract

Many previous studies have focused on impact of anthropogenic aerosols on regional summer monsoon rainfall. This includes a black carbon-induced enhancement and a sulfate-induced suppression, of which encompasses significant Asian (e.g., East Asia and India) and non-Asian sources, but their relative roles in forcing historical global and regional monsoon trends is not well understood. Using targeted 20th century coupled climate simulations from a low resolution coupled-climate model, designed to isolate the impact from anthropogenic aerosols, it is shown that Asian aerosols induce a weak suppression of global summer monsoon, mostly contributed by the East Asian region. The addition of non-Asian aerosols generates an enhancement and broadening of cooler temperatures over Europe and Asia relative to the surrounding oceans, supporting stronger northerly flows that further suppress Asian monsoon rainfall. Atmospheric convection is directed away from the Asian monsoon regions, resulting in an equatorward shift in rainfall. Therefore, non-Asian aerosols exacerbate the impact of Asian aerosols on global monsoon rainfall, particularly across Asia.

Introduction

The global monsoon regions support two-thirds of the world's population so how monsoon rainfall will respond to human-induced climate change is of great importance. One potential factor in altering monsoon intensity and spatial distribution is increasing emissions of anthropogenic aerosols, through their influence on the land-sea thermal contrast (Meehl et al. 2007). Global climate models (GCMs), forced with various aerosol species, are commonly used to understand the impact of anthropogenic aerosols on the monsoon (e.g., Kim et al. 2007, Menon et al. 2002). East Asian sulfates emissions in early boreal spring have been shown to lead to a land surface cooling and a reduction in rainfall over central East Asia in the same season (Kim et al. 2007), while emissions of black carbon over western Asia have been shown to enhance Tibetan Plateau heating drawing in high moisture laden air from the tropical Indian Ocean (Lau et al. 2006). This leads to an intensification in pre-monsoonal rainfall over the Indian subcontinent, whilst at the same time rainfall is suppressed across East Asia.

Although the impact of sulfate loading is to suppress Asia summer monsoon, the relative importance of non-Asian aerosols when combined with Indian and East Asian aerosol emissions is unclear. We therefore use targeted experiment outputs from a fully coupled low resolution GCM to assess the importance of Asian and non-Asian anthropogenic aerosols on 20th century global and regional monsoon trends and examine the associated large-scale dynamics.

Results

The model used is the coarse resolution version of the CSIRO atmospheric GCM with a horizontal resolution of 5.6° × 3.2° (longitude × latitude). A comprehensive and interactive aerosol scheme is included in the model (Rotstayn et al. 2007), including sulfate and carbonaceous aerosols, mineral dust, sea salt and stratospheric aerosols from volcanos. Three sets of eight simulations for the period 1871–1999 are examined: the first set contains "all forcings" (ALL, see Cowan and Cai 2011 for more details). The second experiment set includes "all forcings" with only time-evolving Asian anthropogenic aerosol emissions (AS), while the third set contains "all forcings" except for global anthropogenic aerosols (AXA). The impact of global anthropogenic aerosols is the difference between ALL and AXA; for Asian anthropogenic aerosols, it is the difference between AS and AXA. As comparison to the model, we use rainfall reanalysis outputs from NCEP (Kalnay et al. 1996) for the period 1950–1999.

We focus on the peak monsoon season (summer), and as the GCM has a lower black carbon burden compared to other similar models (Rotstayn et al. 2007) the aerosol-induced impact on monsoon predominantly comes from sulfate emissions. Figure 1 highlights the spatial trend distribution of sulfate emissions since 1871 with both eastern China and eastern Europe showing strong increases over the 20th century.

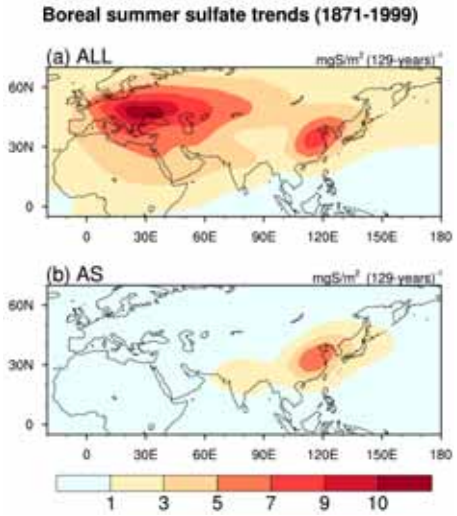

Fig. 1: *Boreal summer trends of vertically integrated sulfate over 1871–1999 for (a) the all forcings (ALL) and (b) all forcings with Asian aerosols (AS) ensembles. Figure taken auxiliary material from Cowan and Cai (2011).*

To quantify the long term changes in global monsoon intensity we first confirm that the GCM simulates the annual range (AR) of rainfall – this is difference between local summer and winter rainfall (Wang and Ding 2006). The AR is defined as summer rainfall minus winter rainfall and (1) must exceed 180 mm, and (2), the summer rainfall must exceed 35% of the total annual rainfall. The GCM performs well at realistically simulating the AR (comparing ALL with NCEP rainfall, figure not shown), generating the six distinct monsoon regions (Indian/East Asia, West Africa, Southern Africa, Australia, Central America and South America).

We next use the average summer rainfall over these monsoon zones to define an index of monsoon intensity for each simulation ensemble (e.g., ALL, AS–AXA, ALL–AXA). In the global aerosol-induced ensemble (ALL–AXA), a reduction in global monsoon intensity is produced, particularly after 1950, dominated by the Northern Hemisphere monsoon regions,

such as India and East Asia. After 1980, intensity over the Asian monsoon regions flattens off, due to global sulfate emissions peaking in the late 1970s and then declining (Fig. 1 of Rotstayn et al. 2007). In the Southern Hemisphere and Australian domains there is very little monsoon change after 1950, opposite to what is seen in NCEP. The Asian aerosol-induced change (AS–AXA) is only statistically significant over East Asia, smaller than the global aerosol-induced trend. In this AS–AXA ensemble the Indian monsoon region is weakly negative; from the mid-century onwards there is very little trend. Only when non-Asian aerosols are added to the model does a substantial reduction in the Indian monsoon emerge. Thus, in the model, a substantial portion of the rainfall suppression over Northern Hemisphere monsoon regions, in particular East Asia and India cannot be simulated without the additional non-Asian aerosols.

To understand the reasons for the changes in the monsoon intensity indices the spatial distribution of trends in surface temperature, mean sea level pressure (MSLP), rainfall, and wind stress over 1871–1999 are generated for the ALL, AS–AXA and ALL–AXA ensembles (see Fig. 3 of Cowan and Cai 2011). The ALL ensemble shows a strong temperature gradient stretching from Europe, Asia and northern America to Africa, southeast Asia and the tropical Indian Ocean. The strong land-sea temperature contrast is associated with a strong rainfall reduction over southeast China, and with smaller declines over southern India. Further south, increasing rainfall over Vietnam and the South China Sea indicate a possible shift in monsoon rainfall to equatorial regions that are less affected by the sulfate-induced cooling. The associated MSLP pattern shows a strong pressure gradient from Asia (high) to the Indian and western Pacific Oceans (low), signifying a redistribution of rainfall that is responding to the aerosol-induced temperature gradients. The redistribution includes a trend of increased subsidence with a wind regime flowing northeasterly against the climatological monsoon flow.

In comparison, Asian (AS–AXA) aerosols generate a strong regional cooling centre over northern India and southern China, along with a corresponding high MSLP centre. The accompanying anti-cyclonic circulation give rise to easterly flows just south of the MSLP centre and strong northerlies to the east of the high. This results in little change in the Indian monsoon, but a weakening in East Asia monsoon. These responses are a part of the regional impact that includes a strong local rainfall reduction over southern China extending to Bangladesh and the Bay of Bengal, accompanied by consistent local reductions in the total cloud amount. The response to regional (e.g., Indian and East Asian) aerosol emissions are somewhat confined, with no evidence of a southward shift in rainfall, meaning that Asian aerosol-induced trends explain only a small portion of the trends seen in ALL ensemble.

The additional non-Asian aerosols (ALL–AXA) greatly intensify the response of Asian monsoonal rainfall and circulation fields. Due to advection by the westerly jets the cooling becomes zonally elongated, extending to almost all longitudes. The cooling is largest over Europe and Asia, enhancing the thermal contrast between the land and the Pacific Ocean. This enhanced east-west thermal contrast further promotes northerly flows, weakening the East Asia monsoon, and curtailing its poleward excursion. In the meridional direction, the cooling area broadens, contributing to the southward shift in monsoonal rain discussed above. The centre of maximum MSLP response remains, but expands in both the zonal and meridional directions. As a consequence, the associated anticyclonic circulation results in northeasterly flows over the Indian monsoon region, extending the rainfall (and cloud) reduction from East Asia to the Indian subcontinent. Thus, only when non-Asian aerosols are included in the model can the surface trend patterns be reproduced (compared to ALL).

This study shows that the addition of non-Asian aerosols (predominantly sulfate emissions) broadens the spatial scale, and increases the intensity, of the land cooling relative to that over the ambient oceans. This gives rise to a broader high MSLP centre situated over the continental Europe and Asia, directing stronger northerly flows into the Indian subcontinent and southeast

China. This suppresses the Asian summer monsoon, leading to a systematic redistribution and equatorward shift in rainfall to monsoon-rim regions less affected by the aerosol-induced cooling. The robustness of the results should be tested using other models, in particular the updated CSIRO Mk3.6 that has improved the emission levels of black carbon, and is run at a higher spatial resolution. Our results, however, conclude the possibility that non-Asian aerosols substantially exacerbate the impact of Asian aerosols on global and regional summer monsoon.

References

Cowan, T. and Cai, W. 2011. The impact of Asian and non-Asian anthropogenic aerosols on 20th century Asian summer monsoon, *Geophys. Res. Lett*., *38*, L11703, doi:10.1029/2011GL047268.

Kalnay, E. *et al*. 1996. The NCEP/NCAR 40-year reanalysis project, *Bull. Am. Meteorol. Soc., 3*, 437–471.

Kim, M.-K., Lau, W.K.M., Kim, K.-M. and Lee W.-S. 2007. A GCM study of effects of radiative forcing of sulfate aerosol on large scale circulation and rainfall in East Asia during boreal spring, *Geophys. Res. Lett., 34*, L24701, doi:10.1029/2007GL031683.

Lau, K.M., Kim, M.K. and Kim K.M. 2006. Asian summer monsoon anomalies induced by aerosol direct forcing: the role of the Tibetan Plateau, *Clim. Dyn., 26*, 855–864.

Meehl, G. A. *et al*. 2007. Global climate projections, in Climate Change 2007: The Physical Science Basis. Contribution of Working Group I to the Fourth Assessment Report of the Intergovernmental Panel on Climate Change, edited by S. Solomon et al., pp. 747–845, Cambridge Univ. Press, Cambridge, U. K.

Menon, S., Hansen, J., Nazarenko, L. and Luo, Y. 2002. Climate effects of black carbon aerosols in China and India, *Science, 297*, 2250–2253.

Rotstayn, L. D. *et al*. 2007. Have Australian rainfall and cloudiness increased due to the remote effects of Asian anthropogenic aerosols?, *J. Geophys. Res., 112*, D09202,doi:10.1029/2006JD007712.

Wang, B. and Ding, Q. 2006. Changes in global monsoon precipitation over the past 56 years, *Geophys. Res. Lett., 33*, L06711, doi:10.1029/2005GL025347.

Remote influence of the tropical Atlantic on the variability and trend in North West Australia summer rainfall

Yun Li

CSIRO Mathematics, Informatics and Statistics, CSIRO Climate Adaptation Flagship
Wembley, WA 6913, Australia, (email: Yun.Li@csiro.au)

Rainfall in North West Australia (NWA) has been increasing over the past decades, occurring mainly in austral summer season (December-March). A range of factors such as decreased land albedo in Australia and increasing anthropogenic aerosols in Northern Hemisphere, identified using simulations from climate models, have been implicated in this wetting trend. However, the impact of land albedo and aerosols on Australian rainfall remains unclear. In addition, previous studies showed that dominant sea surface temperature (SST) signals in the Pacific-Indian Ocean including El Niño-Southern Oscillation (ENSO), ENSO-Modoki and the Indian Ocean dipole mode have no significant impact on the NWA rainfall trend. The present study proposes another viewpoint on the remote influence of tropical Atlantic atmospheric vertical motion on the observed rainfall variability and trend in NWA.

It is found that, with the atmospheric ascent instigated by the warming of SST over the tropical Atlantic, a Rossby wave train is emanating southeastward from off the west coast of subtropical South America to mid-latitudes of the South Atlantic Ocean. It then travels eastward embedded in the westerly jet waveguide over the South Atlantic and South Indian Oceans. The eastward-propagated Rossby wave induces an anticyclonic anomaly in the upper troposphere over Australia, which is at the exit of the westerly jet waveguide. This leads to an in-situ upper-tropospheric divergence, ascending motion and a lower-tropospheric convergence, and the associated increase in rainfall in NWA. Thus, the increasing trend in atmospheric upward motion induced by the warming trend of SST in the tropical Atlantic may partially explain the observed rainfall trend in NWA.

Reference

Lin, Z. and Li, Y. 2012: Remote influence of the tropical Atlantic on the variability and trend in North West Australia summer rainfall. *Journal of Climate* **25**, 2408-2420.

PUZZLING PUZZLES: POTENTIAL CHANGES IN MONSOON ONSET/INTENSITY IN THE AUSTRALIA-ASIAN REGION IN FUTURE CLIMATE

Huqiang Zhang[1], Aural Moise[1], Ping Liang[2], Lawson Hanson[1]

[1]Centre for Australian Weather and Climate Research, a partnership between Australian Bureau of Meteorology & CSIRO, Melbourne, Australia
[2]Shanghai Regional Climate Center, China Meteorological Administration, Shanghai, China

Introduction

As the timing of the start and end of summer monsoon season can directly affect many social and economical practices in the region, studying of Australia-Asian monsoon onset/retreat and factors affecting their behaviours has been one of the foci in monsoon studies. Because of extreme complexities operating in the monsoon system which involves numerous physical and dynamical processes interacting at a range of temporal and spatial scales, it remains as a great challenge for global climate models, often with coarse resolutions, to reproduce detailed characteristics of the monsoon system.

In this study, seasonal variations in both atmospheric precipitable water and wind conditions are used in defining monsoon onset/retreat. Combining these two large-scale variables from ERA-40 reanalysis daily data, we show it gives satisfactory monsoon onset/retreat dates, their detailed spatial patterns as well as interannual variations in the Asian and tropical Australian regions. Then, we use the method to investigate some detailed aspects of monsoon activities from current global climate models which show some skills in reproducing these large-scale variables. We have applied the method to the majority of IPCC AR4 models, using daily data from their three sets of experiments: 20C3m for current climate and A1B and A2 for two future emission scenarios. Throughout the analysis, our focus has been on exploring uncertainties presented in these model results. We have made significant efforts to try to solve these puzzling puzzles by asking three questions to each of these models: what are the dominant processes governing its monsoon onset/retreat; what are the responses of these processes to global warming in the models; and how the changes of these processes influence its simulated changes in monsoon onset/retreat.

Data and method

As pointed out in Zhang (2010), developing a method for defining monsoon onset/retreat which can be applied to global climate model results needs to meet two requirements: one is that it should grasp fundamental features of the monsoon system which owns significant rainfall and circulation seasonal variations; the other is that it can be reasonably simulated by current climate models. Zhang (2010) revised a method by using both atmospheric volumetric precipitable water (PW) and 850hPa horizontal wind conditions for such purposes. Good agreement was seen from the comparisons of results derived from ERA-40 reanalysis data using this method to some published onset data in the Australia-Asian region.

For assessing the potential changes in monsoon onset/retreat in global-warmed climate, we have further analysed 13 IPCC AR4 models. These models were selected because we have access to their model daily data and they give reasonable simulations of the Asian monsoon. In this study, we have analysed three sets of AR4 model experiments: 20C3m which represents the model skill of reproducing current climate; SRESA1B and SRESA2 which represent two different emission scenarios with A2 having a higher emission than A1B. Due to the large amount of data to be retrieved and processed, we were only able to analyse a single run from each of the model data for the 20-yr period of 1981-2000 in 20C3M, and 2081-2100 for A1B and A2.

Results

i) Asian summer monsoon:

Analysis of Zhang et al. (2012a) showed that most models were able to reproduce the observed temporal and spatial evolution patterns of the Asian monsoon system. Nevertheless, there were significant model biases and some models fail in reproducing the broad structure. Under a warmed climate, changes in onset and duration days were only moderate (about 3-10 days), with significant discrepancies among the models, particularly over the East Asia land area where the models were almost equally divided. In the tropical Indian Ocean, maritime continent and Indochina Peninsula, the majority of the models tended to simulate delayed onset and shortened duration while in the western North Pacific most models exhibited an early onset and longer duration.

There were two reasons leading to such uncertainties: (i) the key processes determining the Asian monsoon onset/retreat were different among the models. Some were more influenced by ENSO-like processes. But in some models, monsoon onset/retreat was more significantly correlated to circulations in the tropics. (ii) The model-simulated changes in these dominant processes were different. In some models, surface warming was more intense in the central and eastern Pacific Ocean with El Nino-like patterns, while others did not show such features. If the model-simulated monsoon onset/retreat was correlated to the central and eastern Pacific warming and at the same time the model simulated much larger warming of the central and eastern Pacific Ocean, then it was very likely that these models would show significant delay of south Asian monsoon onset and shortened duration. In some models, the delayed onsets were more related to the reduction of westerlies in the west of the warm pool region. The patterns of anomalous SST and wind conditions identified in this study were consistent with each other and both were likely linked to the weakening and westward shift of Walker circulation in the warm pool and maritime continent region. Increases in precipitable water associated with global warming did not change monsoon rainfall and circulation seasonality much but they could result in increased rainfall intensity once the summer monsoon is established.

ii) Australian summer monsoon

Over Australian summer monsoon region, the analysis of Zhang et al. (2012b) showed that a majority of the models can capture the northwest-southeast evolution of the summer monsoon, which started from the south Sumatra and Java region around later November and then progressively approaches the Australian continent in late December. Nevertheless, significant biases existed in the modeled onset/retreat dates and the extent of the monsoon inland penetration. Under global warming, the agreement among the model projections varied across the domain. In between the Sumatra-Java archipelago and the top end of the Australian continent, over 80% of the models simulated delayed monsoon onset and shortened duration by ~10 days, but less model agreement was seen over interior continent where the model

ensembles showed an approximate 7-day delay of both the onset and retreat with relatively little change in duration.

Correlation analyses suggested that both El Nino – Southern Oscillation (ENSO) and Indian Ocean Dipole (IOD) played important roles in determining the variation of Australian monsoon onset/retreat in the models. Nevertheless, the extent of their influence varied significantly. A large number of the models had IOD-like SST correlation patterns, with positive IOD-like pattern being associated with delayed monsoon onset. This linkage was supported by the correlations of onset dates with 850 hPa wind, with stronger zonal westerly over tropical eastern Indian Ocean and Sumatra-Java region favouring early onset. Furthermore, the model-simulated mean SST warming pattern in the pre-monsoon season had a positive IOD-like pattern in a large proportion of the models. Consequently, most models produced zonal easterly anomalies in the region associated with weakened upward branch of the tropical Walker circulation. This appeared to be the main reason that the models showed delayed onset and shortened duration of the Australian monsoon. Results underline that how the Indian Ocean responds to global warming will have a significant influence on the Australian summer monsoon characteristics in future climate.

Conclusions

This study has underlined the importance of exploring and understanding model uncertainties in their simulations of regional climate changes. Detailed analysis of the divergence of the model results can help us to build up our confidence and strengthen the scientific robustness in delivering regional climate change projections, such as the potential changes of Australia-Asian monsoon in future climate.

Acknowledgment

This collaborative research was supported by the collaboration agreement between the Australian Bureau of Meteorology and China Meteorological Administration.

References

Zhang, H. 2009. Diagnosing Australia-Asian monsoon onset/retreat and using large-scale wind and moisture indices, *Climate Dynamics* DOI 10.1007/s00382-009-0620

Zhang, H., Liang, P., Moise, A. and Hanson, L. 2012a. Diagnosing potential changes in Asian summer monsoon onset and duration in IPCC AR4 model simulations using moisture and wind Indices, *Climate Dynamics*, DOI 10.1007/s00382-012-1289-0

Zhang, H., Moise, A., Liang, P. and Hanson, L. 2012b. The response of summer monsoon onset/retreat in Sumatra-Java and tropical Australian region to global warming in CMIP3 model, *Climate Dynamics*, DOI 10.1007/s00382-012-1389-x

WESTERN PACIFIC MONSOON AND CLIMATE CHANGE

Ian Smith

What do models tell us about changes to be expected in the western Pacific monsoon region as a result of enhanced greenhouse gas concentrations? Here we show: what can happen on the large scale according to CMIP3 and CMIP5 model results. In general, we find little evidence for a change in the low level winds, but substantial evidence for an increase in rainfall. We also present the results from a relatively high resolution model which shows that the projected rainfall changes at the regional scale, where topography is important, can differ from the coarser scale results. In the case of mountainous Papua New Guinea, there is evidence for decreased rainfall in some regions. While the results are preliminary, they do suggest that the mechanism referred to as "the wet get wetter and the dry get drier" can sometimes apply at regional scales.

HIGH-RESOLUTION PROJECTION OF ASIAN/AUSTRALIAN MONSOON SYSTEM

Akio Kitoh
Meteorological Research Institute, Tsukuba, Ibaraki, JAPAN

Abstract

This study focuses on projecting future changes in Asian-Australian monsoon rainfall. Time-slice experiments using a 20-km-mesh MRI-AGCM were performed both in the present-day (1979–2003) and the future (2075–2099). To assess the uncertainty of the climate change projections, 12 ensemble projections (3 different cumulus schemes and 4 different sea surface temperature (SST) patterns) were conducted using 60-km-mesh MRI-AGCMs.

Introduction

Based on multi-model projections, Christensen et al. (2007) assessed increased summertime precipitation over East Asia, South Asia, and most of Southeast Asia due to enhanced moisture convergence under a warmer climate, despite a tendency towards the weakening of monsoonal air flow. In Australian region, large uncertainty exists for summer (DJF) monsoon precipitation. Recent results based on Coupled Model Intercomparison Project phase 5 (CMIP5) show that many models agree in projecting an increase of Australian summer monsoon precipitation (Kitoh et al., 2012).

An increase in the frequency of intense precipitation events is very likely in the Asian-Australian monsoon regions. Higher horizontal resolution models may be needed to better reproduce extreme rainfall associated with tropical cyclones and precipitation systems such as the Meiyu/Baiu rain band. To this end, dynamical downscaling approaches have been developed, including regional climate models (RCM), variable-resolution atmospheric general circulation models (AGCM), and global high-resolution AGCMs. At MRI, we use both a global high-resolution AGCM and an RCM (Kitoh et al., 2009).

Quantifying uncertainty in projections of future climate changes is a critical issue. Kusunoki et al. (2011) assessed future changes in East Asian summer rainfall based on a combination of a single global warming projection experiment with a 20-km-mesh AGCM and ensemble projections with a 60-km-mesh AGCM, using four different SSTs and three atmospheric initial conditions. In their future climate simulation by the 20-km model, precipitation shows an increase over the Yangtze River valley in May–July (Meiyu), over Korea in May (Changma), and over Japan in July (Baiu). Simulations with the 20-km and 60-km models consistently show that the termination of the rainy season over Japan tends to be delayed until August in the future climate.

Recently, we have developed a new model (MRI-AGCM3.2, Mizuta et al., 2012). This model shows improvements in simulating heavy precipitation around the tropical western Pacific, the global distribution of tropical cyclones, the seasonal march of East Asian summer monsoon, and blockings in the North Pacific. Differences in physical parameterization employed in the models as well as differences in SST changes projected by AOGCMs could lead to large uncertainty in

future precipitation projections. Using the MRI-AGCM3.2, we performed climate projections for the end of the 21st century using the 60-km-mesh model under a multi-physics multi-SST framework (twelve ensemble experiments) as well as using the 20-km-mesh model. This approach allows us to address differences of impacts due to model physics and prescribed future SST changes on projected future changes (Endo et al., 2012; Murakami et al., 2012).

Method

The model simulations were run at horizontal resolutions of T_L959 (MRI-AGCM3.2S, the 20-km model) and T_L319 (MRI-AGCM3.2H, the 60-km model). The model is equipped with multiple cumulus convection schemes that can be easily switched. Three cumulus convection schemes were used for the multi-physics ensemble simulations: the prognostic Arakawa–Schubert (AS) cumulus convection scheme; a new cumulus convection scheme named as "Yoshimura scheme (YS)"; and the Kain–Fritsch (KF) convection scheme. The YS scheme is based on the Tiedtke (1989) scheme, but modified as to represent all top-level cumulus plumes by interpolating two convective updrafts with maximum and minimum rates of turbulent entrainment and detrainment (Yukimoto et al., 2011).

A time-slice experiment was conducted, in which the high-resolution AGCM was forced by prescribed sea surface temperatures (SSTs). For the present-day climate simulation, the 20-km model with the YS scheme was integrated for 25 years (1979–2003) with the observed historical SST and sea ice data of HadISST1 (Rayner et al., 2003). We also conducted ensemble simulations with the 60-km model for three different convection schemes (YS, AS, and KF), using experimental settings identical to those for the 20-km model.

For the future climate simulations, the 20-km model with the YS scheme was integrated for 25 years during 2075–2099 with future SSTs. The future SST change was evaluated by the difference between the 20th Century experiment (20C3M) and future simulation under the Special Report on Emission Scenario (SRES) A1B experiments in the CMIP3 dataset. The boundary SST data for the future were prepared by superposing: (1) future change (between 2075-2099 and 1979–2003) in SST projected by CMIP3 multi-model ensemble (MME) mean; (2) the linear trend of SST projected by CMIP3 MME during 2075–2099; and (3) the de-trended observed SST for the period 1979–2003. Future sea-ice distribution was obtained in a similar fashion. Details of the method can be found in Mizuta et al. (2008). The prescribed future SST retains the observed year-to-year variability and El Niño–Southern Oscillation (ENSO) events in the present-day (1979–2003), but with a higher global mean and a clear increasing trend in the future climate. The change in global annual mean SST at the end of the 21st century (2075–2099) relative to the present-day (1979–2003) is +2.17 °C.

To evaluate the uncertainty of future projections due to the choice of convection scheme, simulations using the 60-km model for the YS, AS, and KF convection schemes were conducted similarly for the future as well as the present-day. Although the MME mean of future SST changes projected by CMIP3 models can be considered as one of the best estimates of future SST change, uncertainty of geographical SST distribution especially in the tropics should also be considered. Therefore, three other SST patterns were prepared using a cluster analysis, in which tropical SST anomalies derived from the 18 CMIP3 models were grouped. See Endo et al. (2012) for details.

Results

First, geographical distribution of climatological seasonal mean precipitation, as reproduced in the present-day simulations, is compared with observed data. Figure 1 shows the simulated

December-January-February (DJF) mean precipitation climatology for the 20-km model and for the three 60-km models with the different cumulus schemes. Also shown are two observed datasets: Climate Prediction Center Merged Analysis of Precipitation Version 1103_standard (Xie and Arkin, 1997) with a 2.5 degree grid spacing (CMAP) and Tropical Rainfall Measuring Mission product in version 6 (Huffman et al., 2007) with a 0.25 degree grid spacing (TRMM 3B43). All models successfully reproduced the observed major convection centers over the islands in the Maritime Continent and over the South Pacific Convergence Zone. Among the three 60-km models, KF scheme model (HP_KF) tends to overestimate precipitation. Spatial pattern correlation with CMAP is best reproduced by YS scheme models (SP_YS and HP_YS). We also evaluated precipitation extremes indices (figures not shown). It is found that the AS scheme model underestimates precipitation extremes indices such as maximum 5-day precipitation total (R5d), while other two schemes are close to TRMM dataset. It is noted however that magnitude of R5d differs greatly among different observations.

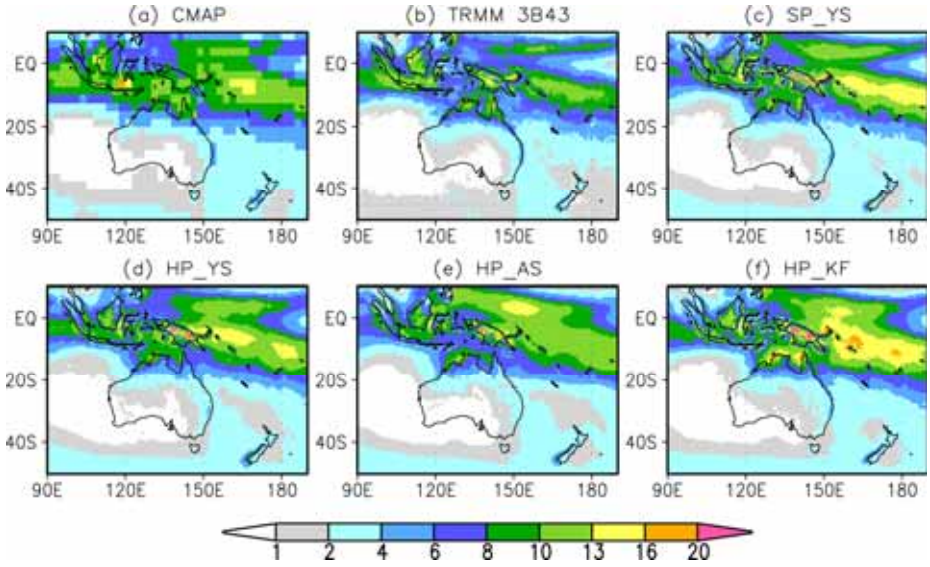

Fig. 1: *December-January-February (DJF) mean precipitation climatology (mm/day): (a) CMAP, (b) TRMM 3B43, (c) 20-km model with YS cumulus scheme (SP_YS), (d) 60-km model with YS cumulus scheme (HP_YS), (e) 60-km model with AS cumulus scheme (HP_AS), and (f) 60-km model with KF cumulus scheme (HP_KF). The average period for the climatology is 1979–2003, except for TRMM 3B43 (1998–2008).*

Figures 2 and 3 show future changes in mean precipitation for the 20-km model and the 60-km models projections in JJA and DJF, and the annual mean for the Asian and Australian regions. For the 20-km model, areas with statistically significant change (at the 10% level) are shaded in color. For the 60-km models, the 12 ensemble experiments (i.e., combination of 3 different cumulus schemes and 4 different assumptions for prescribed future SSTs) are averaged. There is an overall agreement between the 20-km model results and the 60-km models' results. Statistical significance is low over land for the 20-km model projection because sample number is small. For the JJA mean, the models generally project an increase in precipitation over the Asian summer monsoon region, and a decrease in precipitation over inland Asia, the Maritime Continent and coastal Australian region. For the DJF mean, they generally project increased precipitation over the region including East Asia, Bangladesh, the ocean east of the Philippines, the southern part of the Maritime Continent, and southeastern part of Australia. In contrast, they project decreased precipitation over the area between the equator and 20°N in Asia, which coincides with the dry season and is unaffected by mid-latitude synoptic disturbances.

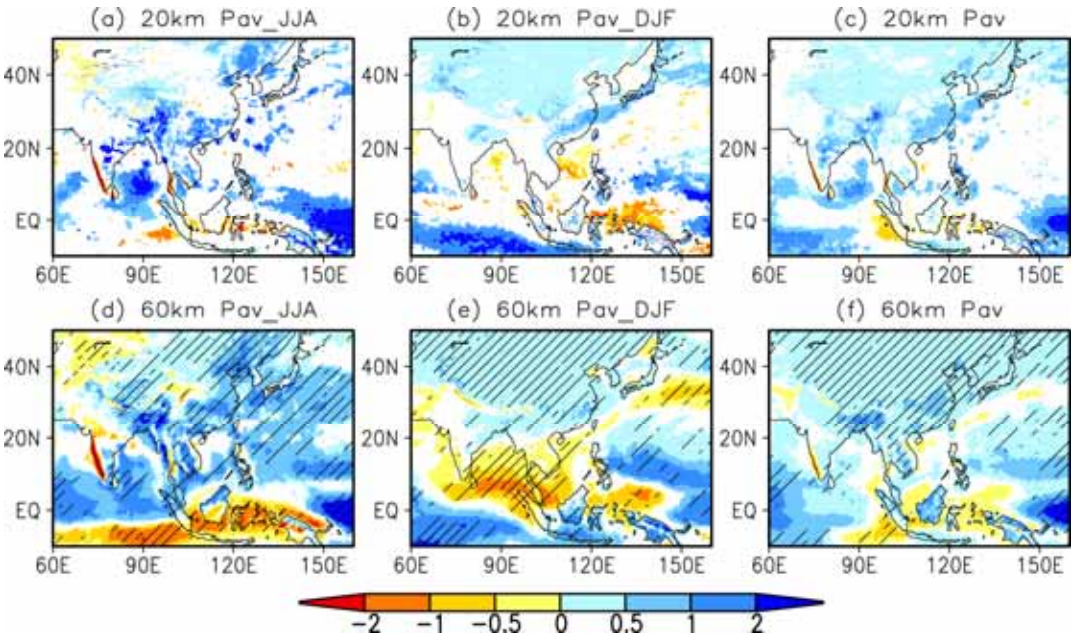

Fig. 2: *Future changes in mean precipitation between the present-day (1979–2003) and the future (2075–2099) for the 20-km model (SP_YS): (a) JJA, (b) DJF, and (c) annual, and for the 60-km model ensemble simulations: (d) JJA, (e) DJF, and (f) annual. In (a)–(c), statistically significant grid points (at the 10% level) are shaded in color. In (d)–(f), statistically significant grid points (at the 5% level) are shaded in color, and grid points where all 12 (>=10) experiments show the same sign of changes are closely (widely) hatched.*

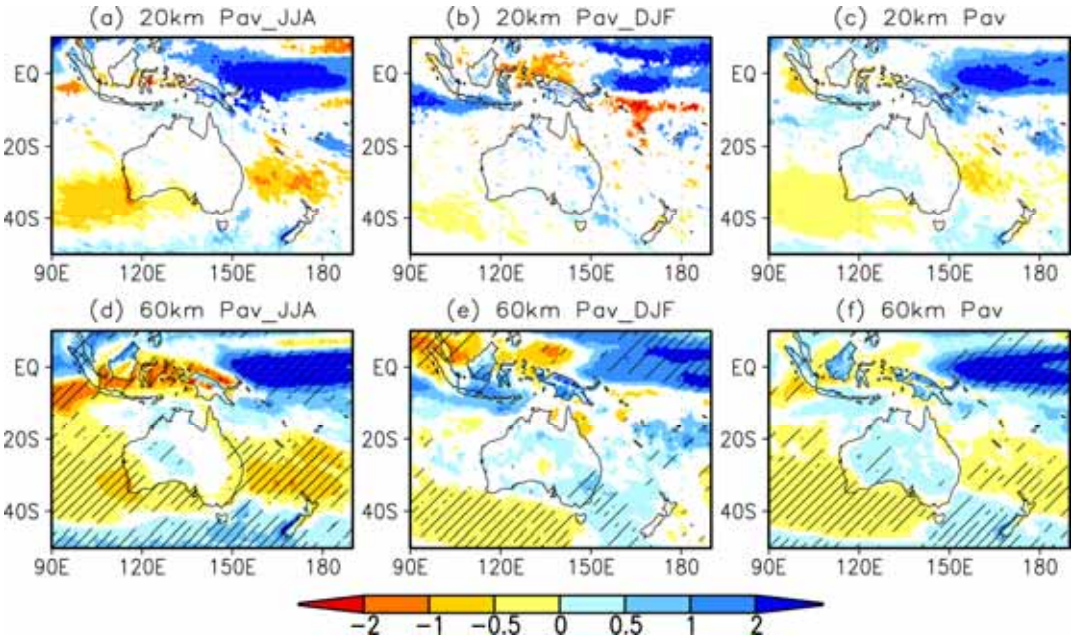

Fig. 3: *As for Fig. 2, but for the Australian region.*

For the annual mean, an increase in precipitation is generally projected over land in Asia. Thus, precipitation tends to be higher in the wet season but lower in the dry-season over tropical Asia, resulting in a greater seasonal contrast than the present-day.

Figure 4 shows future changes in the extreme precipitation indices for the 20-km model and the 60-km models projections. Here we show the simple daily precipitation intensity index (SDII), the maximum 5-day precipitation total (R5d) and the consecutive dry days (CDD). For the future changes, an overall agreement is found between the 20-km model results and the 60-km models. Extreme precipitation (SDII and R5d) is projected to generally increase in Asia-Australian region. Compared with the case for mean precipitation, areas with significant positive changes are larger, particularly over land. At the same time, CDD is projected to increase.

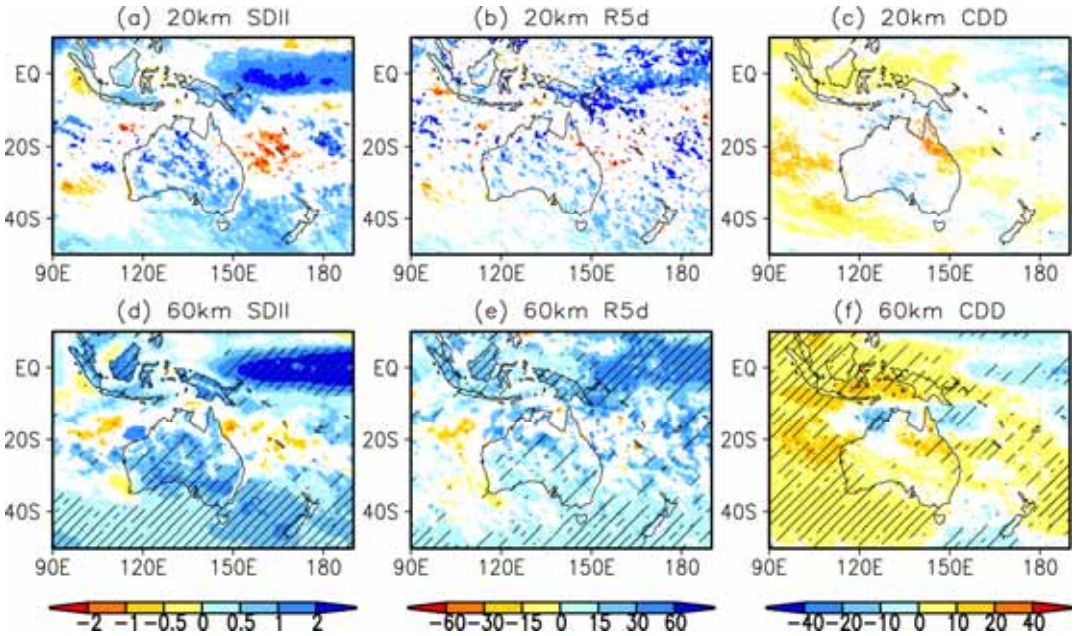

Fig. 4: *As for Fig. 2, but for (a, d) SDII, (b, e) R5d, and (c, f) CDD.*

Figure 5 summarizes the future changes in the precipitation indices averaged over northern Australia land region. In this region, statistical significance of changes is low as indicated by Figs. 3 and 4. For the mean precipitation changes, even with the same YS scheme and same MME SST, the 20-km model and 60-km model show different sign of changes. For DJF, HF_YS projects a decrease in precipitation, while other two schemes project an increase. For JJA, HF_KS projects a decrease in precipitation, while other two schemes project an increase. SDII and R5d tend to increase in this region. Among different SST experiments, Cluster3 SST-forced experiment tends to have different behavior compared to other experiments, probably due to the warmer SST over the western Pacific used in this experiment.

The changes in mean and heavy precipitation show large differences among the projections over many regions including northern Australia, suggesting uncertainty over these regions. In East Asia and Bangladesh, on the other hand, mean and heavy rainfall show consistent increases among the projections, suggesting the projections are reliable over these regions. Further investigation by analysis of variance revealed that uncertainty in the projected precipitation changes in South Asia and Southeast Asia is derived mainly from differences in the cumulus schemes, while the uncertainty originates mainly from differences in the SST anomaly patterns over the Maritime Continent and northern Australia, where a projection of sea surface temperature pattern with a high degree of accuracy is important to reduce the uncertainty.

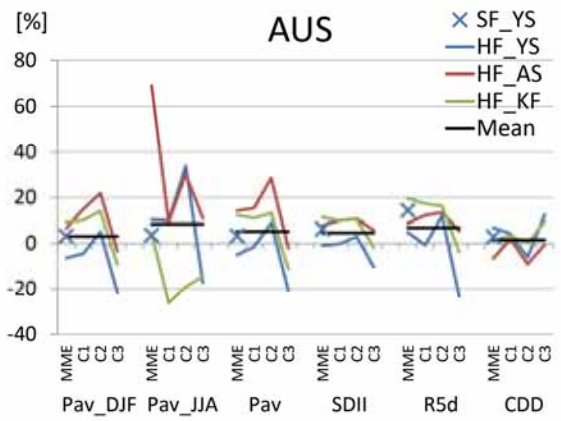

Fig. 5*: Future changes (%) of precipitation indices averaged over northern Australia (120°E-150°E, 20°S-10°S; land). The future changes are shown as the percentage change ((F – P)/P) from the present-day (P: 1979–2003) to the future (F: 2075–2099). The 20-km model is indicated by a cross. The 60-km models are indicated by color line graphs and their averages are denoted by horizontal black lines. Models with different cumulus schemes are indicated by different colors: i.e., blue for YS, red for AS, and green for KF. CMIP3 MME, Cluster1, Cluster2, and Cluster3, which are the SST pattern prescribed in the future climate simulations, are denoted as MME, C1, C2, and C3, respectively.*

References

Christensen, J.H. and Coauthors, 2007: Regional Climate Projections. In *Climate Change 2007: The physical Science Basis*, *Contribution of Working Group I to the Fourth Assessment Report of the Intergovernmental Panel on Climate Change*, S. Solomon et al., (Eds.), Cambridge University Press, New York.

Endo, H., Kitoh, A., Ose, T., Mizuta R. and Kusunoki, S. 2012: Future changes and uncertainties in Asian precipitation simulated by multiphysics and multi-sea surface temperature ensemble experiments with high-resolution Meteorological Research Institute atmospheric general circulation models (MRI-AGCMs). *J. Geophys. Res., 117*, D16118, doi:10.1029/2012JD017874.

Huffman, G.J. and Coauthors, 2007: The TRMM multisatellite precipitation analysis (TMPA): quasi-global, multiyear, combined-sensor precipitation estimates at fine scales, *J. Hydrometeorol.*, *8*, 38–55.

Kitoh, A. and Coauthors, 2009: Projection of changes in future weather extremes using super-high-resolution global and regional atmospheric models in the KAKUSHIN Program: Results of preliminary experiments. *Hydrological Research Letters, 3*, 49-53.

Kitoh, A. and Coauthors, 2012: Monsoons in a changing world: a regional perspective in a global context. *J. Geophys. Res*. (submitted)

Kusunoki, S., Mizuta, R. and Matsueda, M. 2011: Future changes in the East Asian rain band projected by global atmospheric models with 20-km and 60-km grid size. *Clim. Dyn., 37*, 2481-2493.

Mizuta, R., Adachi, Y., Yukimoto, S. and Kusunoki, S. 2008: Estimation of the future distribution of sea surface temperature and sea ice using the CMIP3 multi-model ensemble mean, *Tech. Rep. Meteorol. Res. Inst.*, *56*, 28 pp.
(http://www.mri-jma.go.jp/Publish/Technical/DATA/VOL_56/tec_rep_mri_56.pdf)

Mizuta, R. and Coauthors, 2012: Climate simulations using MRI-AGCM3.2 with 20-km grid. *J. Meteor. Soc. Japan, 90A*, 233-258.

Murakami, H. and Coauthors, 2012: Future changes in tropical cyclone activity projected by the new high-resolution MRI-AGCM. *J. Climate, 25*, 3237-3260.

Rayner, N.A. and Coauthors, 2003: Global analyses of sea surface temperature, sea ice, and night marine air temperature since the late nineteenth century, *J. Geophys. Res.*, *108*(D14), 4407, doi:10.1029/2002jd002670.

Tiedtke, M. 1989: A comprehensive mass flux scheme for cumulus parameterization in large-scale models, *Mon. Wea. Rev.*, *117*, 1779–1800.

Xie, P. and Arkin, P.A. 1997: Global precipitation: A 17-year monthly analysis based on gauge observations, satellite estimates, and numerical model outputs, *B. Am. Meteorol. Soc.*, *78*, 2539–2558.

Yukimoto, S. and Coauthors, 2011: Meteorological Research Institute-Earth System Model version 1 (MRI-ESM1): Model description, *Tech. Rep. Meteorol. Res. Inst.*, *64*, 88 pp. (http://www.mri-jma.go.jp/Publish/Technical/DATA/VOL_64/tec_rep_mri_64.pdf)

HISTORICAL AND PROJECTED AUSTRALIAN MONSOON RAINFALL UNDER DIFFERENT FORCING ASSUMPTIONS

Leon Rotstayn[1,3], Stephen Jeffrey[2], Jozef Syktus[2], Mark A. Collier[1,3], Kenneth Wong[2], Tony Hirst[1,3], Stacey Dravitzki[1,3]

[1]CSIRO Marine and Atmospheric Research, Aspendale, Vic 3195, Australia
[2]Department of Science, Information Technology, Innovation and Arts, Dutton Park, Qld, 4102, Australia
[3]The Centre for Australian Weather and Climate Research. A partnership between CSIRO and the Bureau of Meteorology.

We use a coupled atmosphere-ocean global climate model (CSIRO-Mk3.6) to investigate the drivers of trends in summer rainfall and circulation in the vicinity of northern Australia. As part of the Coupled Model Intercomparison Project Phase 5 (CMIP5), we perform a 10-member 21st century ensemble driven by Representative Concentration Pathway 4.5 (RCP4.5). To investigate the roles of different forcing agents, we also perform multiple 10-member ensembles of historical climate change, which are analysed for the period 1951-2010. The historical runs include ensembles driven by ``all forcings'' (HIST), all forcings except anthropogenic aerosols (NO_AA) and forcing only from long-lived greenhouse gases (GHGAS). Anthropogenic aerosol-induced effects in a warming climate are calculated from the difference of HIST minus NO_AA.

CSIRO-Mk3.6 simulates a strong summer rainfall decrease over north-western Australia (NWA) in RCP4.5, whereas simulated trends in HIST are weakly positive (but insignificant) during 1951-2010. The weak rainfall trends in HIST are due to compensating effects of different forcing agents: there is a significant decrease in GHGAS, offset by an aerosol-induced increase.

Observations show a significant increase of summer rainfall over NWA during the last few decades. The large magnitude of the observed NWA rainfall trend is not captured by 440 unforced 60-yr trends calculated from a 500-yr pre-industrial control run, even though the model's decadal variability appears to be realistic. This suggests that the observed trend includes a forced component, despite the fact that the model does not simulate the magnitude of the observed rainfall increase in response to ``all forcings'' (HIST).

We investigate the mechanism of simulated and observed NWA rainfall changes by exploring changes in circulation over the Indo-Pacific region. The key circulation feature associated with the rainfall increase in reanalyses is a lower-tropospheric cyclonic circulation trend off the coast of NWA. The model shows an aerosol-induced cyclonic circulation trend off the coast of NWA in HIST minus NO_AA, whereas GHGAS shows an anticyclonic circulation trend. This explains why the aerosol-induced effect is an increase of rainfall over NWA, and the greenhouse gas-induced effect is of opposite sign.

Possible explanations for the cyclonic (anticyclonic) circulation trend in HIST minus NO_AA (GHGAS) involve changes in the Walker circulation or the local Hadley circulation. In either case, a plausible atmospheric mechanism is that the circulation anomaly is a Rossby wave response to convective heating anomalies south of the Equator. We also discuss the possible role of air-sea interactions, e.g., an increase (decrease) of sea-surface temperatures off the coast

of NWA in HIST minus NO_AA (GHGAS). Further research is needed to better understand the mechanisms and the extent to which these are model-dependent.

In summary, our results suggest that anthropogenic aerosols may have "masked" greenhouse gas-induced changes in rainfall over NWA and in circulation over the wider Indo-Pacific region. Due to the opposing effects of greenhouse gases and anthropogenic aerosols, future trends may be very different from trends observed over the last few decades.

CLIMATE CHANGE AND THE SOUTHEAST ASIAN MONSOON USING DOWNSCALED SIMULATIONS

Jack J. Katzfey

CAWCR/CMAR, Aspendale, VIC, Australia

Abstract

In this study, six climate simulations downscaled to 60 km globally using the Conformal Cubic Atmospheric Model (CCAM) were analysed to help understand projected changes in the monsoonal rainfall over Southeast Asia. The results suggest that regional differences in increases in sea surface temperatures related to climate change lead to differing amounts of increases in the precipitable water. The pattern of precipitable water changes leads to differing monsoonal rainfall changes. Differences in the model projections appear to be related to differences in the sea surface warming patterns projected by the models.

Introduction

The monsoon rainfall is vitally important for the livelihoods of the Southeast Asian countries. Anticipating what changes may occur due to climate change will allow these countries to plan and possibly adapt to these changes. One of the sources of projection information is the global coupled models (GCMs) run for the Coupled Model Intercomparison Program 3 (CMIP3) used in the Intergovernmental Panel on Climate Change (IPCC) fourth assessment report (AR4) (Meehl et al. 2007). However, these models were run at a relatively course horizontal resolution, on the order of 200 km. In order to assess the projected climate change more regionally, the GCMs can be dynamically downscaled to provide projection information at a higher spatial resolution.

As part of the Pacific Climate Change Science Program, six CMIP3 GCMs were dynamically downscaled globally to 60 km resolution using the CSIRO Conformal Cubic Atmospheric Model, CCAM. In this paper, results from these downscaled simulations are presented for the Southeast Asian monsoon region. The purpose of the paper is to investigate the possible relationship of the projected rainfall changes to changes in precipitable water and surface temperature. The methodology used and details about the CCAM model are given in the next section. In current climate section, the JJA rainfall is validated. Projected changes in the six downscaled simulations for rainfall, precipitable water and surface temperature are then presented in the climate change section. Results are then summarized and conclusions are given in the last section.

Methodology and data used

The model used in this study, CCAM (McGregor and Dix 2008), is a full atmospheric global general circulation model, formulated using a conformal-cubic grid. CCAM uses a semi-Lagrangian advection scheme and semi-implicit time step and includes a fairly complete set of physical parameterizations. The model can be run with only interpolated monthly sea surface temperatures (SSTs) and sea ice from the host GCMs, with CCAM providing the atmospheric response to the projected changes in SSTs.

In this study, six CMIP3 GCMs were downscaled: CSIROMk3.5, GFDLcm2.1, GFDLcm2.0, MPI-Echam5, UK-Hadcm3, and MIROC_medres. Monthly bias-correction of the SSTs was done to ensure that the SST climatology used in the downscaled simulations for the period

1970-2000 was the same as observed. However, the inter- and intra-annual variability, as well as the projected future changes, will be the same as the host GCM. Only GCM outputs from the IPCC high-end emission scenario (A2) were used here. The simulations were completed for the period 1961 to 2100.

Current climate

Evaluation of rainfall in the current climate simulation for JJA for the 20 year period 1979-1999 is presented in Fig. 1. Two observed dataset are shown as well as the results from the CCAM 60 km simulations. For JJA, the wet season over most of Southeast Asia, the model captures the distribution of rainfall rather well, in particular the heaviear rainfall on the upwind sides of mountains over India and Thailand. The model underpredicts rainfall over the South China Sea versus CMAP (Xie and Arkin 1997), but has less bias relative to GPCP (Adler et al. 2003) (not shown).

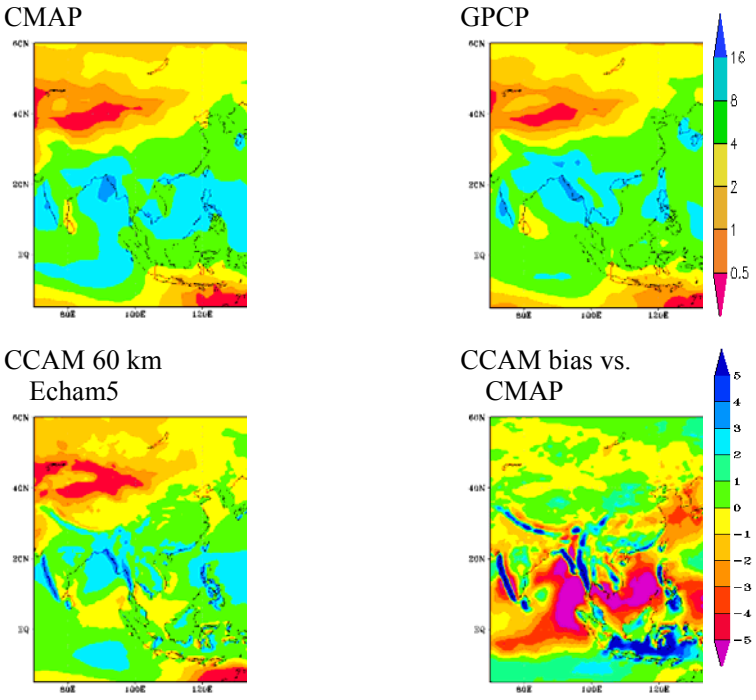

Fig. 1: *Rainfall (mm d^{-1}) for JJA for CMAP and GPCP observed data sets (top row) and the actual rainfall from the CCAM 60 km results using bias corrected SSTs from MPI-Echam5 (bottom left). CCAM biases relative to CMAP are shown on the bottom right. (Colour scale used for rainfall is on upper right, biases on lower right)*

Climate change

The projected effects of climate change are shown by calculating the differences in JJA averages for the 20 year periods 2079-2099 minus 1979-1999. The projected rainfall changes for the six simulations are shown in Fig. 2. Each simulation has its own pattern of change, though all models tend to show rainfall decreases over southern Indonesia. Interestingly, there tends to be a zonal banded structure in the results.

Changes in precipitable water (PW) appear to be an indicator for the rainfall changes (Fig. 3). PW increases everywhere due to more water vapor being held at the warmer temperatures.

However, there are regional differences which appear to be related to the PW changes; there are greater increases of PW where there are rainfall increases and lesser increases of PW in regions of rainfall decreases. This is especially notable in the GFDLcm20 projections over the western North Pacific and in the CSIROMk3.5 projections along the equator east on PNG. For the monsoonal rainfall over eastern China, all models show greater increases than further inland, where most models show rainfall decreases.

To help explain why there are greater PW increases in some regions, changes in surface temperature are shown in Fig. 4. A fairly close relationship exists over the water, where there are greater increases in PW and greater increases in SSTs. For example, the band of rainfall decrease across southern Indonesia is collocated with a band of smaller SST increases. However, the relation does not always hold, as indicated by the larger SST increases over the South China Sea in the MIROC_medres CCAM simulation, leading to larger increases in PW, but not the largest increase in rainfall in this region relative to the other CCAM simulations.

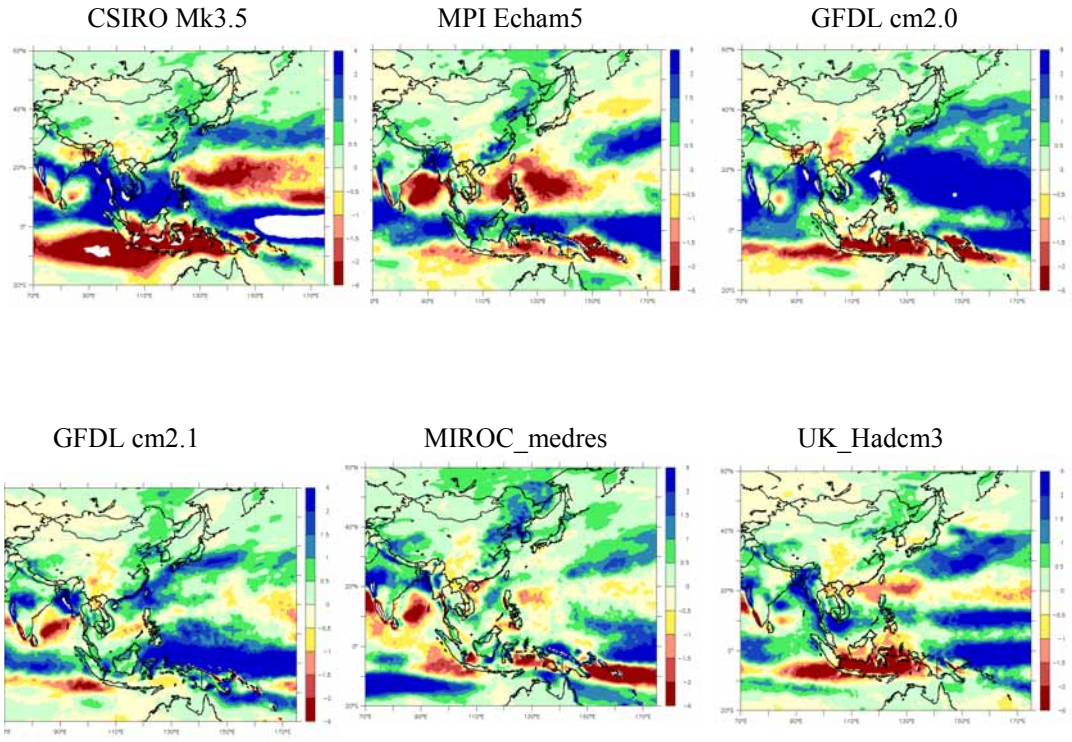

Fig. 2: *JJA rainfall change (mm d^{-1}) for periods 2079 to 2099 minus 1979 to 1999 for CCAM 60 km simulations as labelled.*

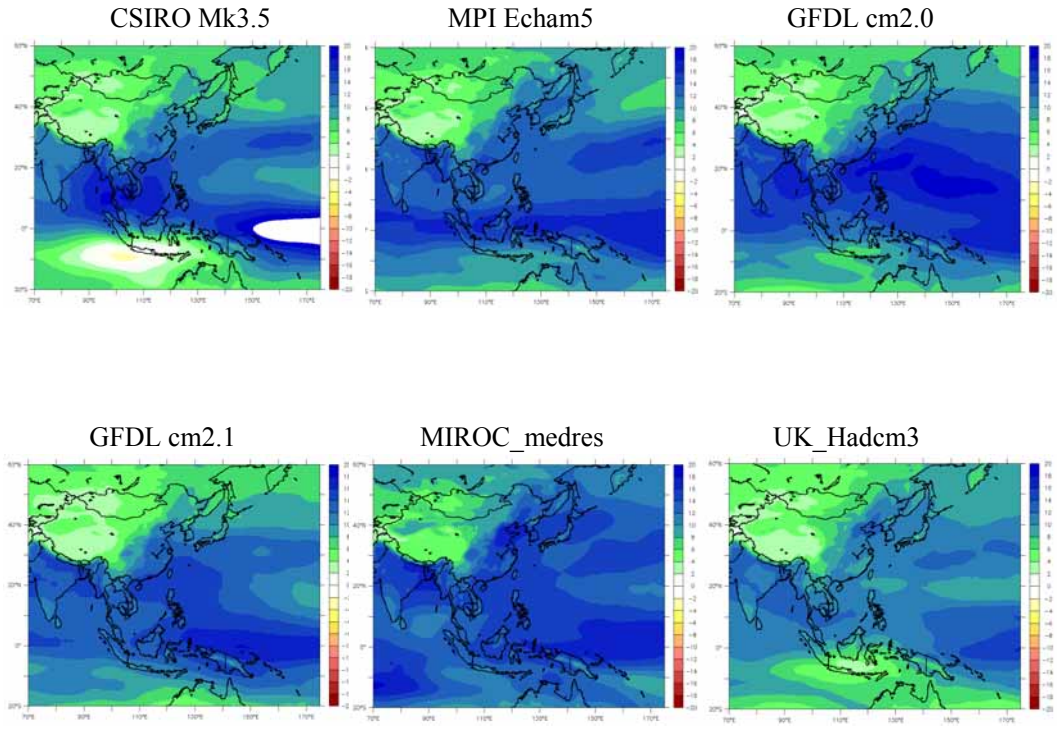

Fig. 3: *JJA precipitable water change (mm) for periods 2079 to 2099 minus 1979 to 1999 for CCAM 60 km simulations as labelled.*

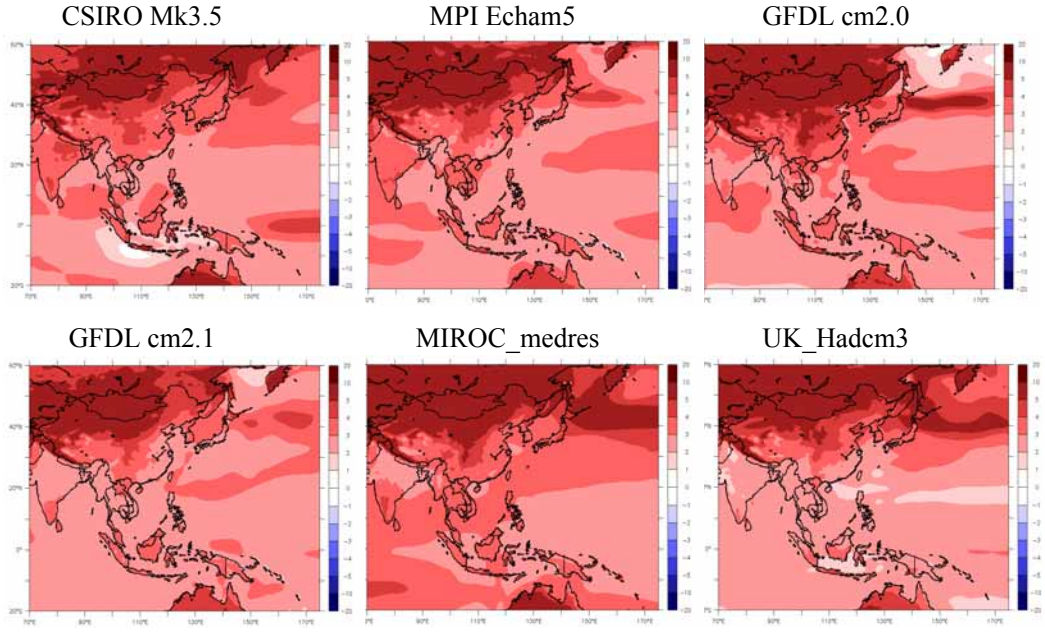

Fig. 4: *JJA surface temperature change (K) for periods 2079 to 2099 minus 1979 to 1999 for CCAM 60 km simulations as labelled.*

Summary and conclusions

In summary, the CCAM 60 km global downscaled simulations using bias-corrected SSTs from six CMIP3 GCMS capture the Southeast Asia monsoonal rainfall in JJA for the current climate reasonably well, including the higher resolution effects related to significant orography. Projected rainfall changes were related to changes in PW, which in turn were partly related to changes in SSTs. Similar relationships were found for other seasons (not shown). In addition, differences in the rainfall changes between various simulations appear to be related to the different PW and SST changes. These results also point out the need for ensemble simulations of climate change and for greater understanding of the reasons for the projected changes.

References

Adler, R.F., Huffman, G.J. , Chang, A., Ferraro, R., Xie, P., Janowiak, J., Rudolf, B., Schneider, U., Curtis, S., Bolvin, D., Gruber, A., Susskind, J. and Arkin, P. 2003. The Version 2 Global Precipitation Climatology Project (GPCP) Monthly Precipitation Analysis (1979-Present). *J. Hydrometeor.*, **4**, 1147-1167.

McGregor, J.L. and Dix, M.R. 2008. An updated description of the Conformal-Cubic Atmospheric Model. In High Resolution Simulation of the Atmosphere and Ocean, eds. K. Hamilton and W. Ohfuchi, Springer, 51-76.

Meehl, G.A., Stocker, T.F., Collins, W.D., Friedlingstein, P., Gaye, A.T., Gregory, J.M., Kitoh, A., Knutti, R., Murphy, J.M., Noda, A., Raper, S.C.B., Watterson, I.G., Weaver, A.J. and Zhao, Z.-C. 2007. Global Climate Projections. In: Climate Change 2007: The Physical Science Basis. Contribution of Working Group I to the Fourth Assessment Report of the Intergovernmental Panel on Climate Change [Solomon, S., Qin, D., Manning, M., Chen, Z., Marquis, M., Averyt, K.B., Tignor, M. and Miller, H.L. (eds.)]. Cambridge University Press, Cambridge, United Kingdom and New York, NY, USA.

Xie P., and Arkin, P.A. 1997. Global precipitation: a 17-year monthly analysis based on gauge observations, satellite estimates, and numerical model outputs. *Bull. Amer. Meteor. Soc.*, **78**, 2539-2558.

21ST CENTURY RAINFALL PROJECTIONS IN CLIMATE MODELS AND THE ROLE OF ENSO

Scott Power[123], François Delage[123], Christine Chung[123], Robert Colman[123], Julie Arblaster[134], Aurel Moise[123], Greg Roff[123] and Harun Rashid[25]

1. Pacific-Australia Climate Change and Adaptation Planning Program (PACCSAP), 2. Centre for Australian Weather and Climate Research, 3. Bureau of Meteorology, Melbourne, Australia; 4. NCAR, USA; 4. CSIRO.

Part 1

Global temperature has increased over the past century (Trenberth et al. 2007), and emissions of greenhouse gases arising from human activities are very likely to have been responsible for most of the warming over the past 50 years (Hegerl et al. 2007). Further warming and further changes in the climate system associated with this warming appear inevitable (Meehl et al. 2007a).

Precipitation is projected to change in many locations across the globe in association with global warming over the 21st century. The last Intergovernmental Panel on Climate Change (IPCC) Fourth Assessment Report was released in 2007. It provided a comprehensive assessment of the current state of climate science at that time and represents a landmark in climate science. It concluded that increases in precipitation are very likely in high latitudes and near major convergence zones in the tropics in some seasons, while decreases are likely in many subtropical land areas (Alley et al. 2007; Christensen et al. 2007; Meehl et al. 2007a; Solomon et al. 2007).

In many areas, fewer than 66% of models agree on the sign of change. This can occur, for example, if some models project a "large" increase while other models project a "large" decrease, making projected changes in such regions very uncertain. This was noted in the 2007 IPCC report by Christensen et al. (2007) who concluded that "for some regions, there are grounds for stating that the projected precipitation changes are likely or very likely. For other regions, confidence in the projected change remains weak". Christensen et al. (2007) also noted that "it is unclear how rainfall in the Sahel, the Guinean coast and the southern Sahara will evolve", that "it is uncertain how annual and seasonal rainfall will change over northern South America, including the Amazon forest" and that "changes in rainfall in northern and central Australia remain uncertain". While some of this uncertainty stems from known model deficiencies and imperfect simulations of twentieth century regional climate (e.g. Randall et al. 2007; Brown et al. 2010; Irving et al. 2011), much of this uncertainty arises because the models do not exhibit a consensus on the sign of projected change in these regions. In fact Africa, Europe, North America, Central and South America, Australia, New Zealand and small island regions were all found to have sub-regions in which no clear consensus on the sign of the projected change was evident. Christensen et al. (2007) also noted that the regions of "large uncertainty" often lie near the boundaries between robust increases at high latitudes and the robust declines in the subtropics, and between these same robust declines in the subtropics and robust increases near major convergence zones at low latitudes.

Large uncertainty is a very undesirable situation because it impedes the ability of the scientific community to provide guidance on future climate in the affected regions. This, in turn, limits the

ability of decision-makers in the wider community to optimise their mitigation and adaptation plans.

But does a lack of consensus on the sign of change definitely indicate greater uncertainty? Suppose, for example, that the externally forced change in every model at a particular grid point in the unshaded region is actually zero. In other words, if each model was run infinitely many times the ensemble mean (EM) of each model is zero. As we only have a finite number of integrations for each model, sampling error arising from essentially random internally generated variability will typically cause the sign of projected change in each run to differ in a random fashion. Some runs will exhibit positive changes, some runs negative. Some individual model ensemble means will therefore give positive projections, with others negative. In other words, we would not expect to see any consensus on the sign of the projections even if the models all agree that the externally forced response is zero.

This highlights the fact that using the degree of consensus on the sign of change will not identify regions where the models agree that the externally forced change is either absent or small compared to internal variability – if such regions actually exist. It is therefore possible that a consensus amongst the models exists, but it is not a consensus on the sign of change.

This motivates the primary purpose of this first part of our investigation: to determine if there are regions where there is a strong consensus that a projected change is small in comparison with the standard deviation of year-to-year variability, even though there is no consensus on the sign of change. In such subregions there is compelling evidence that if there is any externally-forced signal at all, it is very likely small. This is not an uncertain projection. This is a projection of little or no change in which we have a degree of confidence. Our confidence in projections will therefore extend over a greater area than one might infer from the 2007 IPCC report.

We also examine the impact of model co-dependency through the sharing of systematic biases on the statistical significance of projected changes. Previous research has shown that systematic biases in climate models are not independent (Masson and Knutti 2011; Pennell and Reichler 2011). We will test to see if dependency also occurs in climate change projections and not just in the simulation of past climatology. We will then examine the implications the results obtained have for assessing the statistical significance of projected changes.

To address all these issues we examine projected precipitation changes in the late 21st century WCRP/CMIP3 and CMIP5 climate model integrations forced using several emissions scenarios.

In areas with no consensus on the sign of projected change there are extensive sub-regions where the projected change does indeed seem small or absent. “Small” here is defined either as small relative to the size of the interannual variability during the late 20th century or small relative to late 20th century average precipitation.

Interdependency amongst projections is shown to be much weaker than inter-dependency amongst simulations of climatology.

Our results show that there is more widespread consistency amongst the model projections than one might infer from the 2007 Intergovernmental Panel on Climate Change (IPCC) Fourth Assessment report. This discovery highlights the broader need to identify regions, variables and phenomena that are expected to be little affected by anthropogenic climate change, and to communicate this information to the wider community.

Part 2

In the second part of the investigation we investigate rainfall changes over the IndoPacific during El Niño events in the 20th and 21st century. We conduct idealised experiments using the ACCESS Atmospheric General Circulation Model forced with sea-surface temperature (SST) anomalies and changes in atmospheric CO_2 concentrations. Linear increases in the amplitude of the El Niño SST anomaly pattern trigger nonlinear changes in precipitation amounts, resulting in shifts in the location and orientation of equatorial Pacific rainfall, the Intertropical Convergence Zone (ITCZ) and the South Pacific Convergence Zone (SPCZ). In particular, the ITCZ and SPCZ shift eastwards, the ITCZ shifts south towards the equator, and the SPCZ becomes more zonal. The effect of increasing CO_2 levels and warming SSTs is also investigated. The precipitation response over the ocean is dominated by SST changes. Global warming generally enhances the tropical Pacific rainfall response to El Niño. For example, El Niño-driven precipitation increases in the equatorial Pacific are enhanced and El Niño-driven drying in the tropical west Pacific is intensified. While the dependence of projected climate change impacts on seasonal variability is well-established, this study reveals that the impact of global warming on Pacific rainfall also depends strongly on the magnitude of the El Niño event. For example, the centre of the global warming-driven precipitation increase in the equatorial Pacific moves east as the magnitude of the El Niño event increases. The magnitude and structure of the precipitation changes are also sensitive to the spatial structure of the global warming SST pattern.

References

Power, S.B., Delage, F., Colman, R. and Moise, A. 2011: Consensus of 21st century rainfall projections in climate models more widespread than previously thought. J. Climate, 25, 3792-3809, DOI: 10.1175/JCLI-D-11-00354.1.

Chung, C.T.Y., Power, S.B., Arblaster, J.M., Rashid, H.A. and Roff, G.L. 2012: Nonlinear rainfall response to El Niño and global warming in the Indo-Pacific, Climate dynamics (submitted).

INTERACTIONS BETWEEN THE SOUTH PACIFIC CONVERGENCE ZONE AND THE AUSTRALIAN SUMMER MONSOON

Josephine R. Brown, Aurel F. Moise and Robert A. Colman

Centre for Australian Weather and Climate Research, Bureau of Meteorology, Australia.

The South Pacific Convergence Zone (SPCZ) is a band of precipitation and surface wind convergence extending diagonally from the equatorial western Pacific to the south-east. The SPCZ is a major feature of the climate of the South Pacific, with variability on seasonal and interannual time scales that influences many Pacific island nations (Vincent 1994). The western, tropical portion of the SPCZ is formed in the region of the convergence of moist westerly monsoon winds with easterly trade winds (Vincent et al. 2011). The strength of the Australian monsoon low pressure trough, and associated diabatic heating, are thought to influence the intensity of the western portion of the SPCZ (Kiladis et al. 1989). We examine the simulation of the SPCZ in coupled climate models, and consider the interaction with the Australian summer monsoon in historical and future climate simulations.

The ability of Coupled Model Intercomparison Project Phase 5 (CMIP5) models to simulate the SPCZ is evaluated (Brown et al. in press) and compared with previous generation CMIP3 models (Brown et al. 2011; Brown et al. 2012). A subset of CMIP5 models are able to simulate a distinct SPCZ in the December to February (DJF) austral summer in historical simulations, although the position of the SPCZ in these models is too zonal compared with observations (Brown et al. in press). Figure 1 shows the observed (CMAP) SPCZ precipitation band in comparison with the CMIP5 multi-model mean precipitation. The strength of the Australian summer monsoon is also evaluated in the CMIP5 models, and the association between monsoon strength and western SPCZ intensity is investigated for historical climate simulations. Simulations of 21st century climate under the RCP8.5 high emission scenario are examined, and changes in the monsoon strength are compared with changes in the position and intensity of the western portion of the SPCZ.

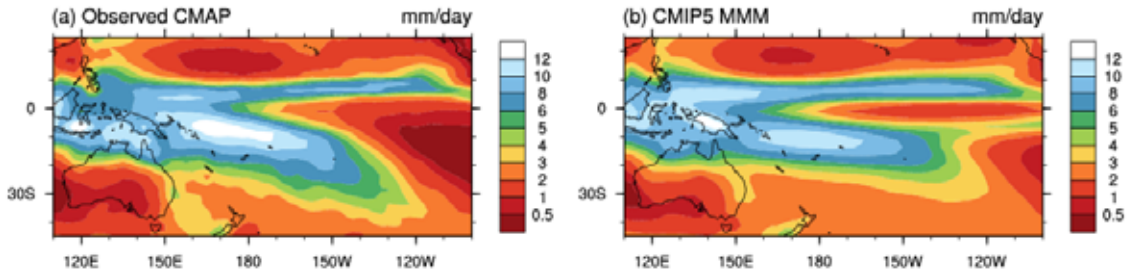

***Fig. 1**: (a) Observed (CMAP) DJF mean precipitation and (b) multi-model mean DJF precipitation from 26 CMIP5 models. Adapted from Brown et al. (in press).*

References

Brown, J. R., Moise, A.F. and Colman, R.A. (in press), The South Pacific Convergence Zone in CMIP5 simulations of historical and future climate, *Climate Dynamics*.

Brown, J.R., Moise, A.F. and Delage, F.P. (2012), Changes in the South Pacific Convergence Zone in IPCC AR4 future climate projections, *Climate Dynamics*, *39*, 1-19, doi:10.1007/s00382-011-1192-0

Brown, J.R., Power, S.B., Delage, F.P. , Colman, R.A., Moise, A.F. and Murphy, B.F. (2011), Evaluation of the South Pacific Convergence Zone in IPCC AR4 climate model simulations of the 20th century, *Journal of Climate*, *24*, 1565-1582.

Kiladis, G.N., von Storch, H. and van Loon, H. (1989), Origin of the South Pacific Convergence Zone. *Journal of Climate*, 2, 1185–1195.

Vincent, D.G. (1994) The South Pacific Convergence Zone (SPCZ): A Review. *Monthly Weather Review, 122,* 1949–1970.

Vincent, E.M., Lengaigne, M., Menkes, C.E., Jourdain, N.C., Marchesiello, P. and Madec, G. (2011) Interannual variability of the South Pacific Convergence Zone and implications for tropical cyclone genesis. *Climate Dynamics, 36*, 1881-1896. doi:10.1007/s00382-009-0716-3

DECADAL VARIABILITY IN TBO-ENSO-MONSOON RELATIONSHIPS

Julie Arblaster[1,2] and Jerry Meehl[2]

[1]Centre for Australian Weather and Climate Research, Bureau of Meteorology
[2]National Center for Atmospheric Research, Boulder, USA

For nearly a century, research has been undertaken to understand the interannual relationships between the Asian-Australian monsoons, land surface processes and sea surface temperatures (SSTs) of the Pacific and Indian Oceans. Sir Gilbert Walker in the early 1920s was the first to attempt a prediction of monsoon strength based on fluctuations in sea level pressure gradient between the Pacific and Indian Oceans. Bjerknes in 1969 described how coupled air-sea interactions could grow SST anomalies and the biennial tendency of these relationships was recognised by Trenberth, Nicholls and others through 1970s and 80s.

A set of dynamically coupled ocean-atmosphere mechanisms was proposed by Meehl (1987) for the Asia-Pacific tropics to produce a dominant biennial component of interannual variability (the Tropospheric Biennial Oscillation or TBO). Namely, a strong Asian-Australian monsoon is often associated with negative SST anomalies in the equatorial eastern Pacific and a negative Indian Ocean Dipole in northern fall between the strong Indian monsoon and strong Australian monsoon, and tends to be followed by a weak monsoon and positive SST anomalies in the Pacific the following year and so on.

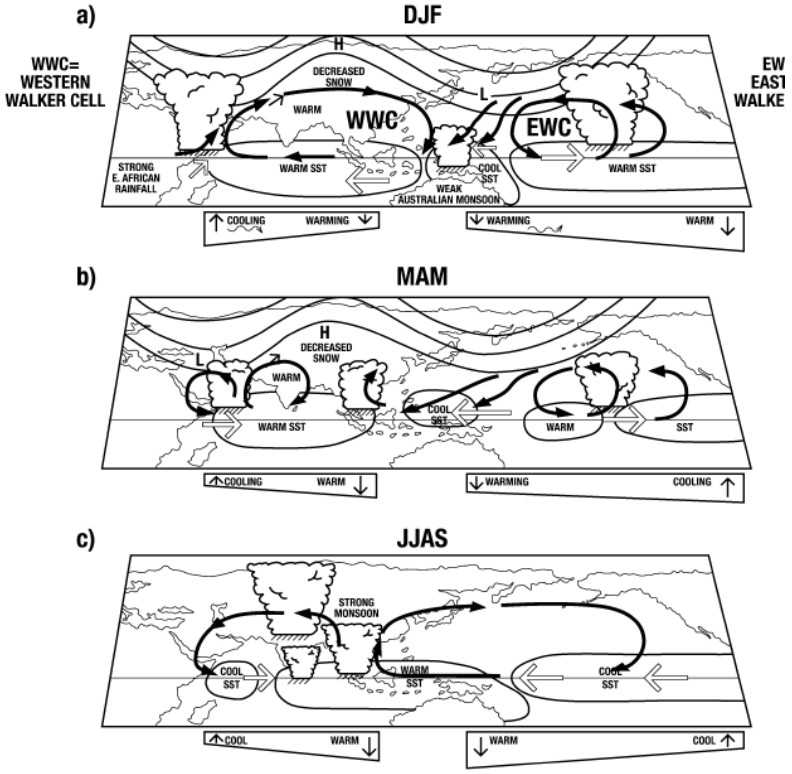

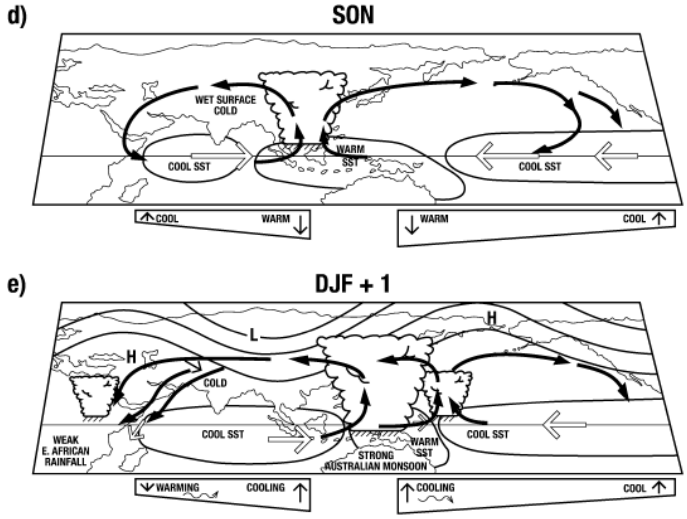

Fig.1*: Schematic diagram indicating anomalous convective activity, SST anomalies, mid-latitude circulation anomalies, surface wind anomalies, and equatorial Indian and Pacific Ocean thermocline orientation for hypothesized TBO evolution for (a) the Australian monsoon season prior to a strong Indian monsoon, (b) the MAM season before a strong Indian monsoon, (c) strong Indian monsoon season, JJAS, (d) SON season after a strong Indian monsoon and prior to a strong Australian monsoon, and (e) strong Australian monsoon following a strong Indian monsoon. Large arrows indicate surface wind anomalies, wedge-shaped outlines below each panel represent thermocline orientation, with the small arrows in those areas indicative of anomalous movement of the thermocline, and wavy arrows indicating Kelvin waves with the arrow at the end representing upwelling Kelvin waves (arrow pointing up), or downwelling Kelvin waves (arrow pointing down). Thick black arrows indicate EWC and WWC, respectively.*

These connections are communicated through the large-scale east-west (Walker) circulation that involves the full depth of the troposphere. However, the Asia-Pacific climate system is characterized by intermittent decadal fluctuations whereby the TBO during some time periods is more pronounced than others. Observations and models are analysed to identify processes that make the system either more or less biennial at certain times due to one or some combination of:

1. increased latitudinal extent of Pacific trade winds and wider cold tongue
2. warmer tropical Pacific compared to tropical Indian Ocean that weakens trade winds and reduces coupling strength
3. eastward shift of the Walker circulation
4. reduced interannual variability of Pacific and/or Indian Ocean SST

Decadal timescale SST variability associated with the Interdecadal Pacific Oscillation (IPO) has been shown to alter the TBO over the Indo-Pacific region by contributing changes in either some or all of the four factors listed above. Analysis of a multi-century control run of CCSM4 shows that this decadal modulation of interannual variability is transferred via the Walker Circulation to the Asian-Australian monsoon region, thus affecting the TBO and monsoon-Pacific connections. Understanding these processes is important to be able to evaluate decadal predictions and longer term climate change in the Asia-Pacific region.

Reference

Meehl, G.A. and Arblaster, J.M. 2011: Decadal variability of Asian-Australian monsoon-ENSO-TBO relationships. J. Climate, 24, 4925-4940, DOI: 10.1175/2011JCLI4015.1

MIP5 EVALUATION OF AUSTRALIAN MONSOON USING REGIME-SORTING OF RAINFALL

Aurel F. Moise, Rob Colman and Jo Brown

Centre for Australian Weather and Climate Research, Bureau of Meteorology

Although populations affected by the Australian monsoon are much smaller than for south or east Asia, regional impacts of any such changes are nevertheless likely to be large particularly on vulnerable indigenous populations and on ecosystems. The exposure risks to climate change of indigenous communities on low-lying island such as the Torres Strait Islands in Northern Australia have previously been highlighted. In this study, large-scale aspects of the Australian rainfall and tropical climate are analyzed in the CMIP5 models, including means and seasonal variations of temperature, mean sea level pressure, winds, and precipitation as well as inter-annual variability of precipitation. Features such as the seasonal reversals of low-level easterlies into Westerlies and the reverse aloft, and skill in the location, orientation, and seasonal progression of the low-level monsoon "shear line" are investigated. Broad-scale features of winds between the equator and the continent in the Australian region are analyzed.

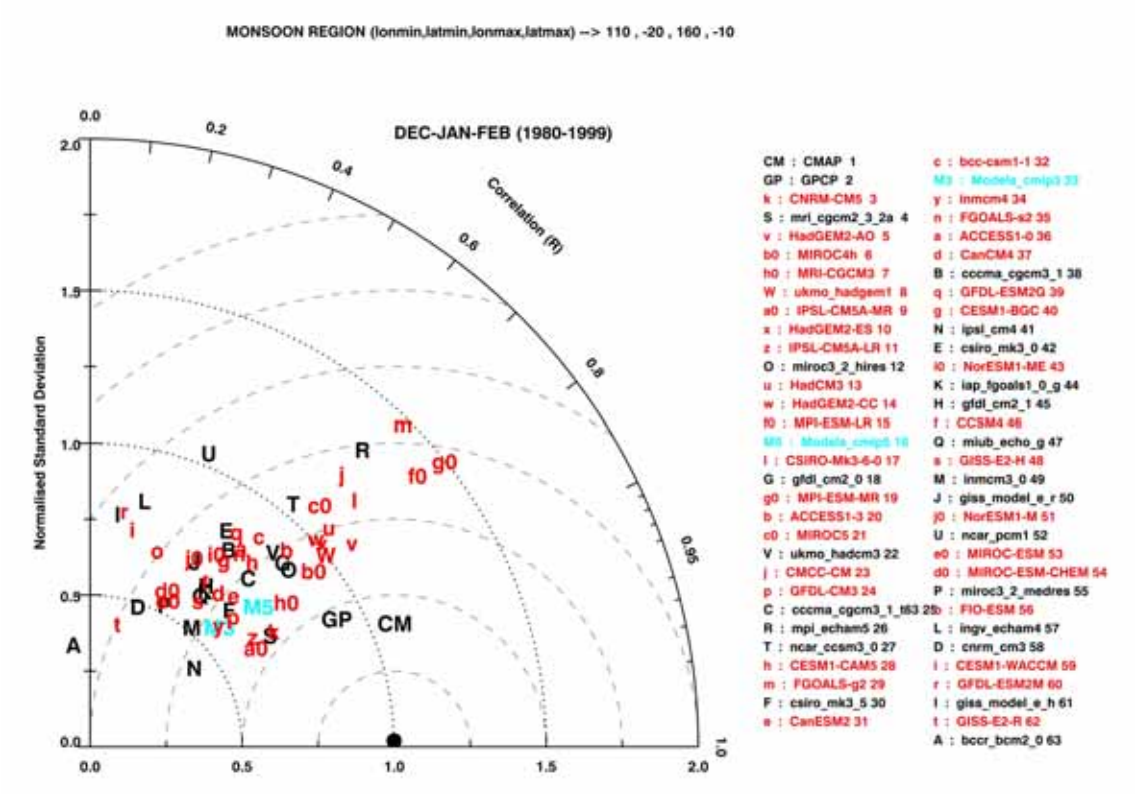

***Fig. 1**: Spatial correlation and normalised standard deviation for DJF precipitation from CMIP5 (red) and CMIP3 (black) models and GPCP and CMAP gridded observational data sets versus reference observed data set (AWAP, black dot) for the Australian tropical region (land only). The model list is a ranking based on the S* score in Taylor (2001). The time period is (1980-1999).*

We have earlier found (Colman et al., 2011) that for CMIP3 simulations, precipitation biases in models were related to differences in occurrence of convection/suppressed vertical motion, and to related precipitation amounts. Our new analysis will investigate if CMIP5 simulations provide a better relationship between the occurrence of convective regimes and associated rainfall amounts.

We will also present results from our CMIP5 based assessment of Australian regional rainfall changes under enhanced greenhouse conditions together with a specific focus on the monsoon. For the latter, we will again focus on the analysis of rainfall changes using regime-sorting techniques which previously has shown for the tropical Australian region offsetting tendencies from thermodynamic changes associated with enhanced atmospheric moisture and dynamic changes associated with a weakened overturning circulation. Early results show a significant improvement in the representation of Australian regional rainfall in some models, particular across the tropical region during the summer season (See Fig. 1 and also Moise et al., 2012).

References

Colman, R.A., Moise, A.F. and Hanson, L.I. 2011. Tropical Australian climate and the Australian monsoon as simulated by 23 CMIP3 models, *J. Geophys. Res.*, *116*, D10116, doi:10.1029/2010JD015149

Moise, A.F., Colman, R.A. and Brown, J.R. 2012. CMIP5 simulations of Australian rainfall with particular focus on the Australian monsoon system: convective regime-sorting of precipitation (in preparation).

Taylor , K.E. (2001) Summarizing multiple aspects of model performance in a single diagram. *J Geophys Res 106:* 7183−7192, doi: 10.1029/ 2000JD900719

ZONAL ASYMMETRIES IN THE WIDENING OF THE TROPICS UNDER CLIMATE CHANGE

Joe Anderson

The changes in the region of the atmosphere that might be considered "tropical" – based on climatic consideration – over the last three decades are investigated using the High-resolution Infra-Red Sounder brightness temperature as a proxy for upper level relative humidity. The trends in the annual mean brightness temperatures are calculated. We observe that the tropics are widening, but the widening is highly asymmetric in the zonal direction. There is an expansion of the moist tropical upper tropospheric signal that is seen over the Indian Ocean and Indonesian region northwards above India, South-east Asia, the Bay of Bengal and the Arabian Sea. The dry region associated with subtropical subsidence over Northern India and the Arabian region appears to by moving to the North-East. Similarly, the subsidence region over West/Central Australia is moving to the south.

Similar analysis of upper level relative humidity trends in the ERA-interim and MERRA reanalyses show qualitative similarities to the observations. The trends in the annual mean vertical velocities taken from the reanalyses are also calculated to investigate the changes in the circulation that may be associated with the changes in the upper level moisture. Both reanalyses show a decrease in the upward velocities associated with the ITCZ, although the trends are less consistent in other regions.

The same analysis is repeated upon the 20th century climate reconstructions within the CMIP3 archive. The trends calculated for the ensemble members differ widely from the satellite observations. It is well known that the climate models fail to reproduce the observed tropical widening but the zonal asymmetries in widening may provide a more tractable approach to addressing the model deficiencies than the zonal mean.

HADLEY CELL UNDER WARMING CLIMATE

Hanh Nguyen

Centre for Australian Weather and Climate Research, Bureau of Meteorology

The Hadley circulation (HC), characterised by a thermally driven circulation, explains a large percentage of the variability of the climate of the tropics and subtropics across the globe. Analysis of the annual cycle of intensity, extent and width of the Hadley circulation across a 31 year period (1979-2009) from all existent reanalyses reveals marked variability at seasonal, interannual and long terms time scales.

During austral summer (DJF), the southern hemisphere is marked by a widest and weakest Hadley cell. Expansion of the Hadley cell in the last few decades is also most pronounced during this season, reaching an average rate of 1^{o} per decade.

Explanations as to the causes of this expansion have focussed on mechanisms driven by increased greenhouse gas concentration or stratospheric ozone depletion. However, because such mechanisms remain to be quantified, it is unclear what impacts are to be expected across subtropical climates under anthropogenic global warming. Projected changes in the Hadley cell are assessed using climate model simulations under natural, anthropogenic and full external forcing. We show that the expansion in the Southern Hemisphere occurs only when anthropogenic alone or combined with natural forcing is present.

THE ASIAN SUMMER MONSOON: AN INTERCOMPARISON OF CMIP5 VS. CMIP3 SIMULATIONS OF THE LATE 20TH CENTURY

K. R. Sperber[1,*], *H. Annamalai*[2], *I.-S. Kang*[3], *A. Kitoh*[4], *A. Moise*[5], *A. Turner*[6], *B. Wang*[2], *and T. Zhou*[7]

[1]*Lawrence Livermore National Laboratory, Livermore, CA, USA*
[2]*International Pacific Research Center, University of Hawaii, Honolulu, HI USA*
[3]*Seoul National University, Seoul 151-742, Korea*
[4]*Meteorological Research Institute, Tsukuba-shi, Ibaraki Pref., Japan*
[5]*Centre for Australian Weather and Climate Research, Australian Bureau of Meteorology, Melbourne, VIC 3001, Australia*
[6]*National Centre for Atmospheric Research-Climate, Dept. of Meteorology, University of Reading, Reading RG6 6BB, United Kingdom*
[7]*LASG, Institute of Atmospheric Physics, Chinese Academy of Sciences, Beijing 100029, China*

Abstract

The boreal summer Asian monsoon has been evaluated in 25 Coupled Model Intercomparison Project-5 (CMIP5) and 22 CMIP3 GCM simulations of the late 20th Century. Diagnostics and skill metrics have been calculated to assess the time-mean, climatological annual cycle, interannual variability, and intraseasonal variability. Progress has been made in modeling these aspects of the monsoon, though there is no single model that best represents all of these aspects of the monsoon. The CMIP5 multi-model mean (MMM) is more skillful than the CMIP3 MMM for all diagnostics in terms of the skill of simulating pattern correlations with respect to observations. The onset of the monsoon over India is typically too late in the models. The extension of the monsoon over eastern China, Korea, and Japan is underestimated, while it is overestimated over the subtropical western/central Pacific Ocean. For both the ENSO-monsoon teleconnection and the East Asian zonal wind-rainfall teleconnection, the MMM interannual rainfall anomalies are weak compared to observations. Though simulation of intraseasonal variability remains problematic, several models show improved skill at representing the northward propagation of convection and the development of the tilted band of convection that extends from India to the equatorial west Pacific.

Introduction

Nearly half of the world's population is dependent on monsoon rainfall for food and energy security. The monsoon is an integral and robust component of the seasonal cycle, though the vagaries of its timing, duration, and intensity are of major concern, especially over semi-arid regions where agriculture is the primary source of food. On interannual time scales the standard deviation of the Indian/South Asian monsoon rainfall is on the order of 10% of the seasonal mean, and the corresponding percentage of East Asian summer monsoon is ~30% (Zhou and Yu 2005). However, subseasonal variations can give rise to much greater swings in rainfall variability and modulate higher frequency variations, including tropical cyclones (e.g. Nakazawa 1986). Foreknowledge of extreme subseasonal variations is particularly important, since this would enable the selection of alternative crops, the adjustment of planting times, and

management of hydrometeorological services (water distribution, etc.) to help cope with the extreme conditions. Improvement in the prospects of monsoon predictability at all time scales, requires (1) an improved understanding of the physical processes that modulate the monsoon, (2) improved observations for processes studies, initialization of forecast models, and long-term monitoring, and (3) better simulation of the monsoon in numerical weather prediction models and climate models.

There are many facets of the atmosphere-ocean-land-cryosphere system that interact to produce monsoon. The seasonal cycle of solar forcing is the basic driver of the monsoon over the Asian region, contributing to the development of a land-sea temperature gradient, including aloft, due to heating of the Tibetan Plateau. The temperature and sea-level pressure gradients that develop promote the formation of the low-level cross-equatorial southwest monsoon circulation. This circulation transports moisture laden air from the ocean to the Asian continent that leads to the onset of the monsoon. Subsequently, the off-equatorial convective heating interacts with the circulation to help maintain monsoon rainfall (Gill 1980; Annamalai and Sperber 2005).

Precursory and/or contemporaneous forcings, especially sea surface temperature (SST; Charney and Shukla 1981), form the basis of seasonal prediction systems with which the seasonal mean monsoon is forecast, either using dynamical models or employing empirical/statistical relationships. The main skill in seasonal forecasting of the monsoon is intimately linked to our ability to forecast the El Nino/Southern Oscillation (ENSO). However, properly representing the location and intensity of the ENSO diabatic heating is essential for getting a response consistent with that expected from statistical teleconnections relationships (Slingo and Annamalai 2000). Other more local interactions, such as Indian Ocean variations (Boschat et al. 2012) and soil moisture (Webster et al. 1998), may play a role in modulating the monsoon.

Given the multitude of physical processes and interactions that influence the monsoon, it is no wonder that simulation and prediction of the monsoon remain grand challenge problems. The challenges of modeling the monsoon and making climate change projections have been discussed in Turner et al. (2011) and Turner and Annamalai (2012). By its very nature, simulating the monsoon requires models with coupling between the atmosphere, the ocean, and land. In prescribed SST experiments observed interannual variations of Asian-Australian monsoon rainfall over land were poorly represented (e.g., Sperber and Palmer 1996). This in part occurred because of the use of prescribed SST's, which forced an incorrect rainfall-SST teleconnection (Wang et al. 2004). Ocean-atmosphere coupling also gives rise to a wide-range of model performance, in which monsoon climate and variability can be adversely affected by poorly representing air-sea interaction. Even so, incremental progress in simulating monsoon has been hard-fought due improvements in local, regional, and global interactions that modulate the monsoon on diurnal through interdecadal time scales (e.g. Wang 2006).

The goal of this paper is to assess the fidelity of boreal summer Asian monsoon in the Coupled Model Intercomparison Project-5 (CMIP5) models as compared to the CMIP3 models and observations. We employ a multitude of diagnostics and skill metrics to present a quantitative assessment of the models' monsoon performance relative to observations. The diagnostics were selected after much deliberation by the CLIVAR Asian-Australian Monsoon Panel (AAMP) Diagnostics Task Team, and helpful comments from the AAMP membership. More complete details of the evaluations performed are contained in the submitted journal article (Sperber et al. (2012).

Models, Observations, and Skill Scores

The CMIP5 models were developed circa 2011, while the CMIP3 models were developed circa 2004. Single realizations for each of the models have been evaluated using the historical simulations from CMIP5 and the Climate of the 20th Century (20c3m) simulations from CMIP3. The period 1961-99 is analyzed herein, when both CMIP5 and CMIP3 had high-frequency (daily) data with which to evaluate intraseasonal variability and the climatological annual cycle of pentad rainfall. These simulations include the modeling groups best estimates of natural (e.g. solar irradiance, volcanic aerosols) and anthropogenic (e.g. greenhouse gases, sulfate aerosols, ozone) climate forcing during the simulation period. From CMIP5 we have analyzed BCC-CSM1.1, CanESM2, CCSM4, CNRM-CM5, CSIRO-Mk3.6.0, FGOALS-g2, FGOALS-s2, GFDL-CM3, GFDL-ESM2G, GFDL-ESM2M, GISS-E2-H, GISS-E2-R, HadCM3, HadGEM2-CC, HadGEM2-ES, INM CM4, IPSL-CM5A-LR, IPSL-CM5A-MR, MIROC-ESM, MIROC-ESM-CHEM, MIROC4h, MIROC5, MPI-ESM-LR, MRI-CGCM3, and NorESM1-M. Detailed documentation of the CMIP5 models can be found at:
http://www.earthsystemgrid.org/search?Type=Simulation+Metadata
From CMIP3 we have analyzed BCCR BCM2.0, CCCMA CGCM3.1, CCCMA CGCM3.1 T63, CCSM3.0, CNRM CM3, CSIRO MK3.0, CSIRO MK3.5, GFDL CM2.0, GFDL CM2.1, GISS AOM, HADCM3, HADGEM1, FGOALS 1.0G, INGV-SXG, INM CM3.0, IPSL CM4, MIROC 3.2 (HI-RES), MIROC 3.2 (MED-RES), MIUB ECHO-G, ECHAM5/MPI-OM, MRI CGCM2.3.2A, an PCM1. Detailed documentation of the CMIP3 models can be found at:
http://www-pcmdi.llnl.gov/ipcc/model_documentation/ipcc_model_documentation.php

For rainfall we use the Global Precipitation Climatology Project (GPCP) data (Huffman et al., 2001) and the Climate Prediction Center Merged Analysis of Precipitation (CMAP; Xie and Arkin 1997) for 1979-2007. For the 850hPa wind we use the Japan Meteorological Agency and the Central Research Institute of Electric Power Industry Reanalysis-25 (JRA-25; Onogi et al. 2007) for 1979-2007, the European Centre for Medium-Range Weather Forecasts Reanalysis-40 (ERA40; Kalberg et al. 2005) for 1961-1999, and the National Centres for Environmental Prediction/National Centre for Atmospheric Research Reanalysis (NCEP/NCAR; Kalnay et al. 1996) for 1961-2007.

Model skill is calculated against a primary observational data set, for example, GPCP in the case of precipitation. We also calculate the skill between different sets of observations, as this is a measure of consistency between the two sets of observations. Due to the large number of models evaluated, spatial patterns of the diagnostics are only presented for the observations and for the CMIP5 multi-model mean (MMM). Additional model figures are presented in Sperber et al. (2012).

Time-mean State

The June-September time-mean patterns of rainfall and 850hPa wind represent key aspects of the monsoon. The intense solar heating in late spring and early summer supports the development of a heat low over the land of south and Southeast Asia. The resulting land-sea thermal and pressure gradients induce the development of cross-equatorial low-level winds that transport an increased flux of moisture onto the Asian landmass, heralding the onset of the monsoon. The strong coupling between diabatic heating and the circulation further amplifies the cross-equatorial flow, the moisture influx, and the rainfall. The orographic structure of the Asian landmass provides anchor points where the observed monsoon rainfall tends to be concentrated, especially adjacent to the western Ghats, the foothills of the Himalayas, the

Burmese coast, and the Philippines (Fig. 1a). Thus, apart from realistic representation of physical processes, the details of the vertical representation of orography and its interaction with the circulation are important for realistic simulation of regional rainfall in models. With a pattern correlation of 0.93 between GPCP and CMAP rainfall, the spatial distribution of observed rainfall is well established.

The MMM is an efficient way to assess the overall performance of the CMIP5 and CMIP3 models. The CMIP5 MMM (Fig. 1b) has an improved representation of rainfall compared to the CMIP3 MMM (not shown). This is reflected by the more realistic magnitude of rainfall adjacent to the western Ghats and in the foothills of the Himalayas. The enhanced skill in representing the precipitation anchor points in the CMIP5 models may be associated with their higher horizontal resolution compared to the CMIP3 models. Even so, the MMM's have smaller pattern correlations than that between GPCP and CMAP, indicating scope for model improvement in the representation of rainfall.

The ERA40 and CMIP5 MMM time-mean 850hPa wind are given in Figs. 1c-1d. Skill is calculated with respect to ERA40. The ERA40 and JRA25 reanalysis (not shown) estimates of the wind structure are highly consistent, with their pattern correlation of 0.99. The main features of the low-level monsoon circulation include the cross-equatorial flow over western Indian Ocean/East African highlands, the westerly flow that extends from the Arabian Sea to the South China Sea, the monsoon trough over the Bay of Bengal, and the weak southerlies over the South China Sea and East

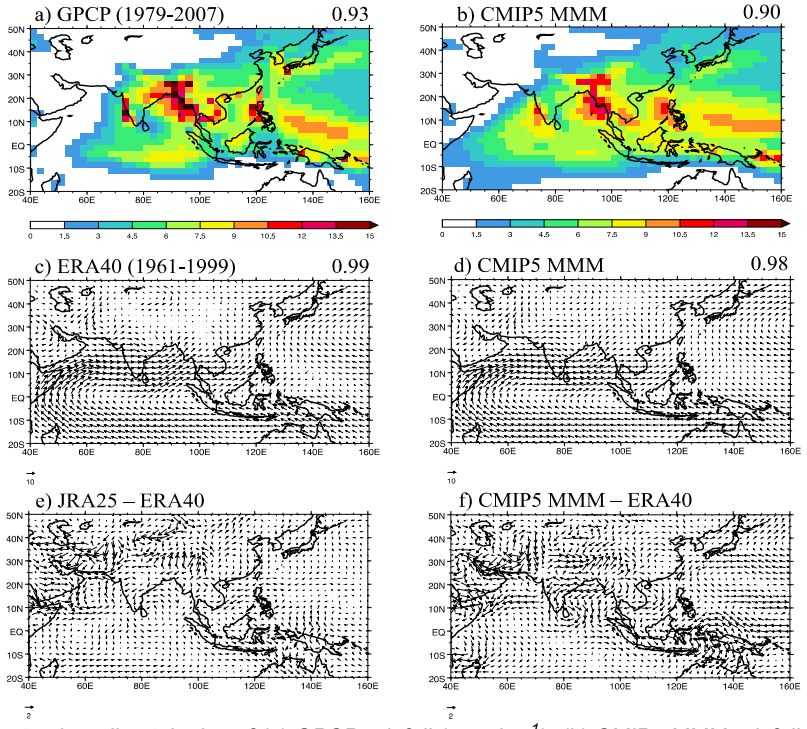

***Fig. 1**: June-September climatologies of (a) GPCP rainfall (mm day^{-1}), (b) CMIP5 MMM rainfall, (c) ERA40 850hPa wind (ms^{-1}), (d) CMIP5 MMM 850hPa wind, (e) JRA25 minus ERA40 850hPa wind, CMIP5 MMM minus ERA40 850hPa wind.*

Asia. The difference between JRA25 and ERA40, seen in Fig. 1e is smaller than that between the NCEP-NCAR and ERA15 reanalyses (Annamalai et al. 1999). The CMIP5 MMM northwesterly wind error over the Saudi Peninsula, and the northerly error over Pakistan and the

Thar Desert, Fig. 1f, is similar to the differences between the reanalyses. This suggests that improved observations are needed to constrain the climate simulations. It is possible that a dearth of rawindsonde reports from remote regions, in conjunction with the way in which the land surface processes and/or orography are handled, may contribute to the observational uncertainty over the land from the reanalyses.

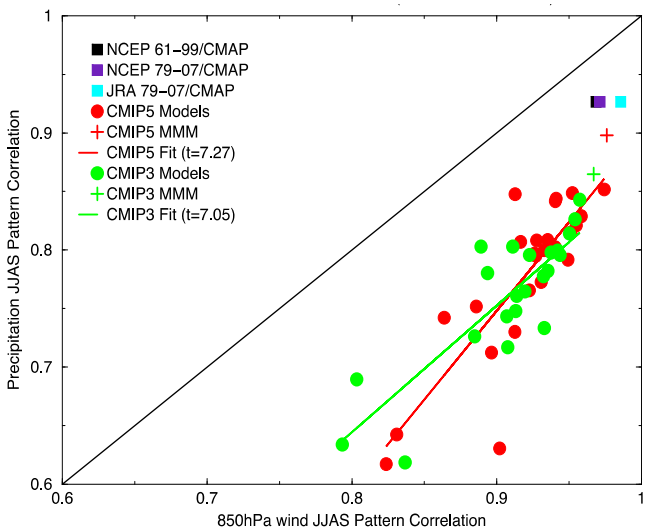

***Fig. 2**: Scatterplot of the pattern correlation with observations of simulated JJAS 850hPa wind climatology vs. the pattern correlation with observations of simulated JJAS precipitation climatology. The skill is relative to ERA40 and GPCP over the region 40°E-160°E, 20°S-50°N.*

The overall skill in simulating the time-mean monsoon is given in Fig. 2, which is a scatterplot of the pattern correlation relative to observations (ERA40 and GPCP) for 850hPa wind vs. precipitation. The results indicate that for all models the 850hPa wind is better simulated than the precipitation. This is perhaps not surprising due to that fact that circulation is a response to integrated diabatic heating and not to the details in regional rainfall. For 850hPa wind, the MMM skill is within the range of observational skill when NCEP/NCAR Reanalysis wind is also considered. For both CMIP5 and CMIP3 there is a better than 1% statistically significant relationship between the skill in representing the rainfall and the 850hPa wind. The statistical relationship suggests that improving the rainfall in the models will result in an improved representation of the wind.

Monsoon Onset

The analysis of the annual cycle of the monsoon using pentad data is restricted to 21/25 CMIP5 models and 18/22 CMIP3 models due to limitations in the availability of high-frequency rainfall data. Our methodology closely follows that of Wang and LinHo (2002). At each gridpoint the pentad time series is smoothed with a five pentad running mean. The smoothing removes high-frequency fluctuations that arise due to the limited sample size, while retaining the climatological intraseasonal oscillation. The January mean rainfall is then removed from each pentad, resulting in the relative rainfall rate. At a given gridpoint, the boreal summer monsoon is taken to occur if the relative rainfall rate exceeds 5mm day^{-1} during May-September. Onset is defined as the first pentad at which this threshold is met or exceeded. Given that the monsoon is defined by a threshold criterion, the monsoon domain will be different for each of the models. Therefore, the MMM is calculated at gridpoints if half or more of the models have monsoon defined at that location. Skill is assessed using pattern correlation for gridpoints where both observations and models have monsoon defined.

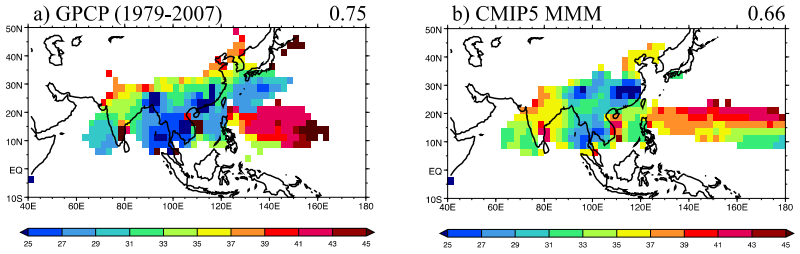

Fig. 3: *Monsoon onset pentad for (a) GPCP and (b) the CMIP5 MMM. The pattern correlation between GPCP and CMAP is also given in (a), and the pattern correlation between the CMIP5 MMM and GPCP is given in (b).*

The observed pentad of onset, seen in Fig. 3a, is consistent with the analysis of Wang and LinHo (2002). Monsoon onset occurs first over southeast Asia, and then subsequently over the South China Sea and to the southwest of India. The onset progresses northward from these locations, subsequently engulfing India, southern China, Korea, Japan, and the western Pacific. The CMIP5 MMM, Fig. 3b, has a larger pattern correlation with GPCP (0.66) than does CMIP3 MMM (0.51), indicating improvement in the ability to simulate the onset of the monsoon. However, for both MMM's, the onset is too late over India, and they overestimate the monsoon extension over the western/central Pacific Ocean. Contrary to the time-mean monsoon, individual models exceed the skill of the MMM.

Indian Summer Monsoon

The relationship between all-India rainfall (AIR) and ENSO is one of the most studied teleconnections (see review article by Turner and Annamalai 2012). Annamalai et al. (2007) provided an analysis of the time-mean state and interannual-interdecadal variability of the Asian summer monsoon in the CMIP3 models. The complexities in representing (1) the spatial distribution of the time-mean monsoon rainfall, (2) the ENSO forcing from the tropical Pacific, and (3) the seasonality of the ENSO-monsoon relationship revealed that only four of the models were realistic in representing the interannual coupled atmosphere-ocean teleconnection between AIR and tropical SST.

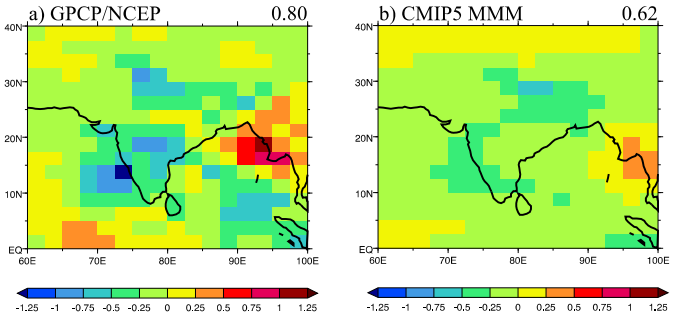

Fig. 4: *Interannual JJAS precipitation anomalies (mm day^{-1}) based on linear regression with JJAS NINO3.4 SST anomalies (a) GPCP rainfall vs. SST used in the NCEP-NCAR Reanalysis (1979-2007) and (b) CMIP5 MMM. The value in (a) is the pattern correlation of GPCP with CMAP, and in (b) is the model pattern correlation with GPCP. The pattern correlations are calculated over the region 60^{o}E-100^{o}E, 0^{o}-30^{o}N.*

The spatial pattern of the ENSO-forced rainfall anomalies is obtained from linear regression of JJAS NINO3.4 SST anomalies with JJAS rainfall anomalies (Fig. 4). The regressions are

presented for one standard deviation of the NINO3.4 SST anomalies, and thus correspond to rainfall anomalies associated with El Nino. From GPCP, the largest rainfall decreases occur adjacent to the western Ghats and near the foothills of the Himalayas, with a secondary rainfall deficit over central India, near 78°E, 18°N (Fig. 4a). Over north-eastern India and near the Burmese coast, above-normal rainfall anomalies prevail, and are also seen in CMAP rainfall (not shown). The CMIP5 MMM, Fig. 4b, has a slightly larger pattern correlation with GPCP (0.62) than does the CMIP3 MMM (0.60) Improvement in the CMIP5 MMM is also noted, since it also has larger rainfall anomalies than the CMIP3 MMM. However, in both cases the MMM anomalies are weaker than observed, given the wide-range of model fidelity in simulating the precipitation teleconnections.

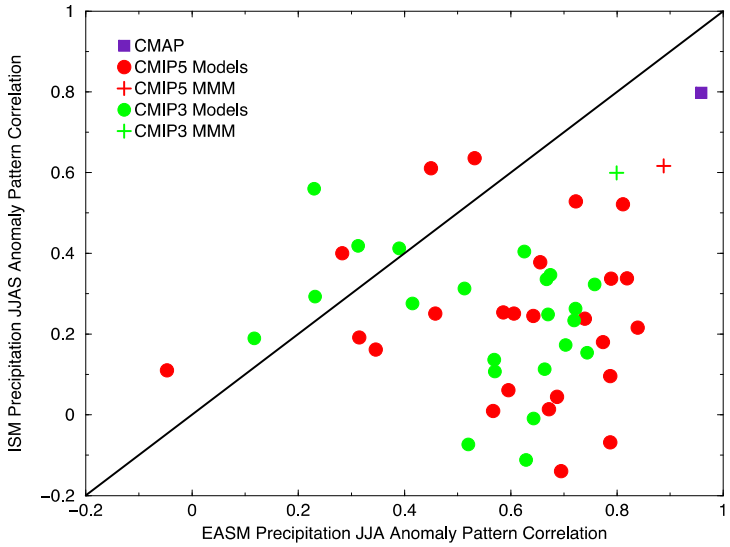

***Fig. 5**: Scatterplot of the pattern correlation with GPCP of simulated JJA precipitation anomalies over the East Asia vs. the pattern correlation with GPCP of simulated JJAS precipitation anomalies over the Indian Summer Monsoon.*

The East Asian summer monsoon (EASM) is a complicated region in that there are many competing mechanisms by which the monsoon is modulated on interannual time scales. We have used the negative of the Wang and Fan (1999) zonal wind shear index to evaluate interannual variations of the Meiyu/Baiu/Changma rainband (not shown). A summary of the ability of the models to simulate the interannual variability of rainfall for the Indian summer monsoon and the East Asian monsoon is given in Fig. 5. Relative to GPCP rainfall, it shows the pattern correlations of the interannual rainfall anomalies over the East Asian Summer Monsoon domain are better simulated than the pattern correlations of the interannual rainfall anomalies over the Indian Monsoon domain. The lack of a statistical relationship between the interannual variations over these regions confirms that the controlling mechanisms are distinct for the two regions, and that progress in modeling monsoon variability requires fidelity in representing a wide variety of processes.

Summary

The CLIVAR Asian-Australian Monsoon Panel Diagnostics Task Team selected the diagnostics presented herein. These diagnostics provide a broad overview of the state-of-the-art in simulating boreal summer Asian monsoon. Sperber et al. (2012) contains a more complete analysis of boreal summer Asian monsoon in the CMIP5 and CMIP3 models that includes additional diagnostics for assessing model improvement. The most important take away message is that in terms of the MMM, the CMIP5 models outperform the CMIP3 models for all of the diagnostics. While the CMIP5 MMM gains in terms of the skill scores are incremental, supporting evidence is noted, such as an improved amplitude of precipitation in the CMIP5 MMM relative to the CMIP3 MMM for the time-mean state, the annual cycle, and interannual variability, as well as a more realistic extent of the monsoon domain. Additionally, boreal summer intraseasonal variability (BSISV) is better represented in CMIP5 compared to CMIP3 (not shown), with several models showing an ability to represent the tilted rainband structure that extends from India to the Maritime continent. This is a pronounced improvement, since previous results indicated that only two climate models, both ECHAM4-based, could represent the BSISV life cycle (Sperber and Annamalai 2008). Furthermore, despite the poor representation of the BSISV in most of the models, the CMIP5 MMM outperforms the individual models. This suggests that a multi-model approach to forecasting the BSISV might be fruitful.

Acknowledgments

We thank the CLIVAR AAMP for helpful comments and encouragement during the course of this work. *We acknowledge the World Climate Research Programme's Working Group on Coupled Modelling, which is responsible for CMIP, and we thank the climate modeling groups for producing and making available their model output. For CMIP, the U.S. Department of Energy's Program for Climate Model Diagnosis and Intercomparison provides coordinating support and led development of software infrastructure in partnership with the Global Organization for Earth System Science Portals.* K. R. Sperber was supported by the Office of Science (BER), U.S. Department of Energy through Lawrence Livermore National Laboratory contract DE-AC52-07NA27344. H. Annamalai was supported by the Office of Science (BER) U.S. Department of Energy, Grant DEFG02-07ER6445, and also by three institutional grants (JAMSTEC, NOAA and NASA) of the International Pacific Research Centre. In-Sik Kang was supported by the National Research Foundation of Korea (NRF-2009-C1AAA001-2009-0093042). Aurel Moise was supported by the Australian Climate Change Science Program, funded jointly by the Department of Climate Change and Energy Efficiency, the Bureau of Meteorology and CSIRO. B. Wang was supported by US NSF award #AGS-1005599.

References

Annamalai, H. and Sperber, K. R. 2005. Regional heat sources and the active and break phases of boreal summer intraseasonal (30-50 day) variability. *J. Atmos. Sci.,* 62, 2726-2748.

Annamalai, H., Hamilton, K. and Sperber, K. R. 2007. The south Asian summer monsoon and its relationship to ENSO in the IPCC AR4 simulations. *J. Clim*.. 20, 1071-1092.

Boschat, G., Terray, P. and Masson, S. 2012. Robustness of SST teleconnections and precursory patterns associated with the Indian summer monsoon. *Clim. Dyn*. 38, 2143-2165.

Annamalai, H., Slingo, J.M., Sperber, K.R. and Hodges, K. 1999. The mean evolution and variability of the Asian summer monsoon: comparison of ECMWF and NCEP-NCAR reanalyses. *Mon. Wea. Rev*., 127, 1157-1186.

Charney, J. and Shukla, J. 1981. Predictability of monsoons. In: Lighthill, J. and Pearce, R. P. (eds.) Monsoon Dynamics. Cambridge University Press, Cambridge, pp. 99-109.

Huffman, G.J., Adler, R.F., Morrissey, M.M., Bolvin, D.T., Curtis, S., Joyce, R., McGavock, B. and Susskind, J. 2001. Global precipitation at one-degree daily resolution from multisatellite observations. *J. Hydrometeorol*., 2, 36–50.

Gill, A.E. 1980. Some simple solutions for heat-induced tropical circulation. *Q. J. R. Meteorol. Soc.* 106, 447-462.

Kallberg, P., Berrisford, P., Hoskins, B., Simmons, A., Uppala, S., Lamy-Thepaut, S. and Hine, R. 2005. ECMWF re-analysis project report series 19. ERA-40 Atlas. European Centre for Medium-Range Weather Forecasts, Reading, UK.

Kalnay, E. et al. 1996. The NCEP/NCAR 40-year reanalysis project. *Bull. Amer. Meteorol. Soc*., 77, 437–471.

Nakazawa, T. 1986. Intraseasonal variations of OLR in the tropics during the FGGE year. *J. Meteorol. Soc. Japan*, 64, 17-34.

Onogi, K. et al. (2007) The JRA-25 Reanalysis. *J. Meteorol. Soc. Japan*, 85, 369-432.

Slingo, J. and Annamalai, H. 2000. 1997: The El Nino of the Century and the Response of the Indian Summer Monsoon. *Mon. Wea. Rev.*, 128, 1778-1797.

Sperber, K.R. and Annamamlai, H. 2008. Coupled model simulations of boreal summer intraseasonal (30-50 day) variability, part 1: systematic errors and caution on use of metrics. *Clim. Dyn*., 31, 345-372. doi:10.1007/s00382-008-0367-9.

Sperber, K.R. and Palmer, T.N. 1996. Interannual tropical rainfall variability in general circulation model simulations associated with the atmospheric model intercomparison project. *J. Clim*., 9, 2727–2750.

Sperber, K.R., Annamalai, H., Kang, I.-S., Kitoh, A., Moise, A., Turner, A., Wang, B. and Zhou, T. 2012: The Asian summer monsoon: An intercomparison of CMIP5 vs. CMIP3 simulations of the late 20th century. *Clim. Dynam.*, (in revision)

Turner, A.G. and Annamalai, H. 2012. Climate change and the south Asian summer monsoon. *Nature Clim. Change*, 2, 1-9. doi:10.1038/NCLIMATE1495

Turner, A.G., Sperber, K.R., Slingo, J., Meehl, G., Mechoso, C.R., Kimoto, M. and Giannini, A. 2011. Modelling monsoons: understanding and predicting current and future behavior. In: Chang, C.-P., Ding, Y., Lau, N.-C., Johnson, R.H., Wang, B. and Yasunari, T. (eds.) The Global Monsoon System: Research and Forecast, 2nd edn. World Scientific Publishing Co., Singapore, pp. 421-454

Wang, B. 2006. The Asian monsoon. B. Wang (ed.) Springer-Verlag, Berlin, Germany.

Wang, B. and Fan, Z. 1999. Choice of South Asian summer monsoon indices. *Bull. Amer. Meteorol. Soc.*, 80, 629-638.

Wang, B. and LinHo. 2002. Rainy season of the Asian-Pacific Summer Monsoon. *J. Clim*., 15, 386-398.

Wang, B., Kang, I.-S. and Lee, J.-Y. 2004. Ensemble simulations of Asian-Australian monsoon variability by 11 AGCMs. *J. Clim.*, 17, 803-818.

Webster, P.J., Magana, V.O., Palmer, T.N., Shukla, J., Thomas, R.A., Yanai, M. and Yasunari, T. 1998. Monsoons: Processes, predictability, and the prospects for prediction. *J. Geophys. Res*., 103, 14,451-14,510.

Xie, P.P. and Arkin, P.A. 1997. Global precipitation: A 17-year monthly analysis based on gauge observations, satellite estimates, and numerical model outputs. *Bull. Amer. Meteorol. Soc.*, 78, 2539–2558.

Zhou, T. and Yu, R.-C. 2005. Atmospheric water vapor transport associated with typical anomalous summer rainfall patterns in China. *J. Geophys. Res.*, 110, D08104, doi:10.1029/2004JD005413

THE INFLUENCE OF CHANGES IN SYNOPTIC REGIMES ON NORTH AUSTRALIAN WET SEASON RAINFALL TRENDS

Jennifer L. Catto, Christian Jakob, Neville Nicholls

Monash University, Clayton, Victoria, Australia

A large proportion of annual precipitation over the north of Australia falls during the wet season between September and April. This rainfall is partly associated with the Australian monsoon system, however a substantial proportion does occur during periods where the monsoon is not active (Nicholls 1984). Many recent studies have shown that precipitation in the north and northwest of Australia increased over the past 50 years, particularly during the summer months (Smith 2004; Taschetto; England 2009). The reason for this increase has been given many possible explanations (Rotstayn et al. 2007; Taschetto; England 2009). It is unclear whether the changes are due to changes in the circulation producing the flow in which precipitation events occur, or if the precipitation per event has increased in intensity.

In previous work by Pope et al. (2009), daily data collected by radiosondes released from Darwin were used to identify five distinct wet season regimes, each associated with a characteristic synoptic circulation pattern and rainfall probability distribution. The five regimes are referred to as the Deep West (the active monsoon regime), Moist East (monsoon break regime), Shallow West (monsoon active east of Australia), East and Dry East (regimes where the flow comes from over the Australian continent and is therefore dry). In the present study (Catto et al. 2012) these five regimes are used to decompose the precipitation trend at Darwin between 1957 and 2008 into two components. The first component is that due to changes in the relative frequency of occurrence of each of the regimes. The second component is that due to changes in the precipitation associated with each regime.

Over the period of interest, the rain associated with each regime does not change significantly for any of the regimes. However, the relative frequency of occurrence of the regimes with the lowest average precipitation values decreases significantly, and increases significantly for the Moist East regime, one of the wettest regimes. The timeseries of the relative frequency of occurrence of these two regimes and the corresponding linear trends are shown in Fig. 1. These changes suggest that changes in the large-scale circulation are a more important contributor to the precipitation trends than are thermodynamic changes.

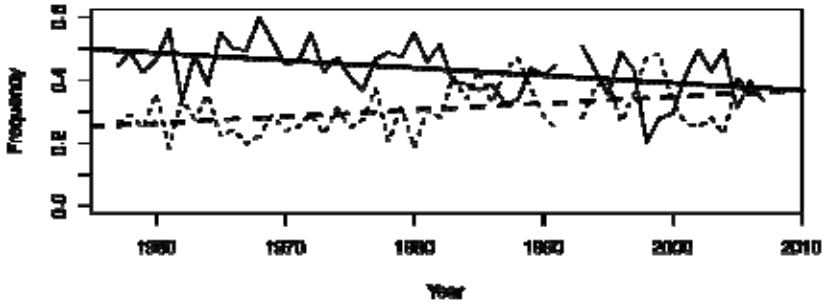

Fig. 7: *Relative frequency of occurrence of the combined Dry East/East (light solid line) and Moist East (light dashed line) regimes, along with the associated linear trends (heavy solid and dashed lines respectively).*

While the largest absolute precipitation trends occur between December and March, associated with changes in the Moist East, Deep West and Shallow West regimes, the largest *relative* changes in precipitation occur in November and April. This indicates a lengthening of the wet season associated with a change in the large-scale circulation to moist easterly flow. Future research will focus on elucidating the potential dynamical reasons for this change in the large-scale flow.

References

Catto, J.L., Jakob, C. and Nicholls, N. 2012: The influence of changes in synoptic regimes on north Australian wet season rainfall trends. *Journal of Geophysical Research-Atmospheres*, **117**.

Nicholls, N. 1984: A SYSTEM FOR PREDICTING THE ONSET OF THE NORTH-AUSTRALIAN WET-SEASON. *Journal of Climatology*, **4,** 425-435.

Pope, M., Jakob, C. and Reeder, M.J. 2009: Regimes of the North Australian Wet Season. *Journal of Climate*, **22,** 6699-6715.

Rotstayn, L.D. and Coauthors, 2007: Have Australian rainfall and cloudiness increased due to the remote effects of Asian anthropogenic aerosols? *Journal of Geophysical Research-Atmospheres*, **112**.

Smith, I. 2004: An assessment of recent trends in Australian rainfall. *Australian Meteorological Magazine*, **53,** 163-173.

Taschetto, A.S. and England, M.H. 2009: An analysis of late twentieth century trends in Australian rainfall. *International Journal of Climatology*, **29,** 791-807.

CIRCULATION OF ANOMALOUS WET AND DRY AUSTRALIAN MONSOON SEASONS AND FUTURE CHANGES FROM CMIP3 SIMULATIONS

Ramasamy Suppiah[1], Aurel Moise[2], Lawson Hanson[2] and Rob Colman[2]

Centre for Australian Weather and Climate Research (CAWCR),

[1]CSIRO Marine and Atmospheric Research and [2]Bureau of Meteorology, Melbourne, Australia

We have analysed current climate and future simulated anomalously wet, dry and normal years of rainfall in the Australian tropics using a set of simulations from the third coupled model intercomparison project (CMIP3) (Meehl et al. 2007) and investigated their link to large-scale circulation anomaly patterns over the region that extends from 30°N to 50°S, 90°E to 160°E. Anomalous wet and dry years have been classified as years above and below one standard deviation of climatological mean rainfall taken for the period representing present climate (1960 to 2000) and also for the period representing future climate (2061-2069) for A2 emission scenario. Other years were classified as normal years. Future changes in anomalous wet years are classified as the difference between average anomalous wet years from 2061 to 2099 and average anomalous wet years from 1961 to 2000 and so on for anomalous dry years. Mean sea level pressure, zonal and meridional winds at 850, 500 and 200 hPa levels and large-scale rainfall have been considered to investigate changes in the regions' atmospheric circulation and rainfall. Models are grouped as projecting rainfall increases (PRI) and projecting rainfall decreases (PRD) based on their simulated changes in rainfall by the end of the 21st century to see any one of these groups can show whether wet years become wetter and dry years become drier under climate change conditions.

Current climate

Almost all of the models considered in this study fairly well captured mean spatial patterns of MSLP, winds and rainfall over the Australian region when simulated long-term climatologies (30-year climatologies, 1961-1990) are compared with observations (Suppiah et al. 2007), but these models fail to capture the observed spatial patterns in anomalous circulation and rainfall patterns. This suggests that the current-generation of models grossly underestimate the observed internnual variability in rainfall and its link to atmospheric circulation patterns. Moreover, model-to-model variations in spatial patterns of rainfall, MSLP and zonal and meridional winds are also large among anomalous wet and dry years. When 16 models are grouped into two categories as PRI and PRD models, some differences in spatial patterns of anomalous winds, MSLP and rainfall have been found between these types of models.

Both zonal and meridional winds at lower levels, represented by the 850 hPa, show models simulate westerly and northerly anomalies over the Australian tropics and easterly anomalies over the continent which are consistent with observations. However, the simulation of winds particularly over north of Papua New Guinea is unrealistic presumably due to central equatorial cold tongue intrusion into this region by in many models. Moreover, the models also overestimate the magnitudes of these winds. At the upper level, 200 hPa, models tend to

underestimate zonal and meridional winds for both anomalous wet and dry conditions. Models also fail to capture the spatial patterns of winds at this level.

Compared to observations, models tend to overestimate rainfall for anomalous wet conditions while under estimate for anomalous dry conditions for the present climate. Most of the models simulate too large rainfall anomalies over Western Pacific presumably due to cold tongue intrusion. In addition to failure of simulating the observed magnitude of winds, the models also fail to get the right location of maximum winds.

Future climate

Winds anomalies at the lower level (850 hPa) simulated by both PRI and PRD models indicate no clear pattern of change for anomalous wet years. For anomalous dry years, PRI models show easterly anomalies over most of the domain, while PRD models show westerly anomalies over northern coast of Australia and easterly anomalies on either sides, which seems unrealistic compared with observations. Strengthening and weakening of meridional winds associated with anomalous wet and dry years are realistically simulated by PRI models, but PRD simulate opposite patterns. While the observation shows a strong positive relationship between strengthening of westerly anomalies and rainfall, both PRI and PRD do not simulate the observed wind anomalies for wet anomalous conditions. However, strengthening of northerly component over Southeast Asia and over Australia during the wet anomalous conditions under enhanced greenhouse conditions suggest an intensified meridional circulation which could lead to stronger monsoon and more rainfall.

Changes in upper level winds at the 200 hPa indicate a slight strengthening of the upper level anticyclone for anomalous wet conditions and weakening for anomalous dry conditions. These changes are clearly found in meridional winds rather than in zonal winds. Although the change in upper level winds shows a slight strengthening of circulation during anomalous wet conditions such changes are loosely linked to low level changes in zonal winds, which show no clear changes. *This suggest, to some extent, that the models simulate an increase in rainfall over tropical Australia independent of the observed (current climate) link with the lower and upper atmosphere anomalous circulations.*

Compared to PRD models, PRI models better simulate circulation patterns associated with anomalous wet and dry conditions in the current climate. Models of PRI in the 21st century show slight strengthening (weakening) of circulation associated with anomalous wet (dry) years and increases (decreases) in rainfall. Models of PRD in the 21st century simulate opposite conditions. This is crucial when produce future projections on anomalous or extreme rainfall events and intensity for tropical Australia as well as other regions of the tropics.

The results, at least from models which are classified as PRI, suggest that *wet years become wetter and dry years become drier over tropical Australia*. The practical implications of the results suggest possible widespread impacts across the region. Such impact can significantly affect marine and terrestrial ecosystem health, agricultural productivity, water resources, fisheries, human health, human migration, tourism, and pest abundance and distribution in the region.

References

Meehl, G.A., Covey, C., Delworth, T., Latif, M., McAvaney, B., Mitchell, J.F.B., Stouffer, R.J. and Taylor, K.E. 2007. The WCRP CMIP3 multimodel dataset: A new era in climate change research. *Bull. American Met. Soc.,88,* 1383–1394. .

Suppiah, R., Hennessy, K.J., Whetton, P.H., McInnes, K., Macadam, I., Bathols, J., Ricketts, J. and Page, C.M. 2007. Australian climate change projections derived from simulations performed for the IPCC 4th assessment report. *Aust. Met. Mag.*, *56,* 131-152.

LARGE-SCALE INFLUENCES ON CHANGES IN AUSTRALIAN MONSOONAL RAINFALL AND CIRCULATION UNDER GLOBAL WARMING.

Ian Watterson

Abstract

Representative changes in far north Australian rainfall under global warming simulated by 23 CMIP3 models ranged from -11% to +11% (both per degree of warming, Watterson 2012). These were rather coherent with Australian average changes, and with the relative surface warming of the regional equatorial Pacific and Indian Oceans. Such large-scale influences are being further examined in both CMIP3 and CMIP5, with a focus on the monsoonal rainfall and circulation. The link to interannual variability will be considered.

The Centre for Australian Weather and Climate Research is a partnership between CSIRO and the Bureau of Meteorology.